PB83-198342

NSF/CEE-82099

JULY 1982

UMEE 82R5

BEHAVIOR OF EXTERNAL REINFORCED CONCRETE BEAM TO COLUMN CONNECTIONS SUBJECTED TO EARTHQUAKE TYPE LOADING

Mohammad Reza Ehsani

James K. Wight

The University of Michigan Department of Civil Engineering

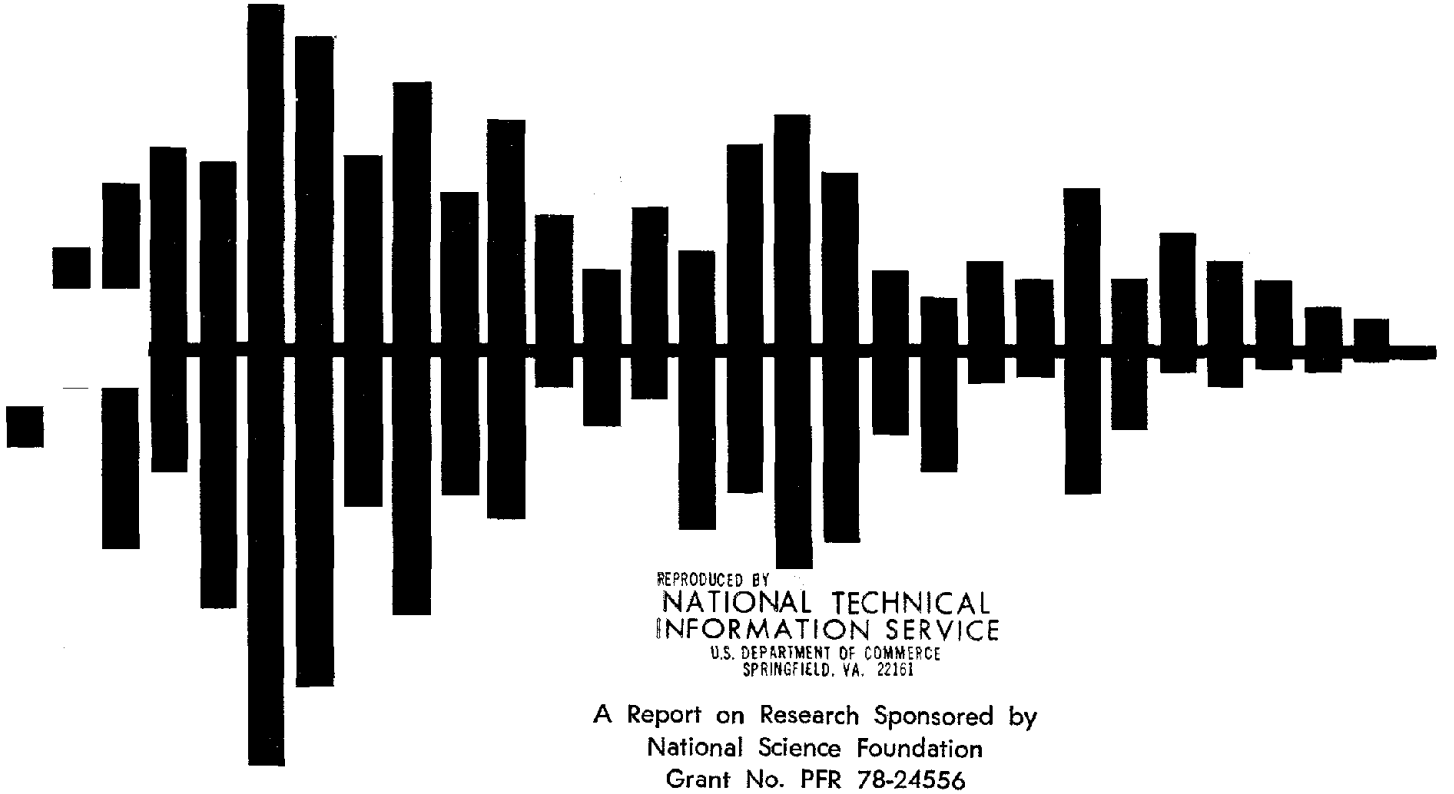

A Report on Research Sponsored by
National Science Foundation
Grant No. PFR 78-24556

50272-101

REPORT DOCUMENTATION PAGE	1. REPORT NO. NSF/CEE-82099	2.	3. Recipient's Accession No. PB83 188362
4. Title and Subtitle: Behavior of External Reinforced Concrete Beam to Column Connections Subjected to Earthquake Type Loading			5. Report Date: July 1982 6.
7. Author(s): M.R. Ehsani, J.K. Wight			8. Performing Organization Rept. No. UMEE 82R5
9. Performing Organization Name and Address: University of Michigan, Department of Civil Engineering, Ann Arbor, MI 48109			10. Project/Task/Work Unit No. 11. Contract(C) or Grant(G) No. (C) (G) CEE7824556
12. Sponsoring Organization Name and Address: Directorate for Engineering (ENG), National Science Foundation, 1800 G Street, N.W., Washington, DC 20550			13. Type of Report & Period Covered 14.

15. Supplementary Notes
Submitted by: Communications Program (OPRM)
National Science Foundation
Washington, DC 20550

16. Abstract (Limit: 200 words)
Twelve full-size exterior beam-to-column subassemblies were constructed and tested. The primary variables studied were: (1) ratio of the sum of the flexural strengths of the columns to that of the beam; (2) amount of transverse reinforcement placed within the joint; (3) shear stress in the joint; and (4) inclusion of transverse beams and slab for half of the specimens. In all bare specimens, diagonal cracks connecting the opposite corners of the joint were observed during the first cycle of loading. In specimens with transverse beam and slab, the flexural cracks formed when the slab reinforcement was in tension did not close completely with the reversal of the loading direction. Conclusions stress the importance of: (1) increasing both the flexural strength and transverse reinforcement ratios; (2) reducing joint shear stress; and (3) including transverse beams and slab.

17. Document Analysis a. Descriptors

Beams (supports)
Columns (supports)
Loads (forces)
Cyclic loads
Reinforced concrete
Displacement
Earthquake resistant structures
Building codes
Joints (junctions)

b. Identifiers/Open-Ended Terms
Transverse reinforcement
J.K. Wight, /PI

c. COSATI Field/Group

18. Availability Statement	19. Security Class (This Report)	21. No. of Pages
NTIS	20. Security Class (This Page)	22. Price

(See ANSI-Z39.18) See Instructions on Reverse

OPTIONAL FORM 272 (4-77)
(Formerly NTIS-35)
Department of Commerce

BEHAVIOR OF EXTERNAL REINFORCED CONCRETE BEAM TO COLUMN CONNECTIONS SUBJECTED TO EARTHQUAKE TYPE LOADING

by

Mohammad Reza Ehsani

James K. Wight

A Report on Research Sponsored by
National Science Foundation
Grant No. PFR 78-24556

Report UMEE 82R5
Department of Civil Engineering
The University of Michigan
Ann Arbor, MI 48109

July 1982

ACKNOWLEDGEMENTS

This report was submitted by Mohammad Reza Ehsani in partial fulfillment of the requirements for the degree of Doctor of Philosophy (Civil Engineering) in The Horace H. Rackham School of Graduate Studies at The University of Michigan. Dr. Ehsani wishes to express his sincere appreciation to Professor James K. Wight, chairman of his doctoral committee, for his invaluable guidance, encouragement and support throughout this research. The authors would like to thank Professors Subhash C. Goel, Robert D. Hanson, Wadi S. Rumman, and Alan S. Wineman (members of his doctoral committee) for reviewing the report and offering helpful suggestions.

The investigation was directed by Professor James K. Wight and sponsored by the National Science Foundation through grant PFR 78-24556. The conclusions arrived at in this report are solely those of the authors and do not necessarily represent the views of the sponsors.

The authors would like to thank Ben Bourland, senior technician in the G.G. Brown Laboratory for his valuable suggestions in solving a variety of problems associated with testing of the specimens. Thanks are also to a

number of graduate and undergraduate students who helped in the testing program at various stages. The assistance of fellow graduate student Ahmad J. Durrani is gratefully acknowledged.

Finally, Dr. Ehsani would like to express his profound gratitude to his parents and his uncle Dr. Mansour Jadalizadeh who provided much needed moral and personal support during the course of this study.

PREFACE

It is suggested that the reader be selective in choosing which chapters to read, depending on the depth of his/her interest in this subject. A general understanding of the report can be achieved by reading Chapter 6 or Chapters 1 and 6.

Chapter 2 provides a detailed description of the specimen fabrication and the testing setup.

Chapter 3 contains information about the manner of deterioration of all specimens. Detailed calculation of yield moments and deflections are presented in Chapter 4. The existing design codes are compared in Chapter 5. Because of the depth of detail which they contain, Chapters 3, 4 and 5 are recommended to be studied only by the most avid reader.

TABLE OF CONTENTS

LIST OF TABLES

LIST OF FIGURES

LIST OF APPENDICES

Appendix

NOTATION

A = cross sectional area of beam or beam and slab ($in.^2$)

A_b = area of individual bar ($in.^2$)

A_c = area of core of specially reinforced column measured to outside diameter of hoops ($in.^2$)

A_{cv} = effective area in shear ($in.^2$)

A_g = cross sectional area of column ($in.^2$)

A_w = cross sectional area of the web portion of beam and slab ($in.^2$)

A_{sh} = cross sectional area of hoop reinforcement ($in.^2$)

A_v = area of shear reinforcement within a distance s_h ($in.^2$)

A_{s1c} = area of tension reinforcement in column ($in.^2$)

A_{s2c} = area of intermediate longitudinal reinforcement in column ($in.^2$)

A_{sc} = area of non-prestressed tension reiforcement in one face of column section ($in.^2$)

A_{sc}' = area of non-prestressed compression reinforcement in one face of column section ($in.^2$)

A_{s1b} = area of outer layer of tension reinforcement in beam ($in.^2$)

A_{s2b} = area of inner layer of tension reinforcement in beam ($in.^2$), or
area of slab longitudinal reinforcement directly above the web portion of main beam ($in.^2$)

A_{s3} = area of slab longitudinal reinforcement on each side of main beam ($in.^2$)

b = width of column transverse to the direction of shear (in.)

b_b = width of main beam (in.)

b_{tb} = width of transverse beam (in.)

c_j = V_{jh} / (V_{jx} + V_{jy})

d_b = nominal column bar diameter (in.)

d_b' = nominal diameter of hooked bar (in.)

D = diagonal dimension of joint (in.)

d_{1b} = distance from compression face to centroid of outer layer of tension reinforcement in beam (in.)

d_{2b} = distance from compression face to centroid of inner layer of tension reinforcement in beam (in.), or distance from compression face to centroid of slab longitudinal reinforcement (in.)

d_{1c} = distance from compression face to centroid of tension reinforcement in column (in.)

d_{2c} = distance from compression face to centroid of intermediate longitudinal reinforcement in column (in.)

E_c = initial slope of concrete stress vs. strain curve (psi)

E_s = measured modulus of elasticity for reinforcing steel (ksi)

E_{sh} = measured slope at the onset of strain hardening for reinforcing steel (ksi)

f_h = stress developed by standard hook (psi)

f_y = specified yield strength of reinforcement (ksi)

f_{yh} = specified yield strength of hoop reinforcement (ksi)

f_c' = compressive strength of concrete (psi)

G_c = shear modulus of concrete = 0.4 E_c (psi)

h_b = total depth of beam (in.)

h= h_c= total depth of column parallel to the direction of shear (in.)

h_{tb} = total height of transverse beam (in.)

h" = core dimension of tied column measured to outside diameter of hoop (in.)

I_b = cracked moment of inertia of beam ($in.^4$)

I_c = cracked moment of inertia of column ($in.^4$)

L_b = length of beam section of specimen between the beam loading point and the front face of column (in.)

L_c = length of column portion of specimens held between simple supports (in.)

l_{dh} = development length of hooked bars measured from the face of the column core to back side of the hook (in.)

l_s = straight embedment length as shown in Fig. 5.1

l_o = development length of hooked bars equal to straight embedment measured from the middle of column to back edge of hooked bar (in.)

M_{col} = moment capacity of column for axial load used during test (k-in.)

M_R = sum of the flexural capacity of columns to that of beam

M_{yb} = yield moment for beam or beam and slab (k-in.)

P_u = design column axial load (kips)

P = applied column axial load during test (kips)

s_h = center to center spacing of hoops (in.)

V_b = shear force applied to beam portion of specimen (kips)

V_c = shear force applied to column portion of specimen (kips)

V_{ch} = ideal horizontal joint shear strength provided by concrete shear resisting mechanism (kips)

V_{cv} = ideal vertical joint shear strength provided by concrete (kips)

V_j = joint shear force (kips)

V_{jh} = horizontal shear force in joint (kips)

V_{jv} = vertical shear force in joint (kips)

V_{jx} = horizontal shear force in X direction (kips)

V_{jy} = horizontal shear force in Y direction (kips)

V_{sh} = design horizontal shear force to be resisted by horizontal joint shear reinforcement (kips)

V_{sv} = design vertical shear force to be resisted by vertical joint shear reinforcement (kips)

V_{yb} = observed yield shear force applied to beam (kips)

V_{yc} = observed yield shear force applied to column (kips)

V_u = design joint shear force (kips)

v_c = nominal permissible shear stress carried by concrete (psi)

v_{jh} = nominal horizontal shear stress in joint (psi)

v_u = factored design joint shear stress (ksi)

α = stress multiplier for flexural reinforcement = 1.25 for earthquake loading

β = factor reflecting loading to be imposed = 1.0

γ = joint shear stress as a multiple of $\sqrt{f_c'}$

γ' = factor reflecting confinement of joint by lateral members = 1.0 or 1.4

γ_j = average joint shear deformation (in./in.)

γ_{1j} = first component of joint shear deformation (in./in.)

γ_{2j} = second component of joint shear deformation (in./in.)

Δ_t = summation of Δ_1, Δ_2, and Δ_3 (in.)

Δ_{yc} = deflection of top column half loading point at yield of beam or beam and slab (in.)

Δ_{yo} = observed yield deflection from plots of applied load vs. load point deflection (in.)

Δ_{ys} = yield deflection measured from plots of applied load vs. strains in beam longitudinal reinforcement at the front face of column (in.)

Δ_1 = theoretical flexural deflection (in.)

Δ_2 = deflection due to shear deformations in beam and column (in.)

Δ_3 = deflection due to shear deformation of joint (in.)

δ_1 = elongation or shortening of LVDT1

δ_2 = elangation or shortening of LVDT2

ε_{sh} = strain in steel at onset of strain hardening (in./in.)

ε_y = strain in steel at the beginning of yield (in./in.)

σ_y = stress in steel at the beginning of yield (ksi)

ρ_t = transverse reinforcement ratio (%)

ρ_{tm} = modified transverse reinforcement ratio (%)

ϕ = strength reduction factor = 0.85

ψ = factor influencing the effect of confinement on capacity of hooked bar

CHAPTER 1

INTRODUCTION

1.1 General

With increasing cost of land in central urban areas, the trend in present reinforced concrete design is towards high rise structures. The design of multistory structures for gravity loads causes no serious problems. However, due to the unpredictability of forces during an earthquake, many aspects of seismic design of structures still need to be investigated. The problem of seismic resistance design is especially significant in reinforced concrete structures, where due to the relatively large mass of the structure, large inertia forces will be generated during an earthquake.

When structures, designed in accordance with building code guidelines (1), are subjected to a severe earthquake, certain components of the structure will undergo cyclic deformations in the inelastic range. For the structure to achieve sufficient energy absorption and dissipation capacity, it is important that these components possess sufficient ductility to sustain large

deformations without significant loss of strength. It is necessary to prevent shear failure, sudden loss of bond and anchorage of reinforcing bars, and premature crushing or splitting of the concrete caused by local buckling of reinforcing bars.

For many years, the "strong column-weak beam" design philosophy has been widely recognized among practicing engineers. Formation of flexural plastic hinges in columns are not generally favored because of the possibility of large lateral deformations leading to larger column moments, in addition to the likelihood of irreparable permanent sway in the structure. It is therefore important when designing reinforced concrete ductile moment resisting frames that provisions be made which limit the formation of flexural plastic hinges to the beams.

To ensure the formation of plastic hinges in the beams, the beam to column connection must be designed to carry the reversing moments, shears and anchorage forces associated with the development of plastic hinges in the beams during an earthquake, without a significant loss of strength or stiffness.

In recent severe earthquakes (2,3), failure of the beam to column joints has seldom been reported. However, in laboratory testing of beam-column subassemblages, the

connection is frequently found to be the weakest component if the adjoining beams and columns are detailed properly. In the field, most failures have occurred at loads well below the strength of the beam to column joints and have usually been due to poor detailing of columns or beams.

1.2 Review of Previous Investigations

Behavior of reinforced concrete beam to column connections has been studied by several researchers in the U.S., Canada, New Zealand, and Japan since the mid 1960's. Hanson and Connor (4-6) conducted the first tests on beam to column connections in the laboratories of the Portland Cement Association. From tests of sixteen exterior and interior connections they demonstrated the importance of a properly detailed joint in achieving ductile frame behavior. The results indicated that adequate energy dissipation can be achieved near the joint if proper attention is given to anchorage of beam bars, shear resistance, and confinement of the joint. They used the design equations developed for shear design of beams, to illustrate that transverse reinforcement is required to resist shear forces in the joint. Furthermore, they indicated that grade 60 reinforcing bars can be used with satisfactory results in

structures which are designed to develop ductile behavior.

Megget (7), Smith (8), Patton (9), and Renton (10) tested a total of thirteen exterior beam to column connections in New Zealand, and the results were summarized by Park and Paulay (11). Their findings were different from those of the U.S. investigators. They concluded that due to excessive diagonal cracking of the concrete in the joint, the contribution of concrete in resisting shear forces in the joint should be ignored. In addition, they rejected the truss analogy, which assumes formation of cracks at a 45 degree angle, as an adequate assumption for determining the shear strength of a joint. They concluded that the shear strength had to be checked on diagonal cracks which extend between opposite corners of the joint. They recognized the need for transverse reinforcement in the joint to provide shear strength and sufficient confinement for the concrete. Park and Paulay's recommendations are probably too conservative due to poor detailing of some specimens. In their early tests, part of the joint transverse reinforcement was placed too close to the top and bottom of the joint. It is now widely recognized that joint transverse reinforcement should be placed near the center of the joint to be considered effective in resisting

joint shear forces (12).

Tests conducted by Uzumeri and Seckin (13) at the University of Toronto reemphasized the importance of proper anchorage of reinforcing bars. Although they used the same shear equations as Hanson and Connor, they concluded that this equation could only be used to predict the cracking shear of a beam to column connection. In addition, they discarded the 45 degree truss analogy as an accurate method in predicting the behavior of the joint.

The results from the above investigations were used by ASCE-ACI Committee 352 to formulate recommendations for the design of beam-column connections (12). These recommendations, which are based on experimental results, use the equations which were developed for calculating the shear strength of beams to calculate the shear strength of a joint.

Lee et al. (14) tested eight exterior beam to column subassemblages and concluded that concrete does carry a significant portion of the total shear force in the joint. Furthermore, they demonstrated that in some cases the specimens carried twice the shear suggested by the recommendations of ACI-ASCE Committee 352 (12).

Tests by Meinheit and Jirsa (15) illustrated that the expression used by Hanson and Connor results in a

good estimate of the load at which the first diagonal crack is formed at the joint, but the contribution of the concrete to the ultimate shear strength of the joint was much larger than the diagonal cracking load.

Scarpas (16) tested three exterior beam to column connections and concluded that the required amount of joint transverse reinforcement can be considerably reduced if the column is reinforced with intermediate longitudinal reinforcement to resist vertical shear forces in the joint.

The more recent research results indicate that confinement is the most important ingredient in the design of beam-column connections to sustain large load reversals. When the joint is adequately confined, deterioration of the concrete in the core of the joint will be delayed and the contribution of the concrete in resisting joint shear forces will increase. In addition, when bars are anchored in well confined joints they will be capable of developing their ultimate capacity, and slippage or pullout of the bars, which is a major source of stiffness degradation, will be eliminated or reduced.

1.3 Objective and Scope

The primary purpose of this investigation is to obtain experimental evidence which would justify a

simplification of the existing seismic recommendations for beam to column connections. The current recommendations from ACI-352 (12) require a very high percentage of transverse reinforcement which makes connections difficult to construct. The experimental portion of this study was designed to determine if joints reinforced with lower amounts of transverse reinforcement than that required by the recommendations (12) would perform satisfactorily under load reversals. The analytical portion of this study used the experimental results from this study and work done by other researchers to develop a design chart for selection of confinement reinforcement. The design chart will indicate the the minimum percentage of transverse reinforcement for various joint configurations to provide adequate confinement, and consequently produce sufficient shear strength and good behavior under large load reversals.

Twelve reinforced concrete beam to column subassemblages were constructed and tested to determine the effect of the following parameters on the overall behavior of beam to column connections. First, the sum of the flexural capacities of the columns to that of the beams, referred to as the flexural strength ratio, which was varied between 1.1 and 2.0. Second, the percentage

of the transverse reinforcement within the joint which ranged from 1.0 percent to 1.5 percent. Third, the shear stress within the joint which was kept at $10\sqrt{f_c'}$ or $14\sqrt{f_c'}$. Fourth, for each set of values of the primary variables, a pair of specimens was tested which were identical except for the addition of transverse beams and slab to one specimen of the pair.

CHAPTER 2

SPECIMEN DESIGN AND EXPERIMENTAL SETUP

2.1 General

Twelve reinforced concrete exterior beam to column subassemblages were constructed and tested for this study. The specimens were designed to approximately represent a typical exterior beam to column connection in the upper levels of a multistory ductile moment resisting reinforced concrete space frame. The origin of the specimens is shown in Fig. 2.1. For each specimen the beam extended from the joint to the mid-span in the first bay of the frame while the column extended from the mid-height of one story to the mid-height of the next story. These mid-span and mid-height points correspond to the approximate points of contraflexure in a symmetrical frame under uniform lateral load. During an earthquake, higher mode effects and fluctuations of gravity loads due to overturning moments will cause a shift of these inflection points from the assumed locations, but the mid-points are expected to represent the mean locations.

2.2 Design of Specimens

The test specimens and appropriate cross sections are shown in Figs. 2.2 through 2.4, with the corresponding dimensions listed in Tables 2.1 and 2.2. The forces acting on an exterior beam to column connection due to lateral loads are shown in Fig. 2.5. Beams and columns for all specimens were designed in accordance with Appendix A of ACI 318-77 (17,18). Design details of shear reinforcement for specimens are discussed in Appendix B of this report.

Four primary variables were selected and their effect on the overall behavior of exterior beam to column subassemblages were studied in this investigation. These variables were: (1) the ratio of the sum of the column flexural capacities at the joint to that of the beam (called the flexural strength ratio in this report M_R), (2) the percentage of transverse reinforcement used within the joint (ρ_t), defined as:

$$\rho_t = (n)\ (A_{sh})\ /\ (b)\ (d-d') \qquad (2.1)$$

where, A_{sh} = area of transverse reinforcement in each set

b = total width of column,

$d-d'$ = distance between the centroid of tensile and compressive reinforcement in beam or beam and slab,

and n = number of sets of transverse reinforcement

TABLE 2.1

PHYSICAL DIMENSIONS OF "BARE" SPECIMENS

Designation*		Specimen Number					
		1	2	3	4	9	11
L_c	(in.)	84.0	84.0	84.0	84.0	87.0	87.0
h_c	(in.)	11.8	11.8	11.8	11.8	13.4	13.4
d_{1c}	(in.)	9.6	9.6	9.6	9.6	11.4	11.4
d_{2c}	(in.)	5.9	5.9	5.9	5.9	6.7	6.7
A_{s1c}		3#6	4#6	3#6	4#6	4#8	3#6
A_{s2c}		2#6	2#6	2#6	2#6	2#8	2#6
L_b	(in.)	60.0	60.0	60.0	60.0	42.0	42.0
h_b	(in.)	18.9	17.3	18.9	17.3	18.9	18.9
b_b	(in.)	10.2	10.2	10.2	10.2	11.8	11.8
d_{1b}	(in.)	16.9	15.4	16.9	15.4	16.9	16.9
d_{2b}	(in.)	15.0	13.4	15.0	13.4	15.0	15.0
A_{s1b}		3#7	3#7	3#7	3#7	3#7	3#7
A_{s2b}		3#6	3#6	3#6	3#6	3#7	2#6
Hoops**		2	2	3	3	2	2
ρ_t (%)		0.87	0.98	1.30	1.48	0.78	0.74

*Refer to Fig. 2.3 for definition of terms.

**Number of sets of hoops in the joint.

TABLE 2.2

PHYSICAL DIMENSIONS OF SPECIMENS WITH TRANSVERSE BEAMS AND SLAB

Designation*		Specimen Number					
		5	6	7	8	10	12
L_c	(in.)	87.0	87.0	87.0	87.0	87.0	87.0
h_c	(in.)	11.8	11.8	11.8	11.8	13.4	13.4
d_{1c}	(in.)	9.8	9.8	9.8	9.8	11.4	11.4
d_{2c}	(in.)	5.9	5.9	5.9	5.9	6.7	6.7
A_{s1c}		3#6	3#6	4#6	4#6	4#8	3#6
A_{s2c}		2#6	2#6	2#6	2#6	2#8	2#6
L_b	(in.)	42.0	42.0	42.0	42.0	42.0	42.0
h_b	(in.)	14.9	14.9	13.3	13.3	14.9	14.9
b_b	(in.)	10.2	10.2	10.2	10.2	11.8	11.8
d_{1b}	(in.)	2.0	2.0	2.0	2.0	2.0	2.0
d_{2b}	(in.)	16.9	16.9	15.4	15.4	16.9	16.9
A_{s1b}		3#6	3#6	3#6	3#6	3#7	3#7
A_{s2b}		3#6	3#6	3#6	3#6	3#7	3#7
A_{s3}		1#6,3#4	1#6,3#4	1#6,3#4	1#6,3#4	1#7,3#4	4#4
h_{tb}	(in.)	14.9	14.9	13.3	13.3	14.9	14.9
b_{tb}	(in.)	10.2	10.2	10.2	10.2	11.8	11.8
Hoops**		2	3	2	3	2	2
ρ_t (%)		0.77	1.16	0.86	1.30	0.68	0.68

*Refer to Fig. 2.4 for definition of terms.

**Number of sets of hoops in the joint.

in the joint,

(3) the inclusion of transverse beams and slab in half of the specimens, and (4) the shear stress in the joint as a multiple of $\sqrt{f_c'}$, defined as:

$$\gamma = V_j / (b)\ (h)\ \sqrt{f_c'} \qquad (2.2)$$

where, b = total width of column,

h = total depth of column,

f_c' = concrete compressive strength,

and, V_j = horizontal joint shear force (Fig. 2.5)

$= T - V_{col}$

where, T = tensile force in beam longitudinal reinforcement including strain hardening effects,

and, V_{col} = horizontal column shear force.

Values for the primary variables in the previous investigations discussed in Chapter 1 are presented in Table 2.3 and Fig. 2.6.

The transverse reinforcement provided in the joint region improves the behavior of the subassemblages in two ways. First, it provides a potential force, which has an upper limit equal to the area of the transverse reinforcement multiplied by its yield stress, to resist the shear forces in the joint. Second, it improves the confinement of the joint core, which will result in delay of the joint deterioration. The contribution of the transverse reinforcement to the confinement of the joint

TABLE 2.3

PRIMARY VALUES FROM PREVIOUS INVESTIGATIONS

Source	Ref. No.	Spec. No.	M_R	$\gamma=\frac{V_j}{bh\sqrt{f_c'}}$	$\rho_{tm}\%$
Hanson	4	1	2.20	11.2	0.91
		2	2.20	11.7	0.53
		3	2.70	11.0	0.98
		4	0.72	15.1	1.16
		5	0.50	17.9	1.18
Hanson	5	4	2.80	12.0	0.50
		5	2.93	12.1	0.74
Megget	7	1	1.33	7.0	0.76
		2	1.33	7.2	0.76
		3	1.33	6.2	0.90
Smith	8	4	1.33	8.3	1.26
Renton	10	1	0.88	15.6	1.00
		2	0.89	12.6	1.40
		3	0.88	16.2	1.80
		4	0.89	14.6	1.80
Uzumeri	13	3	2.59	8.6	0.48
		4	2.47	8.7	0.82
		6	2.26	8.7	1.60
		7	1.95	9.7	0.82
		8	1.43	11.6	1.62
Lee	14	1	4.00	7.9	1.99
		2	4.00	7.3	1.99
		3	4.00	7.4	0.45
		4	4.00	7.5	0.45
		5	3.20	8.3	1.99
		6	3.20	8.4	0.45
		7	3.20	7.6	0.45
		8	3.20	7.2	0.45

TABLE 2.3 (Cont'd)

PRIMARY VALUES FROM PREVIOUS INVESTIGATIONS

Source	Ref. No.	Spec. No.	M_R	$\gamma=\frac{V_j}{bh\sqrt{f_c'}}$	$\rho_{tm}\%$
Scribner	19	1	4.40	6.1	1.60
		2	4.20	6.1	1.60
		3	2.50	9.0	2.30
		4	2.40	9.0	2.30
		5	4.15	7.4	1.60
		6	4.00	7.4	1.60
		7	2.50	11.0	2.30
		8	2.40	10.9	2.30
		9	3.40	12.4	1.70
		10	3.24	12.3	1.70
		11	3.40	12.4	1.70
		12	3.24	12.3	1.70
Scarpas	16	1	2.03	6.5	0.90
		2	1.62	9.8	0.71
		3	2.12	6.0	0.50

core is more directly related to the number and area of the hoops and cross ties than to the yield strength of the bars provided. For the same total area of transverse reinforcement used within a joint, using a larger number of hoops will result in better confinement. However, for the same number and area of hoops, the improvement in the joint behavior is not linearly related to the yield strength of the hoop. Due to this fact, providing fewer hoops with higher yield stresses is less effective than placing a larger number of hoops with lower yield stresses in the joint. Therefore, the actual transverse reinforcement ratios used by other investigators were multiplied by $\sqrt{f_{yh}/40}$, where f_{yh} is the actual yield stress of the hoop in ksi units. These values were called the modified transverse reinforcement ratio (ρ_{tm}). The use of this modified transverse reinforcement ratio also resulted in a more realistic comparison of the values for the joint reinforcement used in other investigations with different hoop yield stresses. The value for the modified transverse reinforcement ratios from other investigations were examined and, based on the location of existing gaps in their data, these values were separated into four groups. The selected modified transverse reinforcement ratio ranges of 0.4-0.7 percent, 0.7-1.0 percent, 1.0-1.7 percent, and greater than 1.7

percent are plotted in Fig. 2.6 with a different symbol for each range. Figure 2.6 clearly demonstrated the area of needed further investi-gation. Selected design values for the primary variables in this study are listed in Table 2.4 and shown with solid symbols in Fig. 2.7.

Most building codes recognize the advantages of providing stronger columns than beams at any connection. However, the minimum code requirements will normally be satisfied by providing a flexural strength ratio slightly greater than 1. Further reevaluation of this minimum value was needed. Therefore, the test specimens were designed to have flexural strength ratios between 1.1 and 2.0.

Because the present ACI Recommendations (12) for design of beam to column joints in monolithic reinforced concrete structures give very little credit for the strength of the concrete in a connection, a large number of hoops are required within the joint region. It was believed that lowering of the amount of the transverse reinforcement in the joint to a certain limit, would not significantly change the behavior of the connection. Except for specimen 4, all specimens had less transverse reinforcement in the joint than that required by the ACI Recommendations. All specimens were constructed with either two or three layers of transverse reinforcement.

TABLE 2.4

SELECTED DESIGN VALUES FOR THE PRIMARY VARIABLES

Specimen Number	M_R	$\gamma = \frac{V_j}{bh\sqrt{f_c'}}$	ρ_{tm} %	Trans. Beams and Slab
1	1.1	14	1.0	No
2	1.5	14	1.0	No
3	1.1	14	1.5	No
4	1.5	14	1.5	No
5	1.1	14	1.0	Yes
6	1.1	14	1.5	Yes
7	1.5	14	1.0	Yes
8	1.5	14	1.5	Yes
9	2.0	14	1.0	No
10	2.0	14	1.0	Yes
11	1.5	10	1.0	No
12	1.5	10	1.0	Yes

As shown in Fig. 2.8, each layer consisted of a square hoop enclosing all column longitudinal bars, plus a diamond shaped tie enclosing only the intermediate longitudinal column bars. Due to changes in the dimension of the joints, the two or three layers of transverse reinforcement led to values for the percentage of transverse reinforcement spread over a range from 0.9 percent to 1.9 percent.

Previous investigations (4,5,6,15) have demonstrated that the addition of unloaded spandrel beams will improve the confinement of the joint, thus leading to better behavior of the subassemblage. However, there was no information on the effect of the presence of the slab on the performance of the subassemblage. For this reason, the specimens were designed in pairs. For each "bare" specimen, another specimen was designed with transverse beams and a slab, keeping all other primary variables constant. The transverse beams were designed with sufficient flexural and shear reinforcement to carry the torsion caused by the loading of the main beam. The slab was designed as a two way slab with the flexural steel in the transverse direction equal to approximately half of that in the main direction of loading.

The present ACI Recommendations limit the allowable shear stress in the joint to $20\sqrt{f_c'}$ (psi units).

However, recent investigations at the University of Texas (15) suggest a reduction in this limit. In order to study the effect of the level of the shear stress in the joint on the overall behavior of the subassemblage, two shear stress levels were considered. In specimens 1 through 10 the design joint shear stress was $14\sqrt{f_c'}$, while for specimens 11 and 12 this value was reduced to $10\sqrt{f_c'}$.

A complete discussion of specific design procedures for a "bare" specimen and a specimen with transverse beams and slab are given in Appendix A.

2.3 Material Properties

Concrete for the specimens was either obtained commercially from a concrete plant or mixed in the laboratory. Average concrete compressive strengths are given in Table 2.5. Complete results of the concrete cylinder tests are presented in Appendix C. The concrete mixes were designed to give a 28 day compressive strength of 4000 psi.

Average steel yield and ultimate stresses are listed in Table 2.6, with a more detailed description appearing in Appendix C. Grade 60 steel was used for column longitudinal reinforcing bars and the transverse reinforcement within the joint. Longitudinal reinforcement used in the

TABLE 2.5

SUMMARY OF CONCRETE CYLINDER TESTS

Specimen Number	Part of Specimen	Average Test Day f_c' (psi)
1	Entire	4870
2	Entire	5070
3	Entire	5930
4	Entire	6470
5	Lower Column	4240
	Beams, Slab	6180
	Upper Column	4390
6	Lower Column	3940
	Beams, Slab	5730
	Upper Column	3910
7	Lower Column	3950
	Beams, Slab	4200
	Upper Column	3930
8	Lower Column	3760
	Joint, Transv. Beams	4260
	Main Beam, Slab	4680
	Upper Column	3900
9	Entire	3530
10	Lower Column	3490
	Beams, Slab, Upper Column	3470
11	Entire	5770
12	Lower Column	3630
	Beams, Slab, Upper Column	5090

TABLE 2.6

SUMMARY OF REINFORCING STEEL PROPERTIES

Bar Size	Grade	σ_y	ε_y	ε_{sh}	E_{sh}
#3	40	48.8	1.70	12.5	0.98
#4	40	51.0	1.79	13.1	1.05
#4	60	63.4	2.18	4.9	1.35
#6	40	50.0	1.79	12.8	1.04
#6	60	71.0	2.46	4.8	1.42
#7	40	48.0	1.69	11.2	0.97
#8	60	60.0	2.05	5.1	1.63

All stresses are expressed in units of (ksi)x10^3.
All strains are expressed in units of (in/in)x10^{-3}.

beams and slabs, and the stirrups used in the columns and the beams, were Grade 40 steel.

2.4 Construction of Specimens

Specimens were constructed by graduate student assistants. Six sets of reusable plywood forms were constructed. The forms were sealed and their interior surface was oiled prior to casting.

A manually operated bar bending device was used to bend the reinforcing bars in accordance with the specifications of the ACI Building Code (17). Stirrups were bent as full rectangles with two legs overlapping and the overlap was welded. Electrical resistance strain gages were bonded to the appropriate locations of the reinforcing bars, following the procedure described in Appendix E. The longitudinal reinforcing bars were supported at their ends with a plywood template to make sure the proper spacing was maintained while stirrups were tied to them, using annealed tie wire.

Specimens without a slab were cast flat on the floor. Reinforcing cages were first placed inside the oiled forms, and then concrete was mixed and delivered in a ready mix truck. After placing the concrete in the form, the concrete was consolidated with a hand held electric vibrator. A minimum of two specimens were cast

on the same day and an average of six concrete cylinders were cast and cured next to each specimen. Half of the cylinders were tested after 28 days and the remaining half were tested on the day the specimen was tested.

Specimens with transverse beams and slab were cast vertically. First, the lower half of the column was cast with concrete mixed in the laboratory (Fig. 2.2(b)). During the next working day, the reinforcing bars for the beams and slab were placed and on the following day concrete for the beams and slab was delivered in a ready mix truck. One day later, the upper half of the column was cast using concrete which was hand mixed in the laboratory. Several concrete cylinders from mixes used for different portions of the specimen were cast and cured next to the specimen. Specimens and the cylinders were moist cured for one week, after which the forms were removed and the specimens and cylinders were cured uncovered until they were tested. A complete description of the construction of the specimens is presented in Appendix D.

2.5 Testing Frames

Two different testing frames were used for testing of the specimens. Testing frame number 1 was used for specimens 1 through 4, and testing frame number 2 was

used for specimens 5 through 12.

Testing frame number 1 (Fig. 2.9), consisted of a steel frame resting on the laboratory floor. The specimens were placed in the frame with the column resting horizontally while the beam was in a vertical position. Each end of the column was tied down to the base beams of the testing frame using four 1¼ in. diameter threaded rods. The rods were pretensioned to stresses near their yield stress to prevent any motion of the specimen relative to its supports during the test. Roller bearings were used to allow rotation of the column at these end supports. The column axial load was then applied through a hydraulic jack.

A steel pipe was cast in the beam at the intended load point. The smooth inner surface of the embedded pipe was oiled before inserting a snug fitting 2 in. diameter solid rod. The hydraulic actuator was secured to the ends of this pin using a specially constructed yoke made out of 1¼ in. thick steel plates. This arrangement provided essentially a moment free connection between the actuator and the beam. Shear forces were applied at the end of the beam through a 50 kip capacity hydraulic actuator.

For testing frame number 2, a smaller 4-hinge frame was added to the support frame of the testing frame

number 1, as shown in Fig. 2.10. The lower beam of the 4-hinge frame was bolted to the base beams of the support frame. Pin ended columns supported the top beam of the 4-hinge frame, which was free to move horizontally in the plane of the frame.

The specimen was placed in the frame with the column portion of the specimen remaining in a vertical position. Two steel base plates with cylindrical surfaces on one side were used at the top and the bottom of the column to allow rotation of the ends of the column. Roller bearings were placed between the column and the brackets to represent points of contraflexure in the column. Using four 1¼ in. threaded rods, the top and the bottom of the column were tied to brackets which were bolted to the beams of the 4-hinge frame.

A specially constructed force link was used to support the free end of the beam during the test. The main section of the force link was a structural steel tube (TS 5x3x¼). One end of the force link was bolted to the lower beam of the 4-hinge frame and the other end was connected to a solid steel pin which was inserted in the embedded pipe at the load point for the beam portion of the specimen. This setup provided an essentially moment free connection at the end of the beam. For specimens with transverse beams and slab, stiffeners were

used at the free end of the slab. As shown in Fig. 2.11, these stiffeners consisted of steel channels bolted together and sandwiching the slab between them.

After the specimen was tied down in place, the column axial load was applied through a hydraulic jack and shear forces were applied to the top of the upper column half using a 250 kip capacity hydraulic actuator. Testing frame number 2 had the advantage of including the P-Δ effect from the column axial load. The testing equipment is described in more detail in Appendix F.

2.6 Data Acquisition

Four data gathering systems were used in this study: (1) a load cell and displacement transducer attached to the hydraulic actuator, (2) electrical resistance strain gages bonded to the reinforcing bars, (3) photographic record of the damage to the specimens, and (4) displacement transducers attached over the joint region of the bare specimens.

A continuous plot of the applied load vs. the specimen displacement at the point of the application of the load was recorded for each specimen using an X-Y plotter. The plots were used to determine the yield displacement as well as to access the overall integrity of the specimen throughout the test.

Electrical resistance strain gages were bonded to the reinforcing bars at the critical sections of the specimens. The gages were applied according to the procedure described in Appendix E. The number of strain gages used in each specimen ranged between twenty four and thirty. Typical location of strain gages for bare and slab specimens are shown in Figs. 2.12 and 2.13 respectively. During each cycle of testing, loading was momentarily stopped at several points while all strain gages were read through an electrical scanning device. The gage readings were automatically punched on a paper tape and typed by a teletype recorder.

Formation of the cracks on the specimens were marked with felt tipped pen using two different colors to distinguish between the two directions of the loading. During each cycle of loading, the loading was discontinued briefly while black and white photographs and color slides of the specimen were shot.

On bare specimens, two Linear Variable Displacement Transducers (LVDTs) were positioned on the lateral face of the specimen. As shown in Fig. 2.14, the LVDTs spanned across the joint, connecting the diagonally opposite corners. Measurements from the LVDTs were recorded automatically at the same time the strain gage readings were recorded. These measurements were used to

determine shear deformations of the joint. Detailed descriptions of the data acquisition equipment are covered in Appendix F.

2.7 Loading Sequence

For all of the tests, the loading was controlled by the displacement of the specimen at the point of load application. The displacement controlled loading history used for specimens 1 through 6 is shown in Fig. 2.15. This loading schedule discloses information on both the strength as well as the stiffness degradation of the specimen. By increasing the maximum displacement for each cycle of loading, the ratio of the load sustained by the specimen in the present cycle vs. the load carried in the previous cycle can be studied. Two different possibilities may occur as shown with dashed lines in Fig. 2.16. Possibility 1 indicates a loss of stiffness only, whereas possibility 2 indicates a loss of both stiffness and strength.

Most building codes have an upper limit for story drift to satisfy the overall stability of the structure and to avoid high overturning moments due to the P-Δ effect. Although the applied displacements in the latter cycles of the proposed loading history may violate this provision of the codes, the use of such a loading history

was justified in order to obtain as much information as possible about the behavior of each specimen.

Due to the large yield displacement observed for specimen 7, and in an effort to subject the specimens to sufficient number of cycles within the limited displacement capacities of the testing frame, the modified loading history shown in Fig. 2.17 was used for speci-mens 7 through 12.

CHAPTER 3

TEST RESULTS

3.1 General Behavior

The overall behavior of each specimen will be analyzed using the following sources of information: (1) plots of applied load vs. specimen displacement at the point of application of the load, (2) cracking patterns for the specimens, (3) strain data from the gages bonded to the reinforcing bars, and (4) data from Linear Variable Differential Transducers (LVDTs) attached over the joint region of the bare specimens. The contribution of each of the above sources to the behavior of the specimens will be covered in this section.

3.1.1 Plots of Load vs. Displacement

Plots of load vs. displacement are one of the most important and perhaps the most easily interpreted source of information available for each specimen. For specimens 1 through 4, the applied shear load to the end of the beam vs. the beam load point deflections were directly recorded and will be presented here. For

specimens 5 through 12, the applied shear to the top column half vs. the displacement at the load point were directly recorded. This latter system of recording load vs. deflection had the advantage of including the P-Δ effect for the subassembly. The P-Δ effect became more significant in the latter cycles of loading. Load vs. displacement curves for specimens 1 through 12 are shown in Figs. 3.1(a) through 3.1(l) respectively. When comparing the two types of hysteresis diagrams for the "bare" specimens, for example, specimen 2 and specimen 9 in Figs. 3.1(b) and 3.1(i) respectively, it can be seen that both types of diagrams demonstrated the general behavior of the subassemblage and that there was no distinct difference in the characteristics of the specimens represented by either type of plot.

As explained in Section 2.7, the loading sequence was selected such that the load vs. displacement curves would indicate the loss of stiffness as well as the change in the load carrying capacity of the specimen in subsequent cycles.

The maximum applied shear to the specimen at each cycle of loading was compared with the maximum applied shear in the first cycle, and the ratios were used to compare the deterioration of the load carrying capacity for different specimens. These ratios are presented in

Table 3.1.

Loss of stiffness in subsequent cycles is shown by the "pinching" of the hysteresis loops at mid-cycle. Two distinct behaviors were observed with respect to stiffness degradation. The first observation was that the stiffness of the specimens reduced during each additional cycle of loading due to the Bauschinger effect in the reinforcing steel, concrete deterioration in and adjacent to the joint, slippage of column longitudinal reinforcement, and pull out of the beam longitudinal reinforcement. The second observation was that after the initial cycle of loading, the stiffness of the specimens was substantially lower in the mid-cycles near the zero displacement point. This loss of stiffness near the zero displacement point is primarily due to unclosed beam flexural cracks near the face of the column. At these cracks the shear stiffness of the beam which is dependent on the doweling action of the beam longitudinal reinforcement is very low. In addition, after the first cycle of loading, the concrete near the load points deteriorated slightly. This deterioration resulted in looser connections between the specimen and the testing frame. The testing setup was such that any looseness between the testing frame and the specimen would be noticed more near the zero load point, when the specimen

TABLE 3.1

CYCLIC LOAD CARRYING CAPACITY OF THE SPECIMENS

Specimen Number	Ratio of the Maximum Load at Each Cycle to that of the First Cycle*					
	Load Cycle Number					
	1	2	3	4	5	6
1	1.00	0.89	0.75	0.65	0.57	—
2	1.00	0.91	0.83	0.74	0.63	0.54
3	1.00	0.95	0.84	0.73	0.60	0.49
4	1.00	1.01	1.04	1.04	0.93	0.80
5	1.00	1.12	1.22	1.18	1.10	1.00
6	1.00	1.11	1.17	1.19	1.11	1.11
7	1.00	1.02	1.02	1.02	0.96	0.91
8	1.00	**	**	**	**	**
9	1.00	0.98	0.95	0.87	0.81	0.74
10	1.00	**	**	**	**	**
11	1.00	1.02	1.02	1.05	1.02	0.95
12	1.00	1.06	1.08	1.07	1.06	1.01

*For bare specimens, the average load for the positive and negative cycles was recorded. For specimens with transverse beams and slab, the load for the positive half cycle was recorded.

**Due to the premature failure of specimens 8 and 10, no values are reported for these two specimens.

was not bearing against the loading brackets. Although minor, this phenomenon caused an additional "apparent" pinching of the load vs. displacement hysteresis loops near the zero load point.

In all slab specimens, there was a noticable unequal pinching of the hysteresis loops in the two directions of loading. As shown in Fig. 2.4 and Table 2.2, for specimens with a slab the total area of top reinforcing steel in the beam and slab, $(A_{s2b}+A_{s3})$, is considerably larger than the bottom reinforcing steel area of the beam, (A_{s1b}). Figure 3.2 illustrates the opening and closing of flexural cracks in the beam and slab for both directions of loading. The reinforcing steel in the top of the beam and slab will yield in tension during the first half-cycle of loading and flexural cracks will form at the slab level and propagate into the beam. When unloading and then reloading the specimen in the opposite direction, these cracks will partially close. However, since the bottom beam bars have a smaller area than that of the top beam bars plus the slab bars, the tensile force generated by the bottom beam bars is not large enough to cause a compression yielding of the top bars. As a result of this, the flexural cracks previously formed at the slab level will not close. In addition, as demonstrated in Fig. 3.2, these cracks will join the

newly formed flexural cracks which started at the bottom of the beam. Because of this extended crack, during the negative half-cycle of loading the contribution of the concrete compressive force to balancing of the tensile forces at that section becomes insignificant. Since the concrete is ineffective at this section, the shear stiffness of the subassemblage depends totally on the dowel action between the reinforcing bars. This phenomenon causes a noticable reduction in the stiffness of the specimen.

For comparison purposes, the stiffness of the specimens at each half-cycle was defined as the slope of a line which was tangent to the load vs. deflection curve and passed through the zero displacement crossing point of that half-cycle. Figure 3.3 shows the lines defining stiffnesses for the first three cycles of specimen 3. Because the bare specimens were subjected to equal displacements in both directions of loading, the stiffness was calculated as the average of the positive and negative half-cycle stiffnesses. For the specimens with a slab, stiffnesses of only the positive half-cycles were recorded. In Table 3.2, for each specimen, the stiffness in subsequent cycles is shown as a percentage of the stiffness of the first cycle of loading.

TABLE 3.2

CYCLIC STIFFNESS OF THE SPECIMENS

Specimen Number	Ratio of the Stiffness at Each Cycle to that of the First Cycle					
	Load Cycle Number					
	1	2	3	4	5	6
1	1.00	0.50	0.29	0.21	0.15	—
2	1.00	0.49	0.34	0.26	0.18	0.13
3	1.00	0.46	0.32	0.21	0.15	0.11
4	1.00	0.48	0.40	0.32	0.24	0.17
5	1.00	0.56	0.50	0.38	0.30	0.23
6	1.00	0.62	0.50	0.39	0.31	0.25
7	1.00	0.51	0.41	0.35	0.29	0.24
8	1.00	*	*	*	*	*
9	1.00	0.50	0.38	0.28	0.23	0.18
10	1.00	0.82	0.68	—	—	—
11	1.00	0.51	0.43	0.36	0.31	0.24
12	1.00	0.48	0.40	0.32	0.27	0.22

*Due to the premature failure of specimen 8, no values are reported for this specimen.

3.1.2 Crack Pattern

In order to simplify the reference to the specimens for location of cracks, the different sides of the specimens for the two testing frames are illustrated in Fig. 3.4.

Diagonal cracks were formed on the lateral faces of the joint region of the bare specimens during the first cycle of loading. Fig. 3.5 shows the general crack pattern at the joint of a specimen without a slab. The crack pattern consisted of two major diagonal cracks connecting the opposite corners of the joint and other smaller cracks parallel to the major cracks. In all specimens, concrete cover at the joint was completely cracked by the end of the test. Cracks were also observed on the back face of the column at the joint level. In the case of specimens 1 through 3, the cracks were so extensive that by the end of the test the cover concrete on the back of the column had spalled off. Figure 3.6 shows specimen 3 at the conclusion of the test.

In all bare specimens, there was a noticeable region of plastic hinging in the beam near the joint. Flexural cracks formed at the top and the bottom of the beam near the joint during the first cycle of loading. In subsequent cycles of loading, the length of these cracks

increased and new cracks formed in the beam further away from the joint. By the end of the test, flexural cracks had spread into the beam for a distance of 1.5 to 2 times the depth of the beam.

In the bare specimens, a few flexural cracks were observed on both the front and the back face of the column. The cracks spread over a distance of 1 to 1.5 times the depth of the column in both directions away from the joint.

In specimens with transverse beams and slab, a few flexural cracks formed on the front and the back face of the column. These cracks spread for a distance equal to the depth of the column away from the joint. In all specimens with a slab, the width of the transverse beams were always smaller than the width of the column. Generally, spalling cracks were observed along the line where the back face of the transverse beams joined the lateral face of the column. As shown in Fig. 3.7, these cracks extended vertically upward near the back face of the column for a distance equal to the column width from the joint. However, at the conclusion of the tests for specimens with a slab, the concrete cover on the back face of the joint always remained in place and attached to the specimen.

For specimens with a slab, wide cracks formed across

the slab parallel to the front face of the column (Fig. 3.8), indicating yielding of the slab longitudinal reinforcement. The crack pattern shown in Fig. 3.8 was typical for all slab specimens tested. Flexural cracks were also observed in the main beam of the slab specimens. With increased cycles of loading, these cracks spread over a region of the beam equal to 1.5 to 2 times the depth of the beam from the joint.

In specimens with transverse beams and slab, loading of the main beam and slab caused torsional forces in the transverse beams. All specimens experienced the same general crack pattern in the transverse beams as shown in Fig. 3.9. A few short inclined cracks started at the back face of the transverse beams and terminated at the joint in the back face of the column. There was always one major spiral torsional crack which started at the back face of the transverse beam and, after crossing a small surface of the slab on top of the transverse beam, continued into the lateral face of the column. The torsion related cracking of the concrete in the upper half column at the slab level reduced the load carying capacity of the upper column half. None of the specimens tested cracked on the front side of the transverse beams, and only half of the slab specimens showed minor cracks on the bottom face of the transverse beams.

3.1.3 Strain Gage Data

Data from the strain gages was important in confirming the conclusions based on other data as well as in revealing certain phenomenon such as slippage of the column bars through the joint, which could not have been detected otherwise.

In testing each specimen, the yield displacement was determined during the test by observing a flattening of the load vs. displacement curve generated on the X-Y plotter. Data from strain gages bonded to the main beam reinforcement at the front face of the column was essential in verifying this observation. A typical example is shown in Fig. 3.10, where yielding of one of the beam longitudinal bars at the front face of the column in specimen 11 between load points number 7 and 8 of Fig. 3.1(k) is confirmed.

For specimens with a slab, wide flexural cracks were noted on the top surface of the slab perpendicular to the direction of the main beam, indicating yielding of the slab longitudinal reinforcement. This observation was later confirmed by the data from strain gages bonded on the slab longitudinal reinforcing bars along the front face of the column. As illustrated in Fig. 3.11 for specimen number 12, the second longitudinal reinforcing bar in the slab away from the main beam yielded during

the second cycle of loading, between load points number 26 and 27 of Fig. 3.1(1).

The measured strains from the transverse reinforcement in the joint helped in determining the load point corresponding to formation of the first crack in the joint. As shown in Fig. 3.12, the first diagonal crack in the joint of specimen 9 was observed between load points number 5 and 6 of Fig. 3.1(i), causing a sudden increase in the strains carried by the joint reinforcement crossed by the crack.

Slippage of column longitudinal reinforcement through the joint was thought to be a major contributing factor to the loss of stiffness of the subassembly and the pinching of the load vs. displacement hysteresis loops. Data from strain gages verified the slippage of some of the column bars. Figure 3.13 illustrates the mechanism of the column bar slippage through the joint. During a positive half-cycle of loading, the column longitudinal reinforcement located near the front face of the column is subjected to tension at the top and compression at the bottom. Integrity of the concrete in the joint is essential in providing adequate bond between the concrete and the reinforcing bar to allow the development of the high stress gradient existing between points A and B of Fig. 3.13. As illustrated in Fig.

3.14, the strain gage located at point A of Fig. 3.13 should measure compressive strains during the positive half-cycles of loading. However, with an increase in the applied load, starting with load point number 5 of Fig. 3.1(i), the measured compressive strains at gage A start to reduce and move towards tensile strains. If slippage of this bar had not occurred, the gage would have recorded larger compressive strains along the path illustrated with a dashed line in Fig. 3.14. It is important to note that as discussed in the previous paragraph, at the same load point number 5 of Fig. 3.1(i), the first diagonal crack was observed in the joint of specimen 9. This observation indicates the significance of the formation of this diagonal crack on the slippage of the column longitudinal reinforcement through the joint.

In all specimens tested, there was a clear indication of slippage of the column bars on the front face of the column. However, only half of the specimens showed slippage of the column longitudinal bars in the back face of the column.

3.1.4 LVDT Data

In specimens without transverse beams and slab, two Linear Variable Differential Transducers (LVDTs) were

mounted on the lateral face of the specimen spanning between diagonally opposite corners of the joint (Fig. 2.14). The measured elongation or shortening of the LVDTs were used to calculate the joint shear deformation. Detailed calculation of the joint shear deformation from the LVDT data is presented in Section 4.3. Due to faulty equipment, the results in only three cases, for specimens 2, 3, and 4, were satisfactory. Plots of the applied load vs. the joint shear deformation for specimens 2, 3, and 4 are shown in Figs. 3.15, 3.16, and 3.17 respectively.

In order to compare the joint shear deformation of different specimens, the maximum load point displacement at the end of each positive half cycle of loading is plotted vs. the corresponding joint shear deformation in Fig. 3.18 Comparing the results for specimens 3 and 4 it is evident that an increase in the flexural strength ratio reduced the joint shear deformation. Results from specimens 2 and 4 indicate that an increase in the transverse reinforcement ratio also reduced the shear deformation of the joint.

3.1.5 Adjusted Values for Primary Variables

Due to unavoidable limitations in the geometry of the specimens and the properties of the construction

materials, the values of the primary variables for the specimens tested were not exactly the same as the proposed design values listed in Table 2.4. The actual tested values for the primary variables are listed in Table 3.3 and presented graphically with solid symbols in Fig. 3.19.

For bare specimens, the design and actual flexural strength ratios were in good agreement. However, for the slab specimens the differences were much larger. In designing the slab specimens, it was assumed that when the slab is in tension, only the first two slab longitudinal reinforcing bars on each side of the main beam will be effective. In testing of the slab specimens, it was noted that all slab longitudinal reinforcing bars yielded in tension, resulting in higher flexural strength for the beam and slab and a lower flexural strength ratio for the subassemblage. The values of the flexural strength ratios for the specimens calculated with the slab partially and fully effective are presented in Table 3.4.

The design values for the transverse reinforcement ratio were 1.0 and 1.5 percent. Obtaining these exact values was not practical because of the limitations on the number of sets of hoops to be used in the joint and the changes in the joint dimensions among specimens. For

TABLE 3.3

ACTUAL VALUES FOR THE PRIMARY VARIABLES

Specimen Number	M_R*	$\gamma = \frac{V_j}{bh\sqrt{f_c'}}$**	ρ_{tm} %	Trans. Beams and Slab
1	1.01	14.20	1.10	No
2	1.35	14.20	1.23	No
3	1.07	12.84	1.64	No
4	1.41	12.53	1.86	No
5	0.89	10.88	0.97	Yes
6	0.87	11.31	1.46	Yes
7	1.17	13.53	1.08	Yes
8	1.16	13.43	1.64	Yes
9	1.93	15.17	0.98	No
10	1.58	14.39	0.86	Yes
11	1.56	8.79	0.93	No
12	1.17	9.06	0.86	Yes

*Assuming that all slab longitudinal reinforcement is effective in tension.

**Assuming that two slab longitudinal reinforcing bars on each side of the main beam contribute to the shear force in the joint.

TABLE 3.4

FLEXURAL CAPACITIES OF THE SPECIMENS

Specimen Number	P (kips)	M_{col} at P* (k-in)	Beam or Slab Moment (k-in)		M_R**
			Yield**	Ultimate**	
1	40	1149	1963	2283	1.01
2	50	1387	1747	2058	1.35
3	50	1238	1989	2322	1.07
4	50	1478	1776	2101	1.41
5	50	1164, 1175	2508 (1938)	2640 (2064)	0.89 (1.13)
6	50	1139, 1136	2450 (1940)	2623 (2050)	0.87 (1.11)
7	50	1358, 1357	2216 (1720)	2313 (1798)	1.17 (1.51)
8	50	1343, 1354	2227 (1724)	2321 (1806)	1.16 (1.49)
9	80	2399	2127	2490	1.93
10	80	2394, 2392	2888 (2383)	3037 (2485)	1.58 (1.93)
11	68	1614	1789	2071	1.56
12	68	1450, 1572	2456 (1905)	2586 (2016)	1.17 (1.50)

*For specimens with slab, the flexural capacity of the lower column half is given first, followed by that for the upper column half.

**Figures in parenthesis are based on the assumption that only the first two slab longitudinal reinforcing bars on each side of the main beam are effective.

all specimens, either two or three sets of hoops were placed in the joint. The two or three sets of hoops led to values of ρ_{tm} spread over a range from 0.9 to 1.9 percent.

The design and actual values for the shear stress levels within the joint were in reasonable agreement. The joint shear stresses were normalized with respect to $\sqrt{f_c'}$, where f_c' is the concrete compressive strength in units of psi. Due to the variations of the actual concrete compressive strength of the specimens from the assumed value of 4000 psi, there were some differences between the design and actual values.

3.1.6 Individual Specimen Behavior

The primary variables for all specimens are listed in Table 3.3. In order to aid the discussion of behavior for each specimen, the flexural strength ratio (M_R), the modified percentage of the transverse reinforcement (ρ_{tm}), the shear stress level in the joint as a multiple of $\sqrt{f_c'}$ (γ), and the inclusion of the transverse beams and slab will be repeated.

Specimen 1 (M_R=1.01, ρ_{tm}=1.1%, γ=14.20, Without Slab)

At the beginning of the test, the beam was accidentally subjected to a displacement approximately

equal to the yield displacement. This was followed by another positive half-cycle of loading to a displacement of 1.8 inches. As shown in Fig. 3.1(a), the specimen was then displaced to the negative yield displacement in accordance with the predetermined loading sequence.

The joint of this specimen was extensively cracked at the conclusion of the first cycle of loading, as shown in Fig. 3.20. By the end of the second cycle of loading, the main diagonal cracks at the joint were visually estimated to be at least 1/8 in. wide. At this point, the joint cover concrete also started to spall off. A few flexural cracks were observed in the column over a distance one column depth away from the joint. All of the flexural cracking in the beam was also in a region of length one beam depth away from the joint. However, as shown in Fig. 3.21, the majority of the damage by the end of test was concentrated in the joint. As shown in Fig. 3.1(a), the load carrying capacity of this specimen was reduced substantially after the first cycle of loading, accompanied by a severe pinching of the hysteresis loops from the second cycle on.

Data from strain gages indicated that during the first cycle of loading the beam longitudinal reinforcement was partially pulled out of the joint and the column longitudinal reinforcement on both the front

and the back face of the column slipped through the joint.

Specimen 2 (M_R=1.35, ρ_{tm}=1.23%, γ=14.20, Without Slab)

The only change between specimen 1 and 2 was the higher flexural strength ratio for specimen 2. The increase in the flexural strength ratio somewhat improved the behavior of specimen 2 compared to specimen 1. At the end of the first cycle of loading there were a few cracks at the joint and the flexural cracks in the beam were spread over a distance of approximately 1.5 times the beam depth from the front face of the column, as shown in Fig. 3.22. A few flexural cracks were also observed in the column over a distance of one column depth away from the joint. At the peak of the second negative half-cycle, a major diagonal crack was formed through the joint and extended through the intersection of the bottom of the beam and the front face of the column (Fig. 3.23). In subsequent cycles the width of this crack increased to as much as 1/4 in. and most of the energy was dissipated in the damaged joint. At the conclusion of the test, the cover concrete had spalled off the lateral sides and the back face of the joint and the concrete in the core of the joint was loose. Figure 3.24 shows specimen 2 at the end of the test, after most

of the loose cover concrete was removed from the joint region.

As shown in Fig. 3.1(b), specimen 2 also experienced a loss of load carrying capacity with sever pinching of the load vs. displacement hysteresis loops starting from the third cycle of loading.

Data from strain gages verified pull out of the beam longitudinal reinforcement from the joint. The column longitudinal reinforcement also slipped through the joint, but the slippage was less severe than that observed for specimen 1.

Specimen 3 (M_R=1.07, ρ_{tm}=1.64%, γ=12.84, Without Slab)

Specimen 3 was similar to specimen 1 except that the joint of this specimen was reinforced with three sets of hoops instead of the two sets used in specimen 1. During the second cycle of loading, two major cracks formed at the joint, connecting the diagonally opposite corners of the connection. The width of these cracks expanded to approximately 3/8 in. by the end of the test. Although the damage was concentrated in the joint, flexural cracking was spread over a length 1.5 times the beam depth into the beam from the joint. A few flexural cracks were also observed in the column over a distance 1.5 times the column depth from the joint.

There was a slight compression crushing of the beam concrete near the joint. Comparison of the strain gage data bonded on the beam longitudinal reinforcing bars for specimens 1 and 3 indicated that larger strains were developed in specimen 3. The above observations supported the notion that the additional hoop provided in the joint of specimen 3 improved the anchorage of the beam longitudinal bars. The concrete in the joint core at the conclusion of the test was more intact (Fig. 3.25), although the cover concrete had spalled off similar to specimens 1 and 2.

Loss of load carrying capacity and stiffness for specimen 3 was similar to that of specimen 2 with severe pinching starting from the third cycle of loading.

There was not sufficient data from the strain gages to make any judgement on the beam bar pull out for this specimen. However, the longitudinal reinforcement on both the front and the back face of the column slipped through the joint.

Specimen 4 (M_R=1.41, ρ_{tm}=1.86%, γ=12.53, Without Slab)

Specimen 4 was similar to specimen 2, but had a higher percentage of transverse reinforcement in the joint. The combined increase in the flexural strength ratio and the percentage of the transverse reinforcement

improved the behavior of this specimen significantly over specimens 1, 2 and 3.

Plastic hinging occurred in the region of the beam near the joint. Flexural cracks extended into the beam over a distance of approximately twice the beam depth from the joint. A few flexural cracks were spread over a distance 1.5 times the column width into the column away from the joint. Although the usual pattern of diagonal cracks was found at the joint, the width of these cracks remained very small and was less than 1/8 in. at the end of the third cycle of loading. Subsequent loading cycles resulted in expansion of these cracks to a width of approximately 3/16 in. at the conclusion of the test. Although the damage for this specimen was concentrated in the joint, the concrete in the core of the joint appeared to have suffered less damage than the core of specimens 1, 2, and 3. Figure 3.26 shows specimen 4 at the termination of the test.

The load carrying capacity of this specimen increased through the fourth cycle and the loss of stiffness was noticably less than that for specimens 1, 2, and 3. Severe pinching of the load vs. displacement curves started after the fouth cycle of loading, as shown in Fig. 3.1(d).

Data from strain gages indicated that the beam

longitudinal reinforcement started to pull out from the joint during the third cycle of loading. Column longitudinal reinforcement on the front face of the column slipped during the first cycle of loading. However, slippage of the column longitudinal reinforcement on the back face of the column was not recorded until the fourth cycle of loading.

Specimen 5 (M_R=0.89, ρ_{tm}=0.97%, γ=10.88, With Slab)

Specimen 5 was designed with the same design values for the primary parameters as specimen 1, except for the addition of transverse beams and slab. Flexural cracks were observed in the beam and the slab during the first cycle of loading. These cracks were spread over a distance 1.5 times the beam depth from the joint. A few flexural cracks were also detected in the column adjacent to the joint. During the second cycle of loading, torsional cracks were detected in the back of the transverse beam. At the maximum negative displacement of the second cycle of loading, a flexural crack was noticed around the periphery of the main beam, covering the lateral sides and the bottom of the beam where it was connected to the column. As described earlier in section 3.1.1, the width of this crack increased to about 1/8 in. by the end of the third cycle.

As explained in the previous section, because the flexural strength ratio for this specimen was less than 1.0, none of the slab longitudinal reinforcing bars yielded. There was a clear hinging of the upper column half just above the slab, accompanied with compression crushing of the column concrete adjacent to the joint. Hinging of the top column half is clearly seen in Fig. 3.27, which shows specimen 5 at the maximum positive displacement in the sixth cycle of loading. The joint cover concrete on the back of the specimen had spalled by the end of the test, but remained attached to the specimen.

The load carrying capacity of this specimen increased through the third cycle of loading and even after six cycles of loading, the specimen was capable of carrying the maximum load carried in the first cycle. As shown in Fig. 3.1(e), severe loss of stiffness for this specimen started from the third cycle of loading.

There was no indication of beam longitudinal reinforcement pull out from the joint of this specimen. Data from strain gages indicated that the front column longitudinal reinforcement slipped during the first cycle of loading. However, slippage of the column reinforcement on the back face was not observed until the fourth cycle of loading.

Specimen 6 (M_R=0.87, ρ_{tm}=1.46%, γ=11.31, With Slab)

This specimen was designed with the same values for the primary parameters as specimen 3, except for the inclusion of transverse beams and slab. Flexural cracks were spread over a length 1.5 times the main beam depth. The first slab longitudinal reinforcing bar away from the main beam yielded during the positive half of the third cycle of loading. In the negative half of the same cycle, a major flexural crack was observed at a distance half the beam depth away from the joint in the main beam. The main cause of this crack was as described in Section 3.1.1, except that here the crack started at a short distance half the beam depth away from the column, whereas in specimen 5, the crack was observed at the face of the connection. Due to higher strain demands in the beam longitudinal reinforcement when the slab was in compression, the width of this cracked increased to 1/8 in. during the last cycle of the test (Fig. 3.28).

There was a distinct hinging of the top column half in this specimen, causing considerable crushing of the concrete on the back of the specimen just above the joint, as shown in Fig. 3.29.

As shown in Fig. 3.1(f), the load carrying capacity of this specimen increased through the fourth cycle of loading, and the subassemblage was capable of carrying

more load at the last cycle than it carried in the first cycle of loading. Stiffness deterioration for specimen 6 was very similar to that for specimen 5.

Data from strain gages indicated that there was no pull out of the beam longitudinal reinforcement for this specimen. The column longitudinal reinforcement did not slip through the joint before the fourth cycle of loading, and because of strain gage failure, there was no information on column bar slippage beyond that fourth cycle.

Specimen 7 (M_R=1.17, ρ_{tm}=1.08%, γ=13.53, With Slab)

Values for the primary design parameters for this specimen were the same as those for specimen 2 except for the addition of transverse beams and slab. During the casting of this specimen, the concrete was not vibrated adequately, causing honeycombing in the back of the joint and on the four sides of the lower portion of the upper column half. The voids were patched with a cement and sand mortar after the removal of the forms from the specimen. The honeycombing and subsequent repair had no apparent effect on the behavior of this specimen.

Flexural cracking of the slab started during the first cycle of loading. The cracks, which crossed the entire width of the slab, spread into the slab over a

distance twice the depth of the beam away from the face of the column. A few flexural cracks were also detected in the column near the joint. Because the flexural strength ratio for this specimen was greater than 1.0, the slab longitudinal reinforcement yielded during the first positive half-cycle of loading.

The slab longitudinal bars were always bent and hooked behind the top longitudinal bar of the transverse beam closest to the back face of the specimen. At the end of the third cycle of loading for this specimen, the bent end of one of these bars was pushed out of the back of the specimen. There was no obvious hinging of the column in this specimen and a slight compression crushing of the concrete was detected at the bottom of the beam adjacent to the joint.

When testing this specimen, no clear yield displacement was observed. As a result of this, the specimen was loaded to a displacement of approximately 2.4 in. during the first cycle of loading. This displacement was noted as the observed yield displacement. However, data from the strain gages after the completion of the test indicated that the actual yield displacement for this specimen was approximately 1.2 in. Due to the large magnitude of the observed yield displacement, it was decided to terminate the first cycle

of loading at the observed yield displacement and increase the maximum displacement for each subsequent cycle by $0.25\Delta_y$, in order to fit enough cycles of loading within the maximum displacement capacity of the hydraulic actuator.

As shown in Fig. 3.1(g), the load carrying capacity of this specimen remained fairly constant throughout the test. Severe pinching of the load vs. displacement hysteresis loops started during the second cycle of loading.

There was no pull out of the beam longitudinal reinforcement from the joint of this specimen. Only a slight slippage of the column longitudinal reinforcement was observed after the fifth cycle of loading.

Specimen 8 (M_R=1.16, ρ_{tm}=1.64, γ=13.43, With Slab)

Specimen 8 was designed with the same values for the primary variables as specimen 4, except for the addition of transverse beams and slab. Flexural cracking of the beam and slab started during the first cycle of loading and spread over a distance 1.5 times the depth of the beam. A few flexural cracks were also observed in the column over a distance of column depth above and below the joint. Because the flexural strength ratio for this specimen was greater than 1.0, the longitudinal

reinforcement in the slab yielded during the first positive half-cycle of loading. There were only two short cracks detected on the transverse beams at the conclusion of the first cycle of loading. Figure 3.30 shows specimen 8 at the end of the first cycle of loading.

During the second cycle of loading and prior to reaching the maximum displacement for this cycle, due to improper detailing of the slab longitudinal reinforcement, the subassemblage failed prematurely at the beam support point. Although the specimen was subjected to three more cycles of loading, almost all of the damage was concentrated at the point of the failure near the end of the beam. The damage in the specimen at the end of the fourth cycle of loading is shown in Fig. 3.31.

Inspection of the specimen at the conclusion of the test revealed that, during the construction of this specimen, the slab longitudinal reinforcement which was to be located above the web of the beam, was accidentally pushed down into the beam (Fig. 3.32). As a result of this, a plane of weakness was created at the bottom level of the slab near the end of the beam, causing the beam and the longitudinal reinforcing bars to separate completely from the slab, as shown in Fig. 3.33.

Due to premature failure of the specimen, no conclusive evidence of beam bar pull out or column bar slippage was observed.

Specimen 9 (M_R=1.93, ρ_{tm}=0.98% , γ=15.17 , Without Slab)

Except for a higher flexural strength ratio, all other design parameters for specimen 9 were the same as specimens 1 and 2. During the first cycle of loading, due to the high flexural strength ratio, flexural cracks were spread in the beam over a distance twice the depth of the beam from the joint. Two major diagonal cracks and several smaller cracks were also observed in the joint on the lateral face respectively. There was no significant flexural cracking of the column.

By the end of the third cycle of loading, the number of diagonal cracks at the joint had increased significantly, as shown in Fig. 3.34. Figure 3.35 shows specimen 9 at the conclusion of the test after some of the loose concrete was removed from the back of the column.

The load carrying capacity of this specimen reduced continuously after the first cycle of loading, but the pinching of the load vs. displacement hysteresis loops was not severe until the fourth loading cycle (Fig. 3.1(i)).

Strain gage data indicated that the beam longitudinal reinforcement for this specimen pulled out from the joint during both positive and negative cycles of loading. One of the column longitudinal reinforcing bars on the front face of the specimen slipped through the joint during the first cycle of loading. Due to strain gage failure, no conclusions were drawn with respect to the slippage of the bars on the back face of the column.

Specimen 10 (M_R=1.58, ρ_{tm}=0.86%, γ=14.39, With Slab)

The only change between the design parameters for specimens 10 and 9 was the presence of transverse beams and a slab in specimen 10. Before the testing of this specimen started, while the specimen was in the testing frame and the bolts tying the specimen to the frame were loose, the actuator was displaced accidentally, causing the loose bolts to become tight and exert forces on the specimen. As a result of this two hairline torsional cracks formed at the back faces of each of the transverse beams. A few shear cracks also developed near the end of the beam, with a large crack near the loading point at the end of the beam (Fig. 3.36).

In order to avoid a failure of the specimen near the beam loading point similar to that for specimen 8, a

1/2 in. diameter seven-strand cable was used to tie the beam to the slab. The cable was passed around the bottom of the beam and its two ends emerged out of the slab through the existing holes in the slab, as shown in Fig. 3.36. The two free ends of the cable were tied to 3/4 in. diameter eye-bolts, and the eye-bolts were tightened on top of the slab to act as additional shear support between the beam end and the slab (Fig. 3.37).

The specimen was then tested in the usual manner. New flexural cracks were observed in the beam and slab. There were no major cracks in the column and most of the energy was absorbed by the damaged area of the beam. The specimen was capable of sustaining three cycles of loading, but the load carrying capacity of the specimen dropped suddenly during the fourth positive half-cycle of loading. Figure 3.38 shows the specimen at the end of the third cycle of loading.

The stiffness of this subassemblage was noticably lower in the first cycle due to the accidental loading, but the relative loss of stiffness during the second and third cycle of loading was moderate. The specimen was capable of sustaining its maximum first cycle load through the third cycle of loading, as shown in Fig. 3.1(j).

No conclusive evidence with respect to beam bar pull

out or column bar slippage through the joint was available for this specimen.

Specimen 11 (M_R=1.56, ρ_{tm}=0.93%, γ=8.79, Without Slab)

Except for the lower joint shear stress present in specimen 11, this specimen was designed with the same design parameters as specimen 2. During the first cycle of loading, a few diagonal shear cracks were observed in the joint. A few flexural cracks were observed in the beam covering a distance 1.5 times the beam depth from the joint. Flexural cracks in the column spread over a distance equal to the column depth. In the second cycle of loading, the beam cracks extended to a distance twice the beam depth into the beam and a few new hairline cracks developed at the joint.

In the third negative half-cycle of loading, two major cracks formed at the bottom of the beam near the column. The shear crack extended into the joint and the flexural crack extended vertically upward into the beam, as shown in Fig. 3.39. The width of these cracks increased with additional cycles of loading and they were visually estimated at 1/8 in. by the end of the fifth cycle of loading (Fig. 3.40). There were a few cracks on the back face of the joint too, but in general, the joint of this specimen was in a good condition at the

termination of the test.

The load carrying capacity of this specimen increased through the fifth positive half-cycle of loading, but the loading in the negative direction reached its maximum at the end of the fourth cycle of loading. Severe pinching of the load vs. displacement hysteresis loops started during the fourth cycle of loading, as shown in Fig. 3.1(k).

Data from strain gages indicated that the beam longitudinal reinforcement started to pull out from the joint only after the fifth cycle of loading. Only the column bars in the front of the specimen slipped through the joint.

Specimen 12 (M_R=1.17, ρ_{tm}=0.86%, γ=9.06, With Slab)

Except for the presence of transverse beams and slab in specimen 12, the other design parameters for this specimen were the same as specimen 11. As a precaution, the beam end loading point of this specimen was externally tied to the slab in the same manner as specimen 10.

Flexural cracks extended for a distance twice the beam depth into the beam and slab during the first cycle of loading. A few cracks were also observed in the back of the column just below the joint, and two hairline

cracks were detected in the back face of each transverse beam. During the third cycle of loading, the width of the major torsional crack at the back face of the transverse beam was visually estimated at 1/8 in. and the cracks penetrated into the column after crossing the top of the slab (Fig. 3.41). In the same cycle, a spalling crack started in the column along the line where the back of the transverse beam joined the column. The specimen was in good condition at the conclusion of the test.

This subassemblage was capable of carrying at least the maximum first cycle load throughout the test. Significant loss of stiffness through pinching of the load vs. displacement hysteresis loops started during the fourth cycle of loading (Fig. 3.1(1)).

There was no evidence of beam longitudinal reinforcement pull out from the joint for this specimen. The column reinforcement on the back face did not slip either. However, there was a slight slippage in the column bars on the front face of the specimen.

3.2 Effect of the Flexural Strength Ratio

The most important effect of the flexural strength ratio was on the location of the failure zone. As the flexural strength ratio increased, the beam flexural hinging region spread further from the joint for

specimens having flexural strength ratios greater than 1.0. For flexural strength ratios approximately equal to 1.0, the beam flexural hinging zone did not spread very far from the joint (less than one beam depth) and the primary damage was in the joint. The effect of the flexural strength ratios can be observed in Figs. 3.21, 3.23, and 3.35, which show specimens 1, 2, and 9 respectively at the conclusion of the tests. The design parameters for these three specimens were identical, except that the flexural strength ratios were 1.01, 1.35 and 1.93 respectively. A similar type of difference was observed between specimens 3 and 4, for which the only change was the increase in the flexural strength ratio. It is interesting to note however that, as shown in Fig. 3.23, even with a flexural strength ratio of 1.35, most of the damage in specimen 2 was concentrated in the joint.

In specimens 5 and 6, where the actual flexural strength ratios were lower than 1.0, flexural hinges were formed at the portion of the upper column just above the slab. Although the advantages of the plastic hinge formation in the column are questionable, the hysteretic performances of these two subassemblages were satisfactory. Both specimens showed stable behavior and maintained their first cycle load carrying capacity

through the fifth cycle of loading.

Changes in the flexural strength ratio also had a distinct effect in the load carrying capacity of the specimens. In general, specimens can be divided into two categories with respect to the cycle to cycle load carrying capacity: (1) specimens with flexural strength ratio equal to 1.0, (2) specimens with flexural strength ratio greater than or lower than 1.0.

For specimens with values of M_R equal to 1.0, the damage was concentrated in the joint region, as shown in Fig. 3.42(b). Due to rapid deterioration of this critical region, the load carrying capacity of these specimens dropped sharply with additional cycles of loading.

For specimens with values of M_R greater or lower than 1.0, the flexural plastic hinging spread further from the joint and into the beam or column respectively, as illustrated in Figs. 3.42(a) and 3.42(c). These specimens demonstrated a more stable behavior and were capable of carrying a larger percentage of the first cycle maximum load in the subsequent cycles of loading. The maximum load carried by the specimen during the fourth cycle of loading as a percentage of that carried during the first cycle of loading is plotted for different flexural strength ratios in Fig. 3.43. The

figure indicates that for specimens with flexural strength ratios greater than 1.0 (specimens 1, 2, 3, 4, and 9), the cyclic load carrying capacity of the specimen increased with an increase in the flexural strength ratio. However, this observation is not valid for specimens 5 and 7. Although the flexural strength ratio for specimen 5 was lower than that for specimen 7, formation of flexural hinging in the column of specimen 5 resulted in an increase in the maximum cyclic load carrying capacity for this specimen. Based on this observation, it is evident that, so far as the cyclic load carrying capacity of the specimen is concerned, specimens for which the flexural hinging occurs outside of the joint region (in beam or column), demonstrate a more stable cyclic behavior than the specimens for which the majority of the damage is concentrated in the joint.

3.3 Effect of the Transverse Reinforcement Ratio

For four pairs of specimens, (1 and 3, 2 and 4, 5 and 6, and 7 and 8), the only change in the primary variables between the two specimens in each pair was the change in the percentage of the transverse reinforcement within the joint. Visual inspection of these specimens during the tests indicated that for specimens with a higher percentage of transverse reinforcement, the damage

in the joint was reduced and although the concrete in the core of the joint was cracked, it was not crushed. An example is shown in Figs. 3.44 and 3.45, which show specimens 2 and 4 at the end of the sixth cycle of loading. However, the increase in the transverse reinforcement ratio did not affect the damage to the joint cover concrete significantly. For the bare specimens, the joint cover concrete was crushed and ineffective by the conclusion of the test, regardless of the transverse reinforcement ratio.

The magnitude of strains in the hoops was also affected by the transverse reinforcement ratio. Figures 3.46 and 3.47 show the strains in the hoops for specimens 5 and 6 respectively. The two specimens were designed identically, except that specimen 5 had two sets of hoops in the joint (ρ_{tm}= 0.97%), while for specimen 6, three sets of hoops were placed in the joint (ρ_{tm}= 1.46%). These figures indicate that when fewer hoops are present in the joint, the share of strains carried by each hoop is larger. Similar behavior was observed in other pairs of specimens for which the only change was the amount of the transverse reinforcement in the joint.

The addition of the extra hoop not only increased the transverse reinforcement ratio, but it also improved the confinement of the joint. This improved confinement

led to a delay or elimination of beam bar pull out and slippage of the column longitudinal bars through the joint.

Because the detection of beam bar pull out was not very clear on plots of load vs. strain, plots of the applied actuator displacement vs. strain were prepared. Beam bar pull out was determined by comparing the strains at the ends of two successive cycles of loading. A reduction, or no change in the strains, while the displacements increased from one cycle to the next, was interpreted as pull out or slippage of the bars. Figures 3.48 and 3.49 show plots of beam load point displacements vs. strains in the beam longitudinal reinforcement at the face of the column for specimens 2 and 4 respectively. It is evident that in specimen 2, the maximum strain was obtained at the end of the first cycle of loading. After that cycle, the maximum strain in each successive cycle was either the same or lower than that of the first cycle even though the maximum displacement was larger, indicating that the bar was pulling out of the joint. In specimen 4, however, there was no indication of bar pull out until the end of the third cycle of loading. The delay of beam bar pull out in specimen 4 compared to specimen 2 is attributed to the improved confinement provided by the additional joint transverse

reinforcement.

The effect of the transverse reinforcement ratio on column bar slippage in specimens 2 and 4 is illustrated in Figs. 3.50 and 3.51 respectively. As shown in Fig. 3.50, the strains in the longitudinal column bar in specimen 2 started to drop after the first cycle of loading. However, for specimen 4, the improved confinement provided by the additional hoop, delayed the slippage of the bar until the fifth cycle of loading, as shown in Fig. 3.51.

3.4 Effect of the Joint Shear Stress

Data from four specimens were used to study the effect of the joint shear stress on the overall behavior of the subassemblage. Specimens 2 and 11, and specimens 7 and 12 were designed with the same values for all the design parameters, except that the design joint shear stress for specimens 11 and 12 was $10\sqrt{f_c'}$ compared to $14\sqrt{f_c'}$ for specimens 2 and 7.

Examination of the specimens during and at the conclusion of the tests indicated that the specimens with lower joint shear stresses suffered less damage than similar specimens with higher joint shear stresses. This observation was especially clear in the case of specimens 11 and 2, where the formation of cracks and deterioration

of the concrete near the joint could be readily seen. However, due to the presence of the transverse beams in specimens 7 and 12, the effect of the lower joint shear stress in reducing the damage to the concrete near the joint was not as clear as that observed for specimens 2 and 11.

Reduction in the joint shear stress had a distinct effect on the load carrying capacity of the specimens. As listed in Table 3.1, the load carrying capacity of specimen 2 dropped significantly after the first cycle of loading. However, specimen 11 was capable of carrying larger forces than that of the first cycle through the fifth cycle of loading. A similar behavior was observed for specimens 7 and 12. As shown in Table 3.1, the load carrying capacity of specimen 12 increased slightly through the third cycle of loading and the maximum load sustained by the specimen at the end of the fifth cycle of loading was six percent larger than that carried during the first cycle of loading. However, specimen 7 reached its maximum load carrying capacity at the end of the second cycle of loading and the force carried by the specimen at the end of the fifth cycle was four percent less than that carried during the first cycle of loading. As expected, due to the additional confinement provided by the presence of transverse beams, the loss of load

carrying capacity between specimens 7 and 12 was not as severe as that observed for specimens 2 and 11.

Deterioration of the concrete in the joint due to higher shear stresses had an adverse effect on the slippage of the column bars. Figures 3.52 and 3.53 show the plot of the load point displacement vs. the strain on the column longitudinal reinforcement in specimens 7 and 12 respectively. The strains measured in specimen 12 extended into compression and tension with every cycle of loading as expected. However, the strains measured for specimen 7 indicated that during the first cycle of loading the column longitudinal reinforcement started to slip. The compressive strains reduced with each cycle and eventually tensile strains replaced the expected compressive strains.

3.5 Effect of the Transverse Beams and Slab

Specimens with transverse beams and slab were stronger for the positive direction of loading (tension in the slab). As a result of this, the shear stresses in the joint were higher during the positive half cycle of loading. As shown in Figs. 3.46 and 3.47, the strain gage data from the transverse reinforcement in the joint verified this behavior. Similar behavior was observed in the hoop strains for all specimens with slabs.

The beneficial effects of the presence of unloaded transverse beams on the overall behavior of the connection have been noted by other investigators (3,14). However, there was no information on the effect of indirectly loaded transverse beams.

In the testing setup used for this study, the applied load at the free end of the main beam and slab was transfered to the transverse beams through the slab. Due to the torsion in the transverse beams, the longitudinal reinforcement of the transverse beam was subjected to tension. These tensile forces caused a more rapid deterioration of the joint than would occur for an unloaded transverse beam. However, the improvement in the confinement of the joint due to the presence of transverse beams was so great that there was a net improvement in the confinement of the joint of specimens with transverse beams and slab.

The improvement in the confinement of the joint reduced the pull out of the main beam longitudinal reinforcement. Figures 3.54 and 3.55 show the plots of load point displacement vs. strains in the main beam longitudinal bars at a distance d/2 away from the face of the column for specimens 9 and 10 respectively. The plots indicate that, while keeping all other parameters constant, addition of the transverse beams and slab in

specimen 10 eliminated the beam bar pull out which was observed after the first cycle of loading in specimen 9.

The addition of transverse beams caused a better distribution of the shear stresses accompanied by less cracking in the joint region. Also, strains in the joint transverse reinforcement were reduced. Figures 3.56 and 3.57 show the hoop strains in specimens 2 and 7 respectively. Specimens 2 and 7 were identical, except that specimen 7 had transverse beams and slab. It is evident from the comparison of these plots that the presence of the transverse beams and slab resulted in lower hoop strains in specimen 7 than in specimen 2.

CHAPTER 4

PREDICTED AND MEASURED BEHAVIOR

4.1 Introduction

Calculated values for several aspects of specimen behavior were compared with the measured results to verify the accuracy of the calibration of the testing equipment as well as to illustrate the validity of certain analytical models.

Comparison for two aspects of specimen behavior are presented here. First, the calculated and measured beam yield moments are compared. Second, the yield deflections are calculated and compared with the measured values.

4.2 Calculated and Measured Beam Yield Moments

Comparison of the calculated and measured beam yield moments were important in verifying the accuracy of the applied loads recorded during the test. In order to calculate the yield moments, all beams and columns were analyzed with a computer program similar to that developed by Wight and Sozen (20). The actual material

properties listed in Appendix C were used for input to the computer program. The program assumes a linear strain variation across a section and has subroutines which model measured stress vs. strain characteristics of the reinforcing steel and concrete.

The flexural strength ratios for specimens 5 and 6 were less than 1.0. This resulted in formation of flexural hinging in the column. In order to make a realistic comparison of the calculated and measured yield moments for these two specimens, the summation of the column yield moment capacities for the upper and the lower half of the column was recorded as the calculated yield moment for the specimen.

For the specimens with a slab, the entire width of the slab was assumed effective when calculating the beam negative (tension near top) yield moments. This assumption resulted in higher yield moments than the design values which were based on the assumption that only two of the slab longitudinal reinforcing bars on each side of the main beam would contribute towards the negative flexural capacity of the beam. The calculated beam yield moments are tabulated in column 2 of Table 4.1.

The measured yield moments were obtained using the observed applied shear force at the observed onset of the

yield. For specimens 1 through 4 the measured yield moment for the beams (M_{yb}) was calculated as follows.

$$M_{yb} = V_{yb} \quad L_b \tag{4.1}$$

where, V_{yb} = observed yield shear force applied to the beam,

and L_b = beam length as shown in Fig. 4.1.

For specimens 5 through 12 the beam yield moment was calculated from the equilibrium of the external forces acting on the specimen (Fig. 4.2), using the following relationship.

$$M_{yb} = \frac{L_c \; V_{yc} + P \quad \Delta_{yc}}{L_b + h_c/2} \tag{4.2}$$

where, h_c = total depth of column as shown in Fig. 4.2,

L_b = beam length,

L_c = column length,

M_{yb} = beam or beam and slab yield moment,

P = column axial load,

V_{yc} = observed yield shear force applied to the column,

and Δ_{yc} = yield displacement of the column.

The measured beam yield moments are shown in column 3 of Table 4.1.

As shown in Table 4.1, the calculated yield moments agree favorably with the measured values. The average difference between the calculated and the measured yield

TABLE 4.1

CALCULATED AND MEASURED YIELD MOMENTS

Specimen Number (1)	Calculated M_{yb} (kip-in) (2)	Measured M_{yb} (kip-in) (3)	Measured M_{yb} / Calculated M_{yb} (4)
1	1963	1980	1.01
2	1747	1680	0.96
3	1989	1920	0.96
4	1776	1800	1.01
5	2124*	2078	0.98
6	2095*	2096	1.00
7	2216 (1720)**	2086	0.94
8	2227 (1724)	2270	1.02
9	2127	2327	1.09
10	2888 (2383)	2778	0.96
11	1789	2078	1.16
12	2456 (1905)	2615	1.06

*Summation of the calculated yield moments for the upper and lower column halves.

**Figures in parenthesis are based on the assumption that only the first two longitudinal reinforcing bars on each side of the main beam are effective.

moments was 4.5 percent.

4.3 Calculated and Measured Yield Deflections

For specimens 1 through 4, beam yield displacements at the point of application of load, and for specimens 5 through 12, column yield displacement at the point of application of load were calculated. The calculated yield deflections were found using the actual material properties for each specimens. Measured yield deflections were obtained from: (1) the data from strain gages bonded to the longitudinal reinforcing bars which detected initial yielding and (2) plots of the applied load vs. the load point deflection which had a significant change of slope at the yield point. Results from these three sources are compared in Table 4.2.

The deflection of the specimens at the loading point consists of several components; (1) rigid body rotation of the joint, (2) flexural deflection of the beam and column, (3) shear deformations in the beam and column, (4) shear deformation of the joint, (5) inelastic flexural rotation of the joint, (6) slippage of the beam and column longitudinal reinforcing bars at the joint, and (7) deformations of the testing frame. Contributions from the first four components were used to calculate the yield displacement.

TABLE 4.2

CALCULATED AND MEASURED YIELD DEFLECTIONS

Specimen Number (1)	Δ_1 (in) (2)	Δ_2 (in) (3)	Δ_3 (in) (4)	Δ_t (in) (5)	Δ_{ys} (in) (6)	$\frac{\Delta_t}{\Delta_{ys}}$ (7)	Δ_{yo} (in) (8)
1	0.54	0.01	—	0.55	—	—	1.20
2	0.46	0.01	0.42	0.89	1.15	0.77	1.10
3	0.53	0.01	0.29	0.83	1.00	0.83	1.20
4	0.45	0.01	0.24	0.70	0.90	0.78	1.10
5	0.97	0.06	—	1.03	1.20	0.86	1.50
6	0.96	0.06	—	1.02	1.40	0.73	1.60
7	0.80	0.06	—	0.86	1.15	0.75	2.35
8	0.81	0.06	—	0.87	1.05	0.83	2.00
9	0.44	0.03	—	0.47	0.85	0.55	1.80
10	0.54	0.07	—	0.61	—	—	2.30
11	0.55.	0.02	—	0.57	0.95	0.60	1.50
12	0.73	0.06	—	0.79	1.50	0.53	2.00

Δ_1 = Deflection due to the flexural deformation of the beam and column.

Δ_2 = Deflection due to the shear deformation of the beam and column.

Δ_3 = Deflection due to the shear deformation of the joint.

Δ_t = Total calculated yield deflection.

Δ_{ys} = Measured yield deflection using data from strain gages.

Δ_{yo} = Measured yield deflection from plots of load vs. deflection.

Displacements due to the elastic flexural rotation of the subassembly at the joint and the flexural deflection of the beam and column was calculated using the moment-area theorem. For specimens 1 through 4, the theoretical flexural deflection was calculated as:

$$\Delta_1 = V_b \left(\frac{L_b^3}{3E_c I_b} + \frac{L_b^2 L_c}{12E_c I_c} \right) \qquad (4.3)$$

where, E_c = modulus of elasticity for concrete,

I_b = cracked moment of inertia for beam,

I_c = cracked moment of inertia for column,

L_b = length of beam as shown in Fig. 4.1,

L_c = length of column,

and V_b = applied shear force to the end of beam.

For specimens 5 through 12, the theoretical flexural deflection at the top of the column was calculated in a similar manner,

$$\Delta_1 = V_c \left(\frac{L_b L_c^2}{3E_c I_b} + \frac{L_c^3}{12E_c I_c} \right) \qquad (4.4)$$

where, V_c = applied shear force to the top of the column as shown in Fig. 4.2.

Other parameters are the same as those in Eq. 4.3.

The deflections due to shear deformations in the beam and column for specimens 1 through 4 were calculated as:

$$\Delta_2 = \frac{V_b}{G_c}\left(\frac{L_b}{A} + \frac{L_b^2}{L_c A_g}\right) \qquad (4.5)$$

where, A = cross sectional area of the beam,

A_g = cross sectional area of the column,

and G_c = shear modulus of concrete = $0.4E_c$.

Other parameters are the same as those in Eq. 4.3.

For specimens 5 through 12, the deflections due to the shear deformations in the beam and column were computed using the following relationship:

$$\Delta_2 = \frac{V_c A}{G_C A_w}\left(\frac{L_c^2}{L_b A_w} + \frac{L_c}{A_g}\right) \qquad (4.6)$$

where, A = total cross sectional area of the beam or beam and slab,

and A_w = cross sectional area of the web of the beam or beam and slab.

Other parameters are the same as those in Eq. 4.3.

In general, in subassemblages where the column is much stronger than the beam, flexural hinging in the beam occurs near the connection. In such cases, flexural deformation at the end of the beam accounts for a large percentage of the total deflection. Due to the relatively low flexural strength ratio values in the specimens tested, shear deformations in the joint region account for a large percentage of the total deflection. Elastic methods of calculating shear deformations are not suitable for calculation of joint shear deformations.

The data obtained from Linear Variable Differential Transducers (LVDTs) attached to the bare specimens over the joint region was used to calculate the shear deformations in the joint. Considering the deformed configuration of a joint (Fig. 4.3), the first component of the joint shear deformation (γ_{1j}) can be calculated as:

$$\gamma_{1j} = (\sqrt{(D+\delta_1)^2 - h_b^2} - h_c) / h_b \qquad (4.7)$$

where, D = diagonal dimension of the joint (Fig. 4.3),

h_b = height of the beam,

h_c = depth of the column,

and δ_1 = measured elongation of LVDT1.

Similarly, the second component of joint shear deformation (γ_{2j}) can be calculated as:

$$\gamma_{2j} = (h_c - \sqrt{(D+\ _2)^2 - h_b^2}\ ) / h_b \qquad (4.8)$$

where, δ_2 = measured shortening of LVDT2.

The average joint shear deformation (γ_j) was calculated using the relationship:

$$\gamma_j = (\gamma_{1j} + \gamma_{2j}) / 2 \qquad (4.9)$$

Due to the presence of transverse beams, LVDTs could not be mounted on specimens with transverse beams and slab. Of the LVDTs mounted on the bare specimens, only three cases, for specimens 2, 3, and 4, led to satisfactory results. Due to malfunctioning of LVDTs, the results for specimens 1, 9, and 11 had to be

discarded. The beam load point deflection due to joint shear deformation, Δ_3, for specimens 2, 3, and 4 was calculated as:

$$\Delta_3 = \gamma_j \quad L_b \tag{4.10}$$

where, all terms have been defined previously.

The components of deflection mentioned above were calculated using the applied shear forces corresponding to the yield moments obtained from the measured load vs. load point displacement relationships and the results are tabulated in Table 4.2. Displacements due to the flexural rotation of the subassemblage at the joint, and the flexural deflection of the beam and column are shown in column 2 of Table 4.2. Load point displacements due to the shear deformation in the beam and column are given in column 3 of Table 4.2. Displacements due to shear deformations in the joint for specimens 2 through 4 are listed in column 4 of Table 4.2. The summation of the above components is listed in column 5 of Table 4.2 and is referred to as the total calculated yield deflection (Δ_t).

Measured yield deflections were obtained using the data from strain gages bonded to the beam longitudinal reinforcement at the face of the column. First, the load corresponding to a sudden change of slope of the load vs. strain diagram was measured. Next, the corresponding

displacement to this load on the measured plot of the applied load vs. load point displacement was recorded as the yield deflection from the strain gage data. The yield deflections obtained from the strain gage data, Δ_{ys}, are listed in column 6 of Table 4.2. The yield displacements could not be determined from the data from strain gages used in specimens 1 and 10. In specimen 1, due to accidental loading, no information was obtained during the first quarter cycle of loading. In specimen 10, the yield displacement could not be determined due to the slippage of the main beam longitudinal reinforcement. For specimen 9, the strain gage located on the beam longitudinal reinforcement at the face of the column did not function properly. However, based on the data from strain gages located on longitudinal bars near the face of the column, the yield displacement was approximated to be 0.85 in.

The yield deflections observed from the load vs. load point deflection relationship during the tests and defined by a significant slope change in load vs. load point deflection curves are listed in column 8 of Table 4.2.

A comparison of the total calculated yield deflections and the measured yield deflections obtained using the data from strain gages indicates a certain

discrepency between the results. The observed smaller values for the calculated yield displacements are due to the fact that the shear deformation of the joint was included only for specimens 2, 3, and 4. In addition, the remaining components of the deflection, namely the inelastic flexural rotation of the joint, slippage of the reinforcing bars, and the deformations of the testing frame were not included in the calculation of the yield displacements for any of the specimens.

As shown in Table 4.2, deflection due to the shear deformation in the joint accounts for a large percentage of the total deflection in specimens 2, 3, and 4. Due to faulty equipment, no useful data was collected for the LVDTs in specimens 1, 9, and 11. It was not possible to use LVDTs to measure the joint deformations in specimens with transverse beams and slab. Exclusion of the joint shear deformation accounts for a large percentage of the difference between the calculated and measured displacements in specimen 1 and specimens 5 through 12.

Inelastic flexural rotation of the joint is another component of the deflection which was not included in the calculations. Even for specimens 2, 3, and 4, the data from the two LVDTs was insufficient to calculate the inelastic flexural rotation of the joint. Flexural rotation of the joint can be measured on joints of bare

specimens, provided that at least two additional LVDTs are used to measure any change in the dimension h_c of the joint (Fig. 4.3). Tests by Scribner (19) indicate that for specimens with large flexural strength ratios, an average of thirty five percent of the total displacement is due to the inelastic flexural rotation of the hinging region at yield displacement. Furthermore, he concluded that this percentage is relatively constant at yield displacement for different specimens. Due to large shear deformation in the joint the inelastic flexural rotation of the joint for the specimens tested in this study are not as high as thirty five percent of the total deflection. However, discounting this component of the deflection does result in lower calculated yield deflections.

Tests by Hawkins (21) indicate that slippage of the longitudinal reinforcing bars contributes towards the overall deflection of a beam-column subassemblage. With the test setup used for this study, inclusion of the bar slippage in the calculation of the components of the deflection was impossible.

The last source of possible error is the deformations of the testing frame. However, due to the high stiffness of the testing frame, the percentage of the total deflection due to the deformations of the

testing frame are considered to be very small.

The yield deflections observed from the load vs. load point deflection relationships were also larger than the calculated yield deflections and were usually larger than those calculated from data from the strain gages. This is due to the difficulties involved in locating the exact yield displacements during the tests. In testing of a subassemblage, all reinforcing bars in the same layer do not yield at the same time. Therefore, there is no sharp flattening of the applied load vs. load point deflection curve, but rather a gradual decrease in the slope of the curve. As a result of this, the observed yield dis-placement from the load vs. load point deflection curves was always larger than the actual yield displacement calculated using the data from strain gages.

CHAPTER 5

COMPARISON WITH DESIGN RECOMMENDATIONS

5.1 Introduction

The design of the beams and columns of the test specimens was in accordance with the seismic provisions in Appendix A of the Building Code for Reinforced Concrete ACI 318-77 (17). Although the design of the tested beam to column connections did not follow any particular code, the recommendations of ACI-ASCE Committee 352 (12) and the gaps in existing research studies discussed in Section 2.2 of this report were used as guidelines. In the following sections, the design of the connections will be compared with three recent design recommendations. The recommendations of ACI-ASCE Committee 352 (17) referred to as "ACI-352" will be studied first. These recommendations, which are the most recently published guidelines for the design of connections in U.S., are currently undergoing revisions. The sixth revised draft of the above recommendations (22) referred to as "ACI-352R" will be studied next. The third set of recommendations to be studied are from the

New Zealand Code of Practice for the Design of Concrete Structures (23), referred to as "NZ Code".

In the following three sections the recommendations of each code, as they apply to exterior joints designed to resist load reversals in the inelastic range, are presented. At the end of each section, the code recommendations are compared with the actual values provided in each test specimen.

5.2 ACI-352

The design recommendations in ACI-352 are based on the concept of "strong column-weak beam". However, the specified minimum value for the flexural strength ratio is only 1.0. These design recommendations specify a minimum increase of 25 percent in the yield stress of the beam longitudinal reinforcement when calculating forces in the joint.

A specified amount of transverse column reinforcement is required for confinement. The transverse reinforcement provided for confinement can also be considered effective in resisting joint shear stresses, but additional transverse reinforcement may be needed if the joint shear stresses are high. When the design column axial load, P_u, is less than 40 percent of the column balanced axial load, the connection should be

designed similar to flexural members. The required area of transverse reinforcement is calculated from the following relationship:

$$A_{sh} = 0.15\, A_{slc}\, \frac{s_h}{d_{lc}} \qquad (5.1)$$

where, A_{slc} = area of non prestressed tension reinforcement,

A_{sh} = cross sectional area of hoop reinforcement,

d_{lc} = distance from extreme compression fiber to centroid of tension reinforcement,

and s_h = center to center spacing of hoops.

However, the center to center spacing of the transverse reinforcement is limited to one quarter of the depth of the column.

When the design axial load is larger than 40 percent of the column balanced axial laod, confinement reinforcement is required in accordance with:

$$A_{sh} = 0.3\, \frac{s_h\, h''\, f_c'}{f_{yh}} \left(\frac{A_g}{A_c} - 1 \right) \qquad (5.2)$$

where, A_c = area of core of specially reinforced column measured to outside diameter of hoops,

A_g = gross area of section,

f_c' = specified compressive strength of concrete,

f_{yh} = specified yield strength of hoop reinforcement,

and h" = core dimension of tied column.

Both concrete and reinforcing steel are considered effective in resisting horizontal shear forces in the joint. The contribution of the concrete in carrying the shear is limited to:

$$v_c = 3.5 \quad \beta\gamma'\sqrt{f_c'} \tag{5.3}$$

where, v_c = nominal permissible shear stress carried by concrete,

β = 1.0 for joints designed to withstand large inelastic deformations,

and γ' = 1.4 when transverse beams cover at least three quarters of the lateral face of the joint, and 1.0 otherwise.

The required area of the shear reinforcement is calculated as follows:

$$A_v \geq \frac{(v_u - v_c)\, A_{cv}\, s_h}{f_{yh}\, d_{lc}} \tag{5.4}$$

where, A_{cv} = effective area in shear,

A_v = area of shear reinforcement within a distance s_h,

d_{lc} = effective depth of joint in direction of shear force,

and v_u = factored design joint shear stress.

In addition, two limitations are imposed on the shear stress levels, requiring that:

$$v_u \leq 20 \sqrt{f_c'} \tag{5.5}$$

and $$(v_u - v_c) \leq 15 \sqrt{f_c'} \tag{5.6}$$

The ACI-352 requires a minimum straight embedment length, l_s, for beam longitudinal reinforcement before a standard hook:

$$l_s = \frac{0.04\ A_b\ (\alpha f_y - f_h)}{\psi \sqrt{f_c'}} \tag{5.7}$$

where, A_b = area of individual bar,

f_h = stress developed by standard hook

= $700\ (1-0.3d_b')\quad f_c'$,

d_b' = nominal diameter of bar,

f_y = specified yield strength of reinforcement,

α = stress multiplier for flexural reinforcement

= 1.25 for earthquake loading,

and ψ = factor influencing effect of confinement on capacity of hooked bar.

However, the value of l_s should be at least $4d_b'$ or 4.0 in. The straight embedment is measured from the outer face of the column longitudinal reinforcement to the start of the hook (Fig.5.1).

Table 5.1 gives a summary of the design of each specimen according to ACI-352. Specimens 5 and 6 did not comply with the design requirements because the flexural strength ratio for these specimens was less than 1.0. Specimens 1 and 2 had horizontal joint shear stress

TABLE 5.1

DESIGN PARAMETERS ACCORDING TO ACI-352

Specimen Number	M_R	v_u (psi)	$\frac{v_u}{20\sqrt{f_c'}}$	v_c (psi)	$\frac{v_u - v_c}{15\sqrt{f_c'}}$	Req'd s_h (in.)	$d_{1c}/4$ (in.)	Provided s_h, (in.)	l_s (in.)	Provided l_s, (in.)
(1)	(2)	(3)	(4)	(5)	(6)	(7)	(8)	(9)	(10)	(11)
1	1.01	1470	1.04	248	1.15	3.7	2.4	4.4	4.0	3.9
2	1.35	1500	1.04	253	1.15	3.6	2.4	3.9	4.0	3.9
3	1.07	1460	0.94	274	1.01	3.8	2.4	3.3	4.0	3.9
4	1.41	1490	0.91	286	0.99	3.7	2.4	3.0	4.0	3.9
5	0.89	860	0.55	385	0.40	7.3	2.5	5.0	4.0	4.8
6	0.87	858	0.57	371	0.43	7.1	2.5	3.7	4.0	4.8
7	1.17	888	0.68	318	0.59	6.1	2.5	4.4	4.0	4.8
8	1.16	889	0.66	328	0.57	6.2	2.5	3.3	4.0	4.8
9	1.93	1155	0.97	208	1.06	3.6	2.8	4.3	4.0	5.9
10	1.58	887	0.75	289	0.68	5.1	2.8	5.0	4.0	5.9
11	1.56	863	0.57	266	0.52	6.1	2.8	4.6	4.0	5.9
12	1.17	853	0.46	350	0.28	10.1	2.8	5.0	4.0	5.9

values larger than the maximum allowable values, and specimens 1, 2, 3, and 9 violated Eq. 5.6 which limits the joint shear stress assigned to transverse reinforcement. Because the column axial load was smaller than 40 percent of the balanced axial load, the confinement requirements were governed by the requirements for flexural members. The maximum allowable spacing of $d_{lc}/4$ was so severe that none of the specimens complied with. The provided hoop spacing within the joint was also larger than the required hoop spacing derived from Eq. 5.4, except for specimens 1, 2, and 9. Due to the high values for the stresses developed by the standard hooks, the calculated straight lead embedment (l_s) from Eq. 5.7 was always smaller than the minimum requirement of 4.0 in. As shown in column 11 of Table 5.1, the provided l_s in specimens 1 through 4 was close enough to 4.0 in. to be considered acceptable. The provided l_s for specimens 5 through 12 was greater than 4.0 in.

5.3 ACI-352R

The revision of ACI-352, which is in progress, contains several major changes in design philosophy. Instead of having separate provisions for the design of joint shear reinforcement, the philosophy reflected in

ACI-352R is that the designer only needs to provide adequate column confinement reinforcement through the connection and limit the nominal joint shear stress to 12 $\sqrt{f_c'}$ (psi units) for external connections. If the joint shear stresses are found to be higher than the allowable value, then the size of the connection must be increased rather than adding more transverse steel which would lead to congestion of reinforcement. The revisions recommend a minimum flexural strength ratio equal to 1.4. There is no change in the required 25 percent increase of the nominal yield stress of the beam longitudinal reinforcement which is used when calculating forces or stresses in the joint. Furthermore, the use of any strength reduction factors when calculating joint shear stresses has been eliminated.

One of the most important changes between ACI-352 and ACI-352R is in the elimination of all reinforcement assigned to carry joint shear forces. According to ACI-352R, confinement reinforcement should be provided regardless of the amount of the column axial load. In addition to Eq. 5.2, the following should be satisfied:

$$A_{sh} \geq 0.12 \frac{s_h \, h'' \, f_c'}{f_{yh}} (1 - 0.01h) \qquad (5.8)$$

where, h= total depth of column.

Also, the center to center spacing between hoops, s_h,

should be limited to the smaller of h/4 or 4.0 in.

Requirements for shear reinforcement within the joint have been eliminated in ACI-352R. However, for external joints, the total design shear force in the joint (V_u) is limited to:

$$V_u \leq 12 \sqrt{f_c'}\ bh \qquad (5.9)$$

where, b and h are the gross width and thickness of the column respectively.

The requirements for development length of hooked bars have been changed to:

$$l_{dh} \geq 0.014\ \alpha f_y\ d_b' / f_c' \qquad (5.10)$$

where, l_{dh} is the development length of hooked bars, measured from the critical section to the back side of the hook (Fig. 5.2). For joints designed to withstand load reversals, the critical section is taken at the face of the core of the column. Also, l_{dh} should be larger than $8d_b$ and 6.0 in. In addition, there are new requirements for development of column bars passing through the joint such that:

$$h_b / d_b \geq 24 \qquad (5.11)$$

where, h_b = total beam depth,

and d_b = column bar diameter.

Table 5.2 summarizes the design of each specimen according to the recommendations of ACI-352R. Only four specimens (4, 9, 10, and 11) passed the requirements for

TABLE 5.2

DESIGN PARAMETERS ACCORDING TO ACI-352R

Specimen Number	M_R	V_u (kips)	$\frac{V_u \times 1000}{12bh\sqrt{f_c'}}$	s_h (in.)	h/4 (in.)	Provided s_h, (in.)	l_{dh} (in.)	Provided l_{dh}, (in.)	Provided h_b/d_b
(1)	(2)	(3)	(4)	(5)	(6)	(7)	(8)	(9)	(10)
1	1.01	128.8	1.05	9.0	3.0	4.4	8.8	7.4	25.1
2	1.35	131.5	1.05	8.6	3.0	3.9	8.6	7.4	23.0
3	1.07	128.4	0.95	7.4	3.0	3.3	8.0	7.4	25.1
4	1.41	131.0	0.93	6.8	3.0	3.0	7.6	7.4	23.0
5	0.89	99.7	0.73	8.9	3.0	5.0	6.7	7.8	25.1
6	0.87	99.9	0.76	9.5	3.0	3.7	7.0	7.8	25.1
7	1.17	103.4	0.92	13.0	3.0	4.4	8.1	7.8	23.0
8	1.16	103.3	0.92	12.2	3.0	3.3	7.9	7.8	23.0
9	1.93	151.4	1.08	18.2	3.5	4.3	10.3	9.4	18.9
10	1.58	135.1	0.98	18.5	3.5	5.0	10.4	9.4	18.9
11	1.56	110.2	0.62	9.6	3.5	4.6	6.9	9.4	25.1
12	1.17	100.3	0.60	10.9	3.5	5.0	8.6	9.4	25.1

the flexural strength ratio. The joint shear forces (Eq. 5.9) were violated for specimens 1, 2, and 9. Due to the relatively small cross sectional dimensions of the columns, Eq. 5.2 led to more conservative values than Eq. 5.8. However, the additional requirement, limiting the spacing of hoops to a quarter of the total column depth was so severe that it governed the maximum hoop spacing within the joint region. Only specimen 4 complied with the design requirements for the spacing of confinement requirement. Beam reinforcement embedment lengths for specimens 4, 5, 6, 11, and 12 were satisfied, but the calculated values from Eq. 5.10 were slightly larger than the provided embedment length in the remaining specimens. The additional requirement of ACI-352R, Eq. 5.11, calls for the ratio of h_b/d_b to be larger than 24. Only half of the specimens (1, 3, 5, 6, 11, and 12) met this requirement. Equation 5.11 becomes particularly difficult to satisfy when larger size column bars are used, such as the No. 8 column bars used in specimens 9 and 10.

5.4 NZ Code

There are two differences in the general principles between the New Zealand code and the American requirements from ACI-352 and ACI-352R. First, the NZ

Code requires that joints be designed in such a way that plastic hinges form outside of the joint core region. However, there is no requirement that the flexural hinges form in the beam. Therefore, flexural strength ratios smaller than 1.0 are permissible. Second, the requirements of this code may be applied to the joints where the beam is wider than the column.

The NZ Code specifies that reinforcement overstrengths should be used when calculating joint forces, but no stress multiplier factor, similar to the 1.25 in ACI-352 is designated. According to the NZ Code, confinement should be provided regardless of the magnitude of the column axial load. The requirements which are modified versions of Eqs. 5.2 and 5.8 are as follows:

$$A_{sh} \geq \frac{0.3\ s_h\ h''\ f_c'}{f_{yh}} \left(\frac{A_g}{A_c} - 1\right) \left(0.5 + \frac{1.25\ P_u}{\phi f_c'\ A_g}\right) \quad (5.12)$$

$$A_{sh} \geq \frac{0.12\ s_h\ h''\ f_c'}{f_{yh}} \left(0.5 + \frac{1.25\ P_u}{\phi f_c'\ A_g}\right) \quad (5.13)$$

where, ϕ = strength reduction factor = 0.85.

Also, s_h should be limited to the lessor of h/5, 8.0 in., or 10 d_b. The extra term in Eqs. 5.12 and 5.13, compared to Eqs. 5.2 and 5.8, modifies the amount of transverse reinforcement as a function of the column axial load

level.

The NZ Code has separate design recommendations for horizontal and vertical shear in the joint. The nominal horizontal shear stress in the joint, v_{jh}, is limited to:

$$v_{jh} \leq 18 \sqrt{f_c'} \quad \text{(psi)} \tag{5.14}$$

The design horizontal shear force to be resisted by the horizontal joint shear reinforcement is given as:

$$V_{sh} = V_{jh} - V_{ch} \tag{5.15}$$

where, V_{ch} is the ideal horizontal joint shear strength provided by concrete shear resisting mechanism. The value of V_{ch} in most cases, and including for the 12 specimens tested, will be equal to zero. The spacing of joint shear reinforcement is then determined from the relationship:

$$s_h \leq \frac{A_{sh} f_{yh} d_{1c}}{V_{sh}} \tag{5.16}$$

The vertical shear forces in the joint, V_{jv}, will be carried by the concrete and the vertical joint shear reinforcement. At least one intermediate column bar should be provided to serve as the vertical joint shear reinforcement. The design vertical shear force to be carried by the vertical joint reinforcement , A_{jv}, is:

$$V_{sv} = V_{jv} - V_{cv} \tag{5.17}$$

where, V_{cv} = ideal vertical joint shear strength provided by concrete,

$$= \frac{A_{sc}'}{A_{sc}} V_{jv} \left(0.6 + \frac{c_j \ P_u}{A_g \ f_c'}\right) \qquad (5.18)$$

where, A_{sc} = area of non-prestressed tension reinforcement in one face of the column section,

A_{sc}' = area of non-prestressed compression reinforcement in one face of the column section,

and $c_j = \frac{V_{jh}}{V_{jx} + V_{jy}} = 1.0$ for the specimens tested,

where, V_{jh} = total horizontal shear force in the joint,

V_{jx} = horizontal shear force in the X direction,

and V_{jy} = horizontal shear force in the Y direction.

However, the value of V_{cv} should be less than $0.2bh\sqrt{f_c'}$.

The NZ Code also has a requirement for the development of bars passing through or terminating with a hook at the joint. For the straight bars with yield stresses of 55 ksi, the ratio of the beam height to the column bar diameter (h_b/d_b) is limited to 25 if plastic hinging occurs in the column, and 20 if plastic hinging occurs in the beam. The development length of the hooked bars for the tested specimens is calculated from the relationship

$$l_o = 0.7 \ l_{hb} \qquad (5.19)$$

where, l_o = development length of hooked bars, equal to the straight embedment between critical

section and back edge of the hooked bar (Fig. 5.3),

and l_{hb} = basic development length for a hooked bar.

The value of l_{hb} can be calculated as:

$$l_{hb} = \frac{795\ d_b}{\sqrt{f_c'}\ (psi)} \qquad (5.20)$$

A major difference exists between the NZ Code and ACI-352R in defining the critical section for the calculation of development length. The NZ Code suggests that in cyclic loading, yielding of the beam bars will penetrate into the joint core. Therefore, the critical section is taken at one half of the column depth or $10d_b$, whichever is less, from the face at which the beam bar enters the column (Fig. 5.3).

The design of each specimen is compared to the NZ Code in Table 5.3. In order to make the comparison of the different codes more meaningful, the yield stress for the beam reinforcing bars was increased by 25 percent in the calculations of the NZ Code. The 25 percent increase is also recommended in the commentary to the NZ Code.

Specimens 1 and 3 violated the code requirements by having flexural strength ratios so close to 1.0 to cause plastic hinge formation in the joint. Confinement hoop spacing, resulting from Eq. 5.12, is easily satisfied for all specimens. However, the requirement of the spacing

TABLE 5.3

DESIGN PARAMETERS ACCORDING TO THE NEW ZEALAND CODE

Specimen Number	M_R	s_h (in.)	h/5 (in.)	Provided s_h, (in.)	$\frac{v_{jh}}{\sqrt{f_c'}}$	s_h (in.) Eq. 5.16	V_{jv} (kips)	A_{jv} ($in.^2$)	l_o (in.)	l_{dh} (in.)	Provided l_{dh}, (in.)	Req'd h_b/d_b	Provided h_b/d_b
(1)	(2)	(3)	(4)	(5)	(6)	(7)	(8)	(9)	(10)	(11)	(12)	(13)	(14)
1	1.01	15.1	2.4	4.4	12.6	4.3	206	1.18	7.0	11.1	7.4	20	25.1
2	1.35	14.2	2.4	3.9	12.6	3.7	193	1.07	6.9	11.0	7.4	20	23.0
3	1.07	12.6	2.4	3.3	11.4	4.3	205	1.17	6.3	10.4	7.4	20	25.1
4	1.41	11.7	2.4	3.0	11.1	3.7	192	1.11	6.1	10.2	7.4	20	23.0
5	0.89	14.2	2.4	5.0	8.8	6.1	159	0.91	5.9	10.0	7.8	25	25.1
6	0.87	16.0	2.4	3.7	9.2	6.1	160	0.91	5.9	10.0	7.8	25	25.1
7	1.17	20.7	2.4	4.4	11.1	5.3	152	0.80	6.4	10.5	7.8	20	23.0
8	1.16	19.6	2.4	3.3	11.0	5.3	152	0.81	6.3	10.4	7.8	20	23.0
9	1.93	26.4	2.8	4.3	13.0	3.5	214	1.01	8.2	13.2	9.4	20	18.9
10	1.58	27.0	2.8	5.0	11.7	4.5	191	0.90	8.3	13.3	9.4	20	18.9
11	1.56	16.3	2.8	4.6	7.4	5.1	156	0.88	6.4	11.3	9.4	20	25.1
12	1.17	18.2	2.8	5.0	7.2	6.1	142	0.79	6.8	11.7	9.4	20	25.1

being limited to one-fifth of the column depth is so severe, that it was violated for all specimens.

The horizontal joint shear stress was always less than the allowable limit of 18 $\sqrt{f_c'}$. Horizontal shear reinforcement spacing, determined from Eq. 5.16 is listed in column 7 of Table 5.3. The spacing was satisfied for all specimens except specimens 9 and 10. The calculated and provided hoop spacing for specimens 1 and 2 were close enough to be considered acceptable.

The vertical joint shear forces were calculated from the geometry of the joint as the product of the horizontal joint shear forces multiplied by the ratio of the total beam depth to the total column depth. The provided vertical shear reinforcement for specimens 1 through 8, and specimens 11 and 12 was equal to the area of two number 6 bars or 0.88 in^2. For specimens 9 and 10, two number 8 bars provided a vertical shear reinforcement area of 1.58 in^2. As shown in column 9 of Table 5.3, the provided vertical shear reinforcement was sufficient for specimens 1 through 6.

Development lengths for the hooked beam bars were calculated and are listed in column 10 of Table 5.3. To make the comparison with the American codes easier, the required development lengths were calculated as measured from the outside face of the column longitudinal

reinforcement where the beam bars frame in (Fig. 5.3), and were recorded under the designation l_{dh} in column 11 of Table 5.3. The column depths were not large enough to develop the hooked bars in any of the specimens tested. The ratios of beam depth to column bar diameter are listed in column 13 of Table 5.3. This ratio was compared with the acceptable value of 20 except for specimens 5 and 6, where due to the flexural hinging of the columns, the acceptable limit is 25. The results were satisfactory for all specimens except for specimens 7 through 10.

5.5 Discussion of the Codes

Recommendations of ACI-352, ACI-352R, and the NZ Code were discussed in detail in the previous sections. The ACI-352 recommendations are based on the results of tests of reinforced concrete beam to column joints, but many of the shear strength design equations came directly from results of tests of reinforced concrete members subjected to a combination of compression, shear, and flexural loading. This conservative assumption has resulted in joints requiring large amounts of transverse reinforcement in the joint.

The ACI-352R employs neither the reinforced concrete member assumptions of ACI-352, nor the complex model used

in the NZ Code. As described in Section 5.3, the design philosophy of this code is that an exterior joint can carry shear stresses up to 12 $\sqrt{f_c'}$ provided that the concrete in the joint is adequately confined. The confinement requirements of ACI-352R are less severe than those of ACI-352 for the specimens tested in this investigation, but they still do not offer any significant simplification in the design of the connections.

The NZ Code recommendations assume that a potential failure plane extends from one edge of the joint to the diagonally opposite edge. The contribution of concrete to resisting horizontal joint shear forces in most cases is assumed to be zero. Both horizontal and vertical reinforcement are required to resist the shear forces. In addition, severe confinement requirements result in a large number of hoops to be placed within the joint.

Although each of the code requirements are important when considered individually, attention must also be paid to the combination of these requirements. Specimen 11 violated the requirements of ACI-352R only in one case; the provided hoop spacing was 4.6 in. compared to the required hoop spacing of 3.5 in. However, this specimen surpassed the minimum code requirements in many other cases. The flexural strength ratio for specimen 11 was

1.56 compared to the minimum code value of 1.4. The joint shear stress was only 62 percent of the allowable value. The provided development length of 9.5 in. for the hooked beam bars was considerably larger than the minimum required length of 6.9 in.

In spite of the noncompliance of specimen 11 with the recommended hoop spacing of ACI-352R, the overall behavior of this specimen was satisfactory. Specimen 11 was capable of sustaining its maximum load of the first cycle through the fifth cycle of loading without any severe loss of stiffness. It is therefore necessary to compare all code requirements with the provided values in a specimen before judgement is made on the acceptability or rejection of the design of a connection.

5.6 Design Recommendations

The load vs. displacement hysteretic behavior is perhaps the best means for judgement of the overall performance of a subassemblage.

A survey of all exterior beam to column connections tested by other investigators was carried out and the plots of applied load vs. displacement were examined. In order to discard any dissimilarities, only specimens with no transverse beams or slabs were studied. Also excluded from the study were specimens with no hoops in the joint

region and specimens in which special beam reinforcing arrangements were made to force the hinging region away from the joint. Exterior joints with stubs at the back face of the joint to provide additional embedment length for the beam bars were not included in the study either. These exclusions led to the study of exterior beam to column connections commonly used in structures.

For each specimen studied, the yield load and the yield displacement were determined as the point where a sudden change of slope or flattening of load vs. displacement curve was observed. Displacement ductilities were then calculated for each cycle as the maximum displacement at the end of that cycle devided by the yield displacement. Because the cyclic load carrying capacity of subassemblages is very important, the displacement ductilities were calculated only for the cycles where the maximum load was greater than the yield load. The displacement ductilities for each applicable cycle and their summation, called total displacement ductility, for the examined specimens are shown in Table 5.4. The total displacement ductility is an excellent representative of the overall cyclic behavior of a specimen.

The actual loading history and the number and levels of inelastic excursions a frame may be subjected to

TABLE 5.4

DISPLACEMENT DUCTILITIES

Source	Ref. No.	Spec. No.	Cyclic Displacement Ductility	Total Displ. Ductility
Hanson	4	1	2.0, 2.4, 4.0, 4.8	13.2*
		2	1.86, 2.6	4.4*
		3	1.8, 2.3, 4.3, 4.9, 5.6, 6.4, 8.2	33.5*
		4	1.0, 2.3	3.3
		5	1.3	1.3
Hanson	5	4	2.0, 3.1, 4.3	9.4*
		5	2.5, 3.1, 5.7, 6.7	18.0
Megget	7	1	2.45, 4.8	7.25*
		2	3.0	3.0*
		3	3.0, 4.7	7.7*
Smith	8	4	2.0	2.0*
Renton	10	1	1.0, 1.2	2.2
		2	4.45	4.45
		3	1.3, 1.6, 3.8	6.7
		4	2.2, 5.8	8.0
Uzumeri	13	3	2.45, 5.3	7.75
		4	1.35, 2.75, 5.5, 5.75, 10.4	25.75
		6	2.4, 4.1, 5.2, 2@6.2, 6.6	30.7
		7	1.9, 2.15, 4.4, 6.2	14.65
		8	1.7, 2.4, 3.8	7.9
Lee	14	1	3@3.1, 3@4.4	22.5
		2	4@4.1, 2@5.2	26.8
		3	2.0, 3@4.0	14.0
		4	4@4.0, 2@5.1	26.2
		5	4@3.65, 4@5.2	35.4
		6	4@3.65, 3@5.2	30.2
		7	2@4.25, 6.3	14.8
		8	3@4.0, 2@6.0	24.0

TABLE 5.4 (Cont'd)

DISPLACEMENT DUCTILITIES

Source	Ref. No.	Spec. No.	Cyclic Displacement Ductility	Total Displ. Ductility
Scribner	19	1	6@3.8, 6@6.65	62.7
		2	6@3.25, 6@5.6	53.1
		3	4@3.8	15.2
		4	6@2.7, 3.6	19.8
		5	6@3.45, 2@5.25	31.2
		6	6@3.9, 4@5.7	46.2
		7	6@4.15, 2@5.3	35.5
		8	3@2.6, 3.3	11.1
		9	5@3.5	17.5
		10	5@3.35	16.75
		11	3@3.5	10.5
		12	3.5, 3@3.7	14.6
Scarpas	16	1	2@1.4, 2@3.0, 2@4.3, 5.0, 5.85	28.25
		2	1.1, 1.8, 2@3.0, 2@4.4, 3@5.85	35.25
		3	2@1.1, 2@2.25, 2@3.4, 2@4.5, @25.5	33.50
This Study	—	1	1.4, 1.6	3.0
		2	1.35	1.35
		3	1.5	1.5
		4	1.5, 2.0, 2.5, 3.0, 3.5	12.5
		9	1.3, 1.6, 2.0	4.9
		11	1.4, 1.6, 2.0, 2.4, 2.7, 3.0, 3.3	16.4

*Rotational ductilites are listed from plots of applied load vs. specimen curvature.

during an earthquake is of course difficult, if not impossible to predict. Although in many investigations, specimens are subjected to displacement ductilities as large as 4.0 or 6.0, the effectiveness of such large displacements in terms of their applicability to actual structural frames subjected to an earthquake remains questionable. These high ductilities are accompanied by very large story drifts which are not permissible by most building codes. Considering the overall stability of a structure, displacement ductilities ranging between 2 and 3 more realistically represent the average deformations which a subassemblage may undergo.

For the purpose of evaluation of the existing test data, a sum of displacement ductilities greater than or equal to 10 was selected as the lower limit for satisfactory behavior under severe earthquake loading. Specimens with total displacement ductilities equal to or larger than 10 can sustain their yield load for four cycles of loading at displacement ductility of 2.5. This criterion was used to "accept" or "reject" the behavior of the surveyed specimens. The results of this acceptance criteria are shown in Fig. 5.4, where the accepted specimens are shown with full symbols, while hollow symbols are used to indicate the rejected specimens.

Of the four design parameters discussed in section 2.2, information about three of them is included in Fig. 5.4. The flexural strength ratio and the joint shear stress are shown on the vertical and the horizontal axis respectively. The amount of the joint transverse reinforcement is incorporated into the figure by the use of different symbols. The data points were divided into four groups depending on the value of the transverse reinforcement ratio. Due to the large scatter of the existing data points, it was not practical to choose uniform increments for the modified transverse reinforcement ratios. The fourth variable, effect of transverse beam and slab, is not included in Fig. 5.4. However, since the additional confinement provided by the transverse beams improves the behavior of the subassemblage, the information in Fig. 5.4 could be safely applied to the connections where transverse beams and slabs are present.

In order to develop a simplified design chart, a lower limit for the flexural strength ratio and an upper limit for the joint shear stress were selected. Although it is possible for specimens with flexural strength ratios less than 1.0, such as specimens 5 and 6 of this study, to perform satisfactorily, the design recommendations presented here are based on the "strong

column-weak beam" philosophy, where hinging of the column is to be avoided. The minimum flexural strength ratio is selected as 1.4 to make sure that flexural hinging will occur in the beam. The limit of 1.4 was chosen based on the result of specimen 4, where a flexural strength ratio of 1.41 resulted in flexural hinging and most of the damage being limited to the beam.

A few specimens, including specimen 4 of this study, performed satisfactorily with joint shear stresses greater than $12\sqrt{f_c'}$. Although more data is needed for specimens with joint shear stresses larger than $12\sqrt{f_c'}$, based on the available information, the upper limit for the joint shear stress was selected as $13\sqrt{f_c'}$.

The next step in the development of the design chart was to divide the recommended portion of the chart into a few regions with different joint transverse reinforcement ratios.

The first line, line A, for recommended modified transverse reinforcement ratio of 0.7 percent, was drawn through the two points representing two specimens with modified transverse reinforcement ratios ranging from 0.41 to 0.70 percent which had performed satisfactorily. This line divided the chart into two regions. All specimens designated with a "square" symbol and to the left of line A are shown with solid squares, indicating

that they performed satisfactorily. The specimens designated with a square and to the right of line A are shown with a hollow symbol, meaning that their performance was unsatisfactory.

The second line, line B, was drawn parallel to line A through the solid "hexagon" symbol furthest to the right of line A.

There are very few test data points available to the right of line B. For the region to the right of line B, based on the satisfactory performance of specimen 4 of this study with ρ_{tm} equal to 1.86 percent, a conservative modified transverse reinforcement ratio of 2.0 percent is recommended.

The primary advantages of this chart are its simplicity and convenience to use. For any exterior beam to column connection in a frame, the flexural strength ratio and the joint shear stress can be calculated readily. Knowing the values for these two parameters, the corresponding recommended joint transverse reinforcement ratio can be obtained from the chart. For example, a connection with flexural strength ratio of 2.0, and joint shear stress of $8\sqrt{f_c'}$ will perform satisfactorily if at least 1.0 percent transverse reinforcement is provided within the joint. In all cases, at least two sets of hoops should be placed within

the joint. The spacing of the hoops should be kept uniform in accordance with the recommendations of ACI-352R.

As discussed earlier, this chart is derived for specimens without transverse beams and slab. Considering the beneficial effects, resulting from the presence of transverse beams on the behavior of specimens tested in this investigation, these design recommendations could be safely applied to specimens where transverse beams and slabs are present. Additional data will be helpful in redefining the location of the recommended regions and choosing more uniform increments in the modified transverse reinforcement ratios. Because larger shear stresses are often encountered in most joints, additional data for specimens with shear stresses between $10\sqrt{f_c'}$ and $14\sqrt{f_c'}$ and flexural strength ratios ranging between 1.4 and 2.0 could make a significant contribution towards the improvement of this design chart.

CHAPTER 6

SUMMARY AND CONCLUSIONS

6.1 Summary of Research Program

Design of reinforced concrete beam to column joints according to the present recommendations of ACI-ASCE Committee 352 (12) results in congested connections which are usually very difficult to construct. The primary objective of this investigation was to obtain sufficient experimental evidence which would justify a reduction in the amount of transverse reinforcement placed in some joints without jeopardizing the overall cyclic load carrying capacity of the subassemblage.

To satisfy the above objective, twelve full-size exterior beam-column subassemblies were constructed and tested. The primary variables which were studied consisted of the ratio of the sum of the flexural strengths of the columns to that of the beam (flexural strength ratio), the amount of transverse reinforcement placed within the joint, the shear stress in the joint as a multiple of $\sqrt{f_c'}$, and the inclusion of transverse beams and slab for half of the specimens.

Based on the available data from previous studies by other investigators, the following ranges were selected for the above variables. The flexural strength ratio varied between 1.1 and 2.0. The transverse reinforcement in the joint was limited to two or three sets of ties which resulted in a percentage of transverse reinforcement that ranged from 0.86 to 1.86. In all cases, except for specimen 4, there was less transverse reinforcement in the joint than that recommended by the ACI-ASCE Committee 352 recommendations. The design joint shear stress varied between $10\sqrt{f_c'}$ and $14\sqrt{f_c'}$ (psi units). Because in most structures connections are confined by transverse beams, specimens were designed in pairs. For each bare specimen, a similar specimen was constructed with transverse beams and slab while the remaining design parameters were kept the same. Beam and column portions of the specimens were designed according to the guidelines of Appendix A of ACI Building Code for Reinforced Concrete (17).

Two different testing frames were used in this study. Specimens 1 through 4 were tested with the column portion of the specimens placed horizontally in the testing frame. Columns were tied to the testing frame near their free end points with roller bearings to represent points of contraflexure. Cyclic shear loads

were applied near the free end of the beam portion of the specimens. Specimens 5 through 12 were placed in the testing frame such that the column portion of the specimens remained vertical. In addition to the two ends of the column, the free end of the beam portion of the specimens were also tied down to the testing frame with simple supports. Shear forces were then applied near the free end of the upper column half.

Specimens were subjected to a displacement controlled loading history. In the case of specimens 1 through 6, loads were applied slowly until the specimen had reached a displacement 1.5 times that of its observed yield displacement. The direction of loading was then reversed and the specimen was loaded in the negative direction to a displacement equal to 1.5 times its yield displacement. Specimens were subjected to five more cycles of loading and the maximum displacement at each cycle increased by 0.5 times the yield displacement from the previous cycle. For specimens 7 through 12 the first cycle of loading terminated at the yield displacement and the maximum displacement for each of the five subsequent cycles of loading was increased by 0.25 times the yield displacement. In all cases the column portion of the specimens were subjected to an axial load which remained constant throughout the test.

A continuous plot of the applied load vs. the load point displacement was recorded during the tests. Electrical resistance strain gages were bonded to the longitudinal and transverse reinforcing bars in critical regions and their measurements were recorded at discrete points. In bare specimens, Linear Variable Differential Transducers (LVDTs) were placed on the lateral face of the joint to measure the joint shear deformations. The LVDT measurements were also recorded at discrete load points throughout the test.

Several observations were common among all specimens. In all bare specimens diagonal cracks connecting the opposite corners of the joint were observed during the first cycle of loading. Many shorter and narrower cracks were also observed parallel to the two major diagonal cracks. In bare specimens there was a flexural hinging region in the beam portion of the specimen near the joint. In specimens with transverse beams and slab, due to unequal longitudinal reinforcement in the beam and slab, the flexural cracks formed when the slab reinforcement was in tension did not close completely with the reversal of the loading direction. This resulted in unequal pinching of the hysteresis loops. Flexural cracks crossed the entire width of the slab and the size of the cracks indicated that even the

slab longitudinal reinforcement furthest away from the main beam may have yielded in tension. Torsional cracks which started at the back face of the transverse beam, moved spirally upward and after crossing a small portion of the slab penetrated into the upper column half. Data from the strain gages indicated that there was always some pull out or slippage of the longitudinal reinforcement from the joint.

6.2 Conclusions

The following conclusions are drawn based on the results of the specimens tested in this investigation and the work done by other researchers:

1. The flexural strength ratio for beam-column subassemblies should be larger than 1.4. The flexural strength ratio is very important in stabilizing the cyclic load carrying capacity of beam-column subassemblies. Although specimens 5 and 6 with flexural strength ratios smaller than 1.0 developed flexural plastic hinges in the columns and were capable of sustaining their maximum first cycle load throughout the test, to ensure that plastic flexural hinges form in beams rather than columns, the flexural strength ratio for bare subassemblies should be greater than 1.4.

2. To postpone rapid deterioration of joint

concrete, the shear stress in the joint should be kept below $13\sqrt{f_c'}$ (psi units). The hysteretic behavior of the subassemblages was closely linked to the shear stress level in the joint as a multiple of $\sqrt{f_c'}$. In specimens with low shear stresses (less than $12\sqrt{f_c'}$) deterioration of the joint concrete was delayed significantly and the cyclic load carrying capacity of the subassemblages were more stable throughout the test. Lower shear stresses in the joint also resulted in delay or elimination of beam bar pull out or column bar slippage.

3. Larger percentages of transverse reinforcement did improve the behavior of the beam to column joint. The increase in the transverse reinforcement ratio in the joint provided additional confinement for the joint concrete and delayed the deterioration of the concrete in the joint. The improved confinement provided by the additional transverse reinforcement resulted in a delay or elimination of beam bar pull out or column longitudinal reinforcement slippage from the joint.

4. The additional confinement provided by the transverse beams which were not directly loaded significantly increased the energy dissipation and the stability of the hysteretic response. The beneficial effects of transverse beams proved to be so great that

their presence in an actual design should not be ignored. The improved confinement of the joint led to better anchorage conditions for the reinforcing bars and delayed the initiation of main beam bar pull out and column longitudinal reinforcement slippage from the joint.

5. Slippage or pull out of the bars was reduced or postponed with: (1) increases in the flexural strength ratio, (2) increases in the transverse reinforcement ratio, (3) reduction in the joint shear stress, and (4) presence of transverse beams and slab.

6. The design chart prepared from both the data from this study and the work done by other researchers is an excellent guide for the design of exterior beam to column connections. This design chart sets a lower limit of 1.4 for the flexural strength ratio and an upper limit of $13\sqrt{f_c'}$ for the joint shear stress. There is sufficient experimental evidence indicating that when designing a beam to column connection, all design parameters should be considered collectively. In most cases the recommendations of this design chart lead to lower amounts of joint transverse reinforcement than that suggested by ACI-ASCE Committee 352 (12). Because the presence of transverse beams was shown to improve the behavior of subassemblies, the design chart which is developed for bare specimens could be safely applied to

the design of specimens with transverse beams and slab.

7. Based on the experimental results and the design chart developed from this and other experimental studies, it is apparent that excessive amounts of transverse reinforcement are not required for satisfactory behavior of most beam to column connections. However, in some cases where the flexural strength ratio is near 1.4 and the joint shear stresses are high (i.e. near $14\sqrt{f_c'}$), congestion of reinforcement in the joint can not be avoided.

6.3 Recommendations for Further Research

Although this study answered many questions with regards to the behavior of beam to column connections, several questions were raised as a result of these tests which deserve further investigation. The following topics are the more important questions which need to be answered.

1. The effective width of slabs in tension should be studied further. In calculating the flexural strength ratio for connections, where in many cases slabs are present, more information is needed for estimating an effective width for the slab beyond which the contribution of the slab longitudinal reinforcement to the flexural strength of the beam and slab could be

ignored.

2. Distribution of shear stresses in joints confined by transverse beams need to be investigated. This problem is especially complicated where slabs are present. In such cases a part of the input shear force is distributed along the transverse beam near the joint rather than being concentrated at the core of the joint.

3. More information is needed on the effect of the loading history on the overall behavior of subassemblages. In judging the behavior of subassemblies by criteria which depend on displacement ductilities, such as the one used in Chapter 5 of this report, it is important to understand what effect, if any, the loading history may have on the total displacement ductility sustained by a subassemblage.

4. Specimens should be tested to provide more information for the ranges of joint shear stresses between $10\sqrt{f_c'}$ and $14\sqrt{f_c'}$ (psi units) and the flexural strength ratios between 1.4 and 3.0. Presently there is little data available for this region of the design chart presented in Chapter 5. Additional data points are needed to locate the defining boundary lines more precisely.

BIBLIOGRAPHY

BIBLIOGRAPHY

1. Uniform Building Code, 1979 Edition, International Conference of Building Officials, Whittier, California, 1979.

2. Lew, H.S., Leyendecker, E.V., and Dikkers, R.D., "Engineering Aspects of the 1971 San Fernando Earthquake," National Bureau of Standards, December 1971, 412 pp.

3. EERI Reconnaissance Report, "Managua, Nicaragua Earthquake of December 23, 1972," May 1973, 214 pp.

4. Hanson, N.W., and Conner, H.W., "Seismic Resistance of Reinforced Concrete Beam-Column Joints," Journal of the Structural Division, ASCE, No. ST5, October 1967, pp. 533-560.

5. Hanson, N.W., "Seismic Resistance of Concrete Frames with Grade 60 Reinforcement," Journal of the Structural Division, ASCE, No. ST6, June 1971, pp. 1685-1700.

6. Hanson, N.W., and Conner, H.W., "Tests of Reinforced Concrete Beam-Column Joints under Simulated Seismic Loading," Portland Cement Association Research and Development Bulletin, RD012.01D, 1972.

7. Megget, L.M., "Anchorage of Beam Reinforcement in Seismic Resistant Reinforced Concrete Frames," Master of Engineering Report, University of Canterbury, New Zealand, February 1971, 68 pp.

8. Smith, B.J., "Exterior Reinforced Concrete Joints with Low Axial Load under Seismic Loading," Master of Engineering Report, University of Canterbury, New-Zealand, 1972, 86 pp.

9. Patton, R.N., "Behavior under Seismic Loading of Reinforced Concrete Beam-Column Joints with Anchorage Blocks," Master of Engineering Report, University of Canterbury, New Zealand, 1972, 94 pp.

10. Renton, G.W., "The Behavior of Reinforced Concrete Beam-Column Joints under Seismic Loading," Master of Engineering Thesis, University of Canterbury, New Zealand, 1972, 181 pp.

11. Park, R., and Paulay, T., "Behavior of Reinforced Concrete External Beam-Column Joints under Cyclic Loading," Proceedings, Fifth World Conference on Earthquake Engineering, Rome, Italy, June 1973, pp. 772-781.

12. ACI-ASCE Joint Committee 352, "Recommendations for Design of Beam-Column JOints in Monolithic Reinforced Concrete Structures," ACI Journal, July 1976, pp. 375-393.

13. Uzumeri, S.M., and Seckin, M., "Behavior of Reinforced Concrete Beam-Column Joints Subjected to Slow Load Reversals," Publication No. 74-05, Department of Civil Engineering, University of Toronto, March 1974.

14. Lee, D.L.N., "Original and Repaired Reinforced Concrete Beam-Column Subassemblages Subjected to Earthquake Type Loading," Report No. UMEE 76S4, Department of Civil Engineering, University of Michigan, April 1976, 206 pp.

15. Meinheit, D.F., and Jirsa, J.O., "The Shear Strength of Beam-Column Joints," CESRL Report No. 77-1, Department of Civil Engineering, University of Texas at Austin, January 1977, 271 pp.

16. Scarpas, A., "The Inelastic Behavior of Earthquake Resistant Reinforced Concrete Exterior Beam- Column Joints," Report No. 81-2, Department of Civil Engineering, University of Canterbury, New Zealand, February 1981, 84 pp.

17. American Concrete Institute, Committee 318, Building Code Requirements for Reinforced Concrete (318-77), Detroit, Michigan: American Concrete Institute, 1977.

18. American Concrete Institute, Committee 318, Commentary on Building Code Requirements for Reinforced Concrete (318-77), Detroit, Michigan: American Concrete Institute, 1977.

19. Scribner, C.F., and Wight, J.K., "Delaying Shear Strength Decay in Reinforced Concrete Flexural Members under Large Load Reversals," Report No. UMEE 78R2, Department of Civil Engineering, University of Michigan, May 1978, 221 pp.

20. Wight, J.K., and Sozen, M.A., "Strength Decay of Reinforced Concrete Columns under Shear Reversals," Journal of the Structural Division, ASCE, Vol. 101, No. ST5, May 1975, pp. 1053-1065.

21. Hawkins, N.M., Kobayashi, A.S., and Fourney, M.E., "Reversed Cyclic Loading Bond Deterioration Tests," Structural and Mechanics Report SM 75-5, University of Washington, Seattle, Washington, November 1975.

22. Sixth Draft of Revised Recommendations from ACI-ASCE Joint Committee 352, material obtained from J.K. Wight, a committee member, October 1981.

23. Standards Association of New Zealand, "Code of Practice for the Design of Concrete Structures," Draft Standard DZ 3101, June 1980.

24. Soleimani, D., Popov, E.P., and Bertero, V.V., "Hysteretic Behavior of Reinforced Concrete Beam-Column Subassemblages," ACI Journal, November 1979, pp. 1179-1195.

25. Viwathanatepa, S., Popov, E.P., and Bertero, V.V., "Seismic Behavior of Reinforced Concrete Interior Beam-Column Subassemblages," Report No. UCB/EERC-79/14, Earthquake Engineering Reasearch Center, University of California at Berkeley, June 1979, 184 pp.

26. Beckingsale, C.W., "Post-Elastic Behavior of Reinforced Concrete Beam-Column Joints," Ph.d. Thesis, University of Canterbury, New Zealand, 1978, 359 pp.

27. Birss, G.R., "The Elastic Behavior of Earthquake Resistant RC Interior Beam-Column Joints," Research Report 78-13, University of Canterbury, New Zealand February 1978, 96 pp.

28. Jirsa, J.O., "Seismic Behavior of RC Connections (Beam-Column Joints) State-of-the-Art, "Proceeding, 7WCEE, Istanbul, Turkey, September 1980.

29. Jirsa, J.O., et al., "Factors Influencing the Shear Strength of Beam-Column Joints," Proceedings of the U.S. National Conference on Earthquake Engineering, Ann Arbor, Michigan, June 1975, pp. 297-305.

30. Uzumeri, S.M., "strength and Ductility of Cast-in-Place Beam-Column Joints," Reinforced Concrete Structures in Seismic Zones, SP-53, American Concrete Institute, Detroit, 1977, pp. 293-350.

31. Zhang, Liande, and Jirsa, J.O., "Shear Strength of Reinforced Concrete Planar Frame Joints," Paper presented at the US/PRC Workshop on Seismic Analysis and Design of RC Structures, University of Michigan, Ann Arbor, May 1981.

32. Park, R., and Paulay, T., Reinforced Concret Structures, John Wiley & Sons, New York, 1975, 769 pp.

33. Popov, E.P., "Seismic Behavior of Structural Subassemblages," Journal of the Structural Division, ASCE, Vol. 106, No. ST7, July 1980, pp. 1451-1474.

34. Paulay, T., Park, R., and Priestley, M.J.N., "Reinforced Concrete Beam-Column Joints under Seismic Actions," ACI Journal, November 1978, pp. 585-593.

35. Megget, L.M., "Exterior Reinforced Concrete Joints With and Without Intersecting Beams under Seismic Loading," Bulletin, New Zealand National Society for Earthquake Engineering, Vol. 11, 1973, pp. 115-167.

36. Blakeley, R.W.G., et al. "Performance of Large Reinforced Concrete Beam-Column Joints under Cyclic Loading," Proceedings, Sixth World Conference on Earthquake Engineering, New Delhi, India, January 1977, pp. 3095-3100.

37. Bertero, V.V., and Popov, E.P., "Hysteretic Behavior of Reinforced Concrete Flexural Members with Special Web Reinforcement," Proceedings, U.S. National Conference on Earthquake Engineering , Ann Arbor, Michigan, June 1975, pp. 316-326.

38. Mitchell, D., and Collins, M.P., "Diagonal Compression Field Theory - A Rational Model for Structural Concrete in Pure Torsion," ACI Journal, Vol. 71, No. 8, August 1974, pp. 396-408.

39. Park, R., et al., "Tests on Interior Reinforced Concrete Beam-Column Joints," Bulletin of the New Zealand National Society for Earthquake Engineering, Vol. 14, No. 2, June 1981, pp. 81-92.

FIGURES

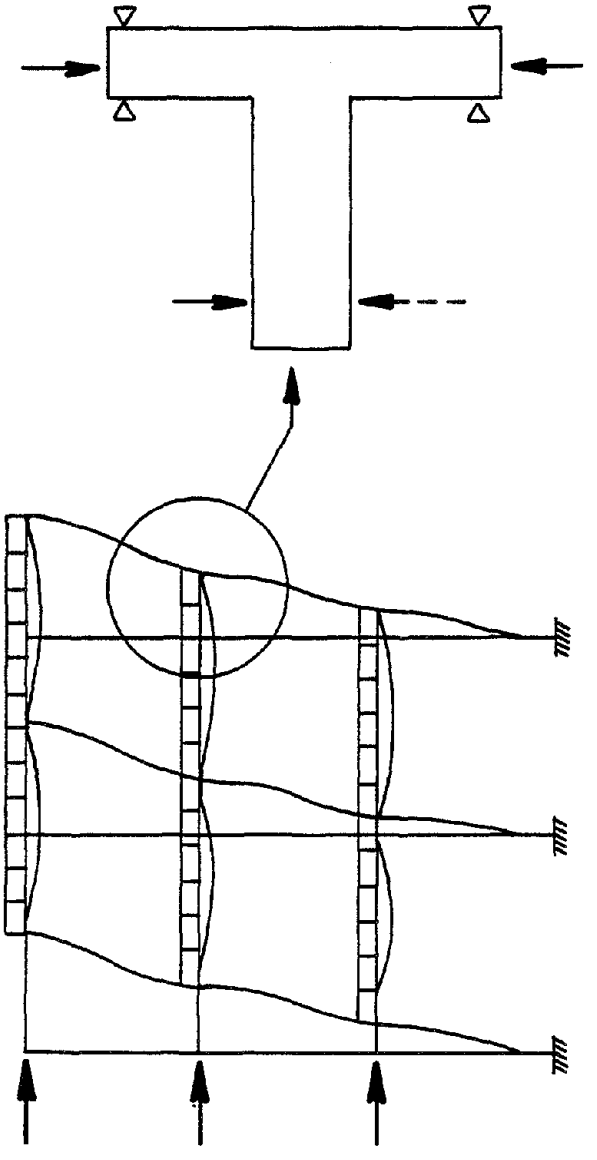

Fig. 2.1. Origin of Test Specimens.

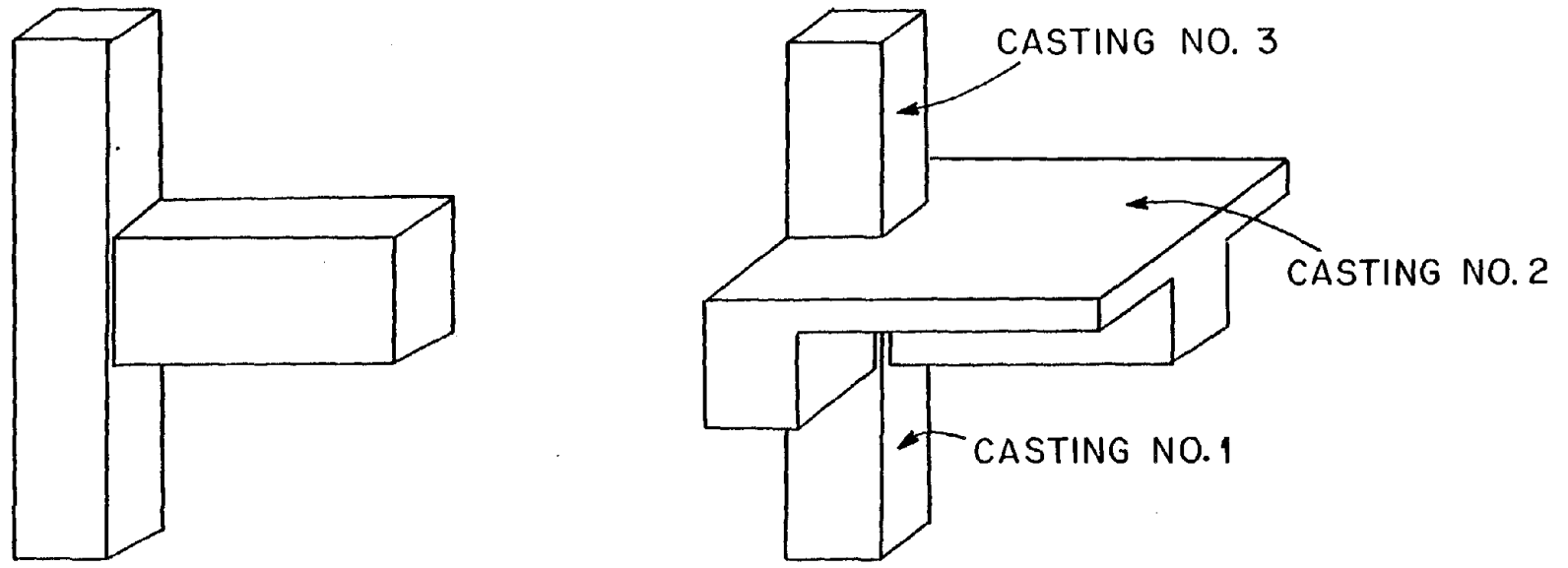

Fig. 2.2. General View of Test Specimens.

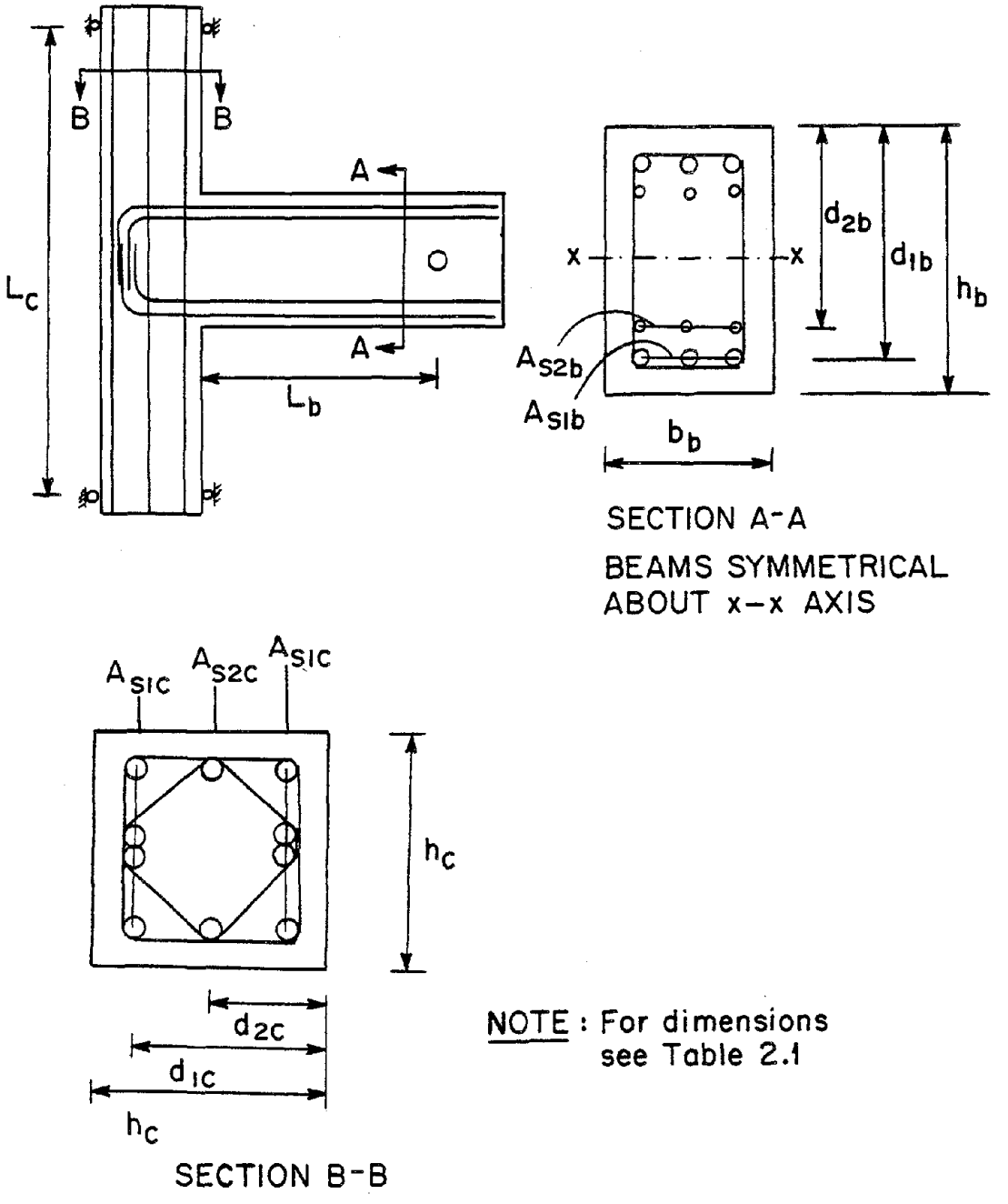

Fig. 2.3. Configuration and Dimension Designation for Bare Specimens.

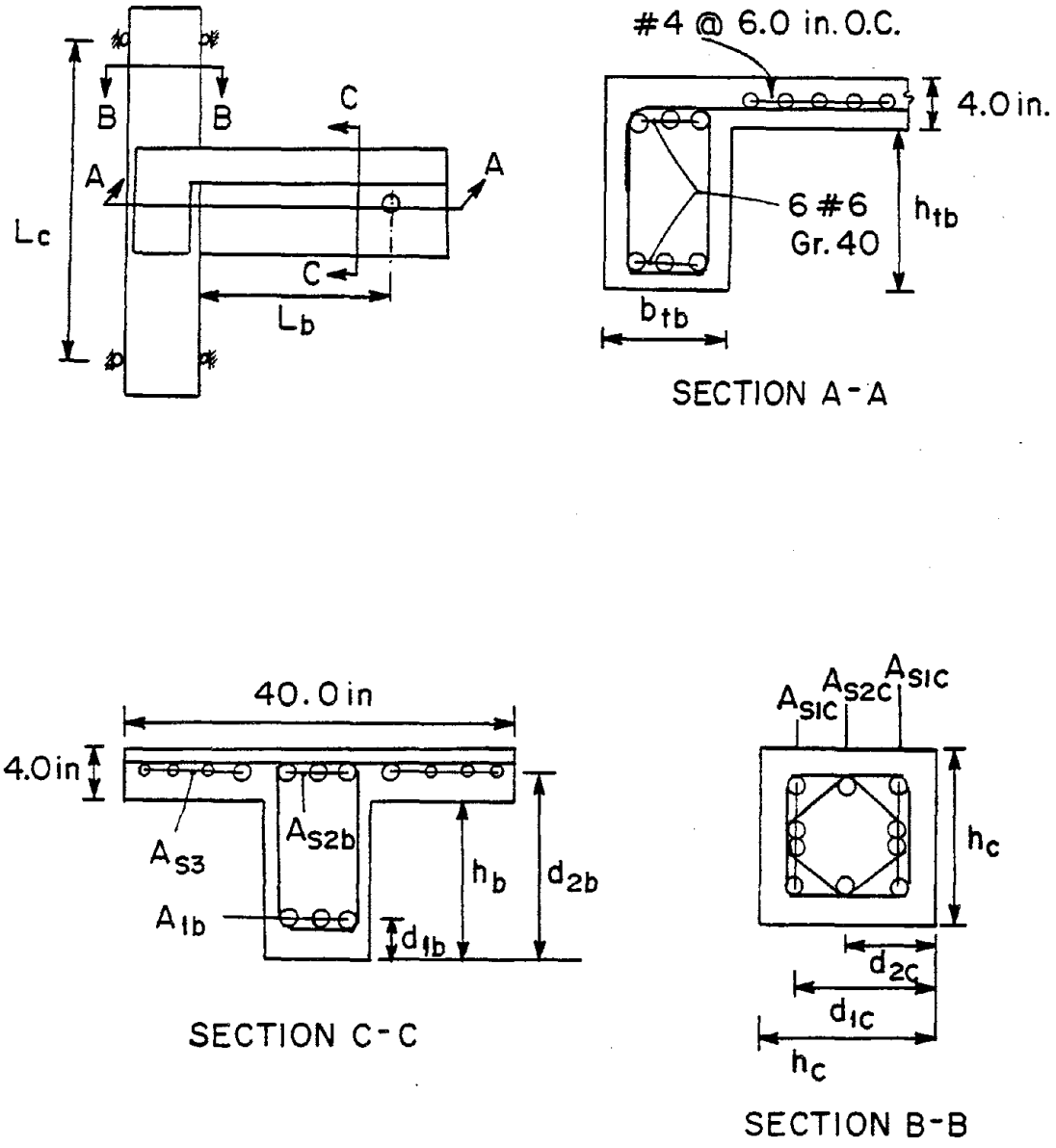

NOTE: For dimensions see Table 2.2

Fig. 2.4. Configuration and Dimension Designation for Specimens with Transverse Beams and Slab.

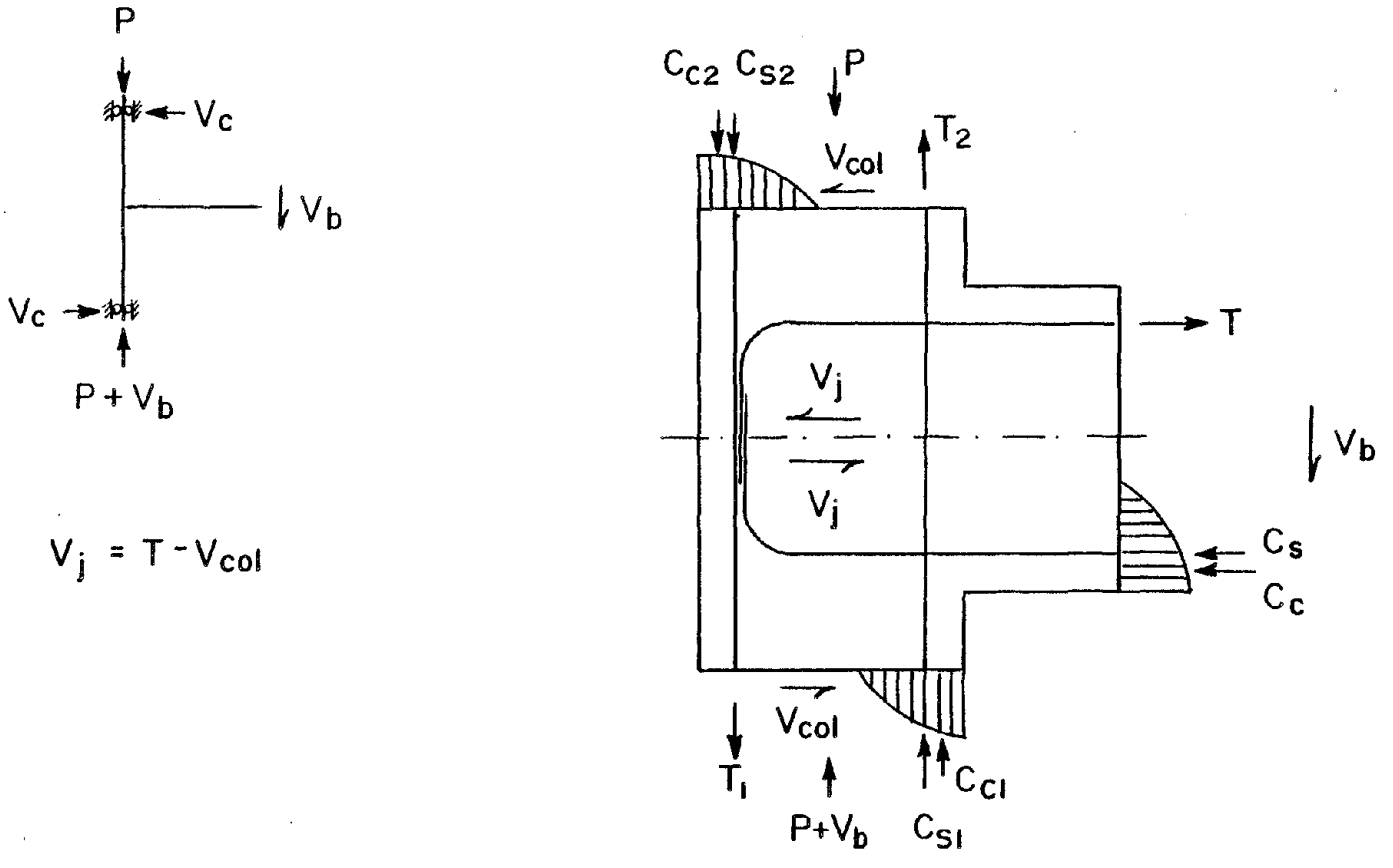

Fig. 2.5. Forces Acting on an External Joint.

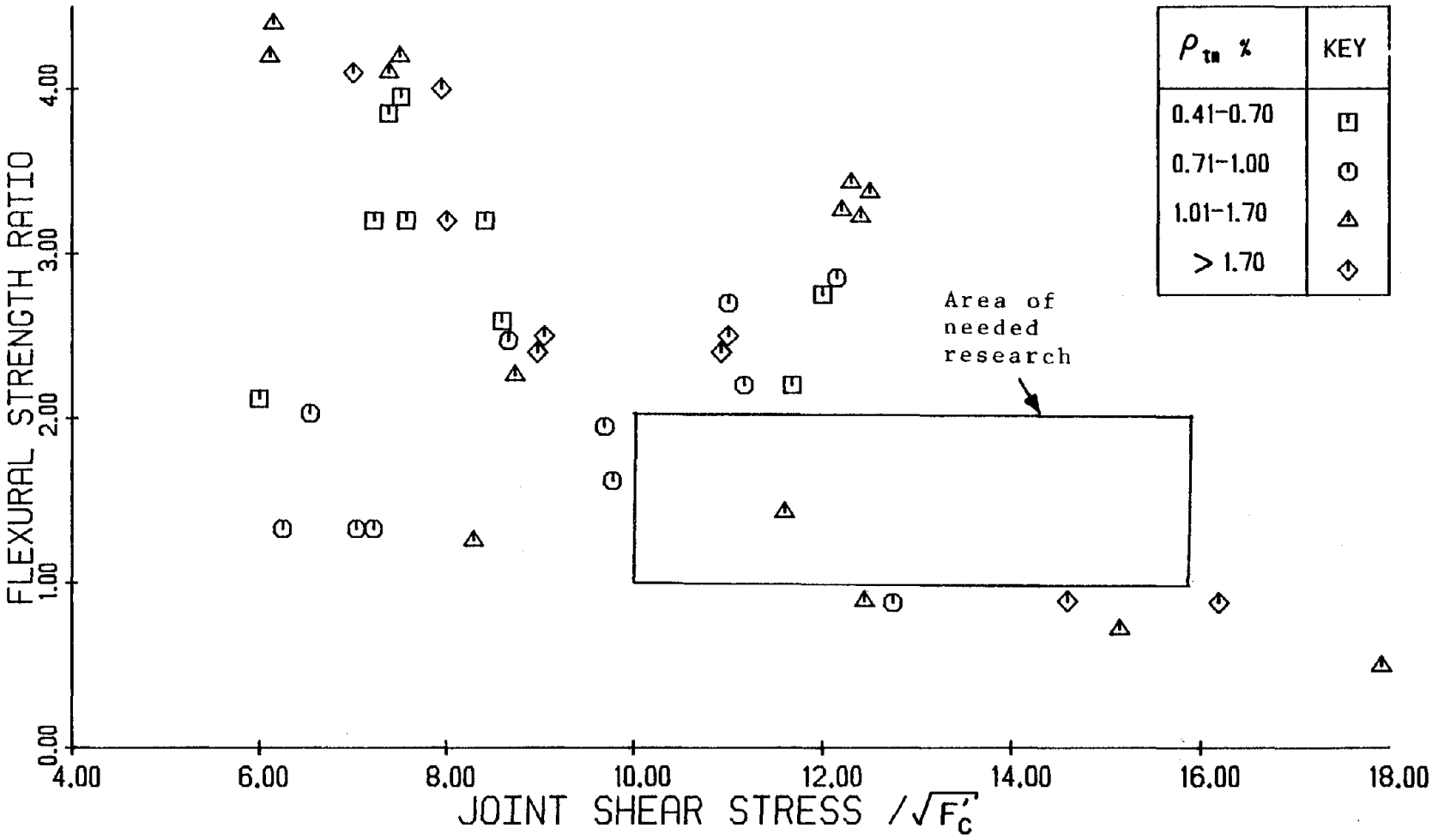

Fig. 2.6. Specimens Tested by Other Researchers.

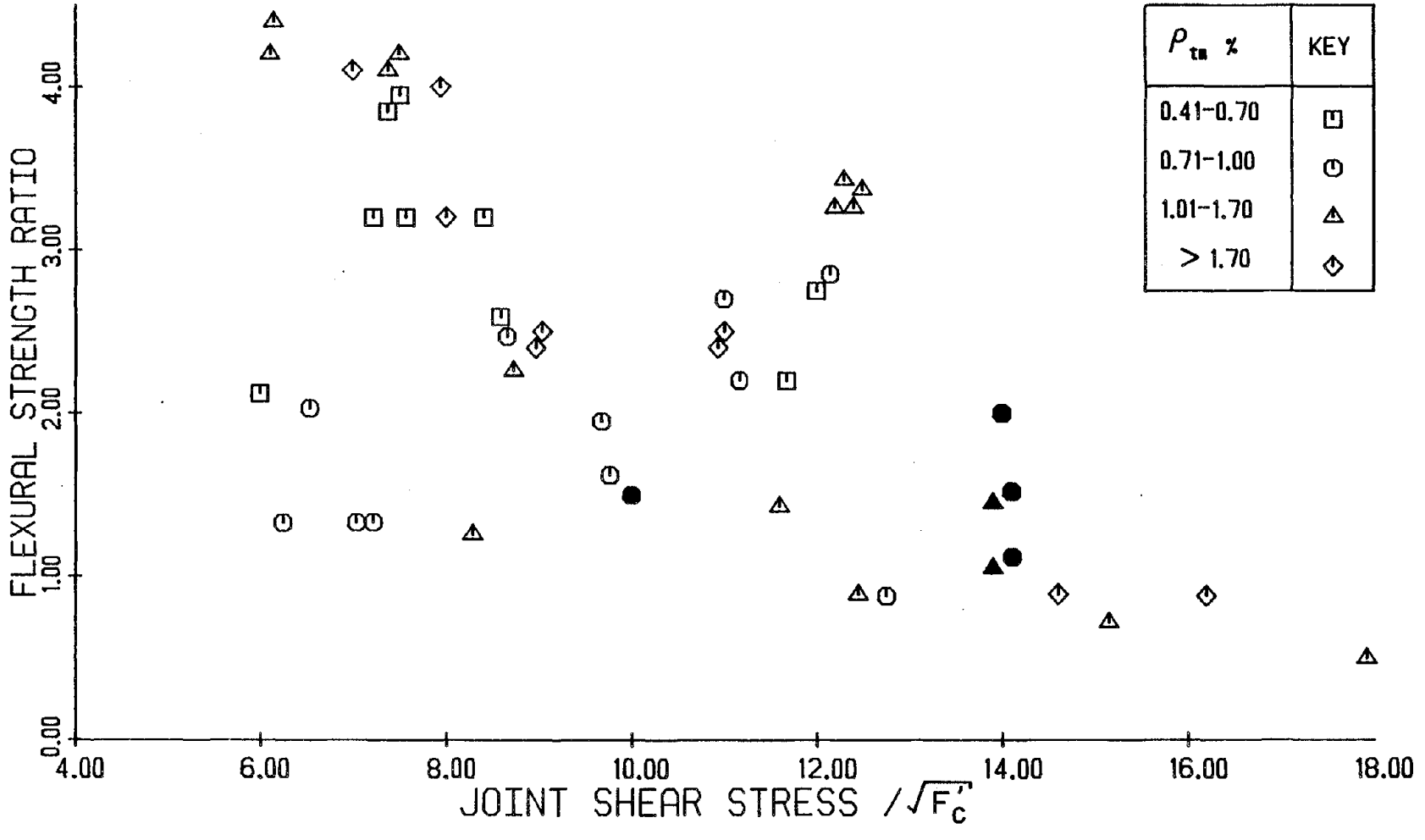

Fig. 2.7. Selected Design Values for the Primary Variables in Tested Specimens.

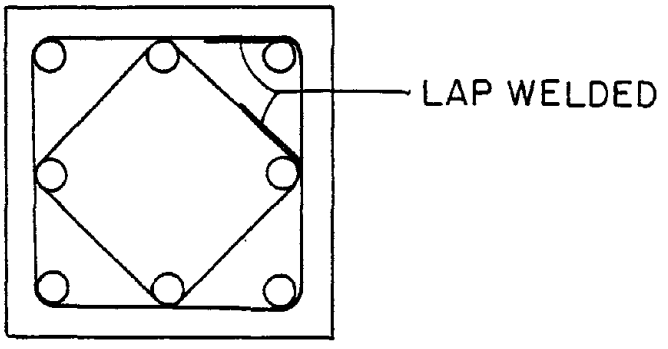

Fig. 2.8. Configuration of Transverse Reinforcement Used in Columns.

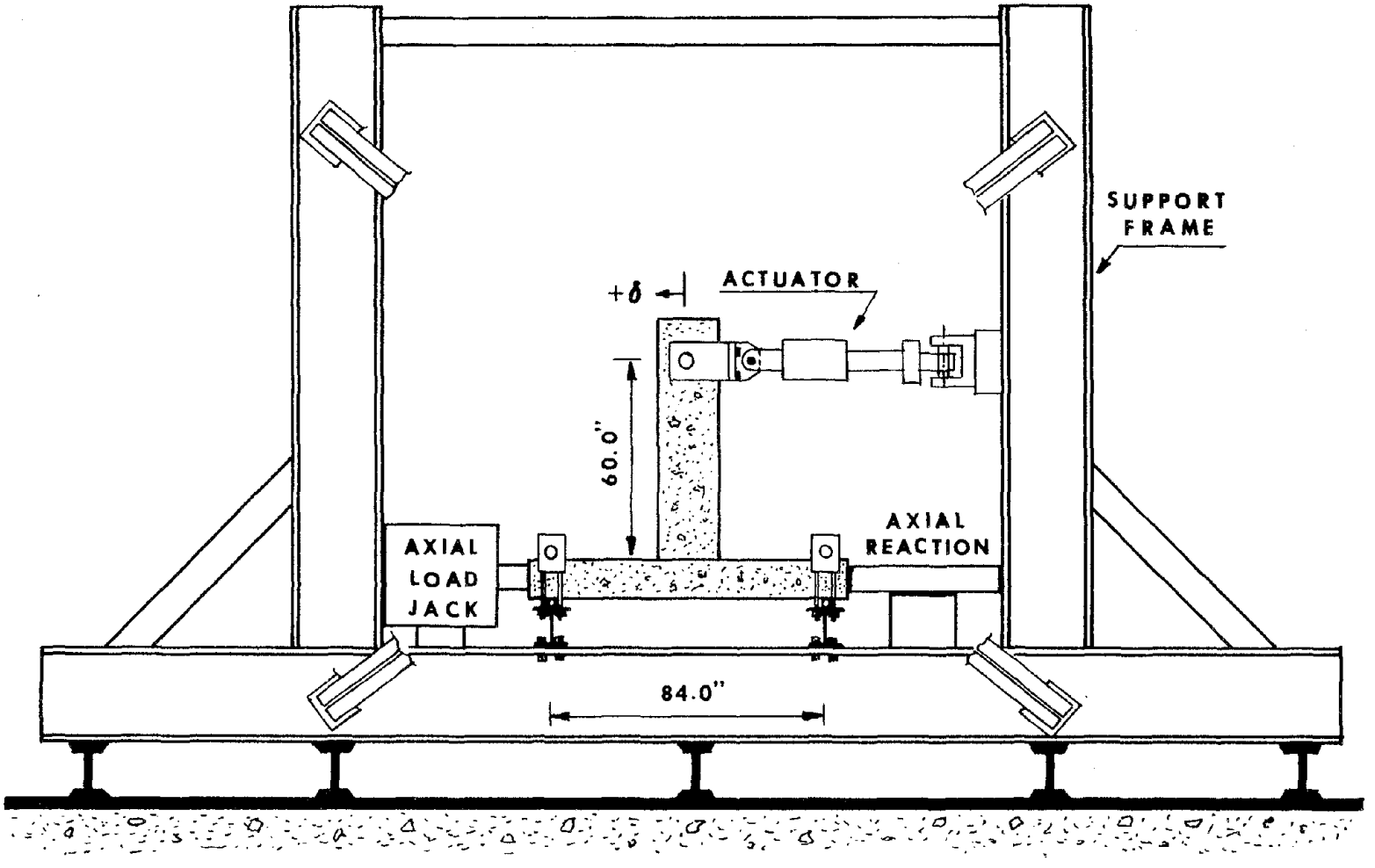

Fig. 2.9. Testing Frame 1, Used for Specimens 1 through 4.

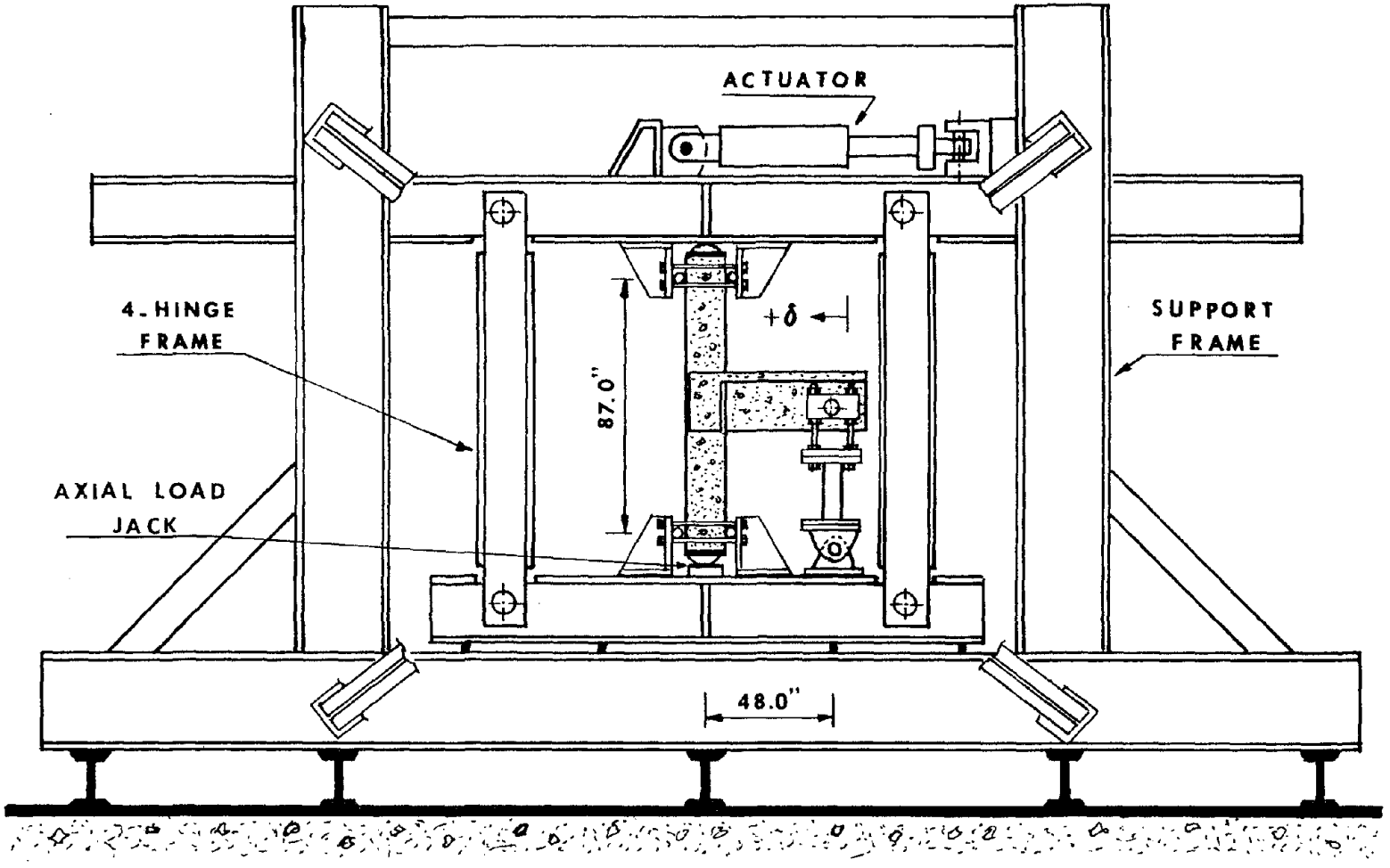

Fig. 2.10. Testing Frame 2, Used for Specimens 5 through 12.

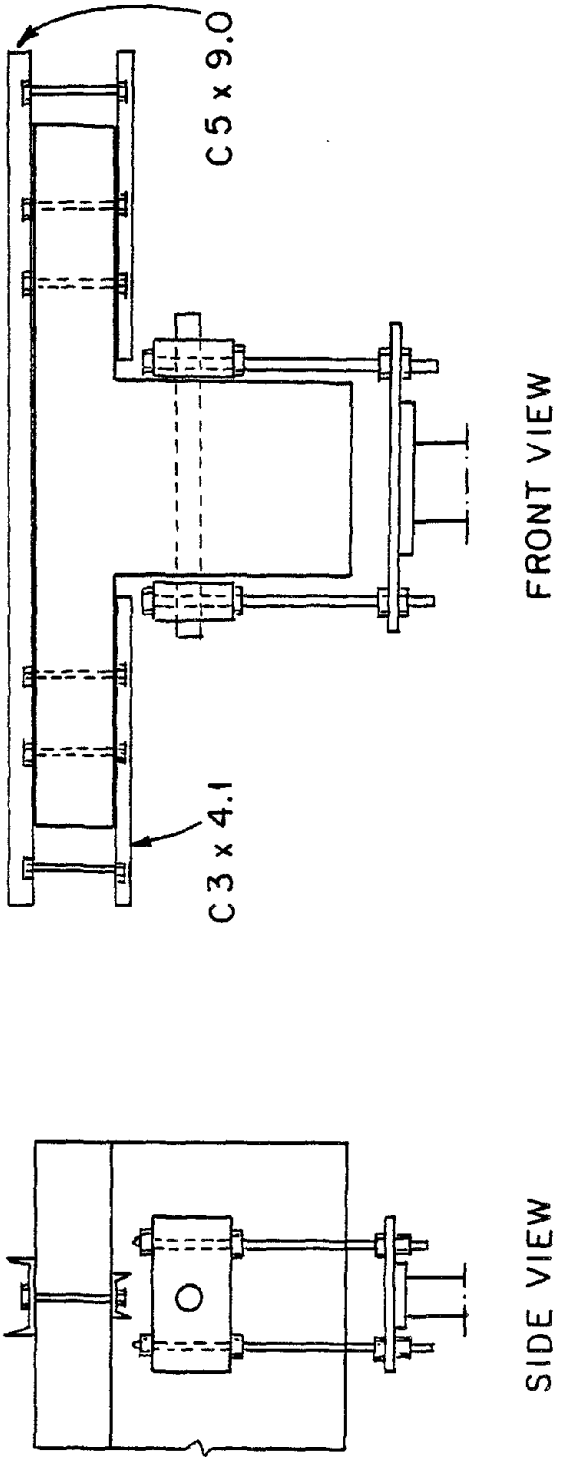

Fig. 2.11. Slab Load Point Stiffeners.

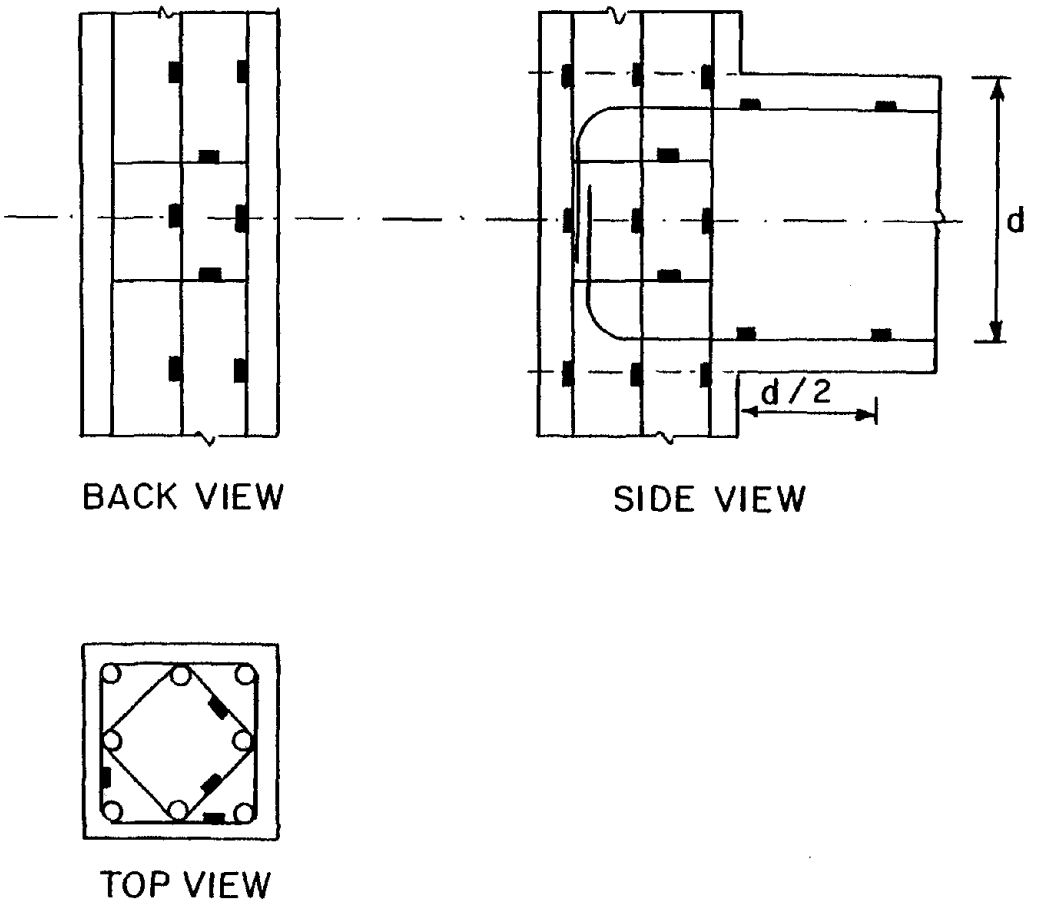

Fig. 2.12. Location of Strain Gages in Bare Specimens.

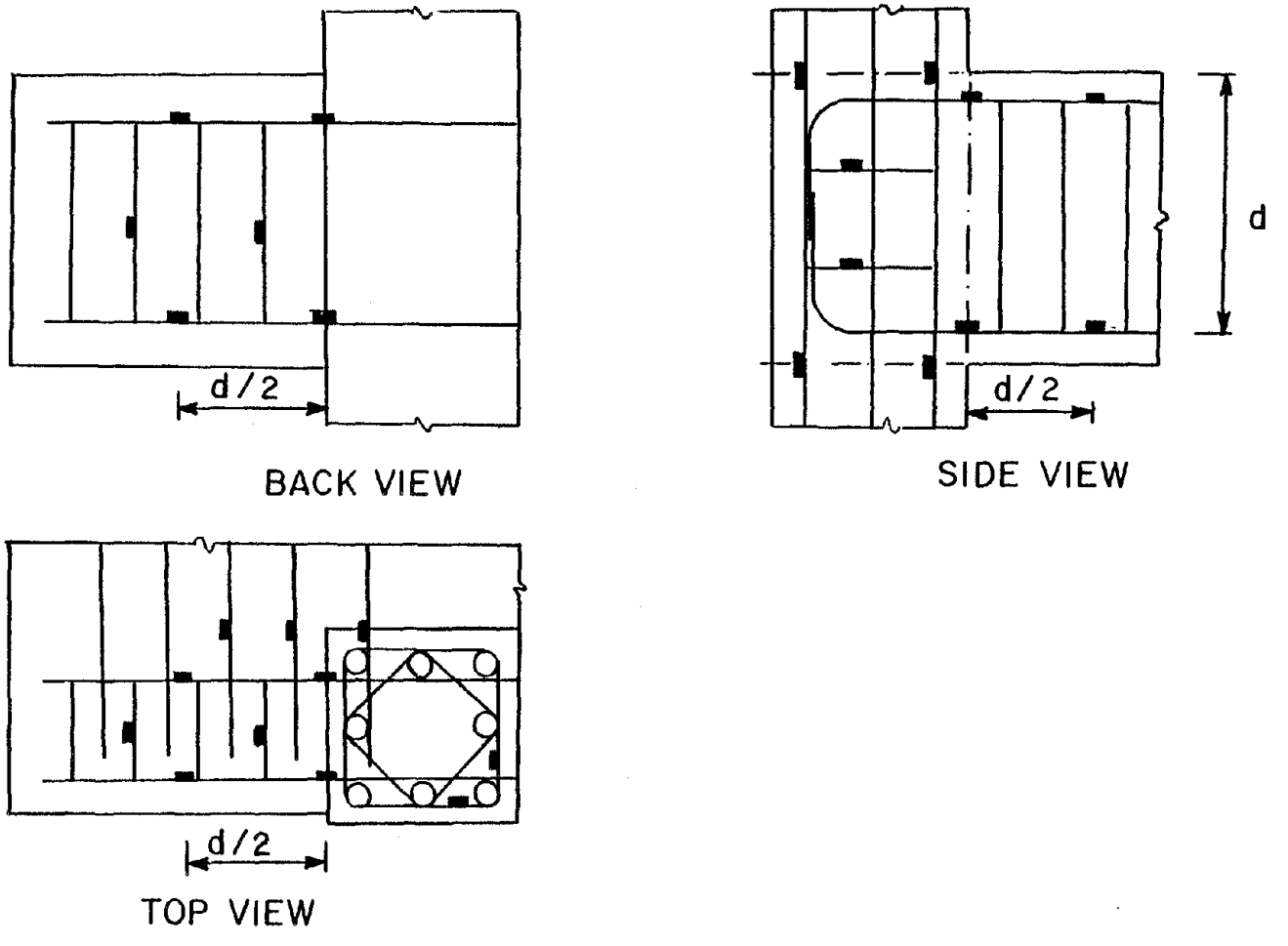

Fig. 2.13. Location of Strain Gages in Specimens with Transverse Beams and Slab.

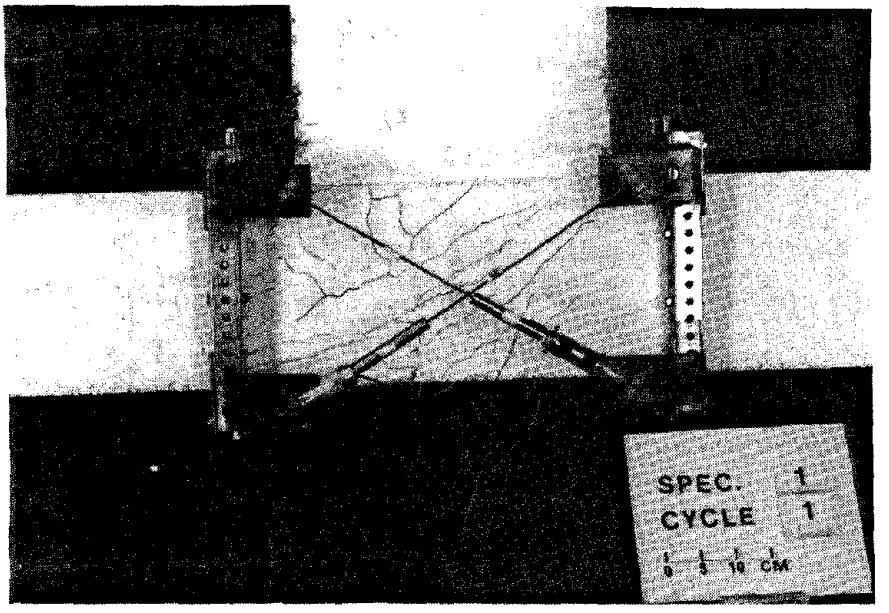

Fig. 2.14. Location of LVDTs in Bare Specimens.

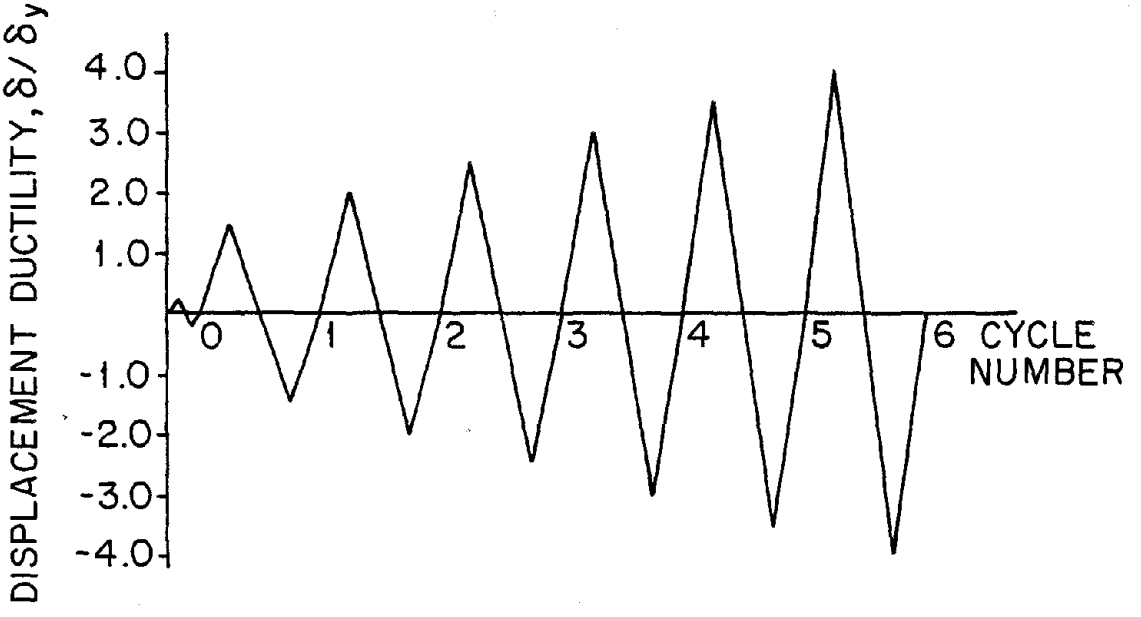

Fig. 2.15. Loading History for Specimens 1 through 6.

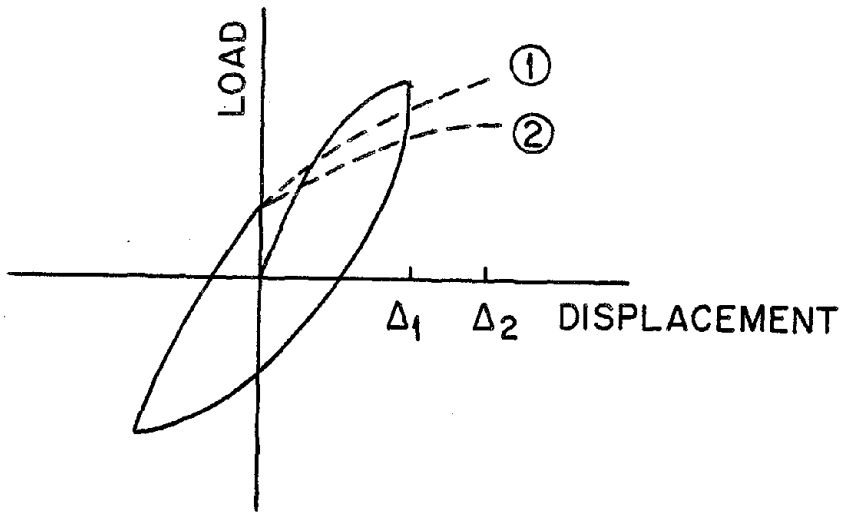

Fig. 2.16. Two Possible Load-Displacement Paths in Subsequent Cycles.

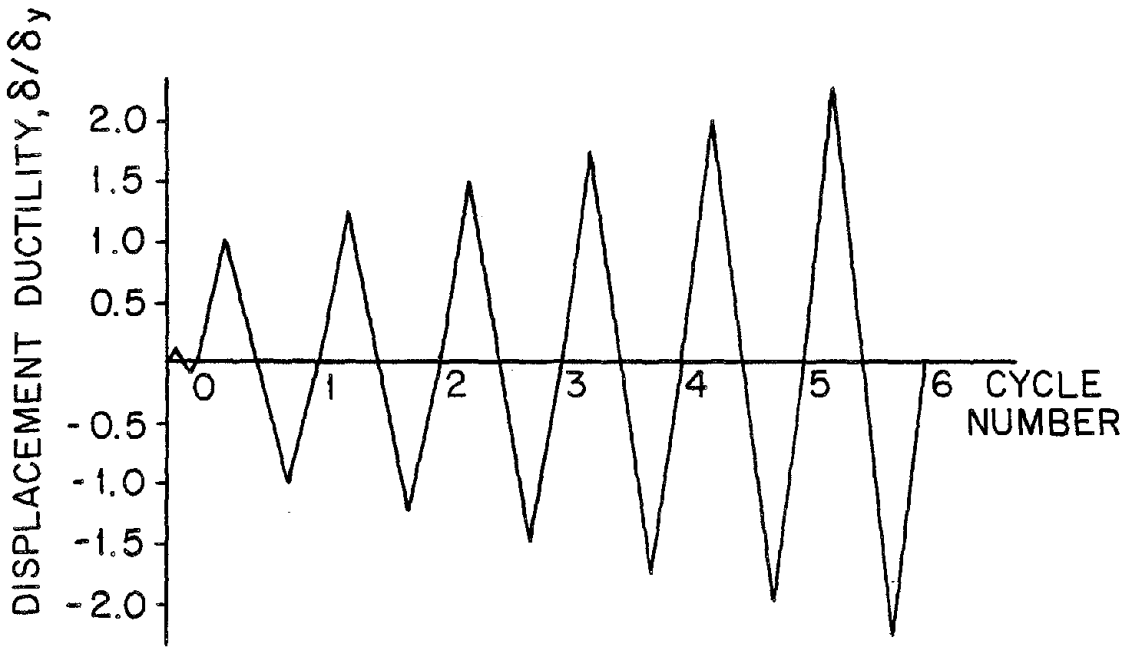

Fig. 2.17. Loading History for Specimens 7 through 12.

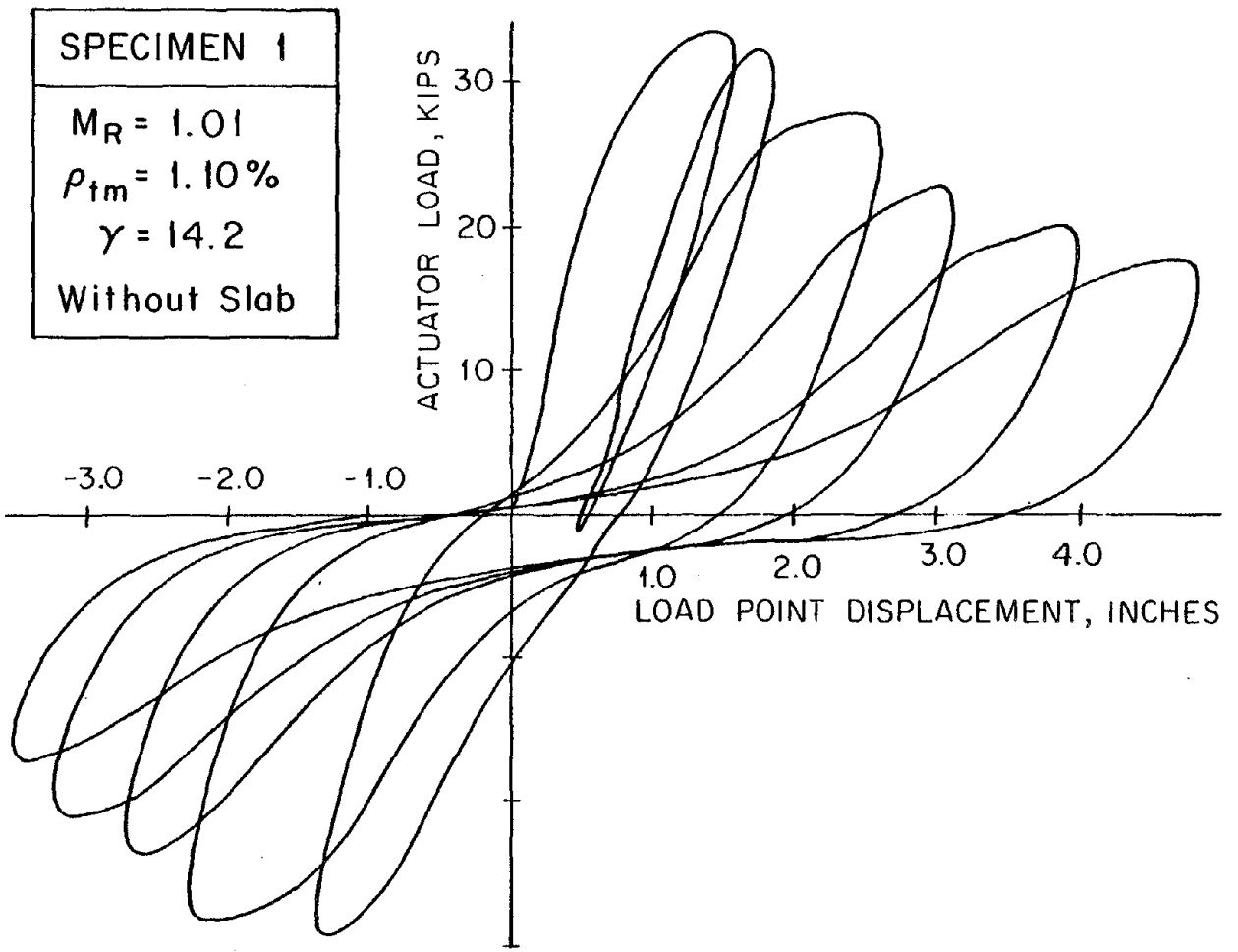

Fig. 3.1(a). Load vs. Deflection Response of Specimen 1.

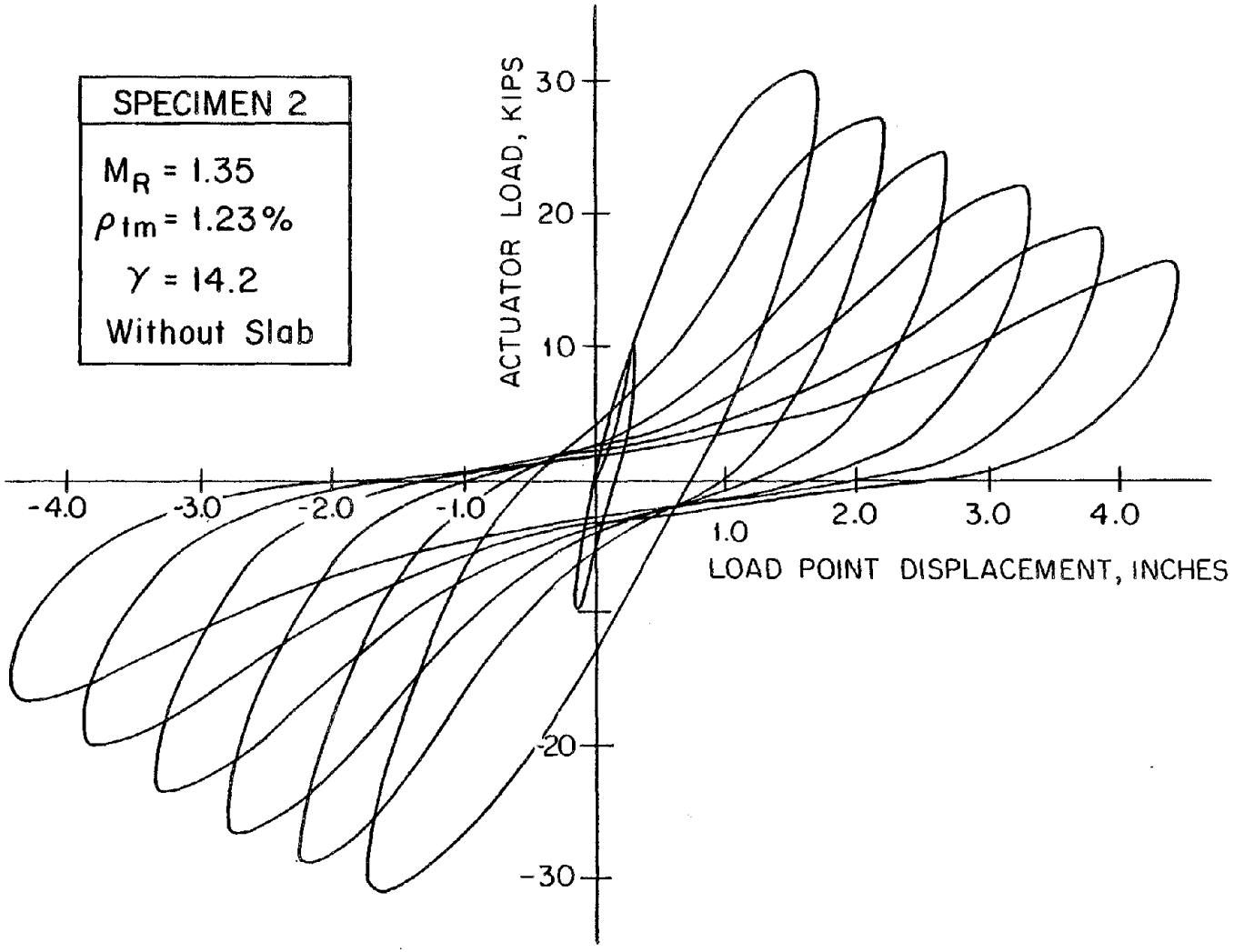

Fig. 3.1(b). Load vs. Deflection Response of Specimen 2.

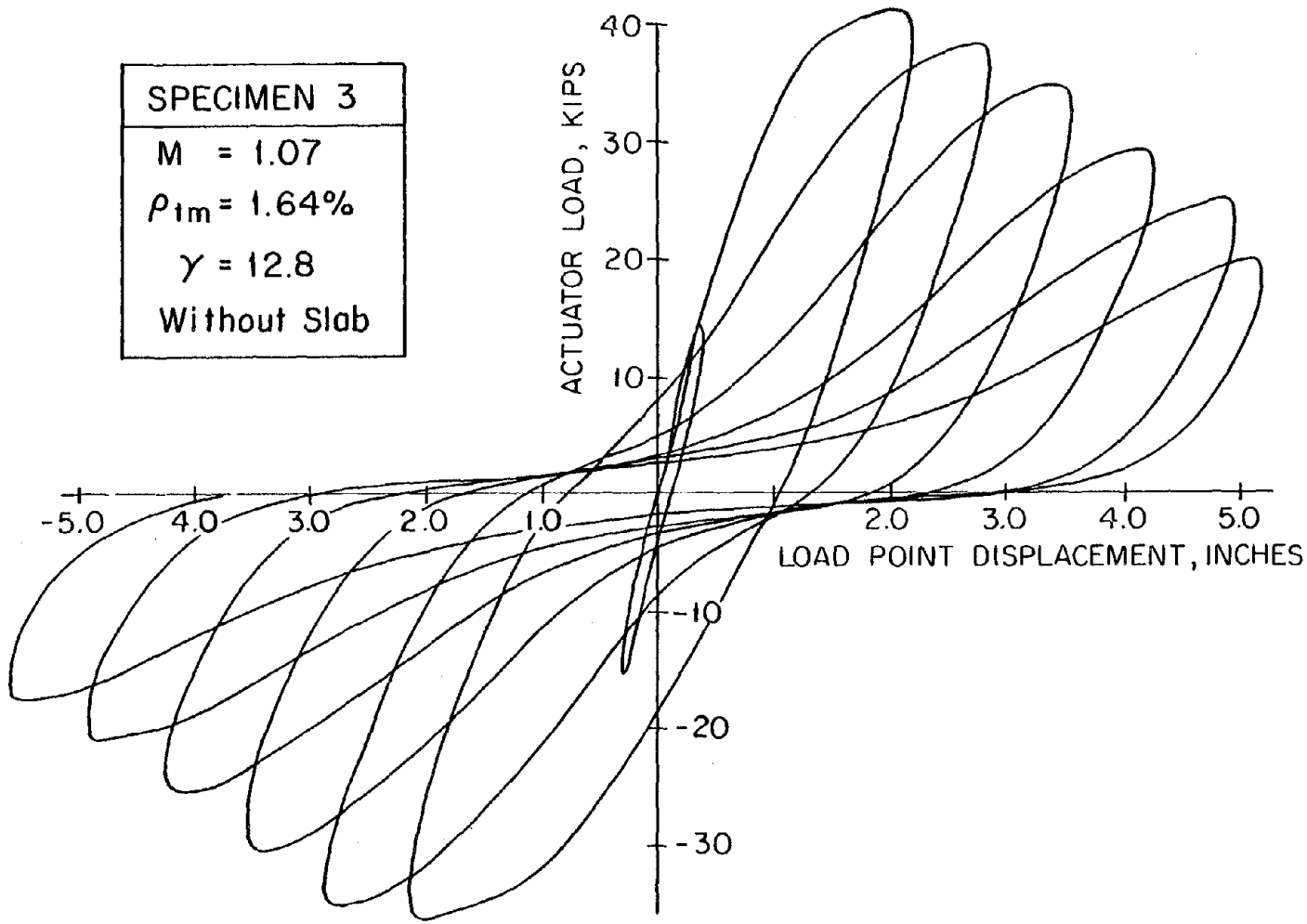

Fig. 3.1(c). Load vs. Deflection Response of Specimen 3.

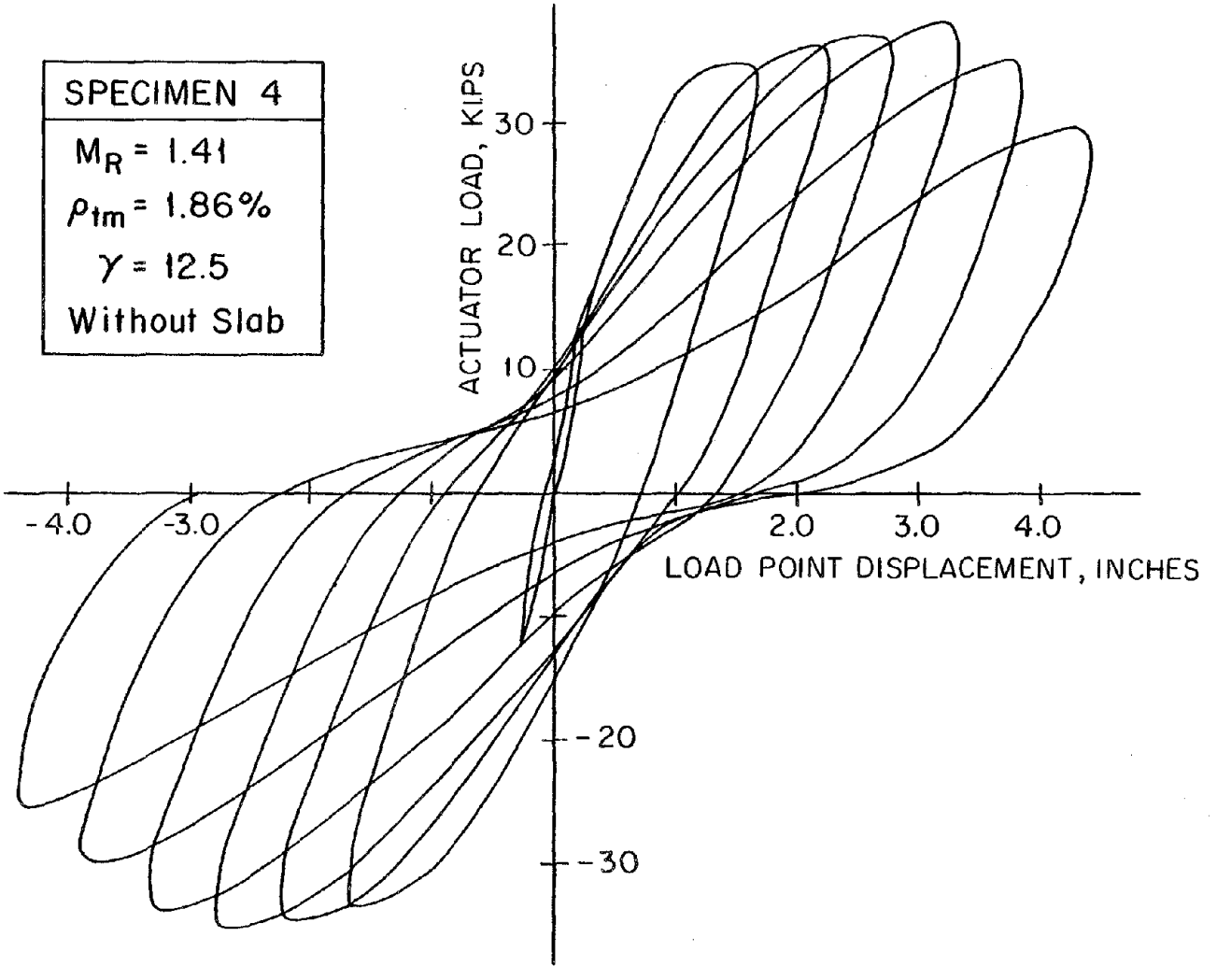

Fig. 3.1(d). Load vs. Deflection Response of Specimen 4.

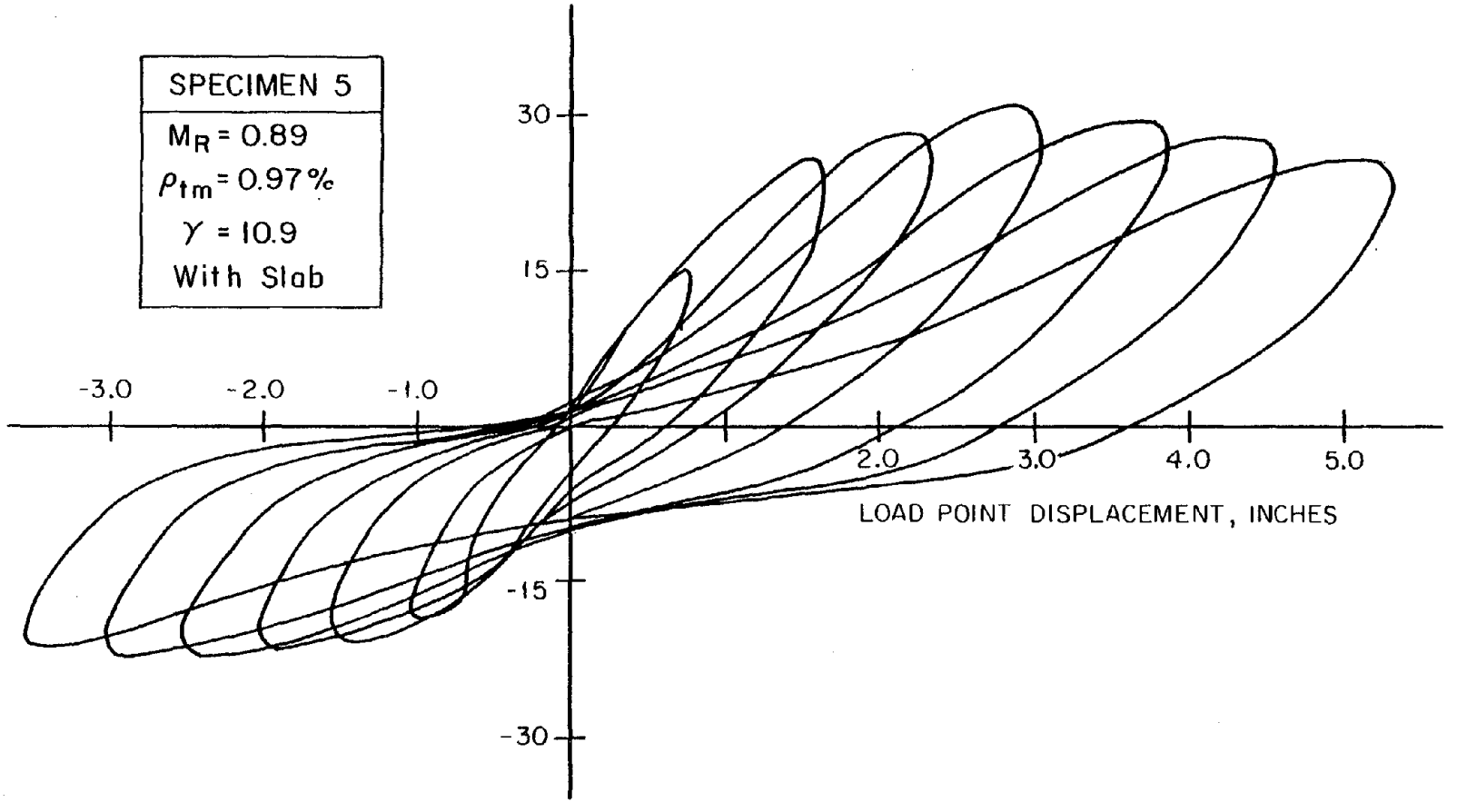

Fig. 3.1(e). Load vs. Deflection Response of Specimen 5.

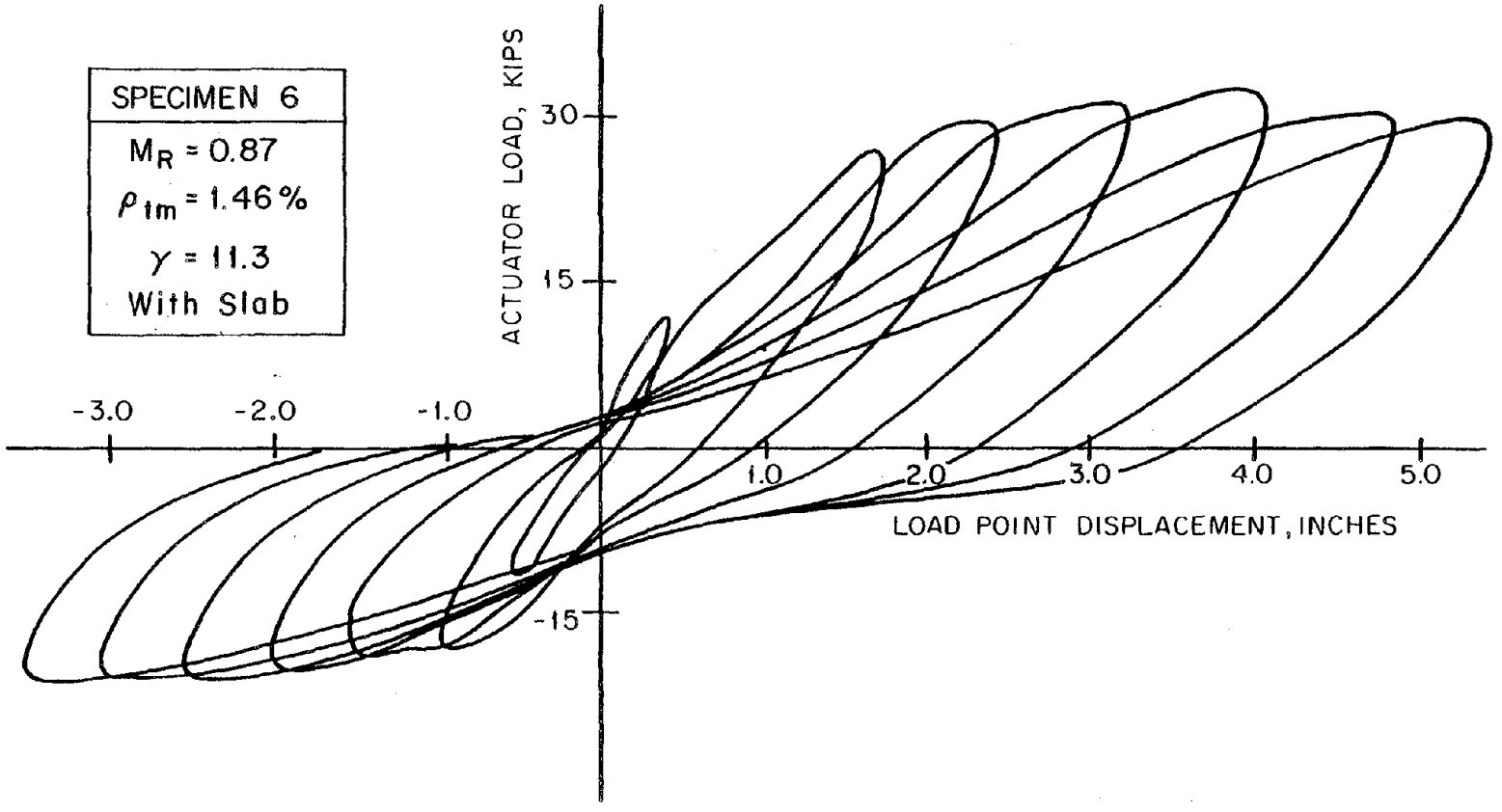

Fig. 3.1(f). Load vs. Deflection Response of Specimen 6.

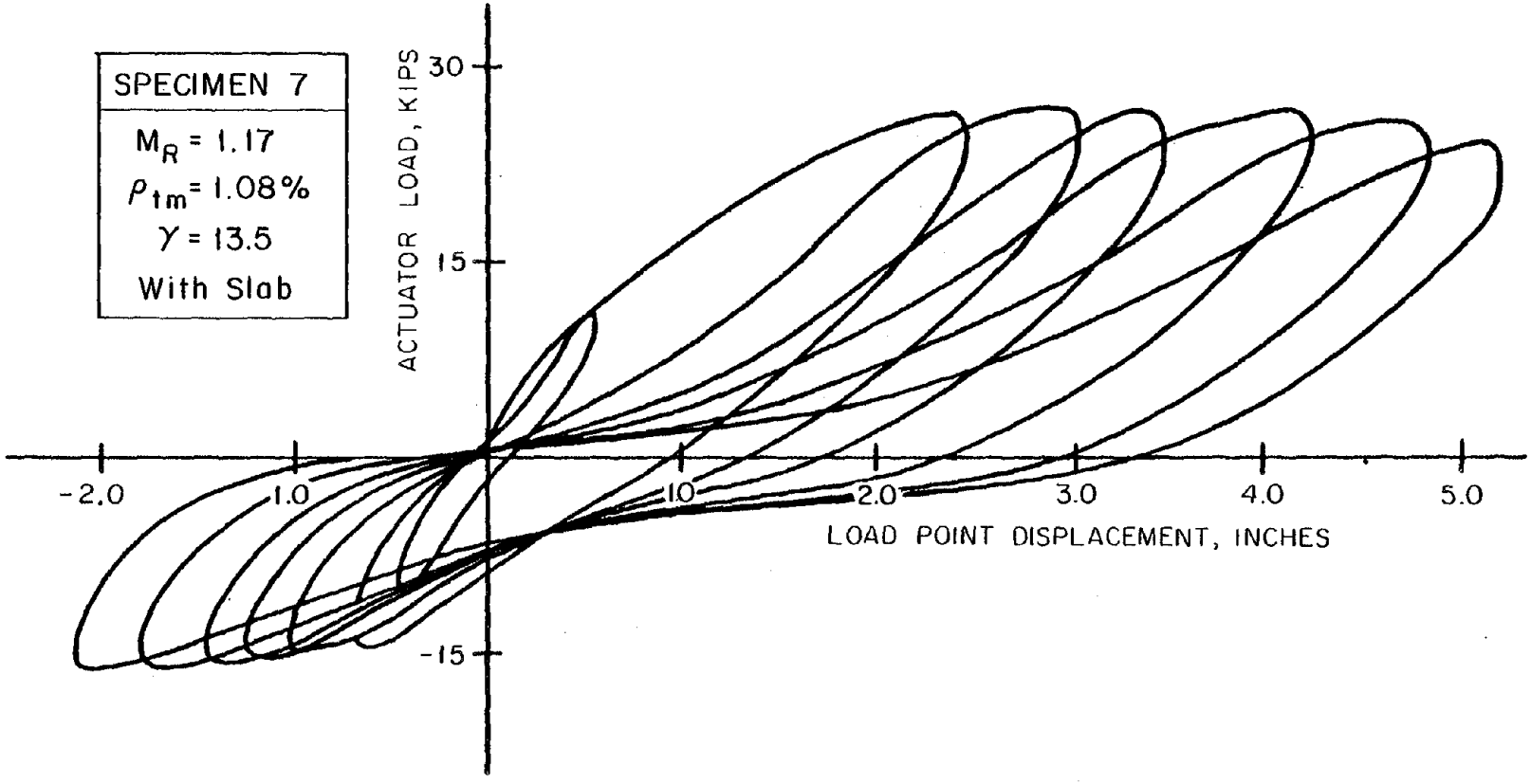

Fig. 3.1(g). Load vs. Deflection Response of Specimen 7.

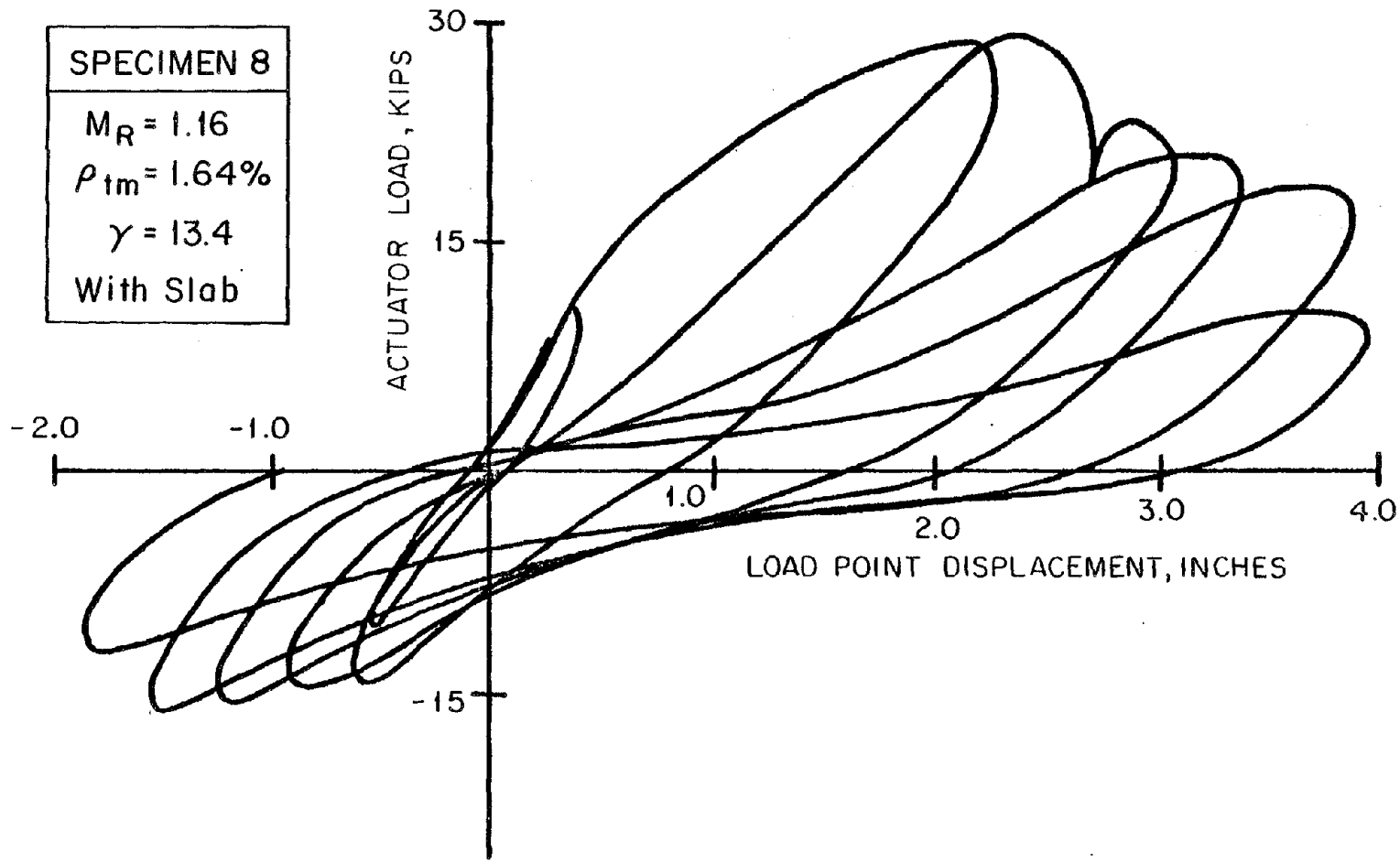

Fig. 3.1(h). Load vs. Deflection Response of Specimen 8.

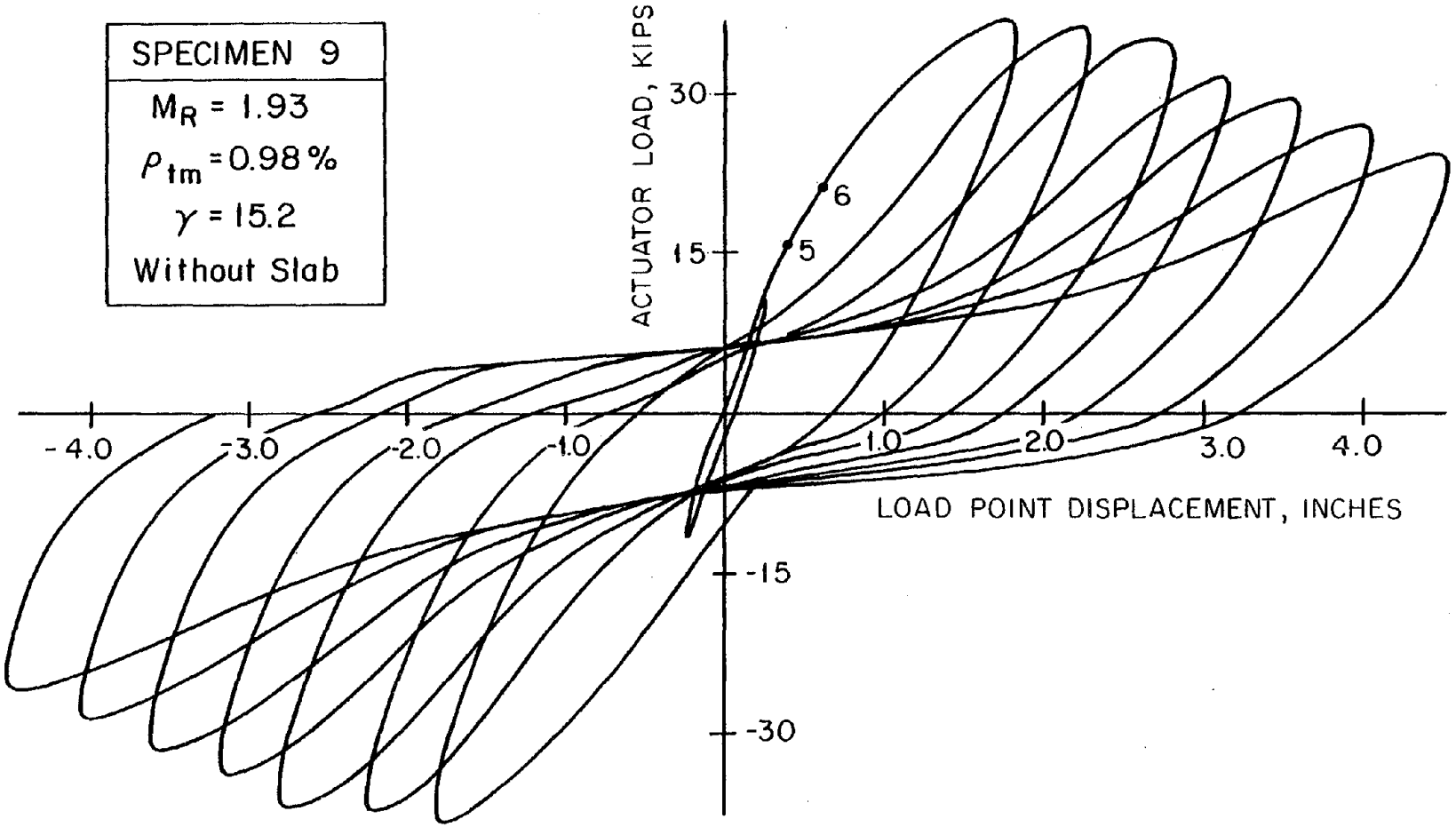

Fig. 3.1(i). Load vs. Deflection Response of Specimen 9.

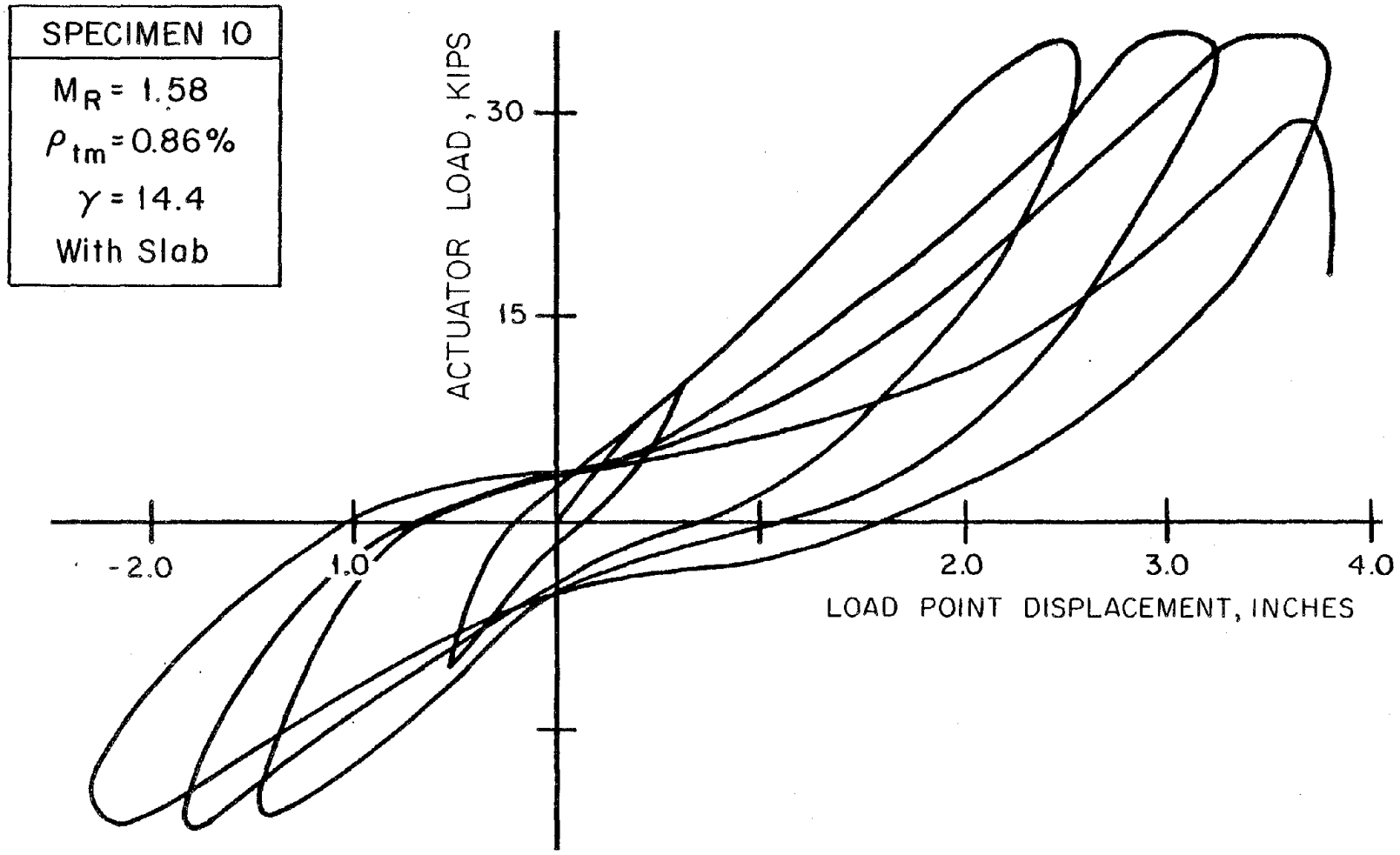

Fig. 3.1(j). Load vs. Deflection Response of Specimen 10.

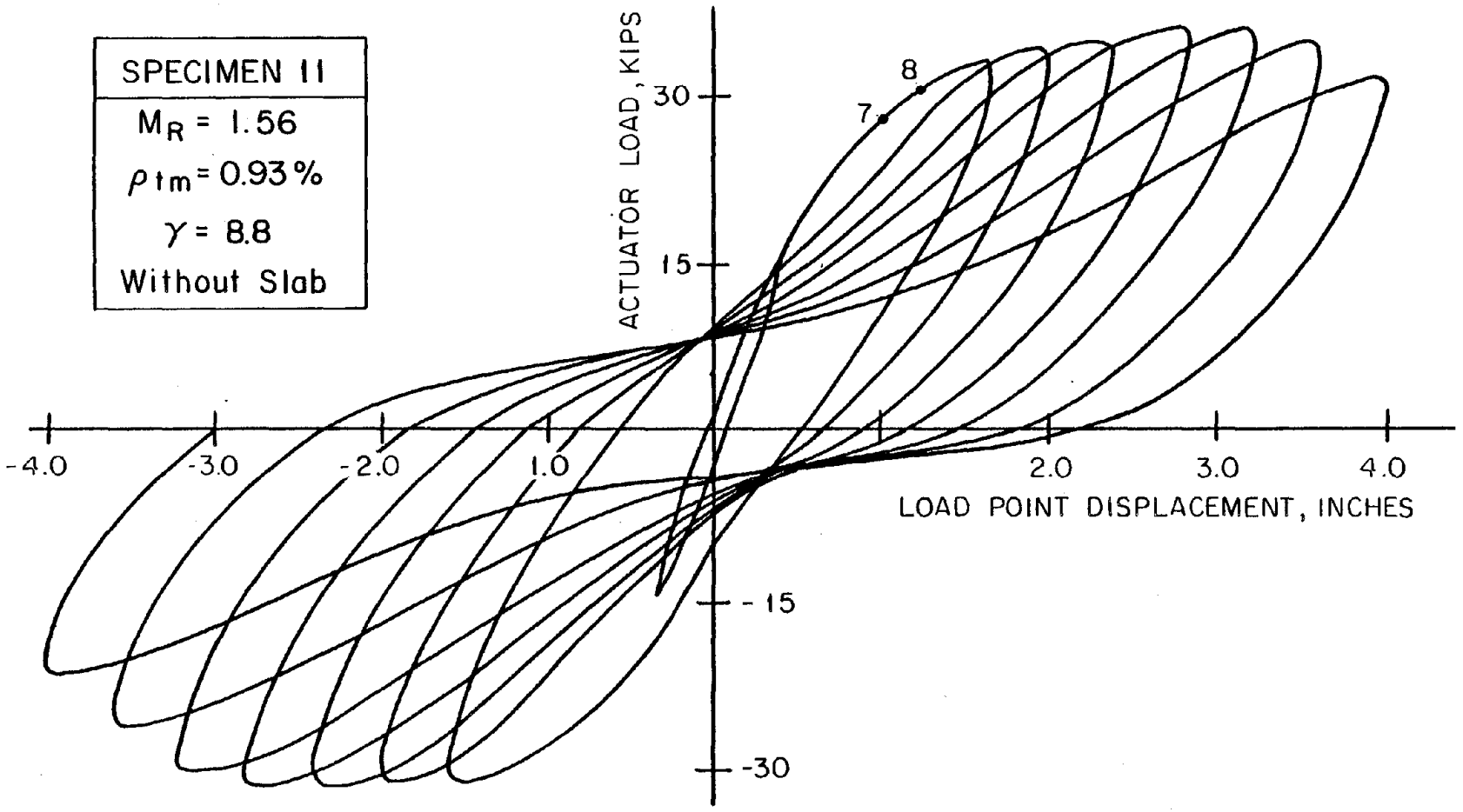

Fig. 3.1(k). Load vs. Deflection Response of Specimen 11.

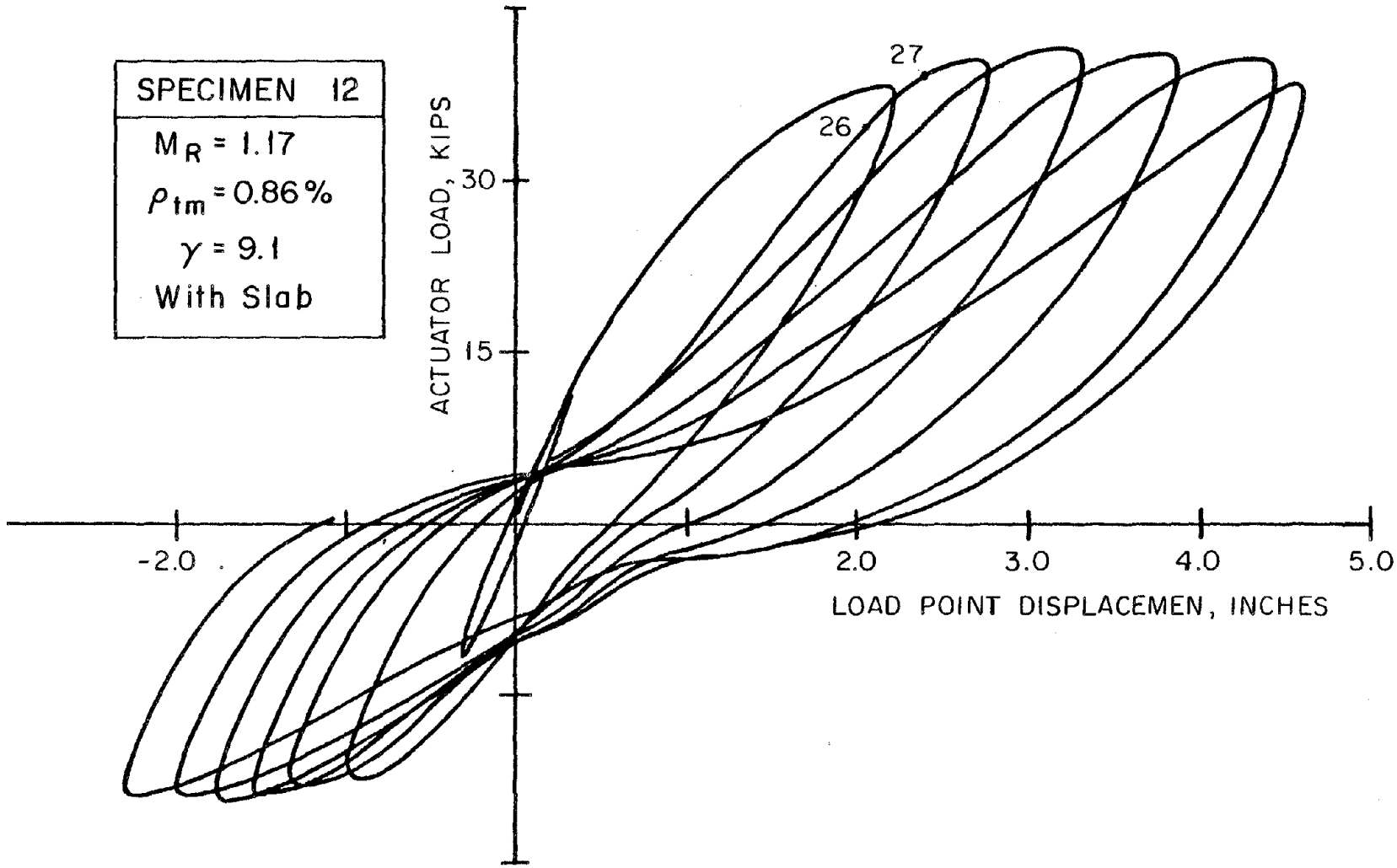

Fig. 3.1(1). Load vs. Deflection Response of Specimen 12.

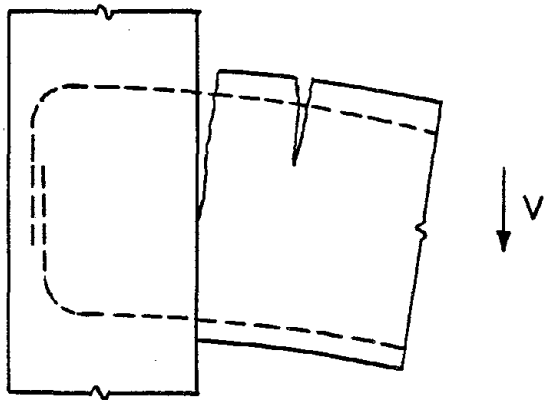

(a). Loading in the positive direction.

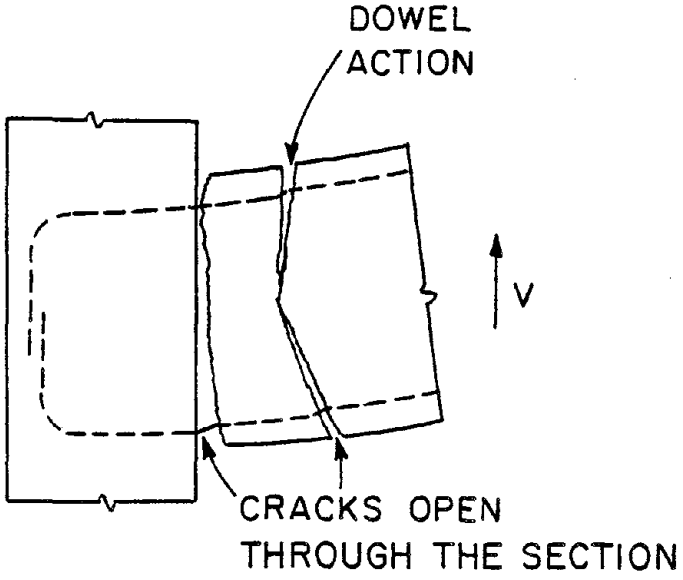

(b). Loading in the negative direction.

Fig. 3.2. Opening and Closing of Flexural Cracks in Specimens with Transverse Beams and Slab.

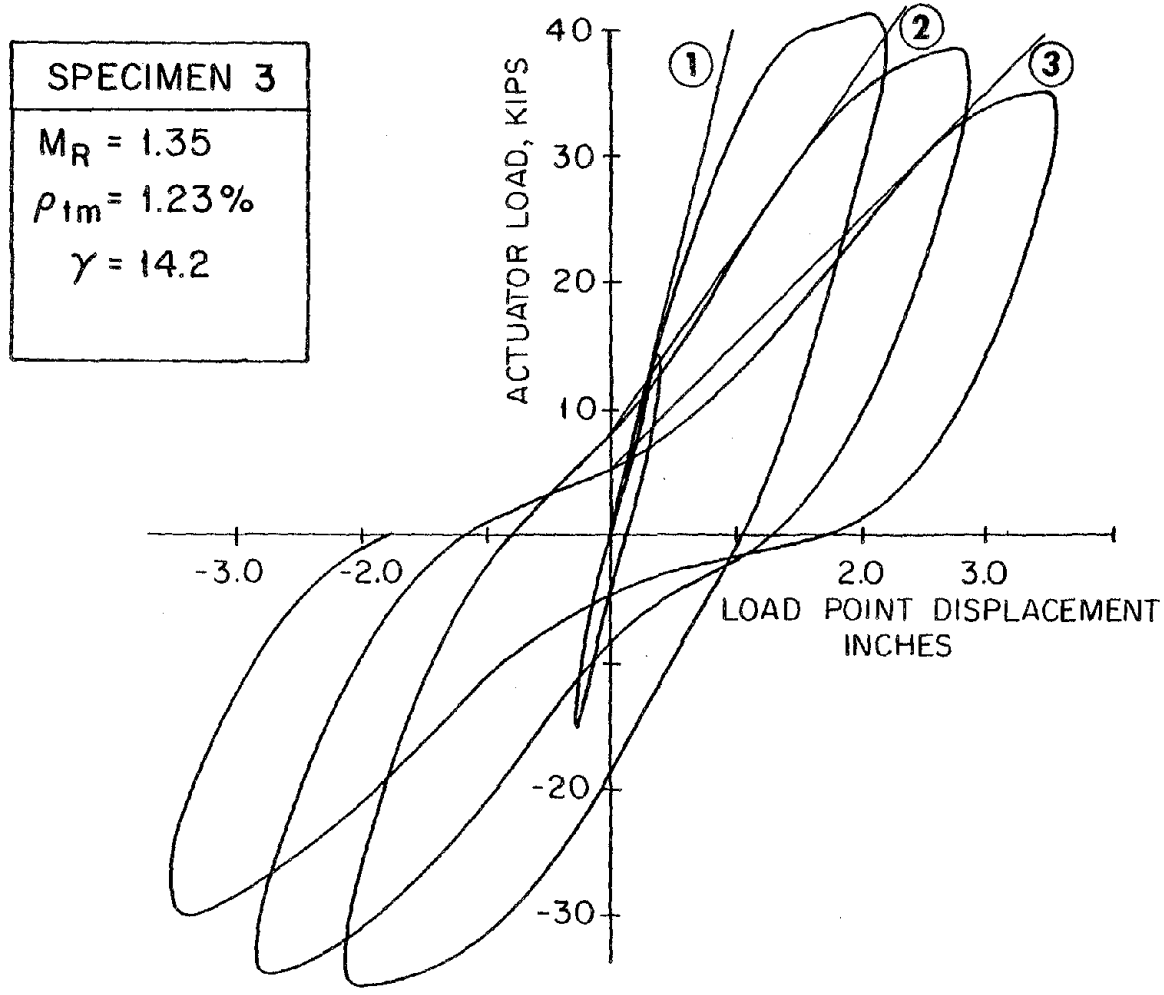

Fig. 3.3. Lines Defining Stiffness for the First Three Loading Cycles of Specimen 3.

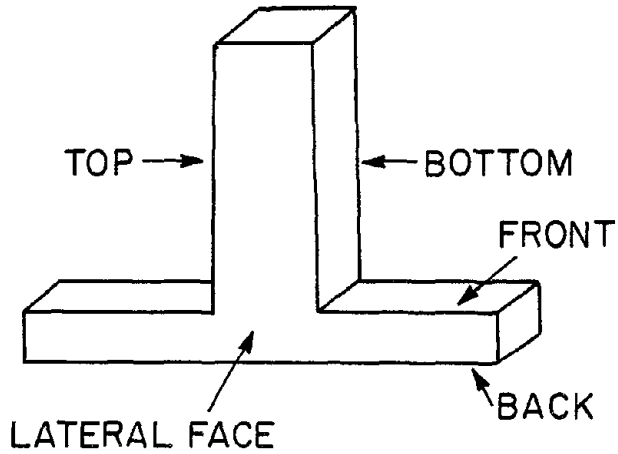

(a). Sides of specimens 1 through 4.

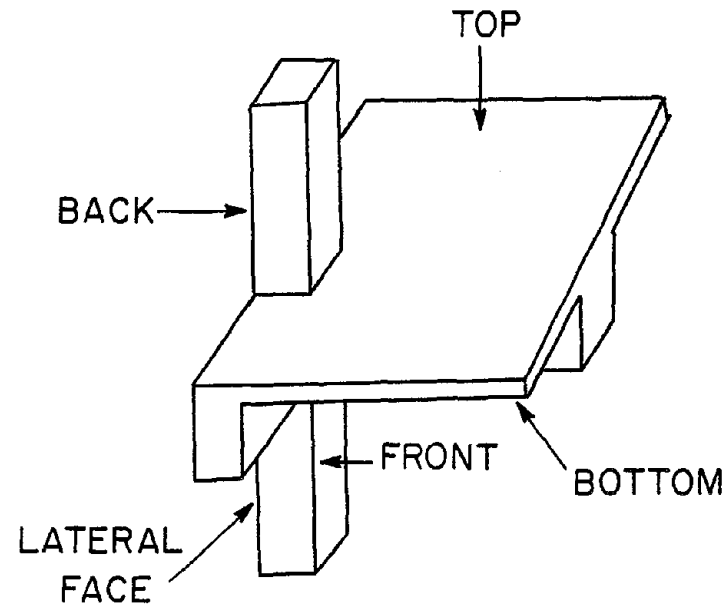

(b). Sides of specimens 5 through 12.

Fig. 3.4. Different Sides of Specimens.

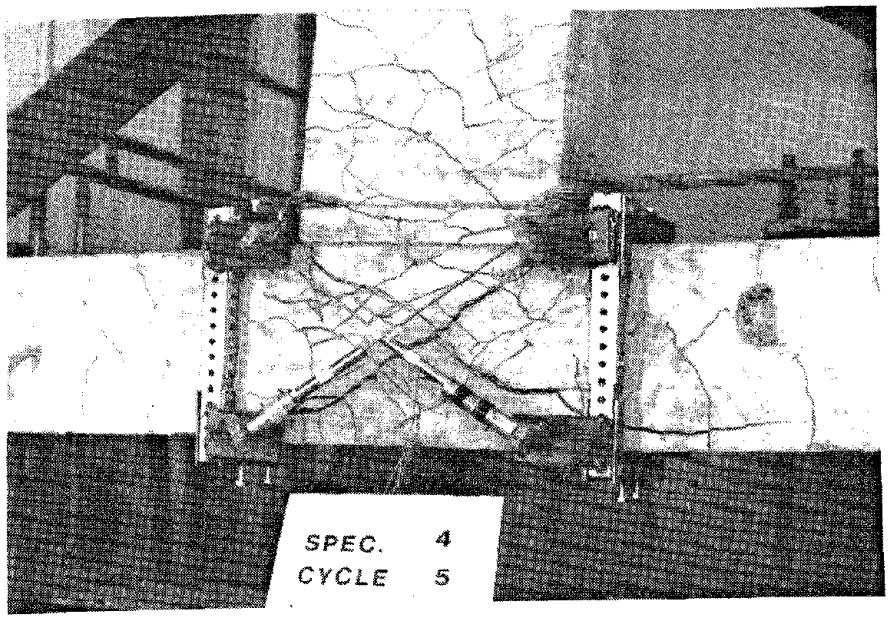

Fig. 3.5. Cracking Pattern on the Joint of a Bare Specimen.

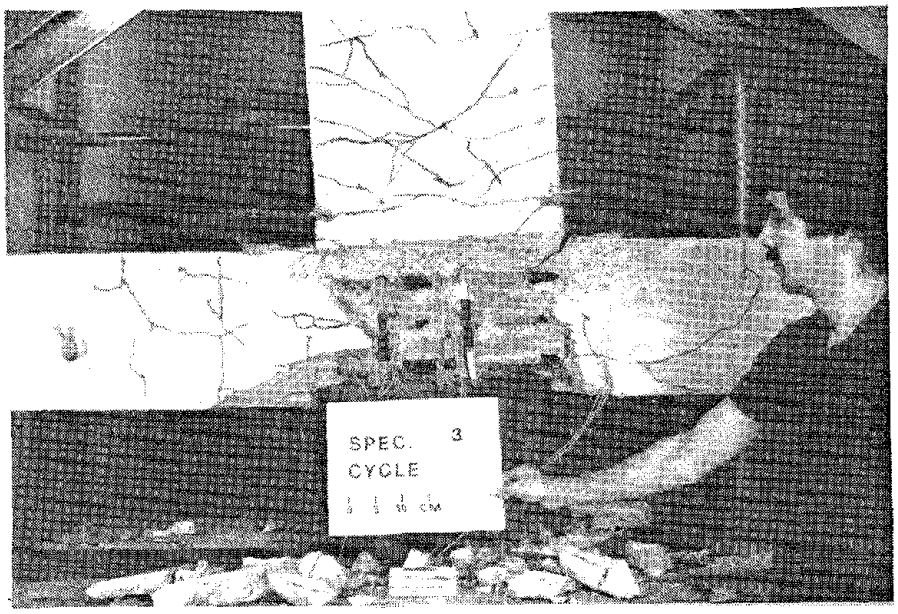

Fig. 3.6. Spalling of Cover Concrete on the joint of a Bare Specimen.

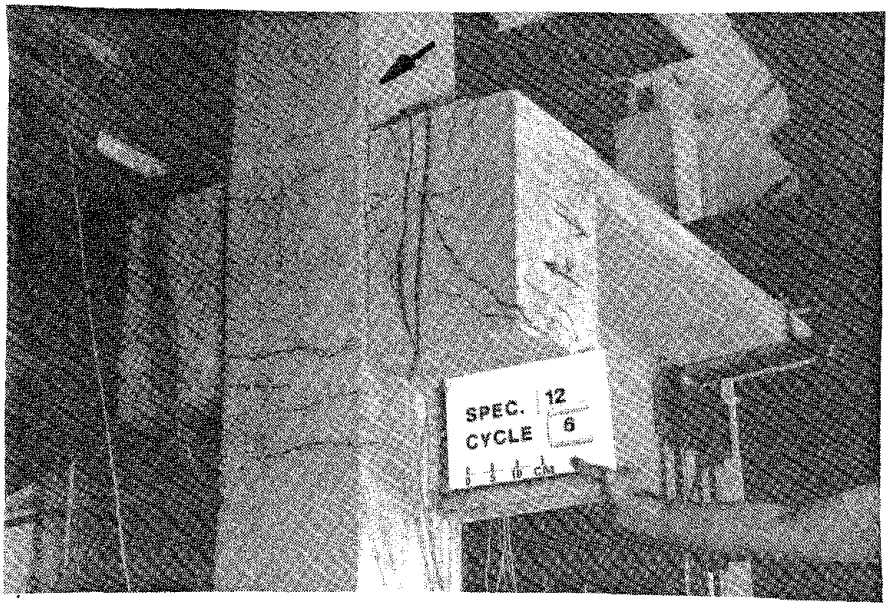

Fig. 3.7. Extension of Cracks into the Column of Specimens with Slab.

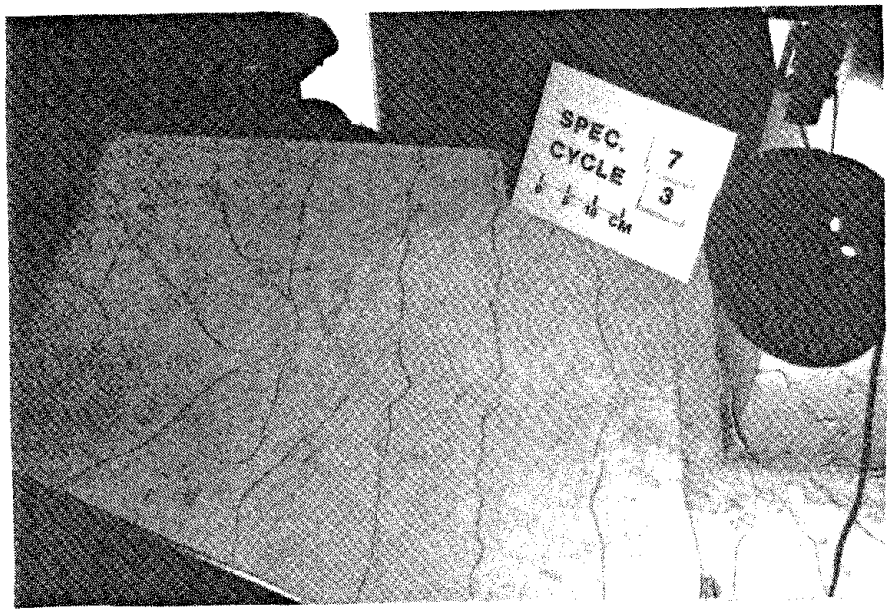

Fig. 3.8. Cracking Pattern of the Slabs.

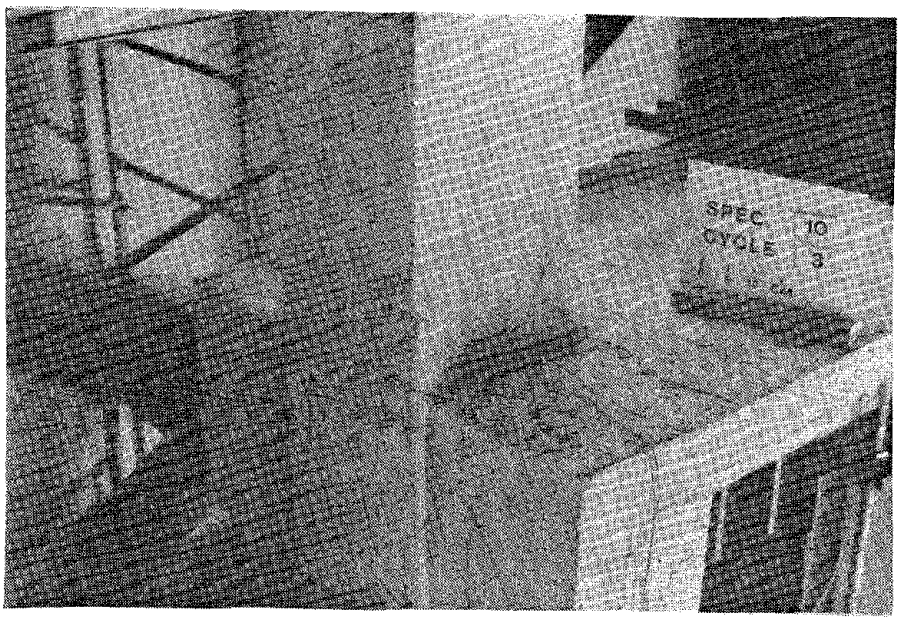

Fig. 3.9. Torsional Cracks in the Transverse Beams and Columns of Specimens with Slab.

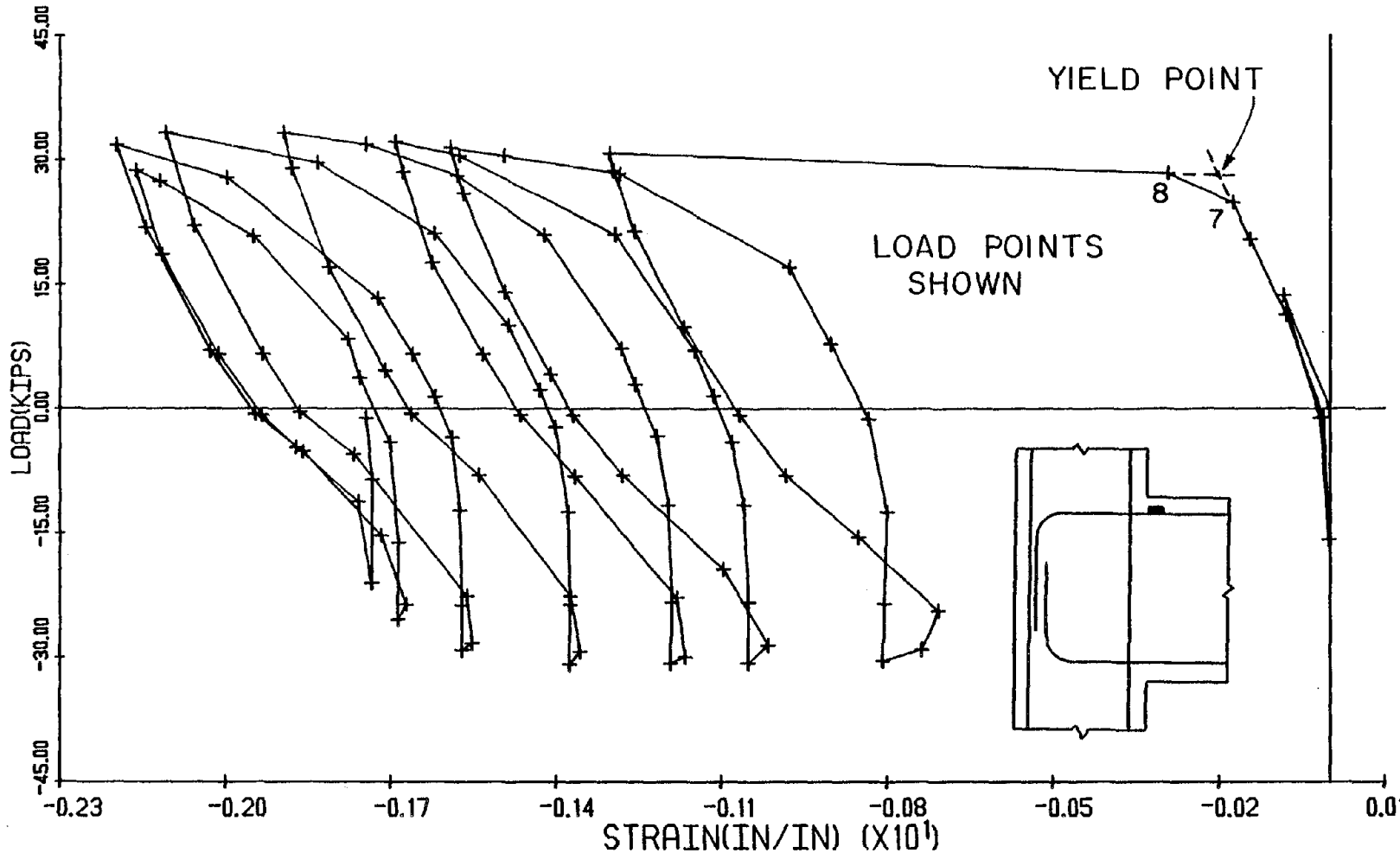

Fig. 3.10. Yielding of the Main Beam Longitudinal Reinforcement at the Face of the Column Between Load Points 7 and 8 of Fig. 3.1(k).

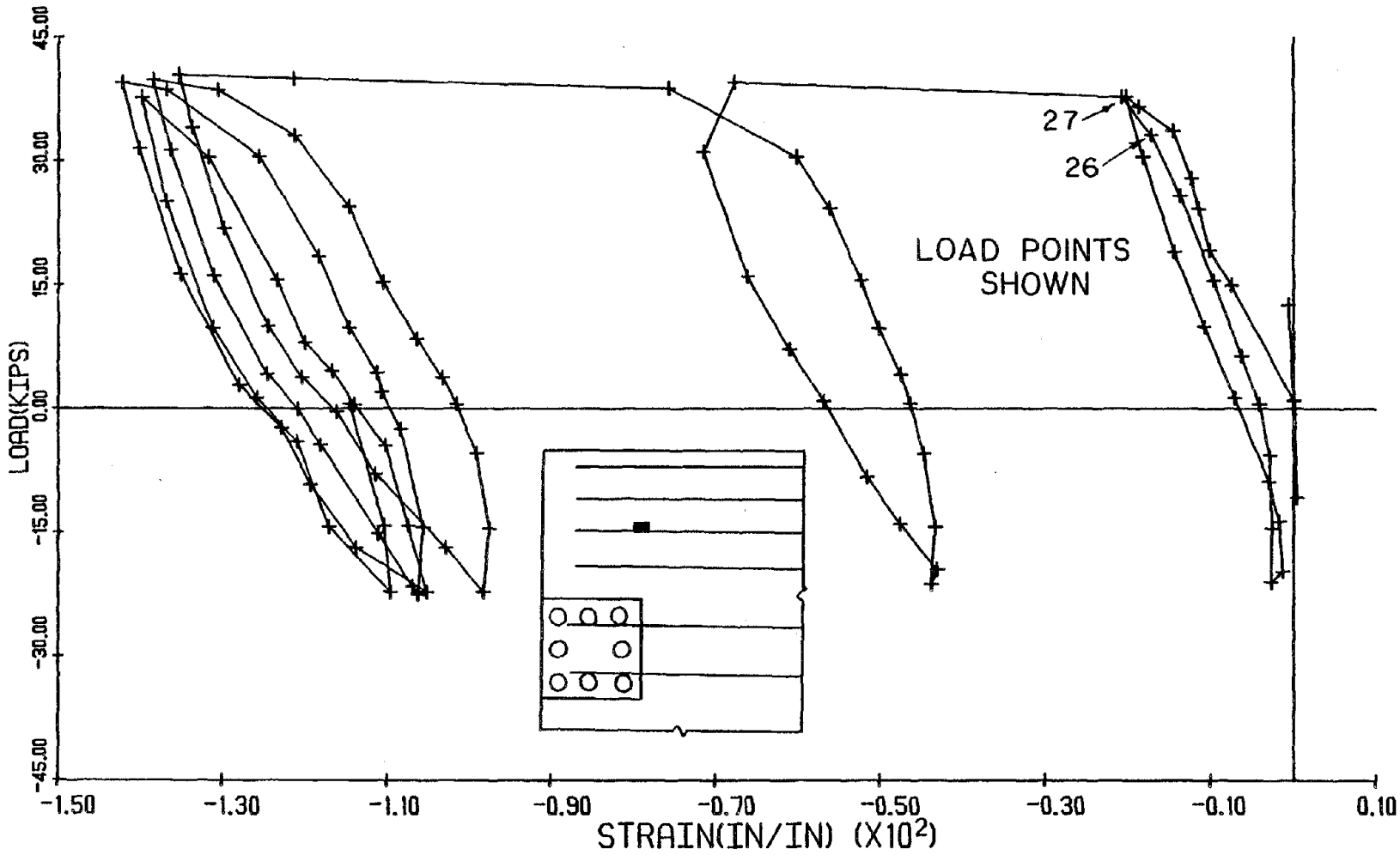

Fig. 3.11. Yielding of the Slab Longitudinal Reinforcement Along the Front Face of the Column Between Load Points 27 and 28 of Fig. 3.1(1).

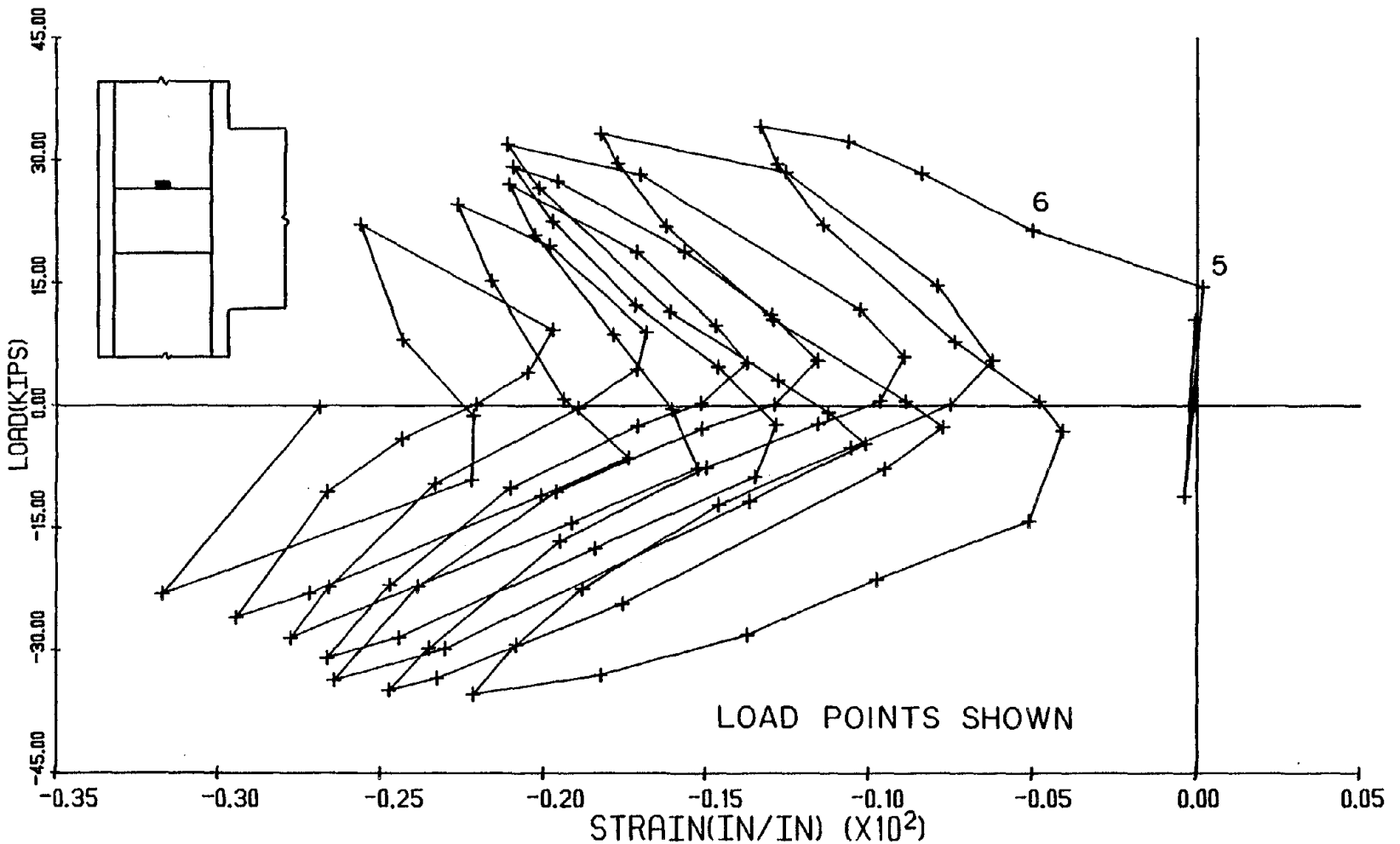

Fig. 3.12. Increase in the Strains of the Joint Transverse Reinforcement in Specimen 9 Between Load Points 5 and 6 of Fig. 3.1(i).

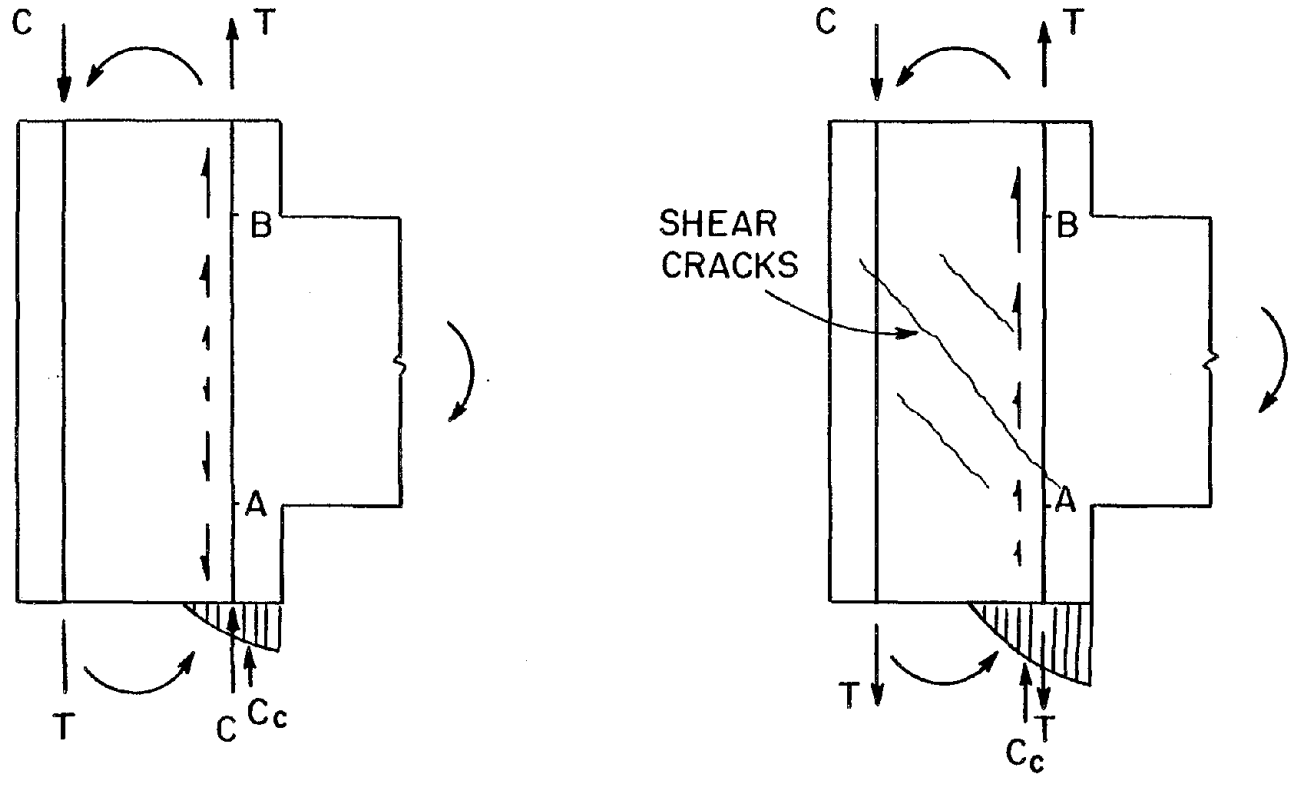

Fig. 3.13. Mechanism of Slippage of Column Longitudinal Reinforcement Through the Joint.

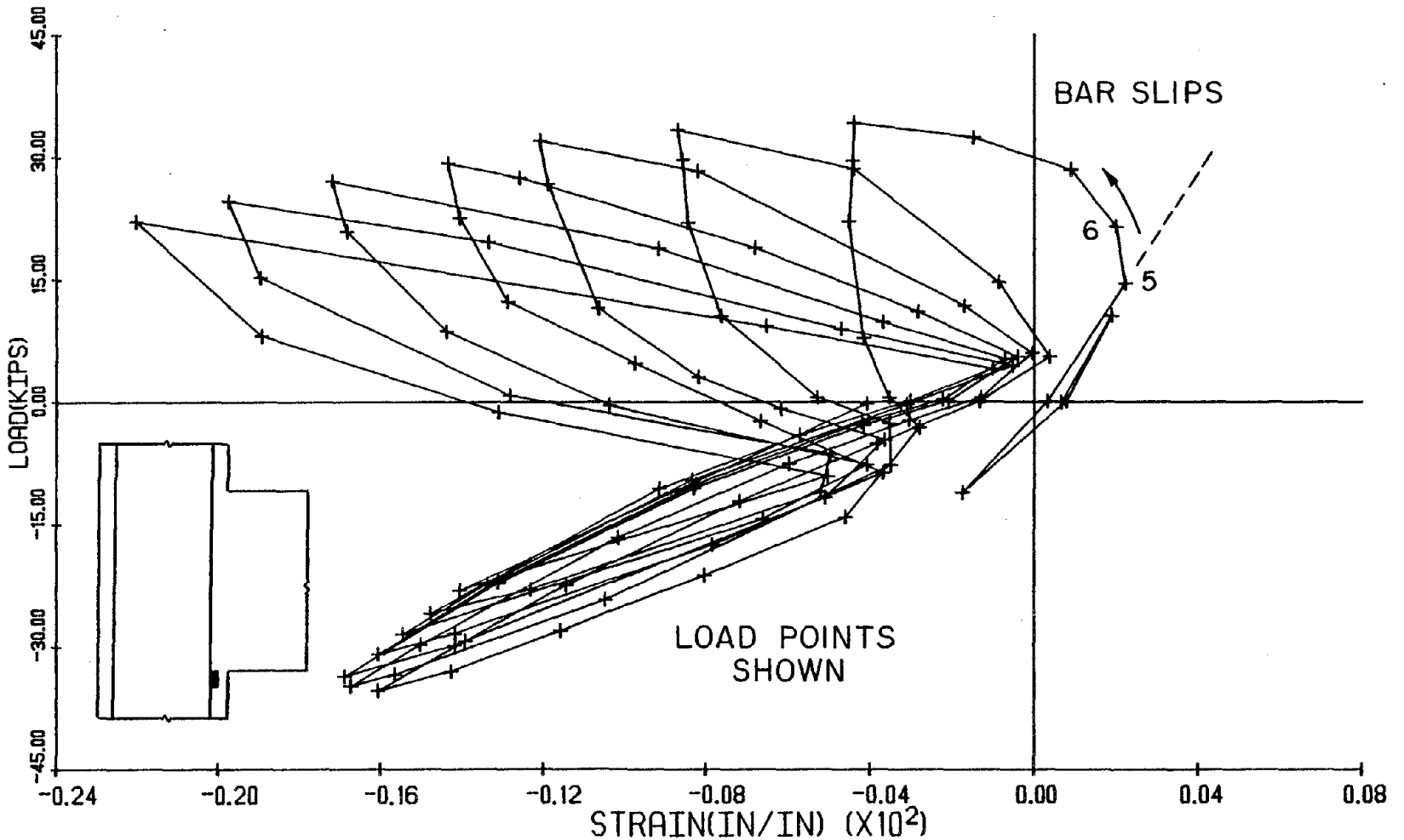

Fig. 3.14. Slippage of the Column Longitudinal Reinforcement in Specimen 9 at Load Point 5 of Fig. 3.1(i).

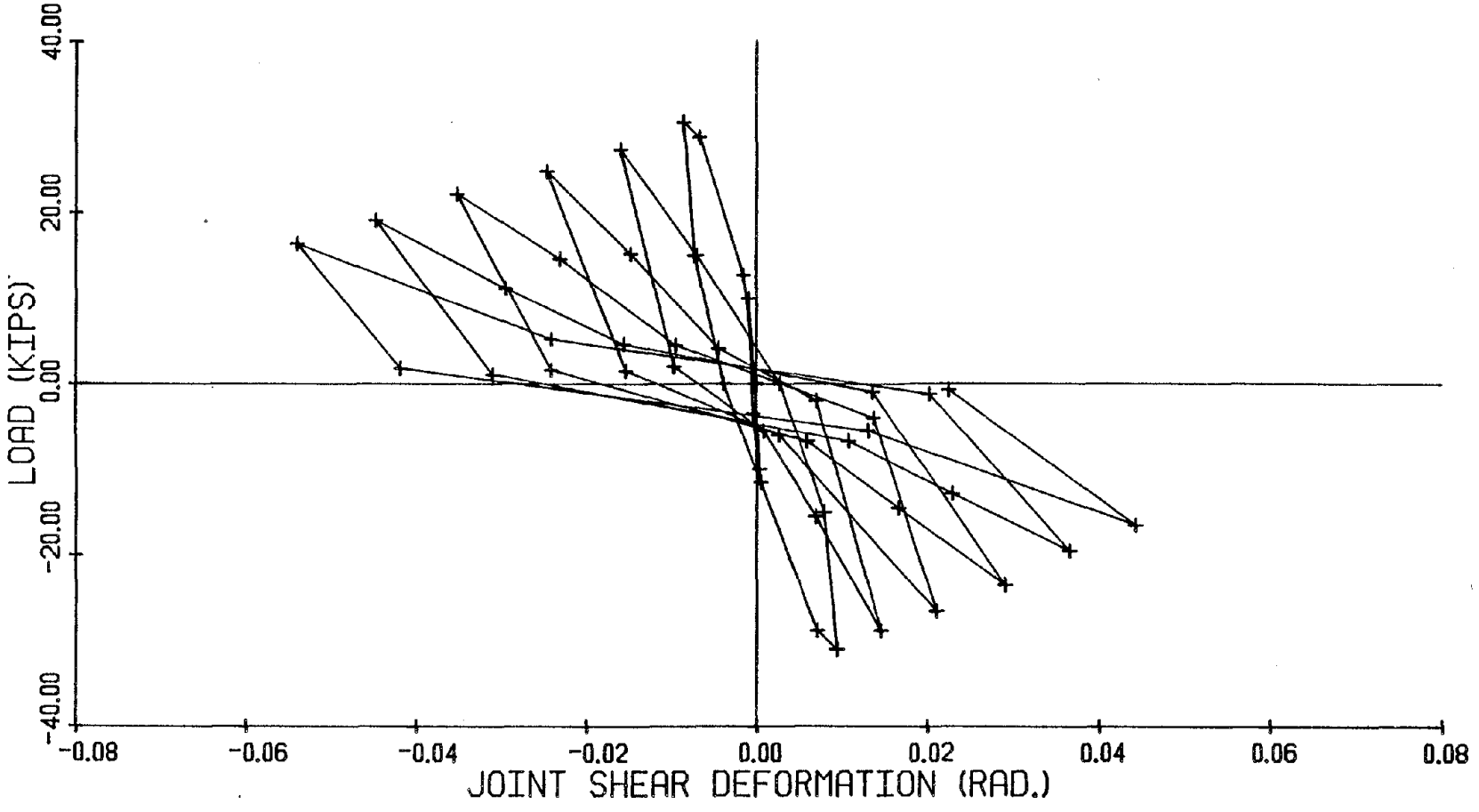

Fig. 3.15. Applied Load vs. Joint Shear Deformation - Specimen 2.

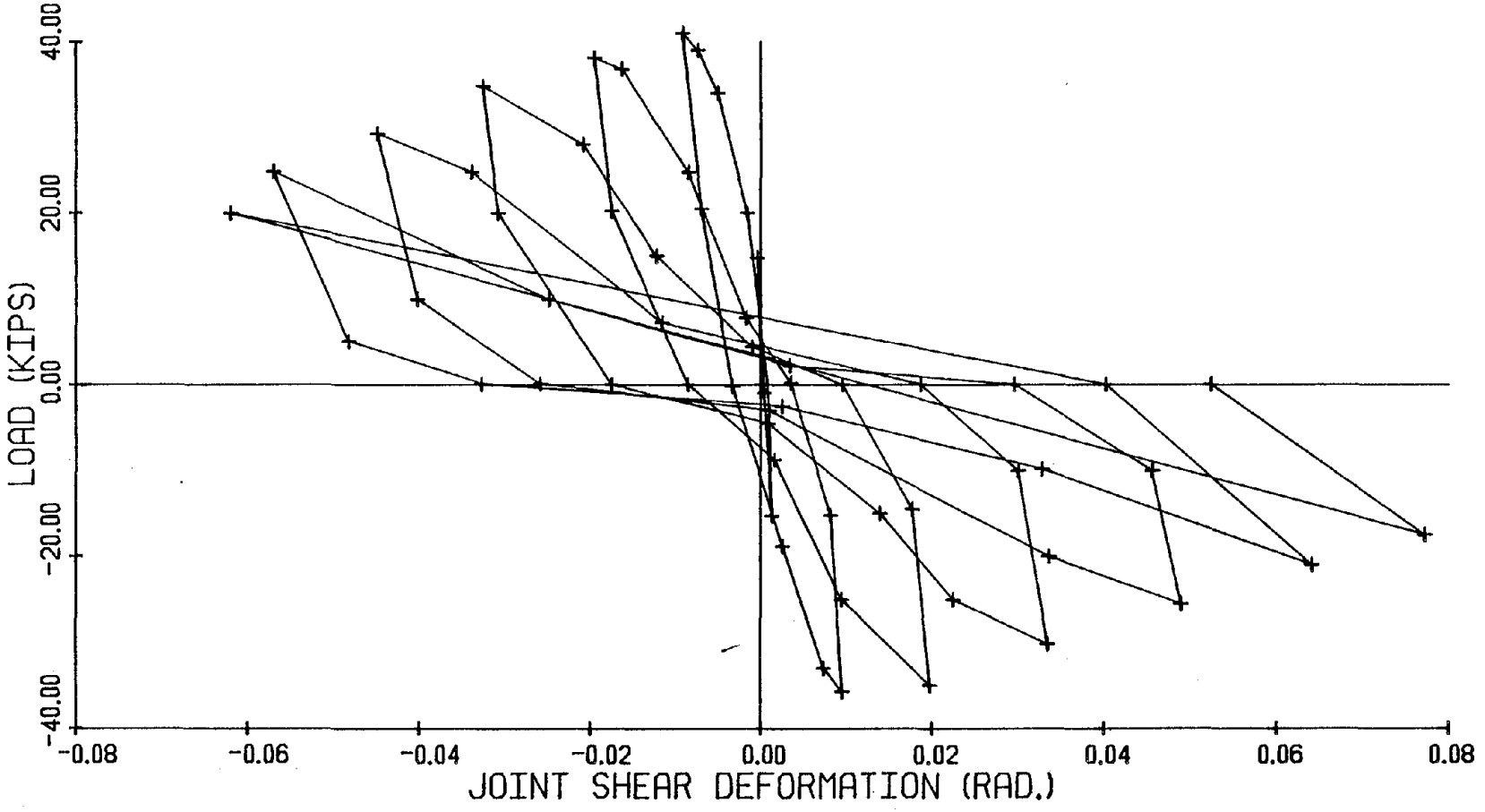

Fig. 3.16. Applied Load vs. Joint Shear Deformation - Specimen 3.

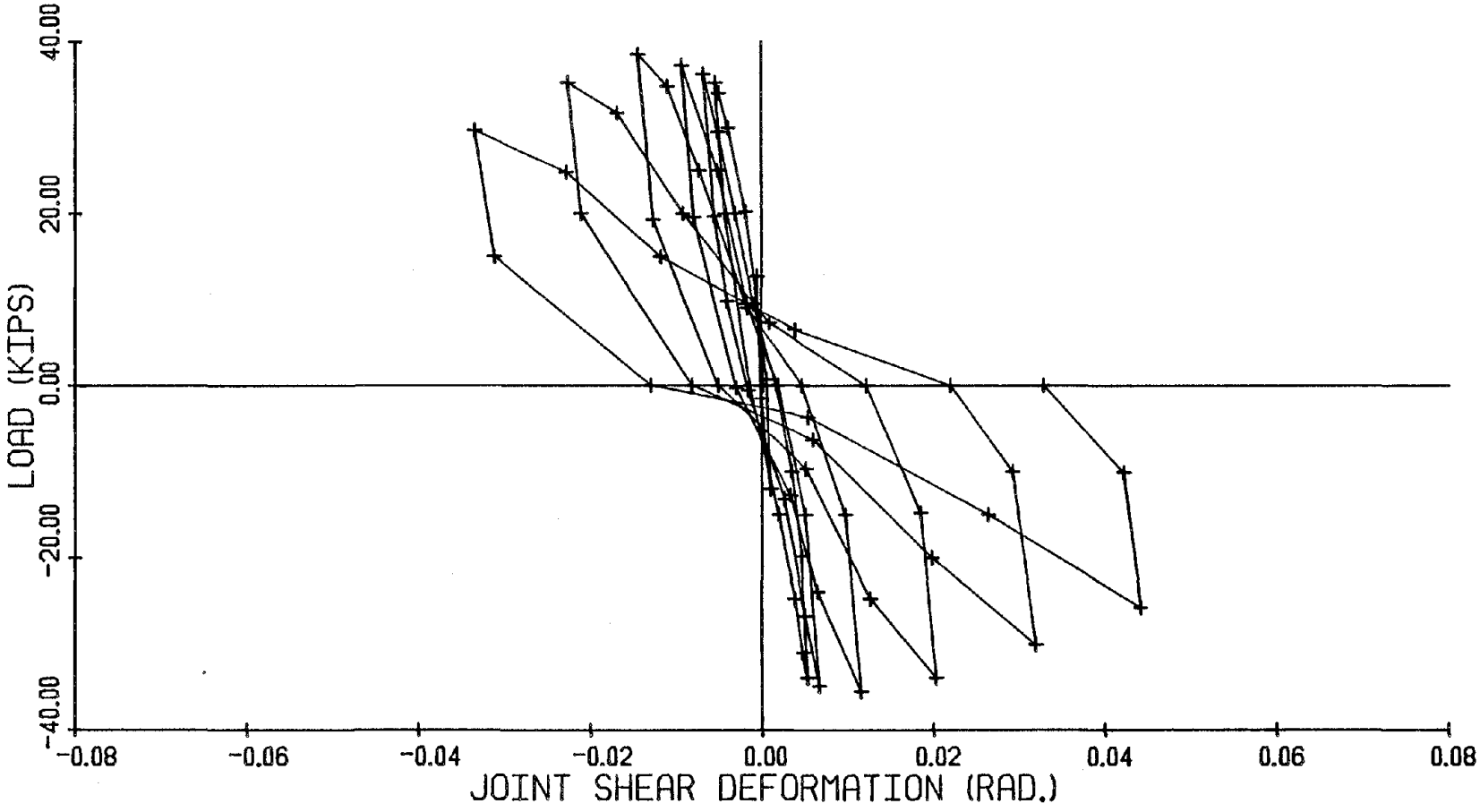

Fig. 3.17. Applied Load vs. Joint Shear Deformation - Specimen 4.

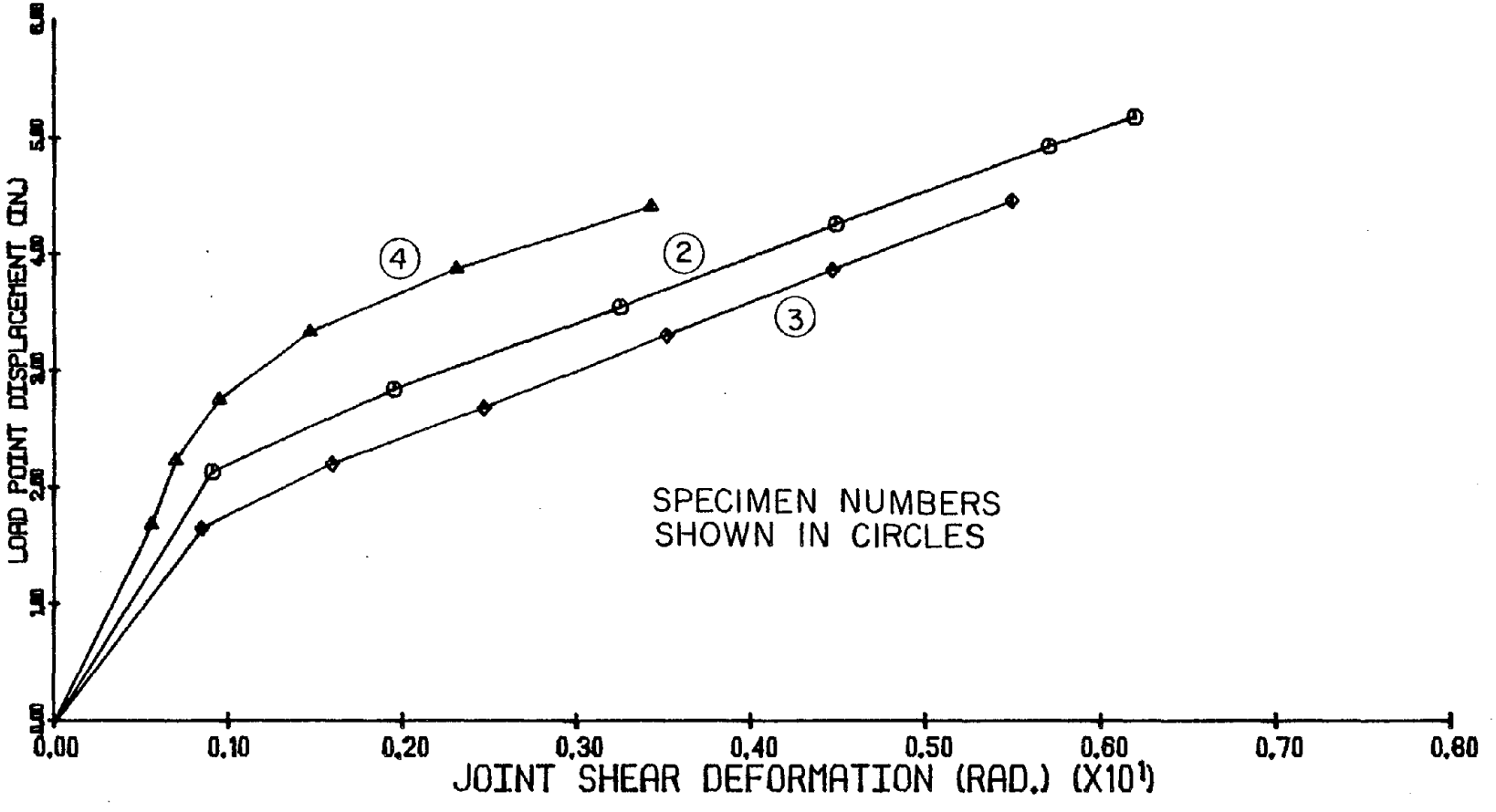

Fig. 3.18. Maximum Positive Half-Cycle Displacement vs. Joint Shear Deformation for Specimens 2, 3, and 4.

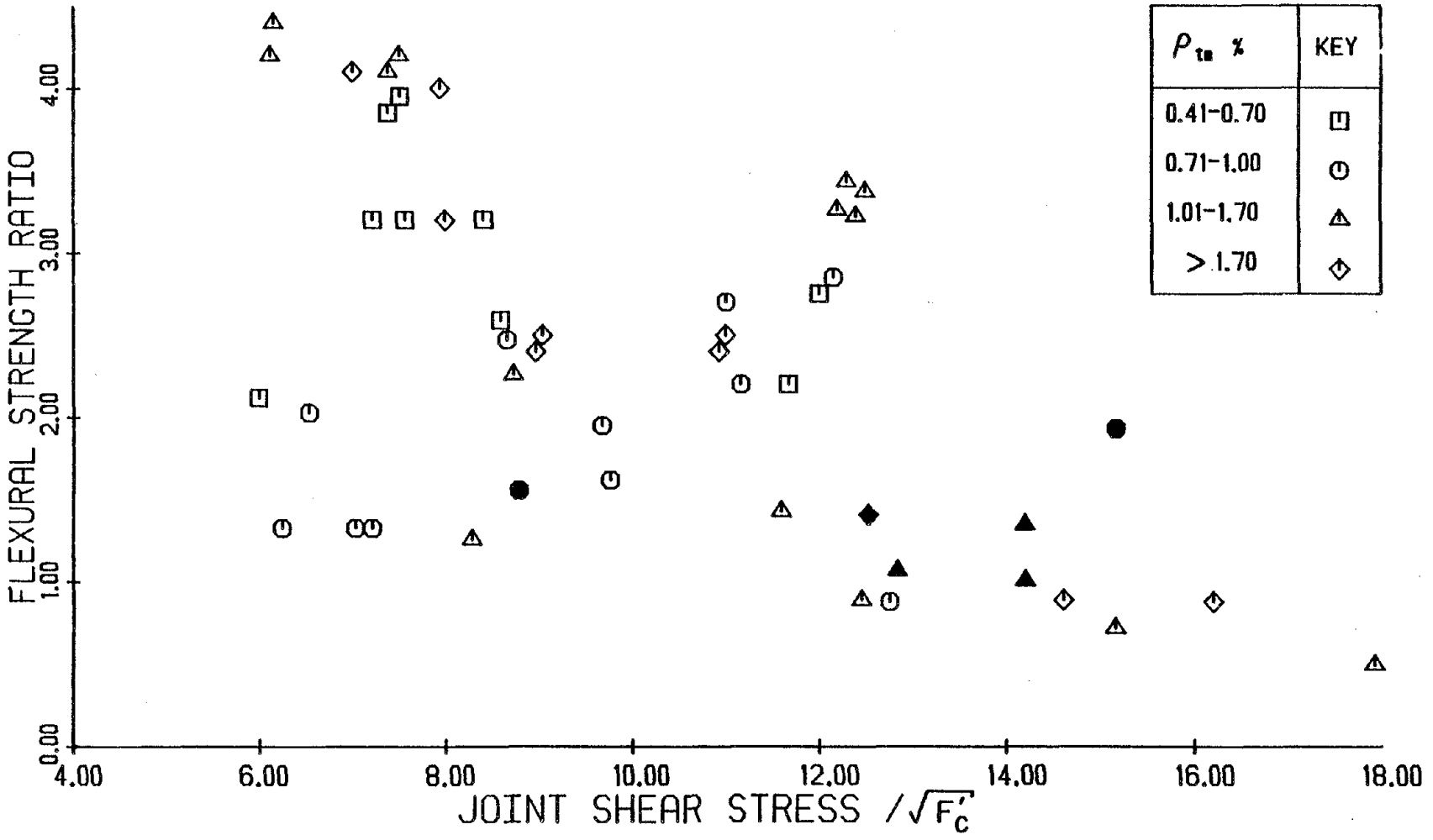

Fig. 3.19. Actual Values For the Primary Variables in Tested Specimens.

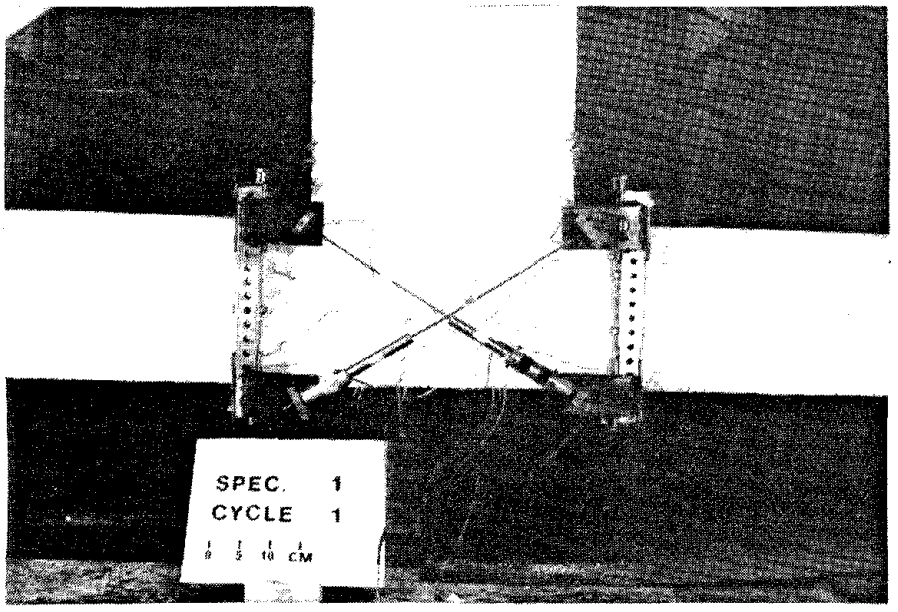

Fig. 3.20. Specimen 1 at the Conclusion of the First Cycle of Loading.

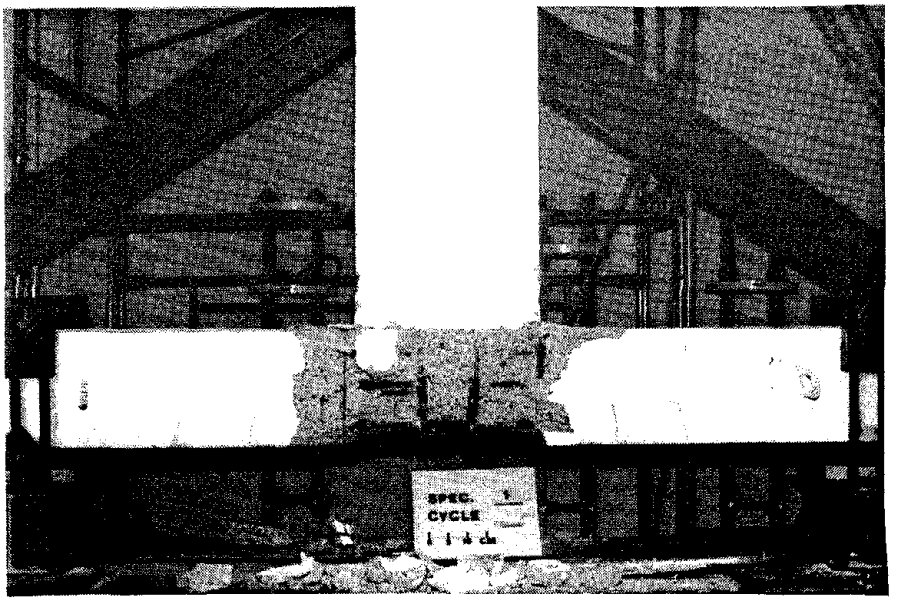

Fig. 3.21. Specimen 1 at the Conclusion of the Test.

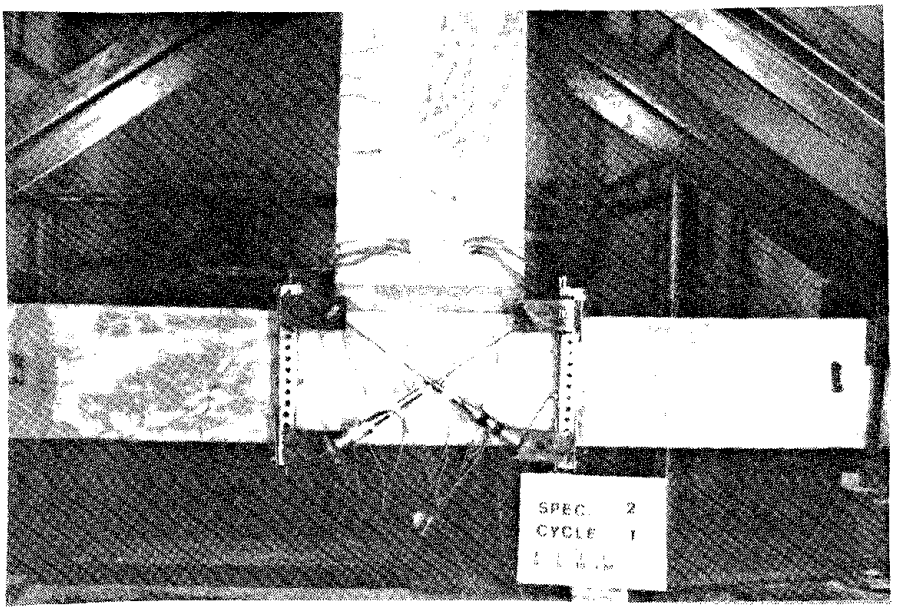

Fig. 3.22. Specimen 2 at the Conclusion of the First Cycle of Loading.

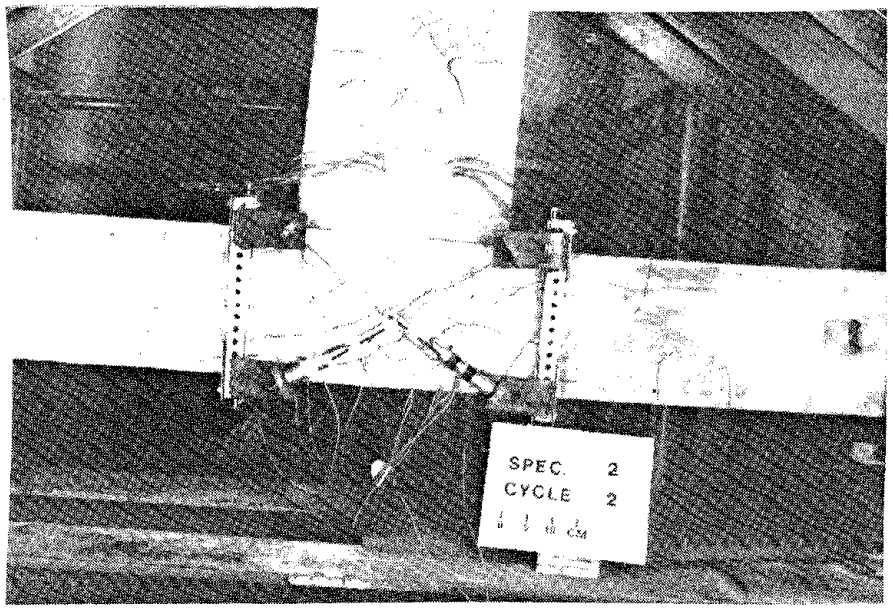

Fig. 3.23. Specimen 2 at the Conclusion of the Third Cycle of Loading.

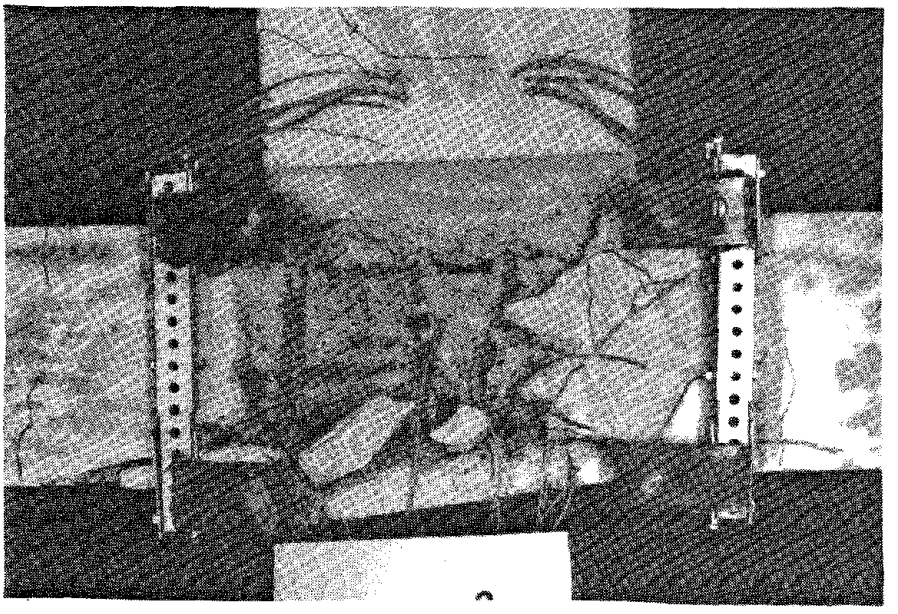

Fig. 3.24. Specimen 2 at the Conclusion of the Test.

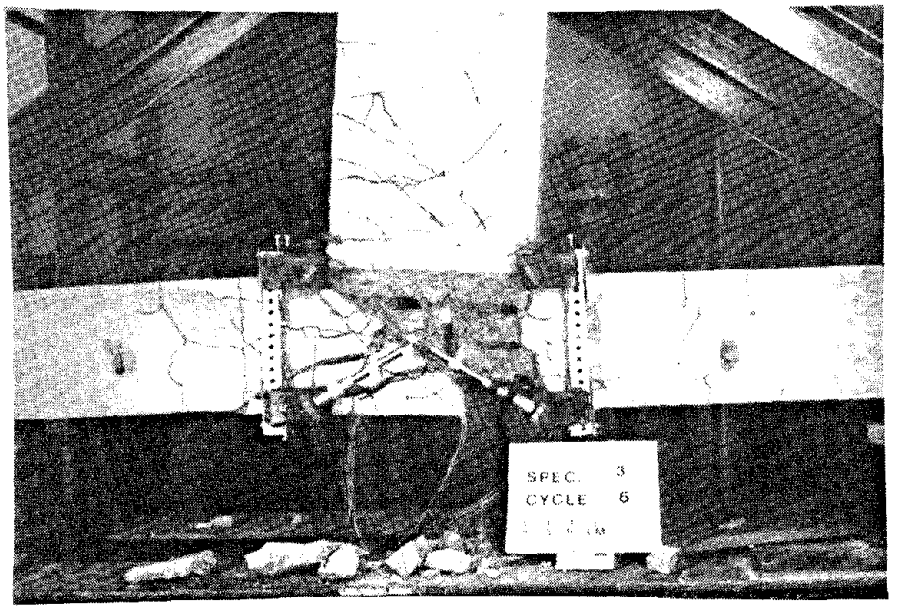

Fig. 3.25. Specimen 3 at the Conclusion of the Test.

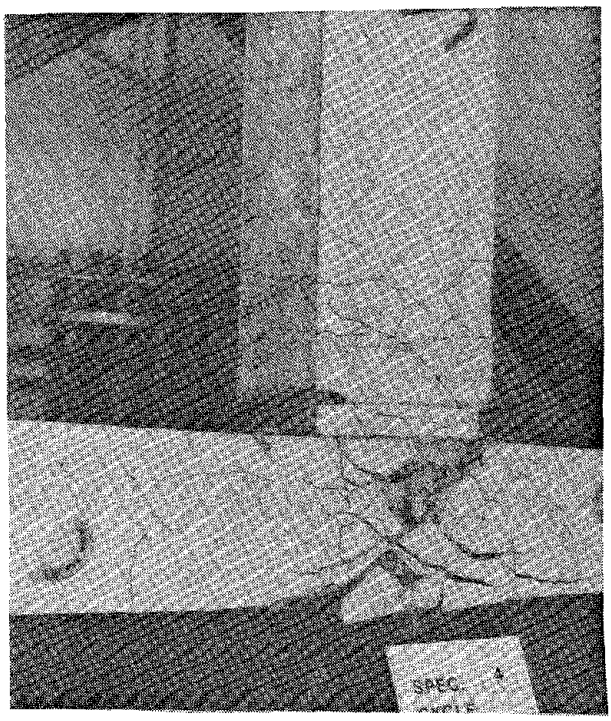

Fig. 3.26. Specimen 4 at the Conclusion of the Test.

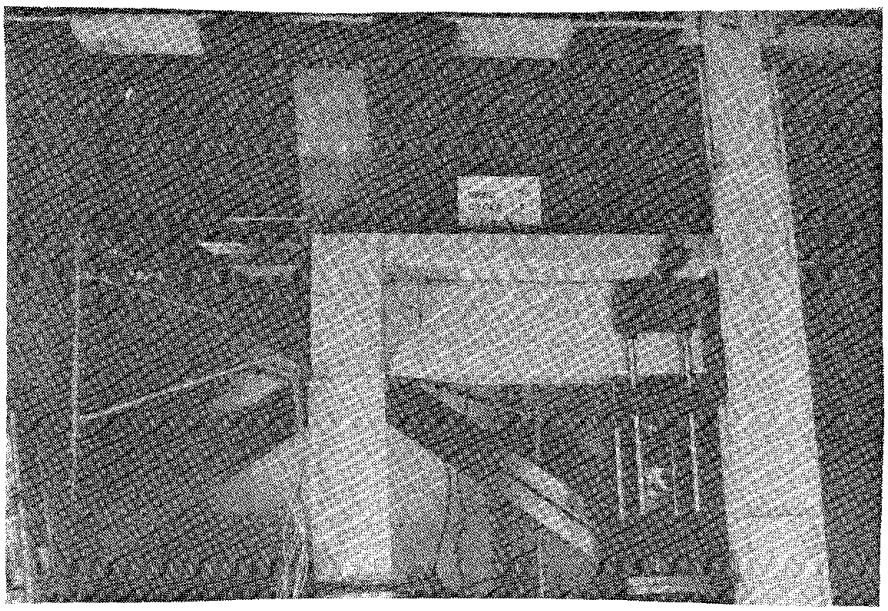

Fig. 3.27. Hinging of the Top Column Half of Specimen 5 Above the Slab During the Sixth Cycle of Loading.

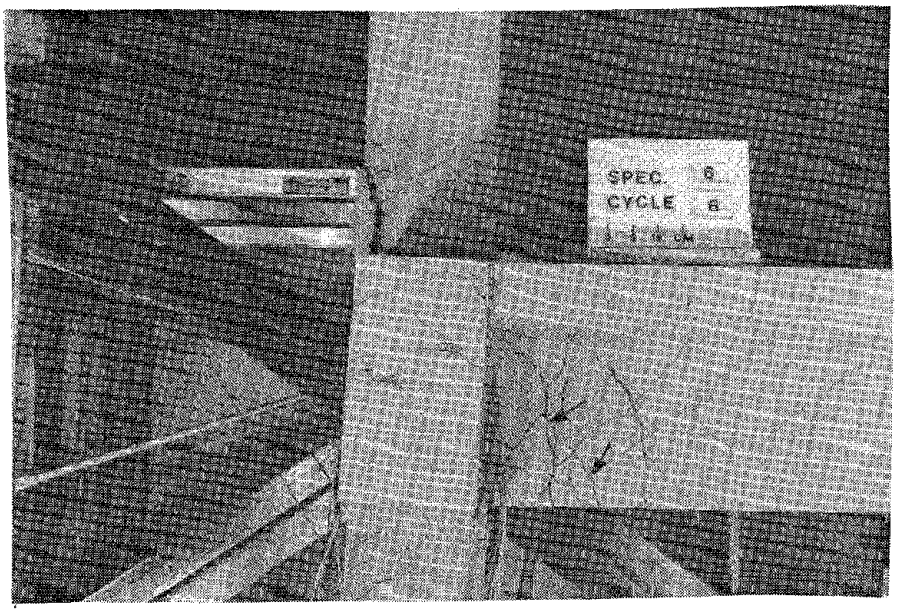

Fig. 3.28. Opening of the Beam Flexural Cracks Near the Column in Specimen 6.

Fig. 3.29. Crushing of the Concrete Due to the Hinging of the Upper Column Half - Specimen 6.

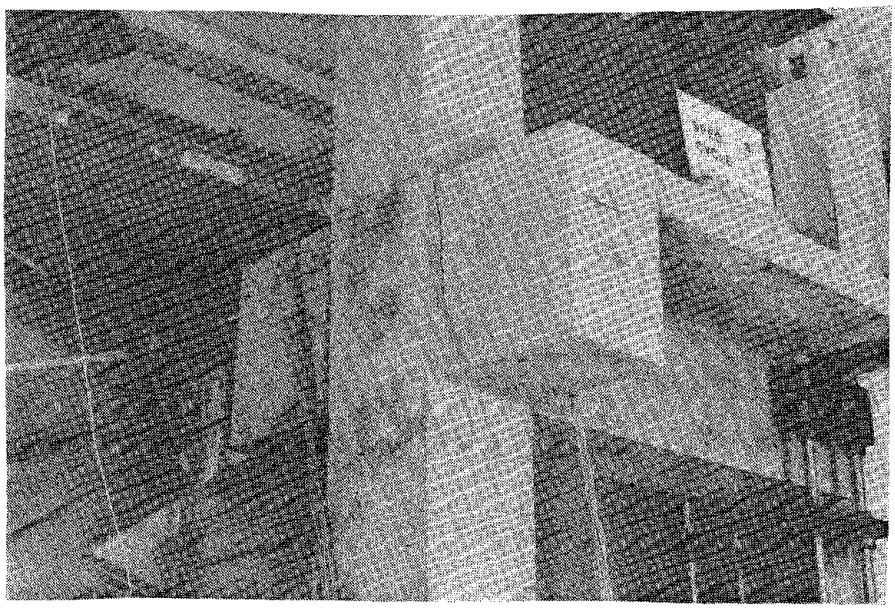

Fig. 3.30. Specimen 8 at the Conclusion of the First Cycle of Loading.

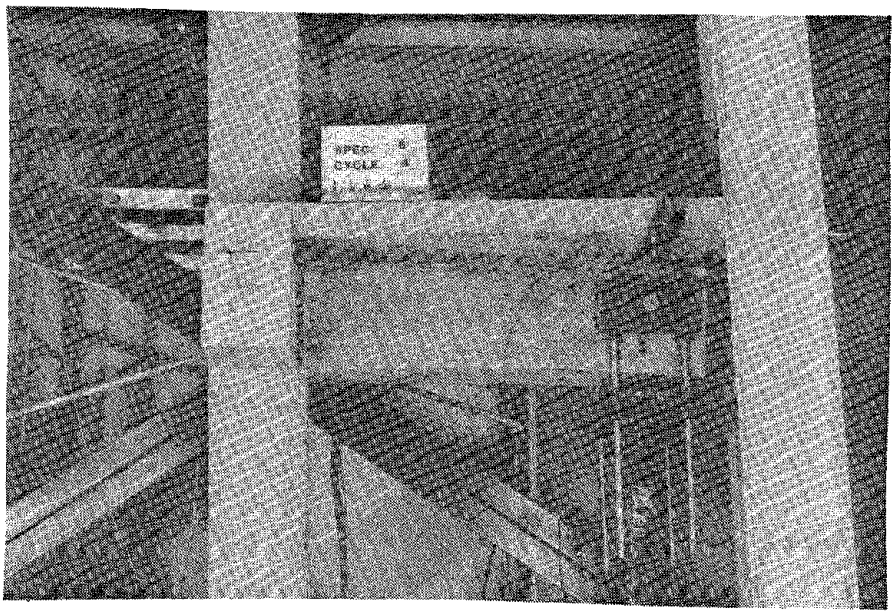

Fig. 3.31. Concentration of Damage Near the Beam Loading Point in Specimen 8.

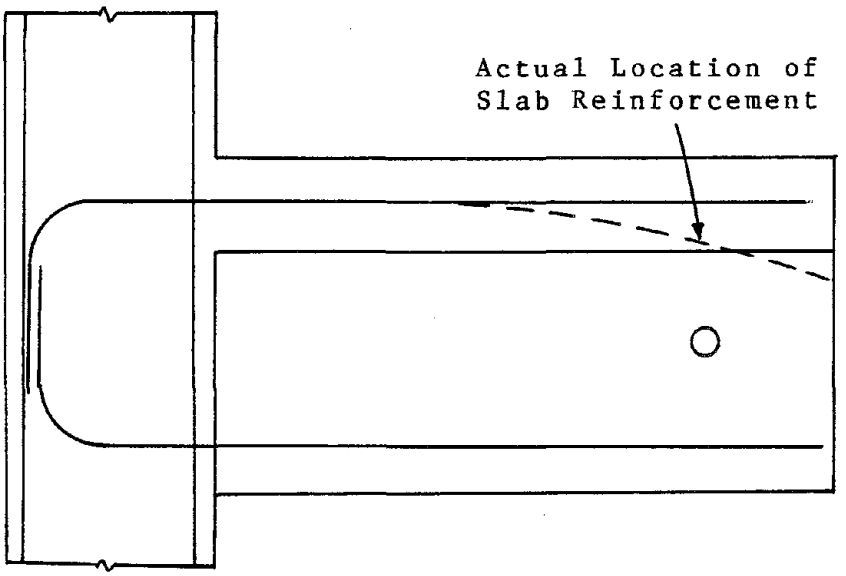

Fig. 3.32. Actual Location of Slab Longitudinal Reinforcement in Specimen 8.

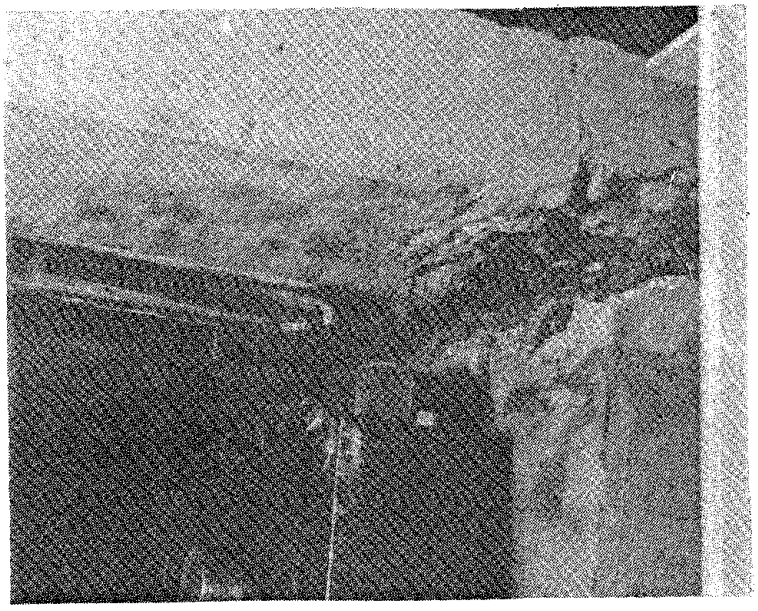

Fig. 3.33. Separation of the Beam from the Slab Near the Free End of the Beam - Specimen 8.

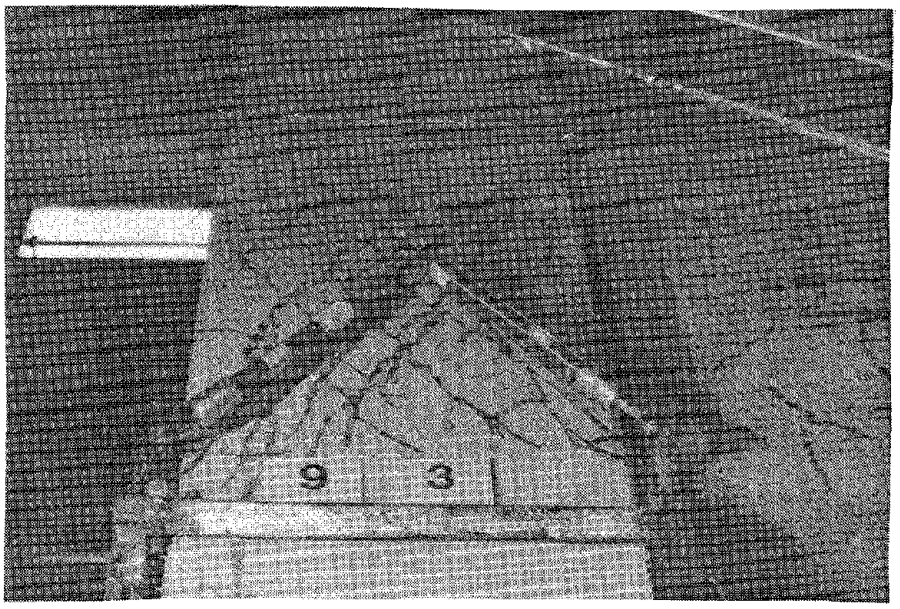

Fig. 3.34. Specimen 9 at the Conclusion of the Third Cycle of Loading.

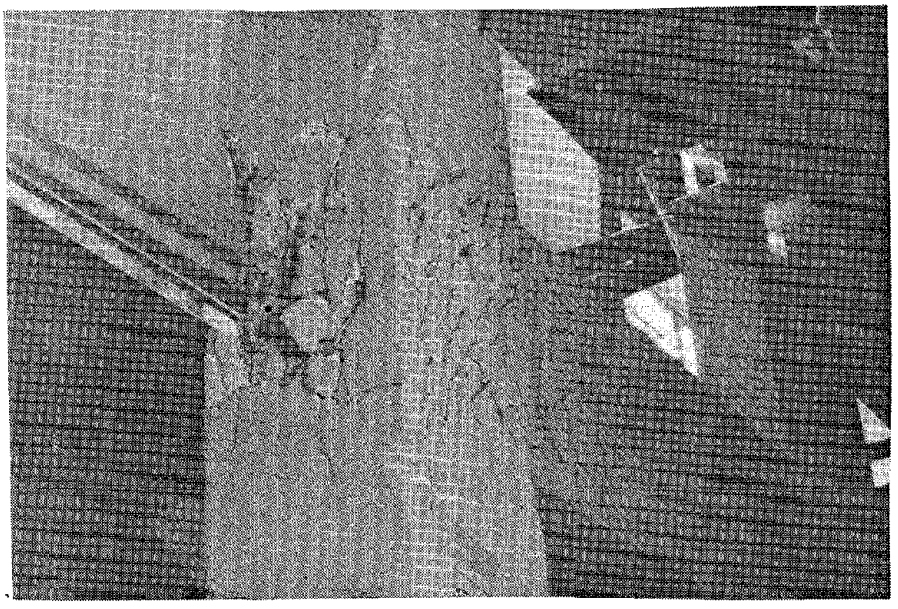

Fig. 3.35. Specimen 9 at the Conclusion of the Test.

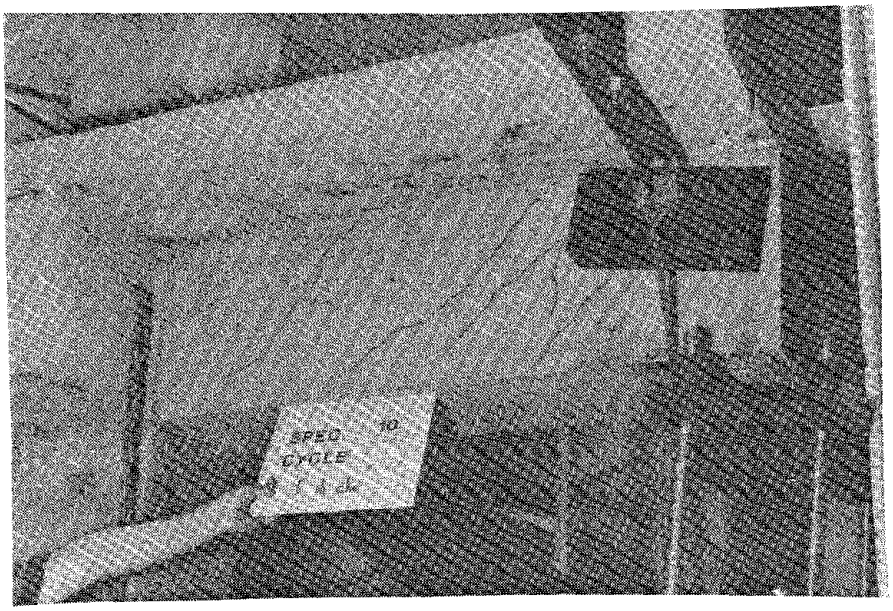

Fig. 3.36. Specimen 10 Before the Start of the Test.

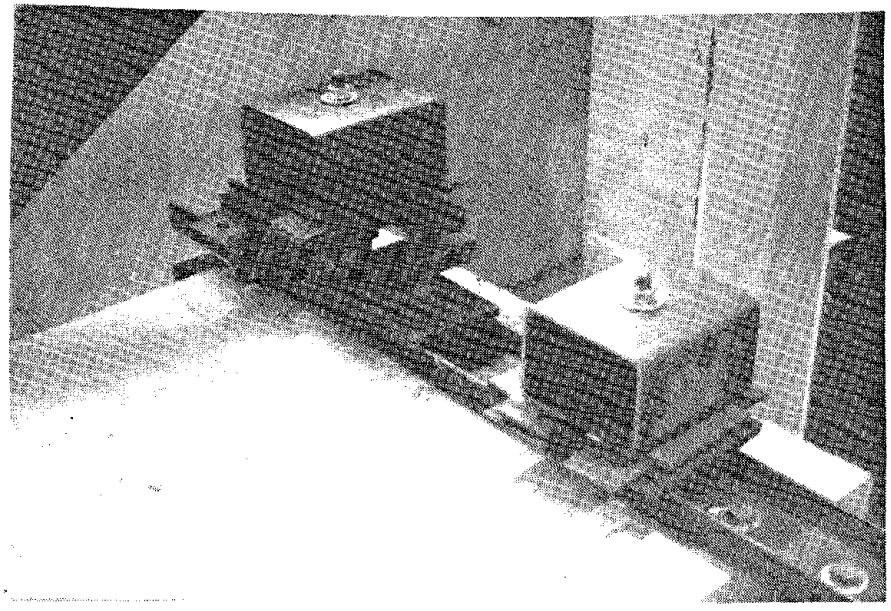

Fig. 3.37. External Tie Mechanism for Specimen 10.

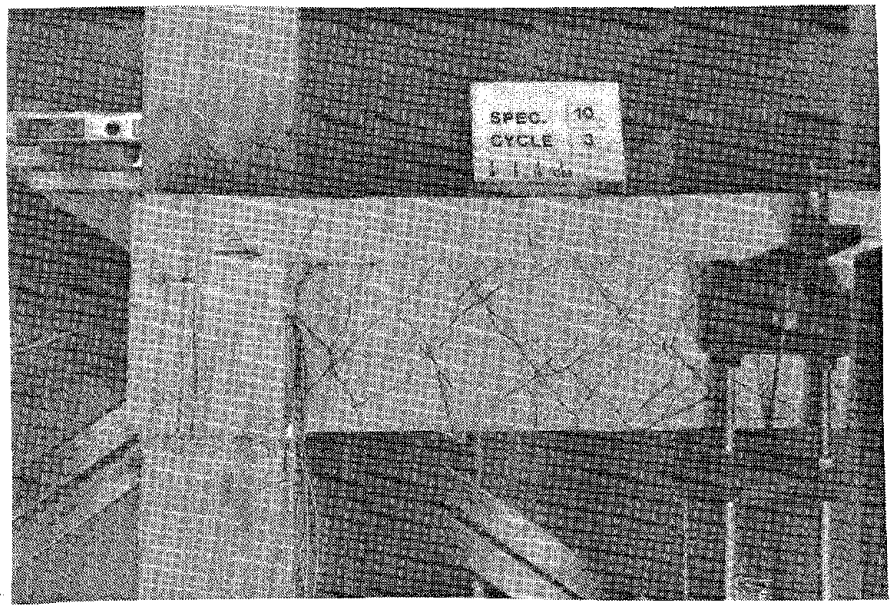

Fig. 3.38. Specimen 10 at the Conclusion of the Third Cycle of Loading.

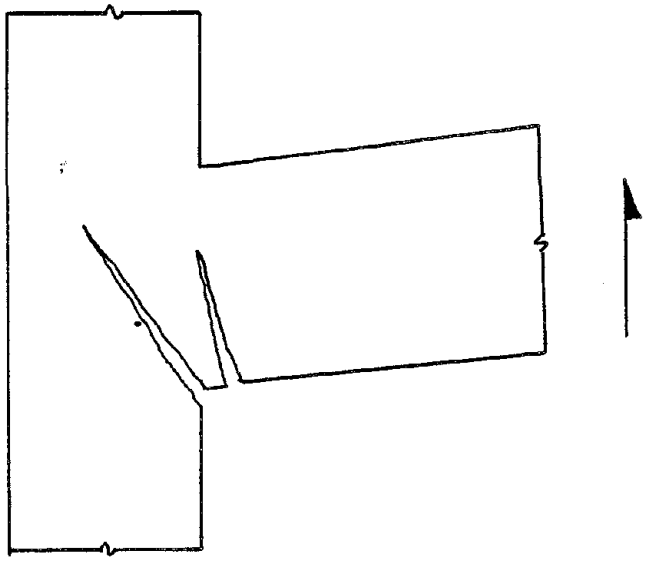

Fig. 3.39. Location of Large Shear and Flexural Cracks in Specimen 11.

Fig. 3.40. Specimen 11 at the Conclusion of the Fifth Cycle of Loading.

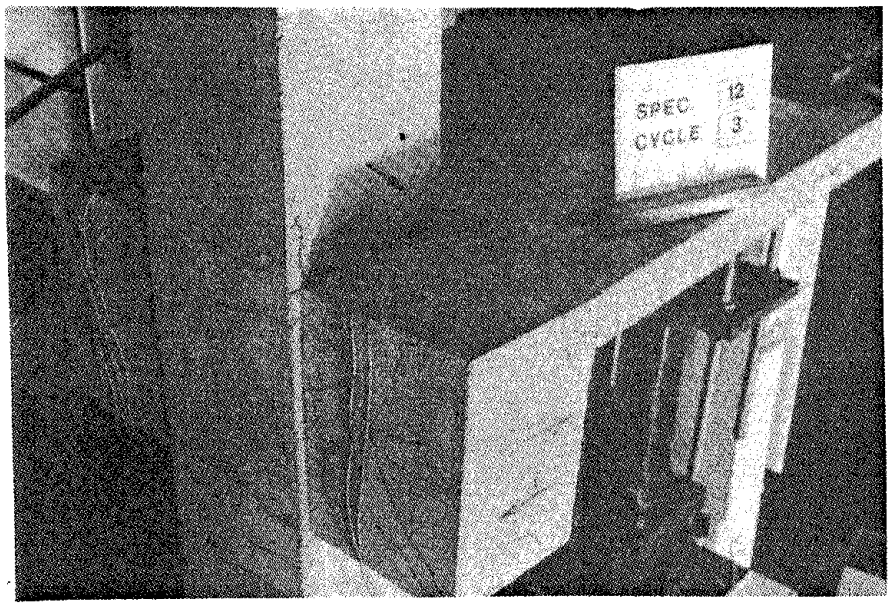

Fig. 3.41. Propagation of the Cracks into the Column Portion of Specimen 12.

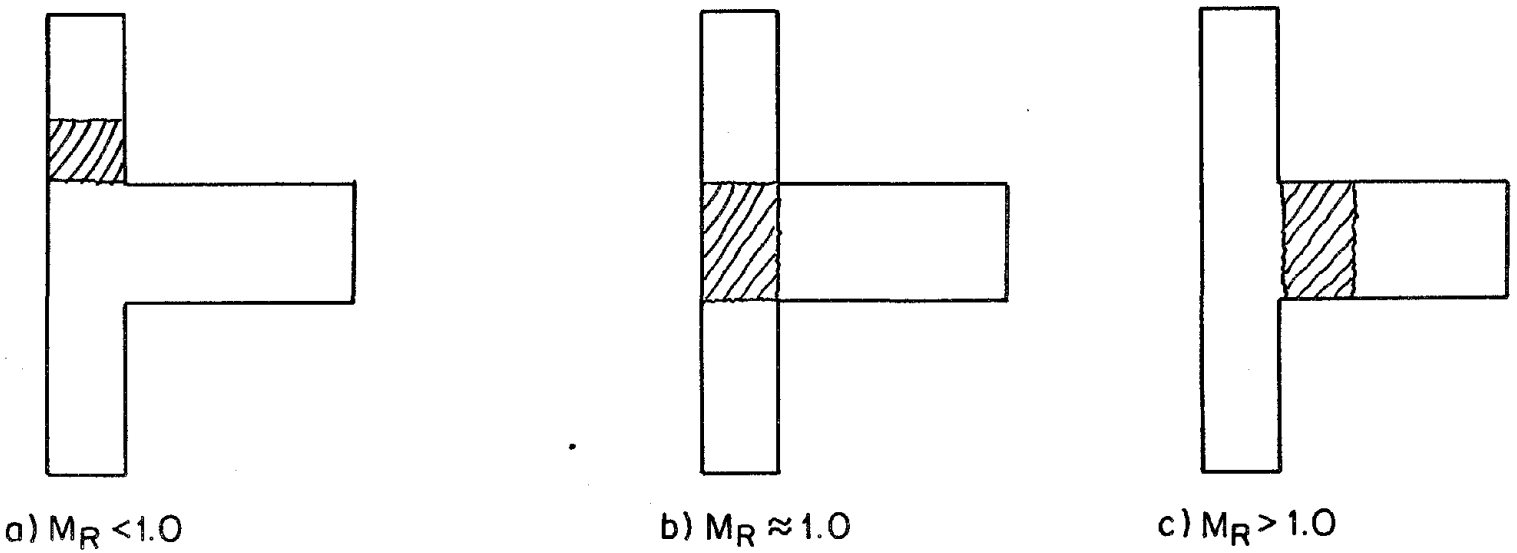

Fig. 3.42. Location of Plastic Hinges in Specimens with Different Flexural Strength Ratios.

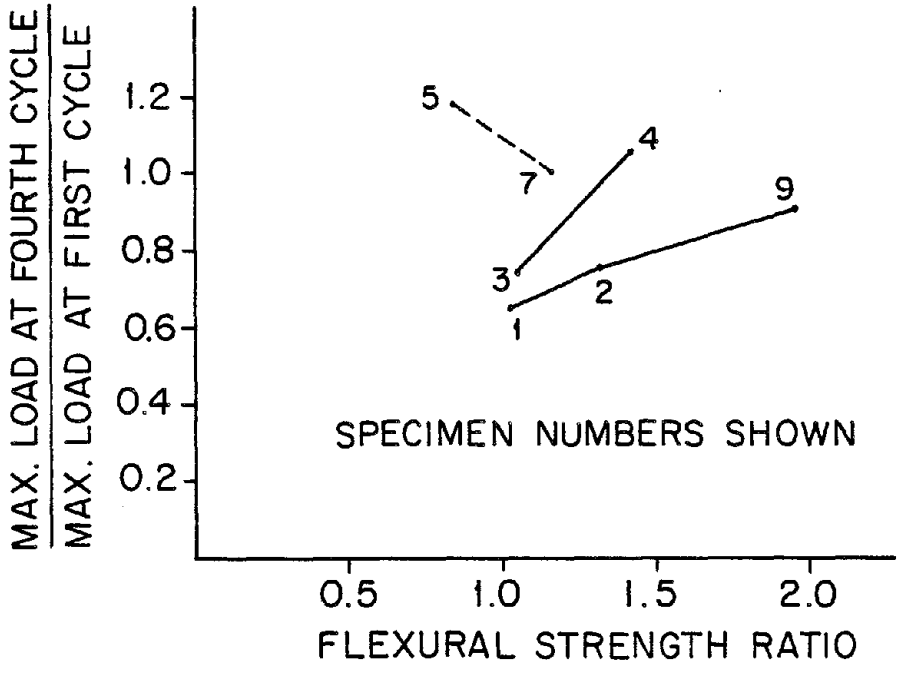

Fig. 3.43. Effect of the Flexural Strength Ratio on the Cyclic Load Carrying Capacity of the Specimens.

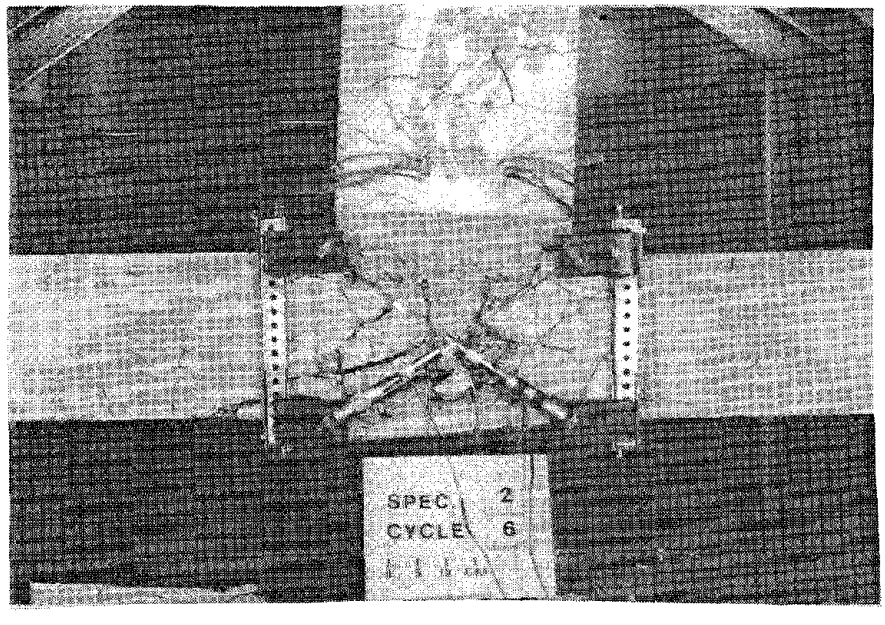

Fig. 3.44. Specimen 2 at the Conclusion of the Test.

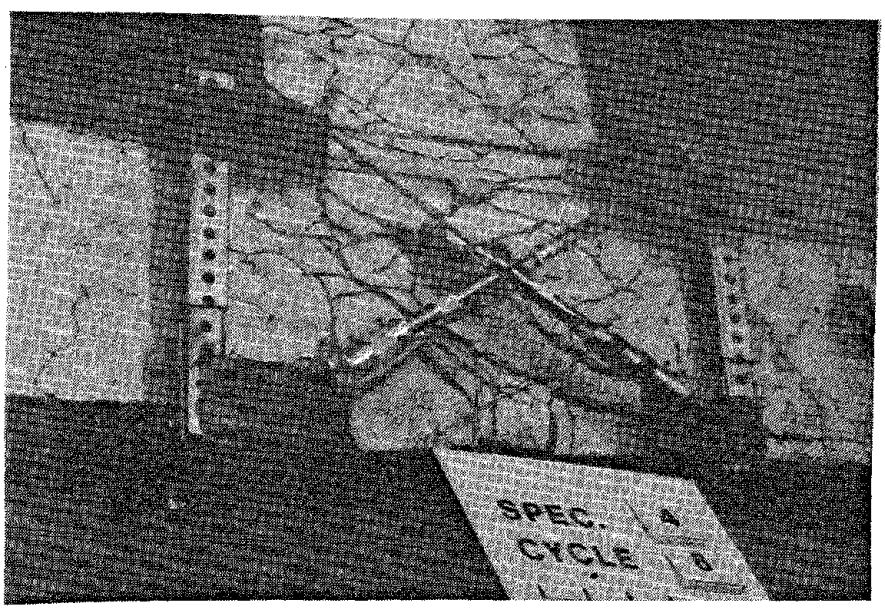

Fig. 3.45. Specimen 4 at the Conclusion of the Test.

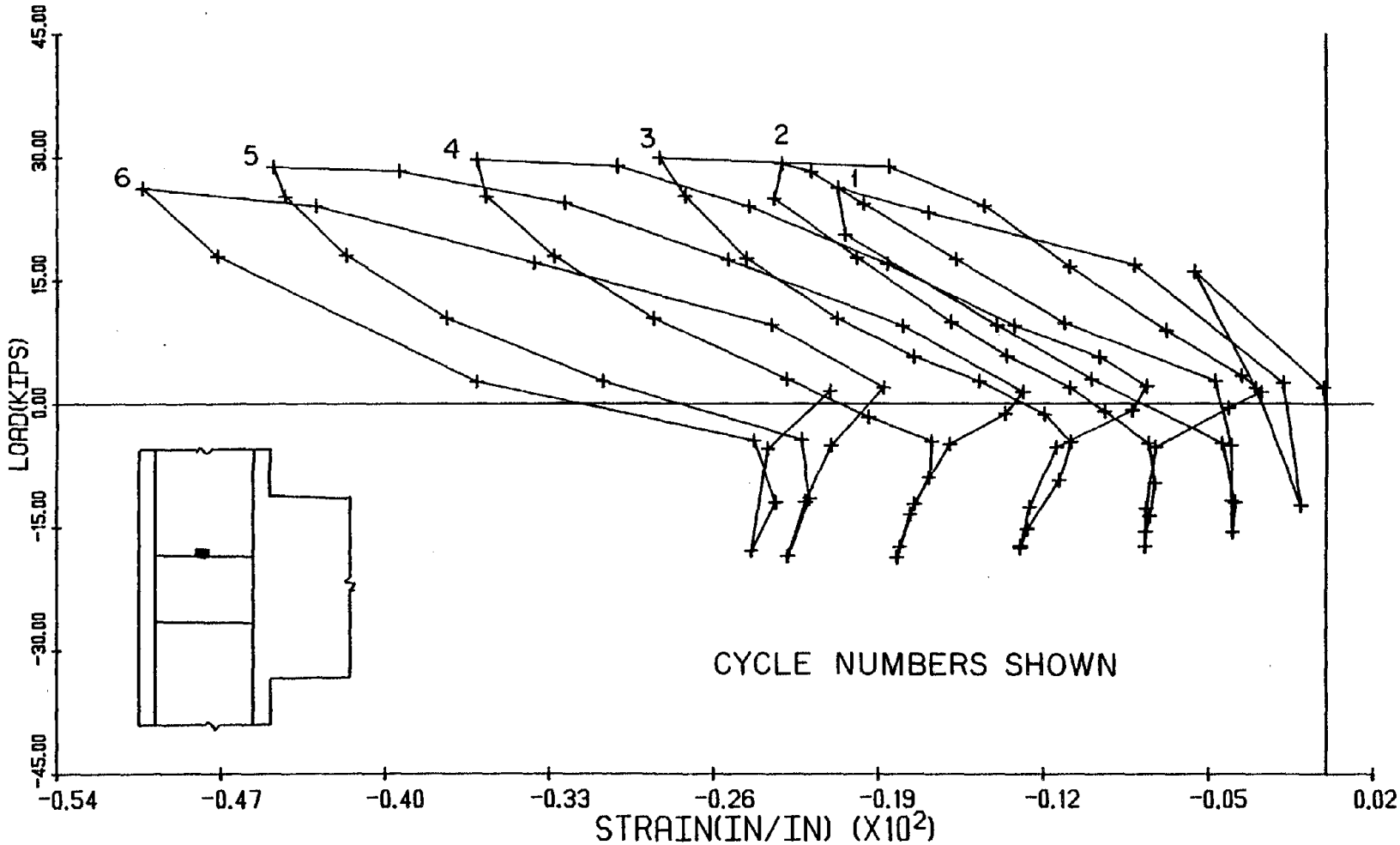

Fig. 3.46. Applied Load vs. Strain in the Hoop - Specimen 5.

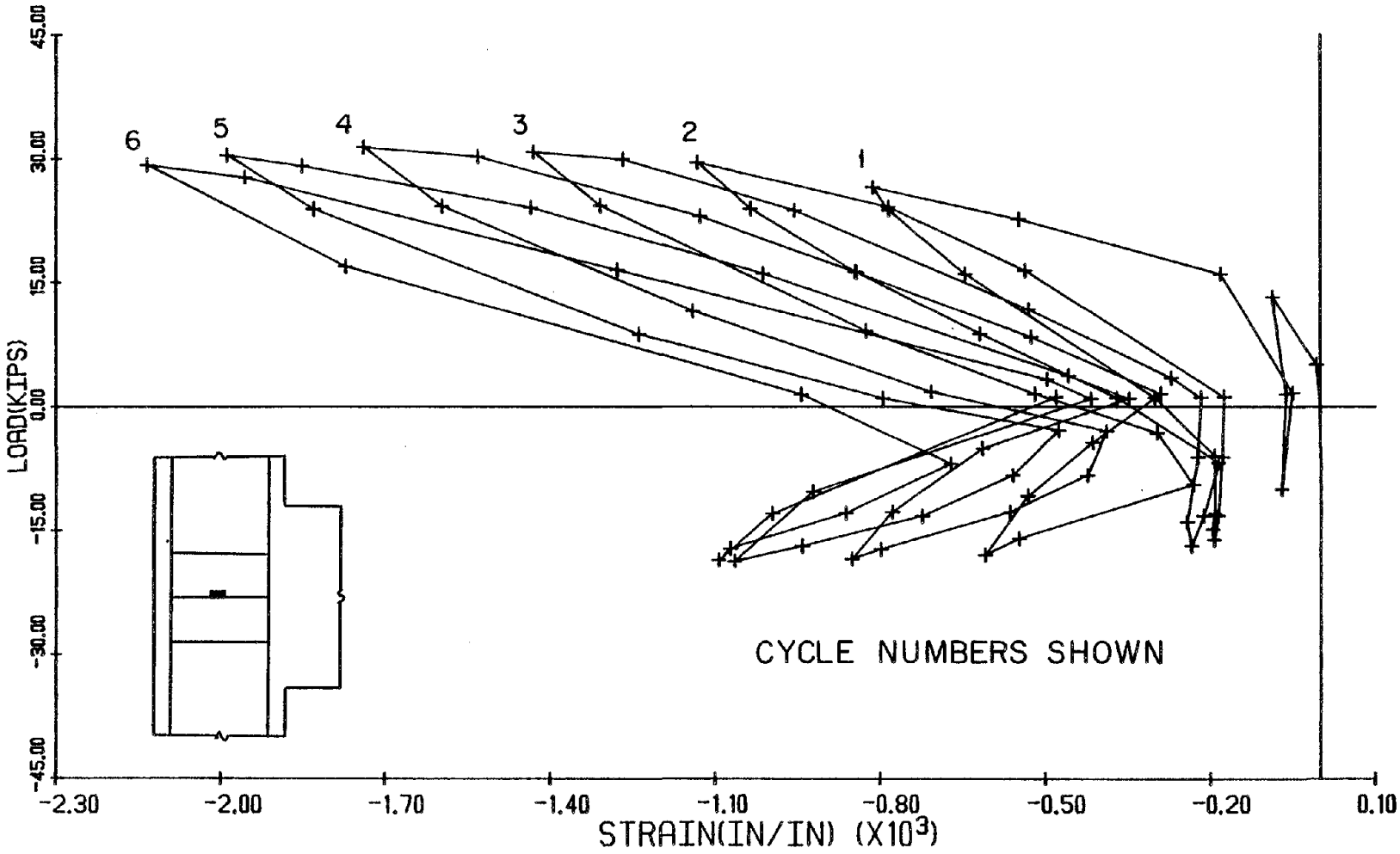

Fig. 3.47. Applied Load vs. Strain in the Hoop - Specimen 6.

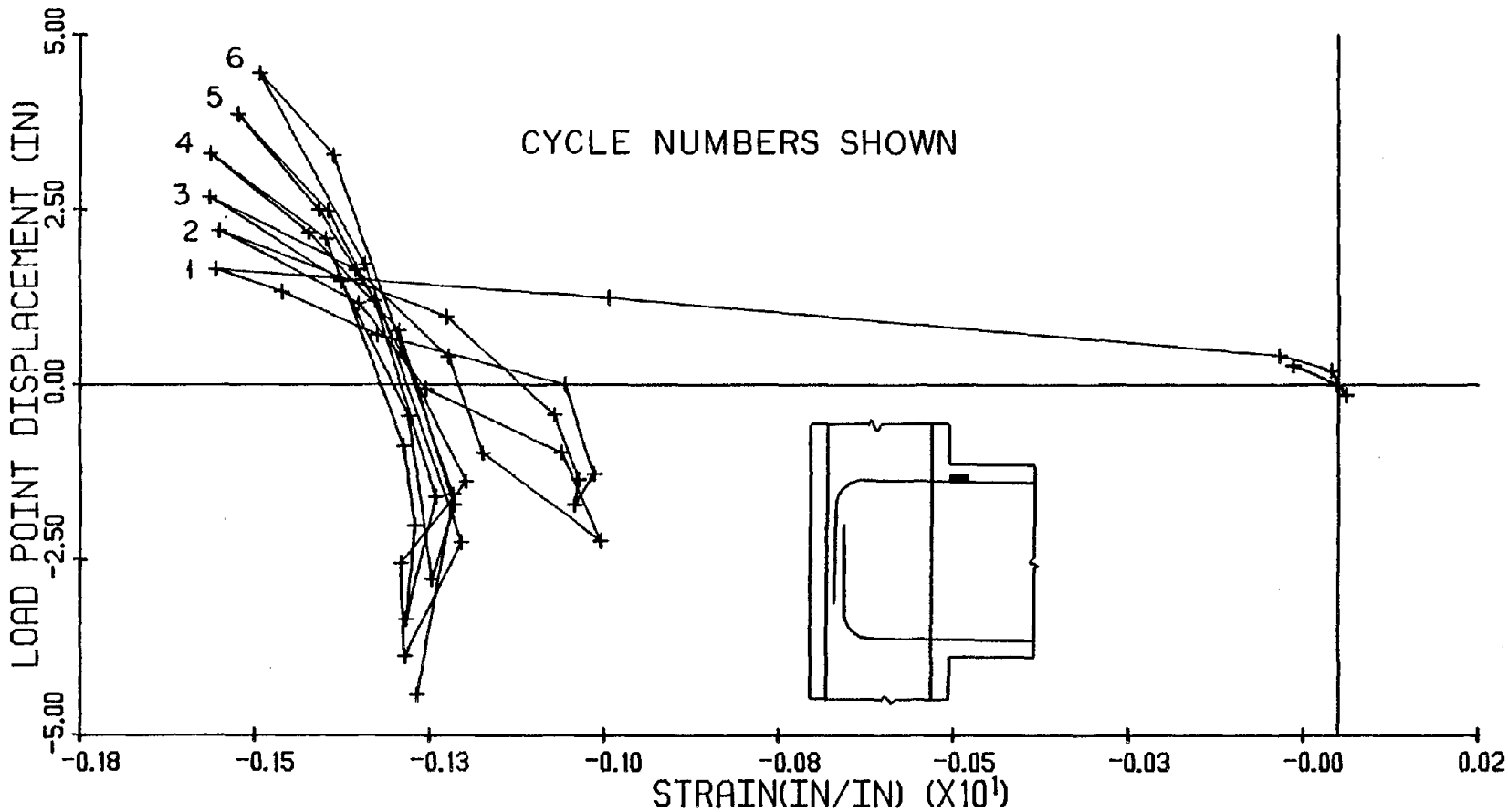

Fig. 3.48. Load Point Displacement vs. Strain in the Beam Longitudinal Reinforcement - Specimen 2.

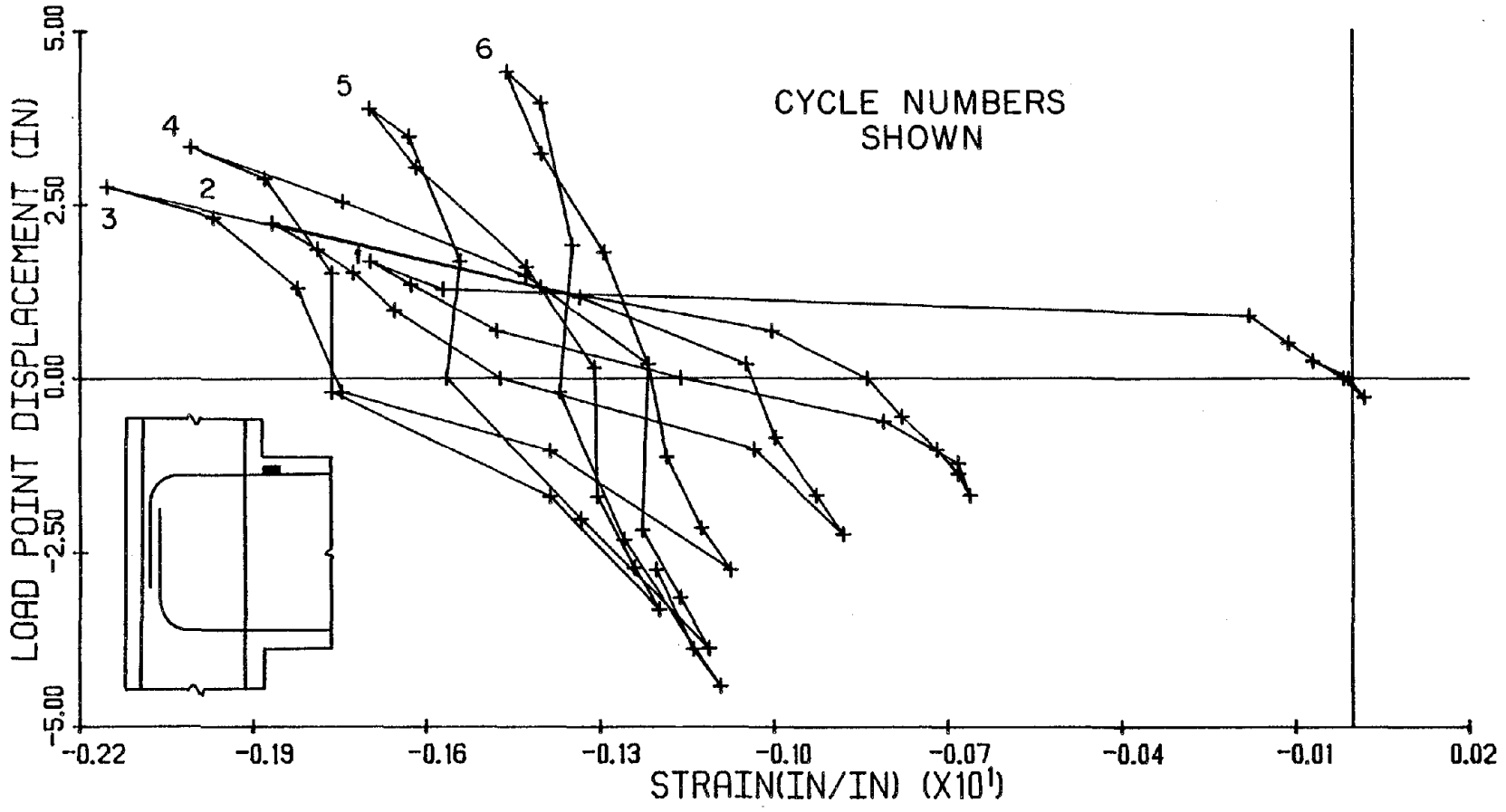

Fig. 3.49. Load Point Displacement vs. Strain in the Beam Longitudinal Reinforcement - Specimen 4.

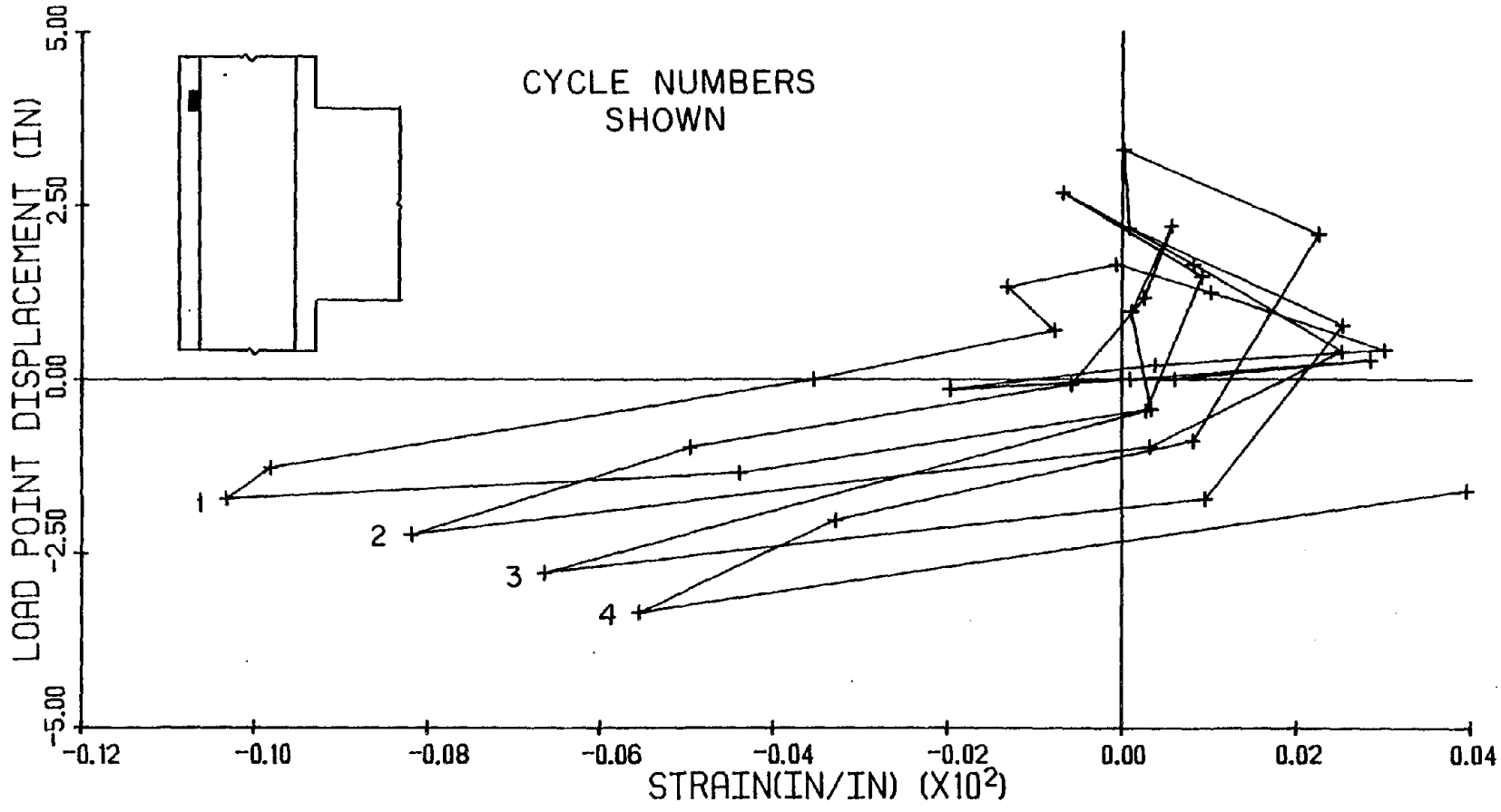

Fig. 3.50. Load Point Displacement vs. Strain in the Column Longitudinal Reinforcement - Specimen 2.

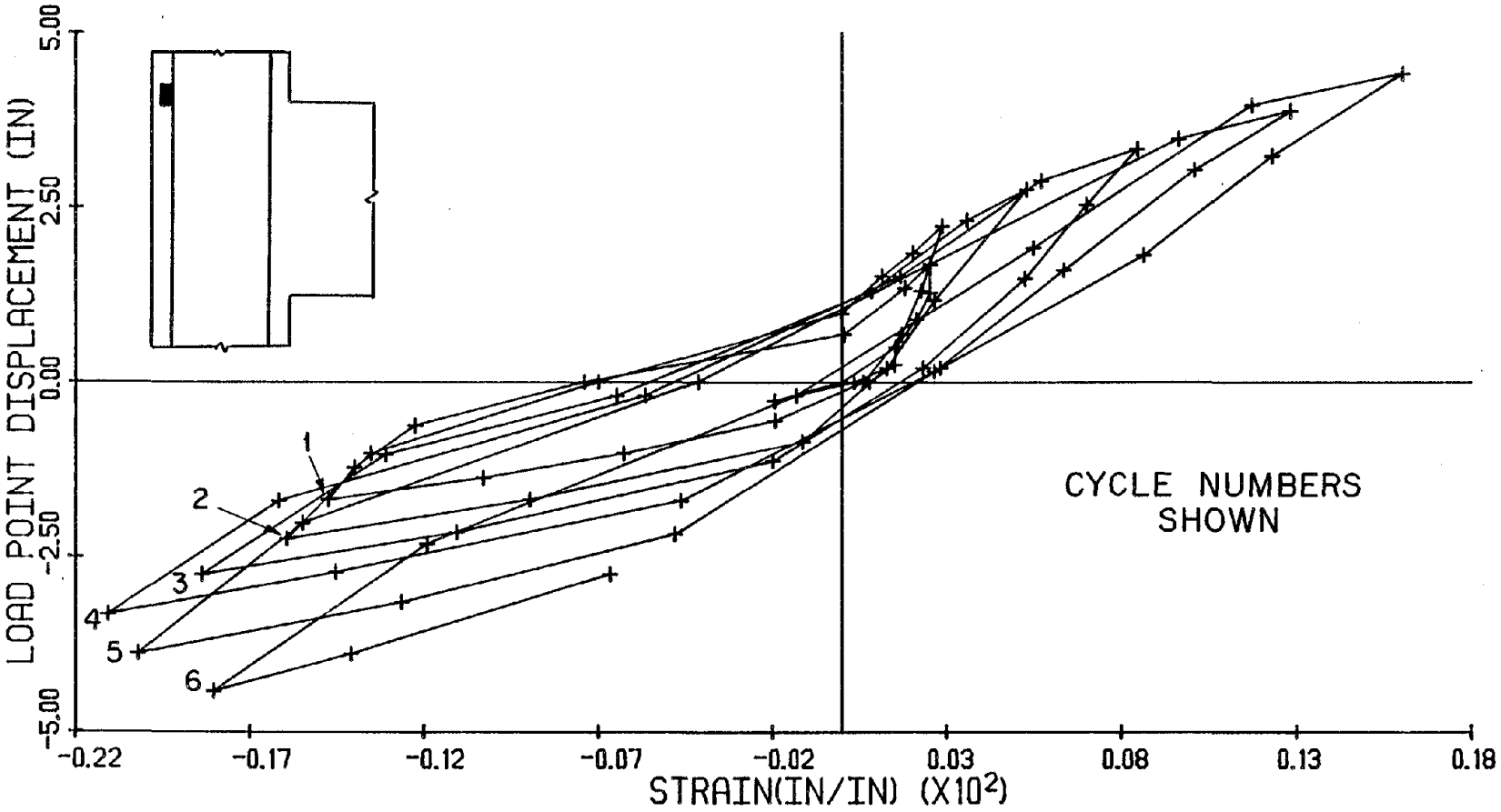

Fig. 3.51. Load Point Displacement vs. Strain in the Column Longitudinal Reinforcement - Specimen 4.

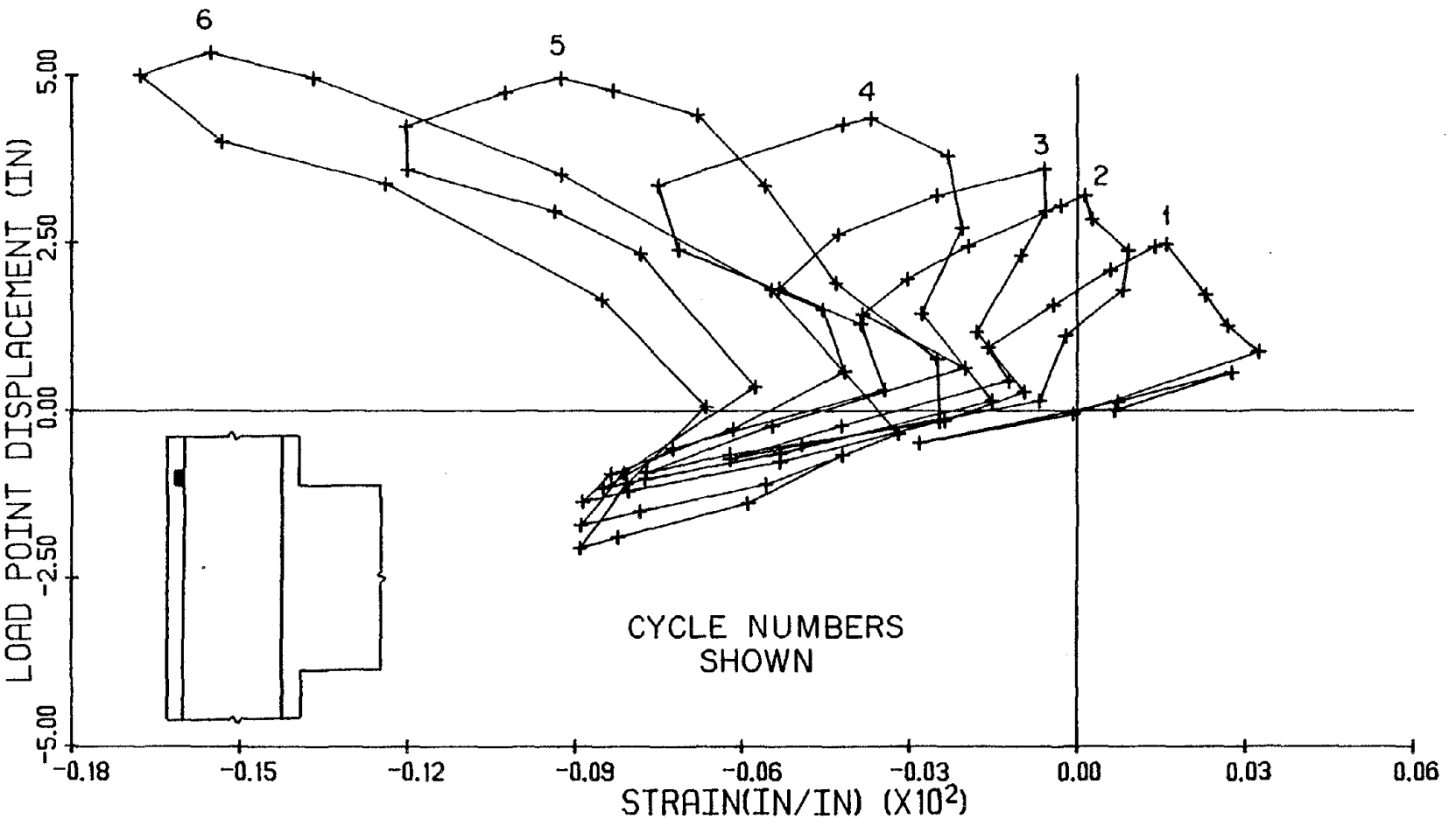

Fig. 3.52. Load Point Displacement vs. Strain in the Column Longitudinal Reinforcement - Specimen 7.

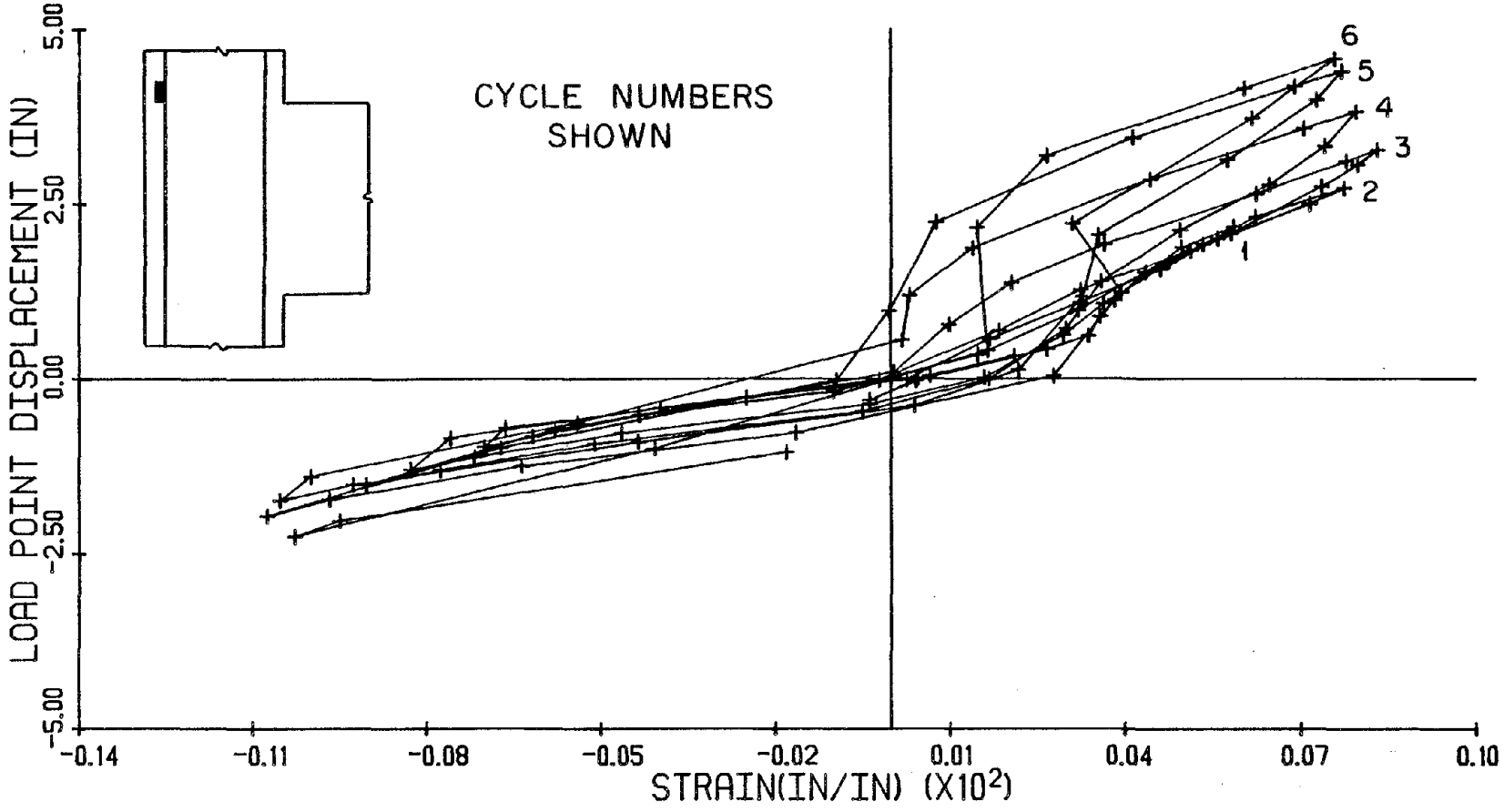

Fig. 3.53. Load Point Displacement vs. Strain in the Column Longitudinal Reinforcement - Specimen 12.

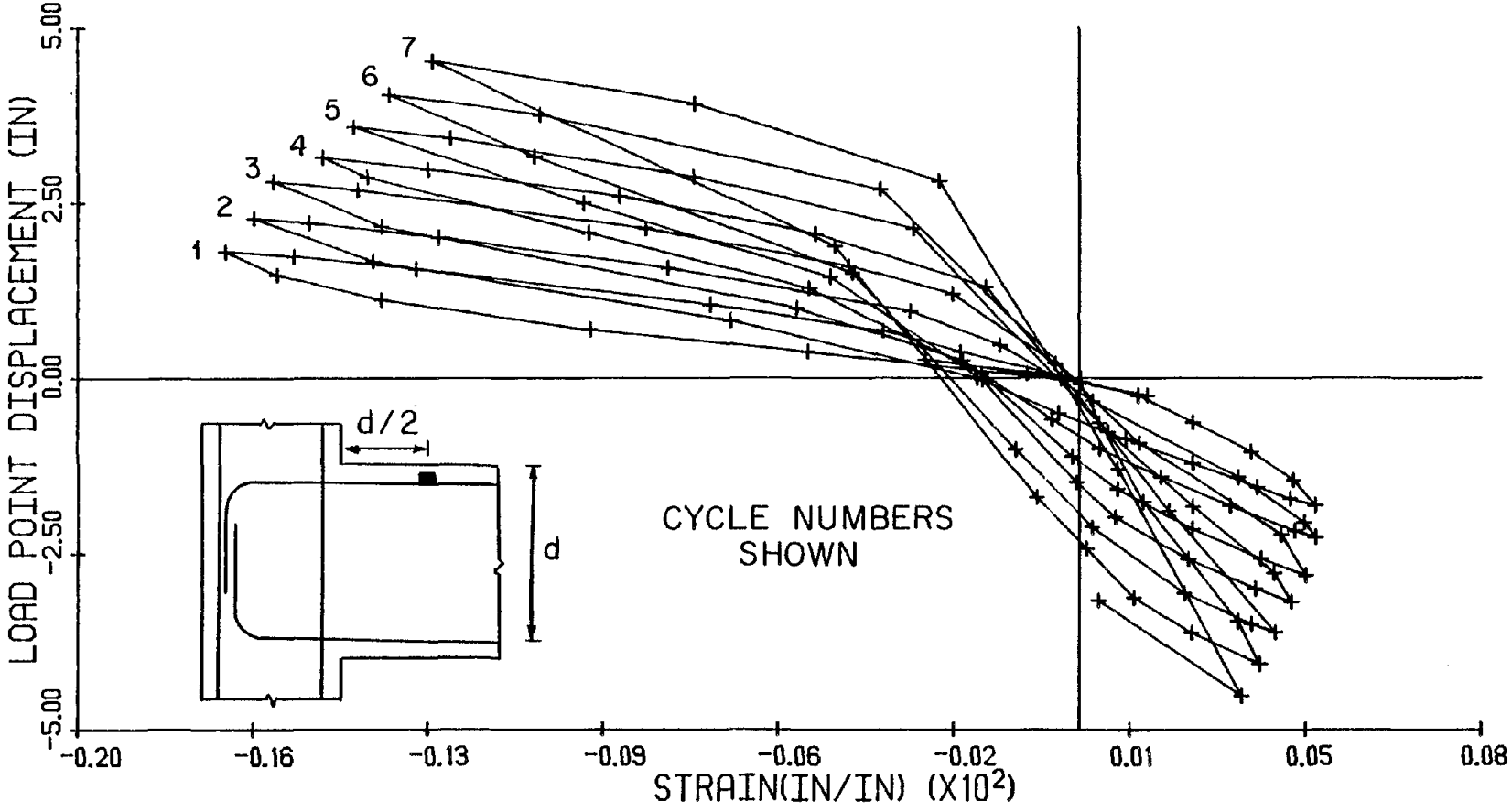

Fig. 3.54. Load Point Displacement vs. Strain in the Beam Longitudinal Reinforcement - Specimen 9.

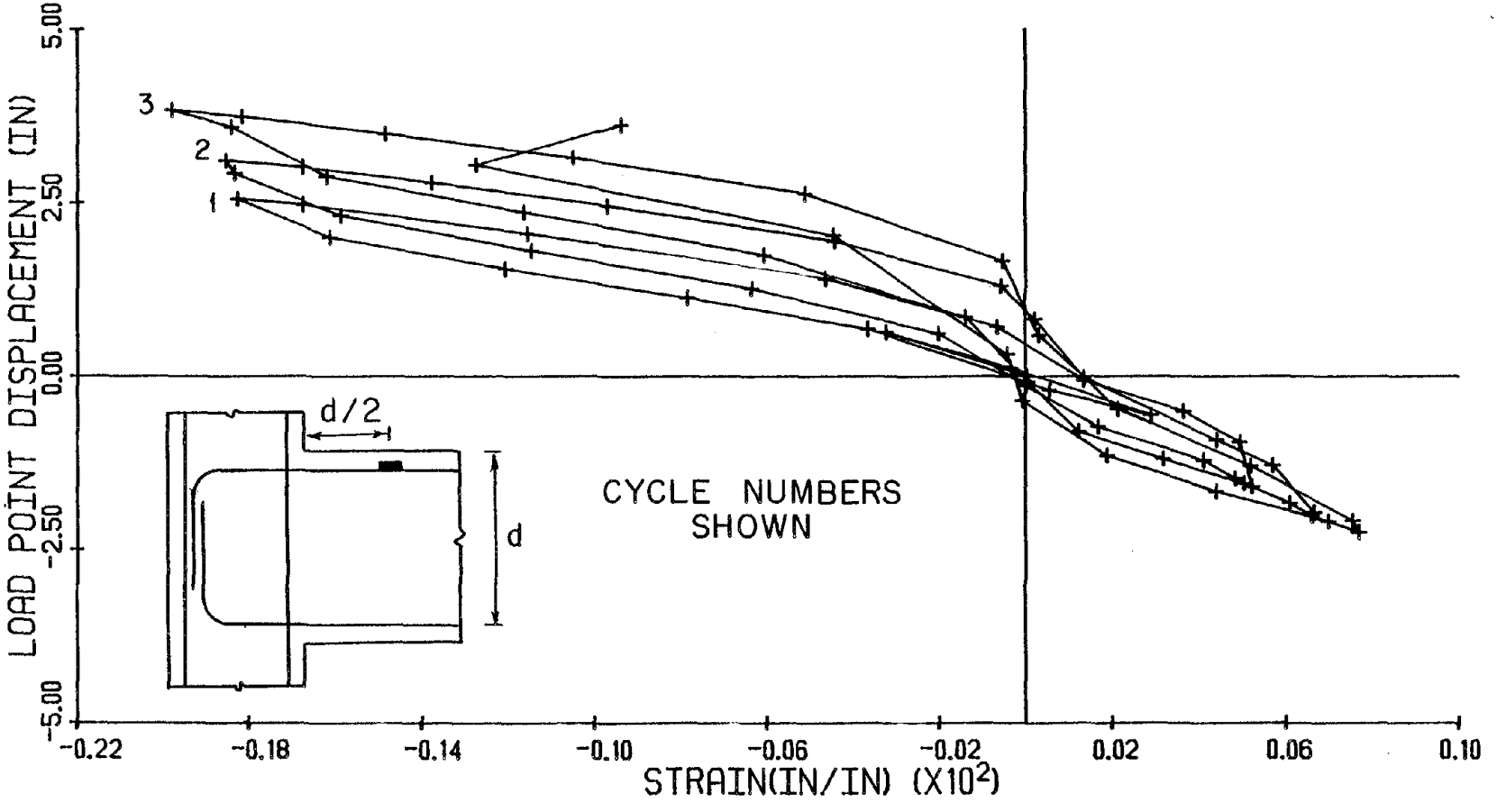

Fig. 3.55. Load Point Displacement vs. Strain in the Beam Longitudinal Reinforcement - Specimen 10.

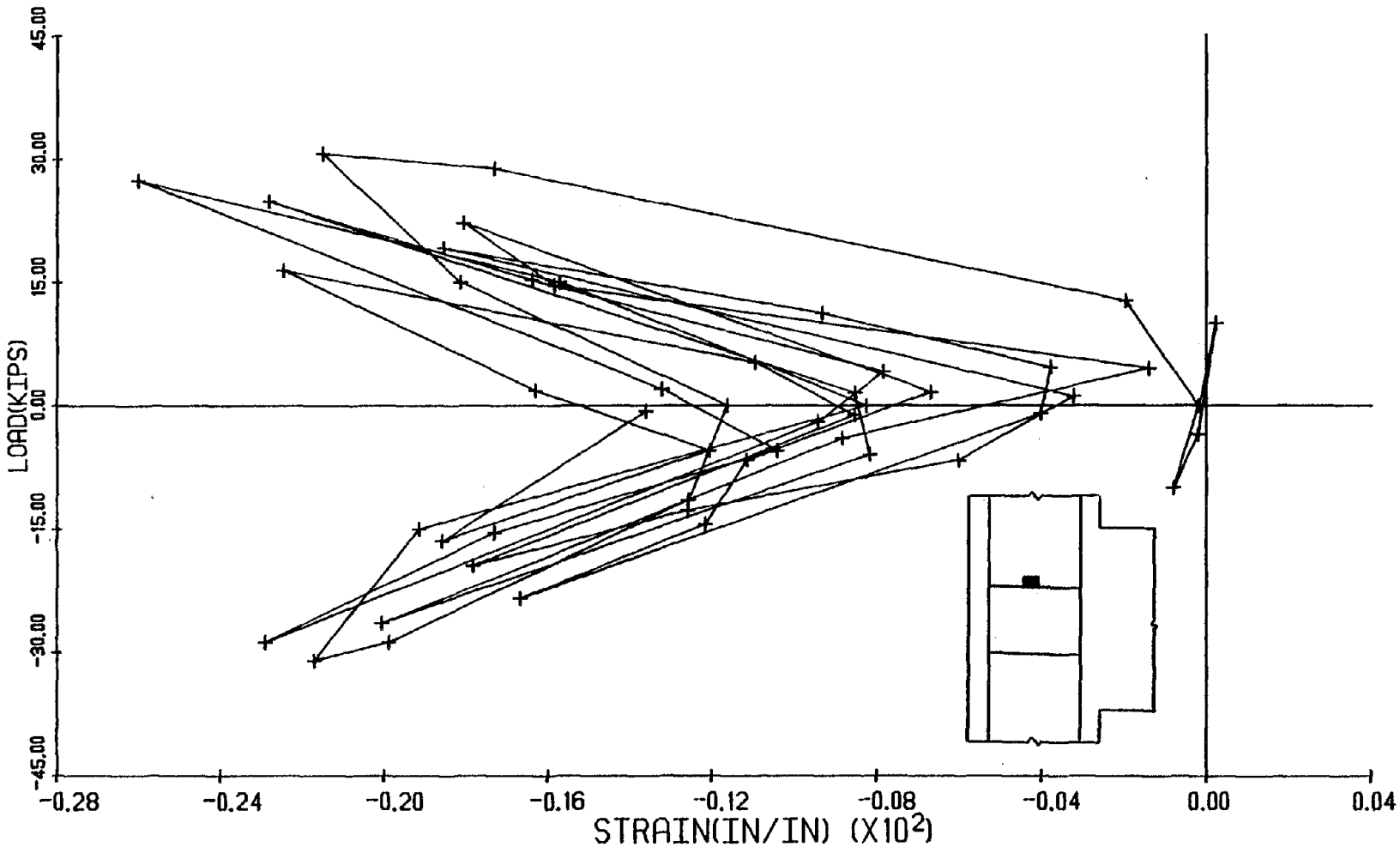

Fig. 3.56. Applied Load vs. Strain in the Hoop - Specimen 2.

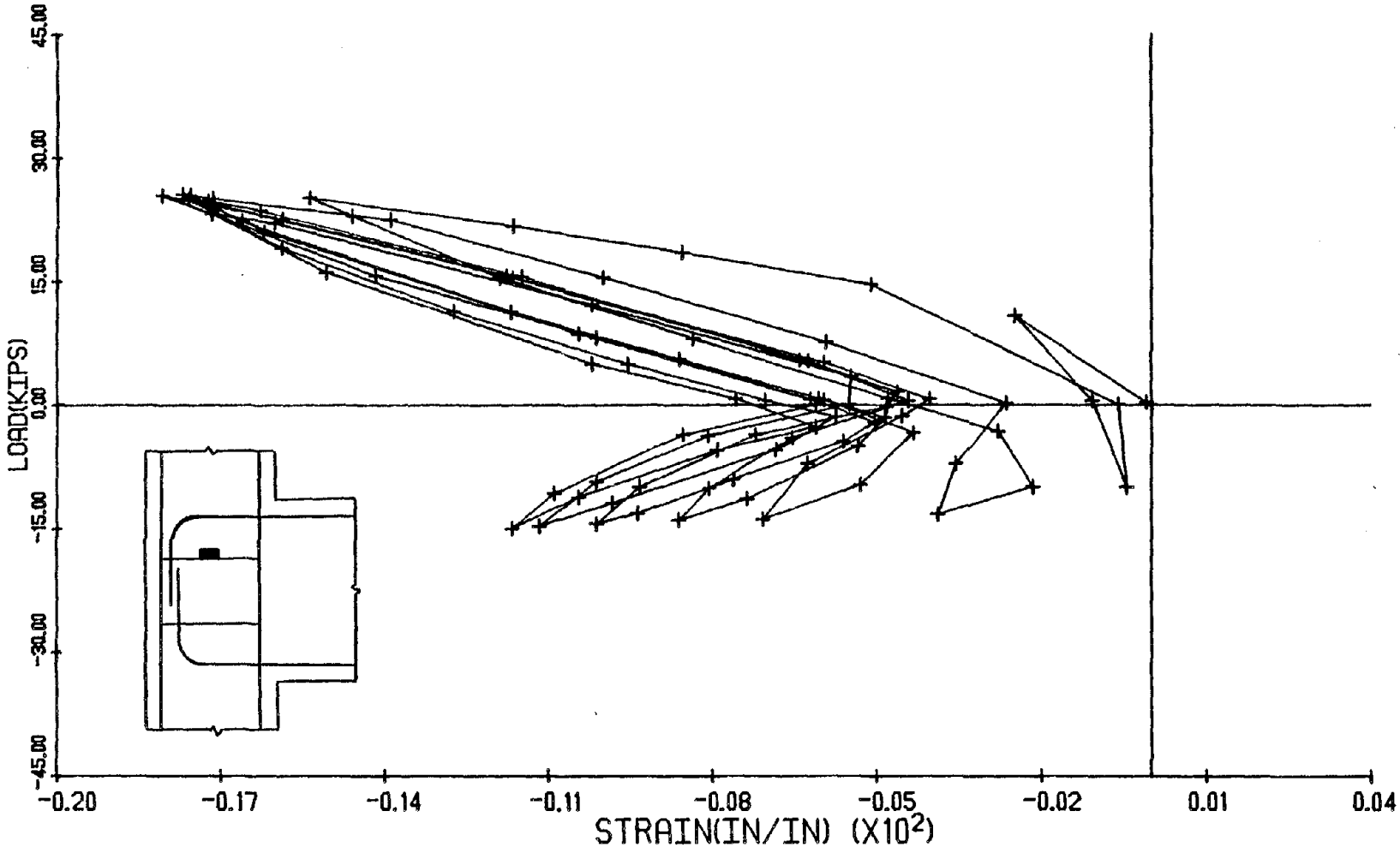

Fig. 3.57. Applied Load vs. Strain in the Hoop - Specimen 7.

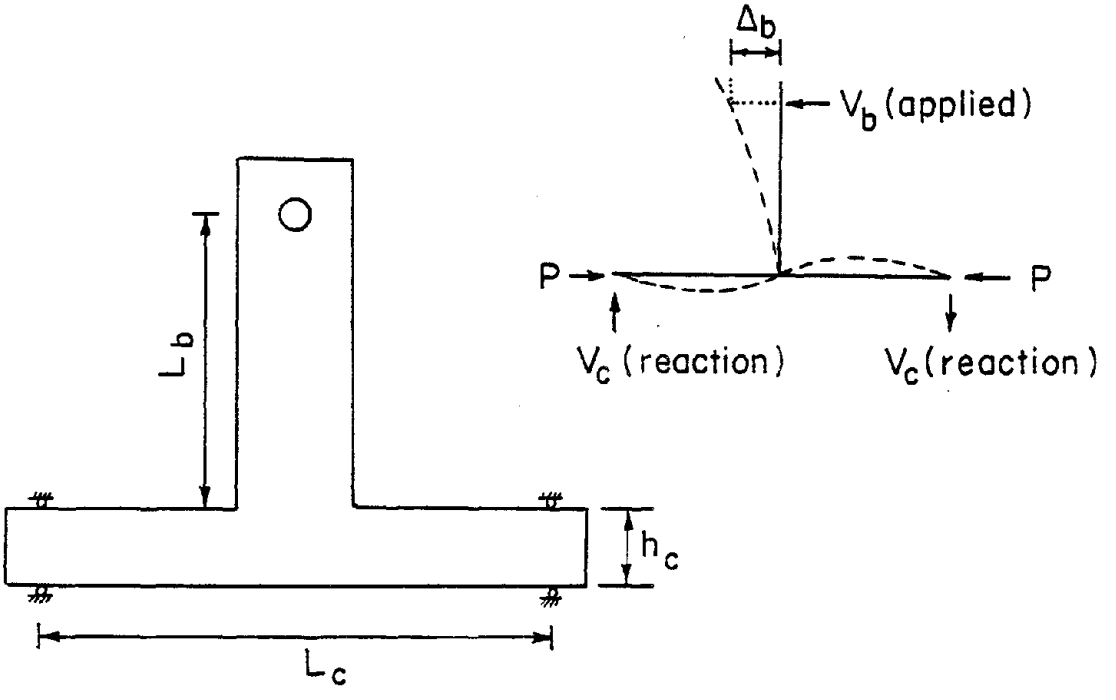

Fig. 4.1. Deflected Shape of Specimens 1 through 4.

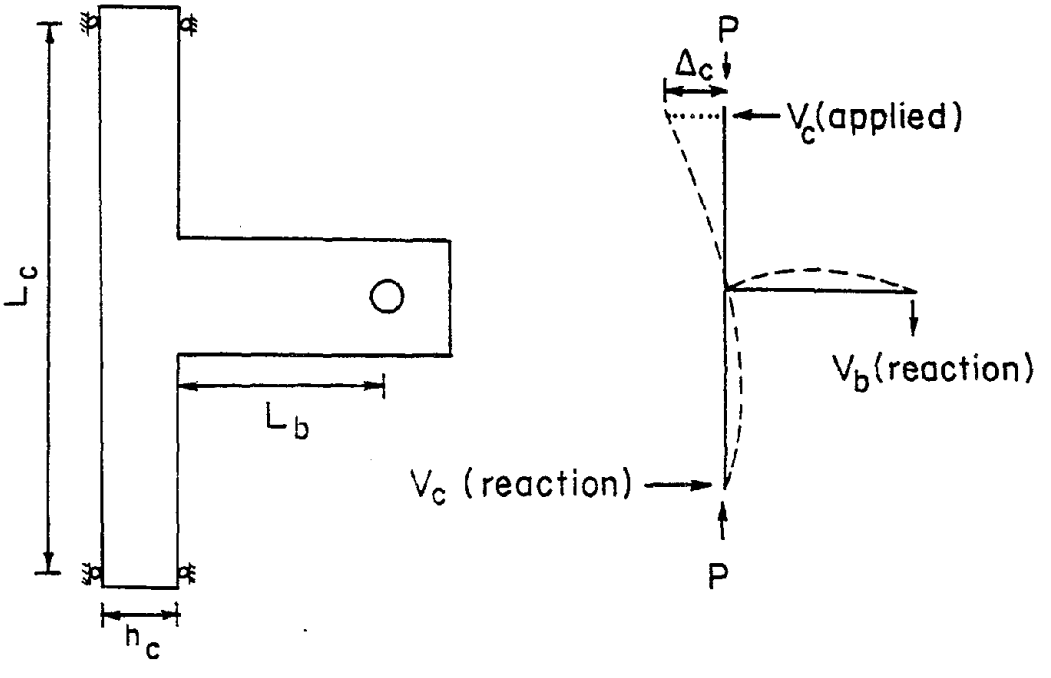

Fig. 4.2. Deflected Shape of Specimens 5 through 12.

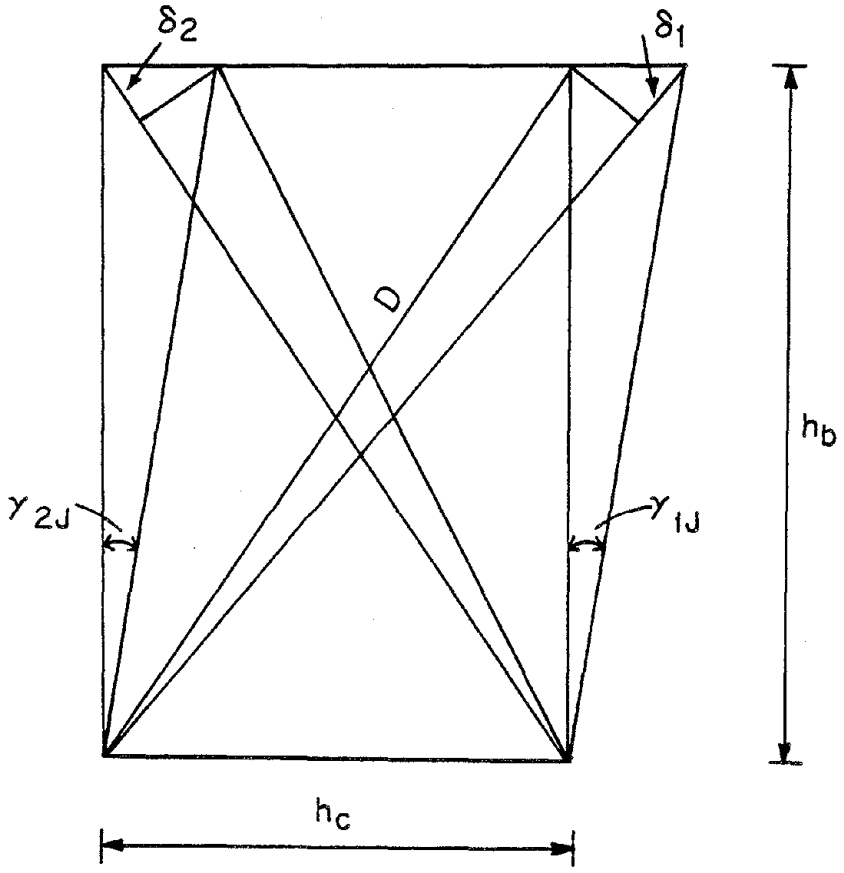

Fig. 4.3. Schematic Diagram to Measure Joint Distortion.

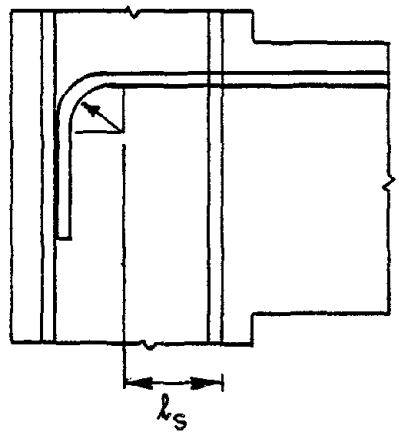

Fig. 5.1. Straight Development Length Before Hook According to ACI-352.

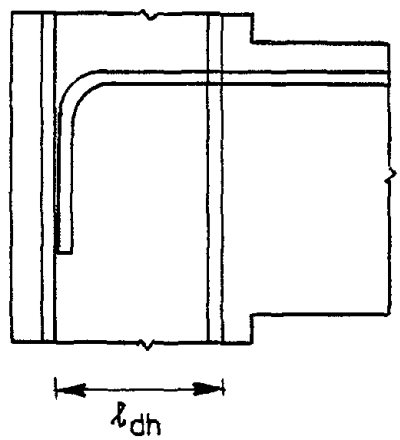

Fig. 5.2. Hooked Bar Development Length According to ACI-352R.

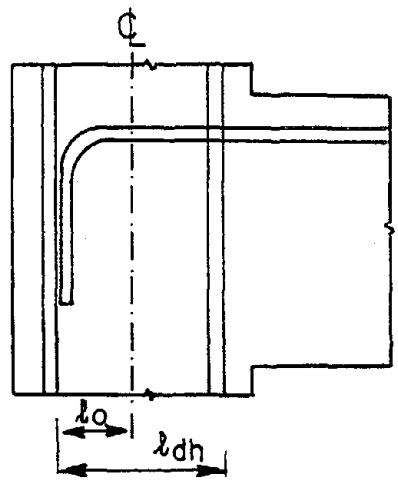

Fig. 5.3. Hooked Bar Development Length According to the NZ Code.

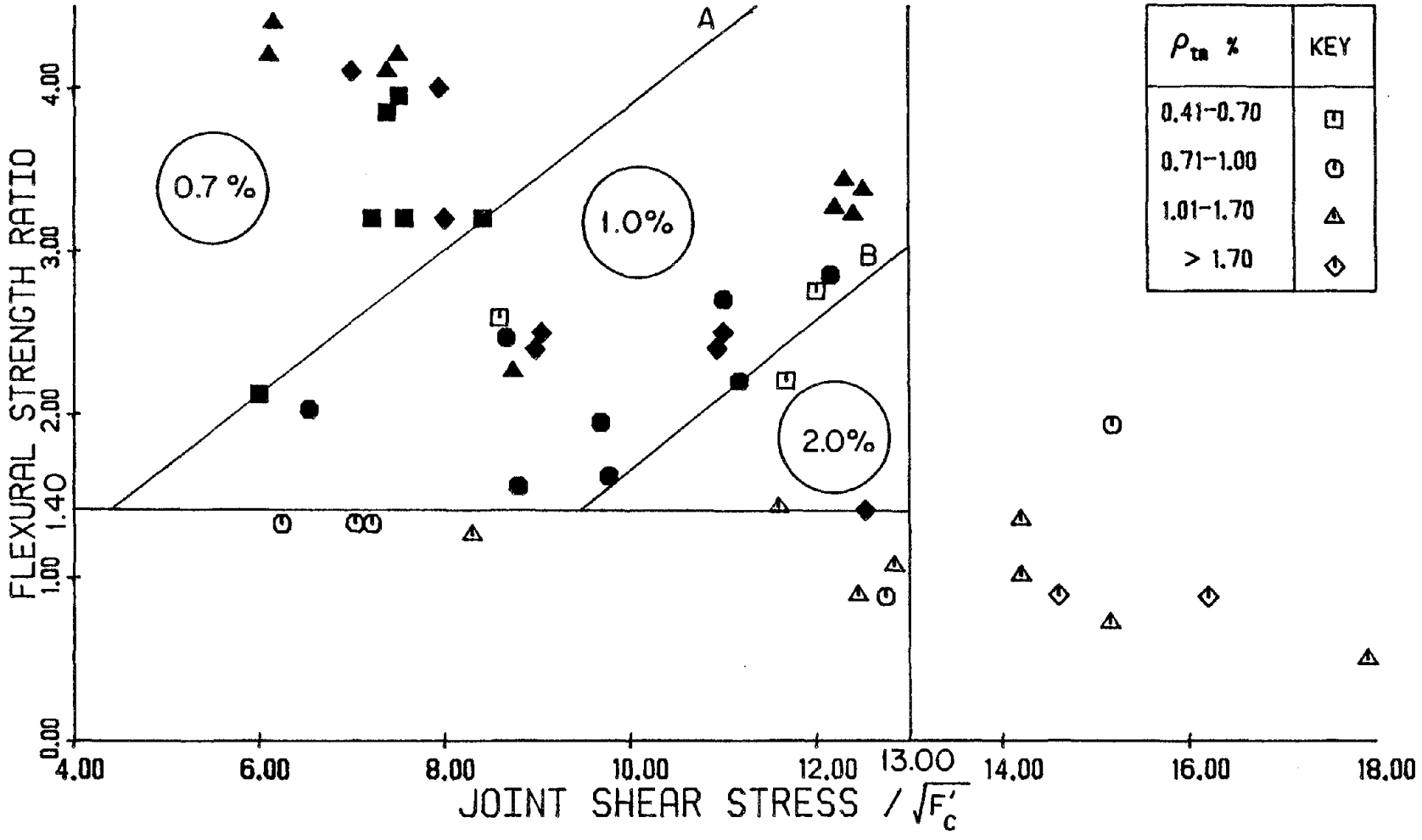

Fig. 5.4. Recommended Design Chart for Exterior Beam to Column Connections.

APPENDICES

APPENDIX A

DESIGN OF SPECIMENS

A.1 General

In designing the specimens the following factors were considered: (1) the overall dimensions of the specimens were to be such that they would fit within the existing testing frames, (2) the flexural capacities of the specimens were to be such that the specimens could be loaded to failure within the capacity of the testing equipment, and (3) the specimens were to be designed so that the beam or column elements would not fail in shear.

The values for the flexural strength ratio, joint shear stress, and the transverse reinforcement ratio for each specimen were predetermined based on the location of existing gaps in the data available from previous investigations. Because these values were fixed in advance, the design of the specimens was a trial and error procedure. For each specimen, several trial beams and columns were designed before a beam and column were selected which had values very close to the target design values. In the following sections, the procedure used

for the design of a bare specimen and a specimen with transverse beams and slab will be presented. Where applicable, numerical examples will be provided for the design of specimens 9 and 10.

A.2 Flexural Design of Beams

After the preliminary selection of dimensions and number and sizes of reinforcing steel, the beam sections were analyzed using the measured yield stress for the reinforcing steel and a concrete compressive strength of 4000 psi. The joint shear stress was then calculated and the design of the beam section was modified until the target design joint shear stress was obtained.

For the beam of specimen 9, the ultimate flexural capacity was M_{ub} = 2511 k-in. The shear force in the column, V_{col}, was calculated from the equilibrium of the external forces acting on the specimen as:

$V_{col} = M_{ub} / L_c = 2511 / 87 = 28.9$ kips

where, L_c = length of the column between roller supports. The tensile force in the beam, T_b, was calculated with a 10 percent increase in the measured yield stress of the longitudinal reinforcement. This tensile force for 6 No. 7 Grade 40 bars used in the beam of specimen 9 was equal to:

$T_b = 1.1(6)(0.6)(48.0) = 190.0$ kips.

The joint shear force was then calculated as:

$V_j = T_b - V_{col} = 190.0 - 28.9 = 161.1$ kips.

Finally the joint shear stress as a multiple of $\sqrt{f_c'}$ was calculated using gross column dimensions which were assumed to be 1.6 in. larger than the width of the beam:

$\gamma = V_j\ (1000) \ / \ bh\ \sqrt{f_c'}$

$= 161.1\ (1000) \ / \ (13.4)(13.4)\ \sqrt{4000} = 14.2$

This value was close to the design value of 14 and the flexural design of the beam was considered satisfactory.

A.3 Flexural Design of Slabs

Flexural design of the slabs was carried out similar to that for the beams, assuming that only the first two longitudinal reinforcing bars on each side of the main beam contributed to the flexural capacity of the beam and slab. For the beam and slab of specimen 10, the ultimate flexural capacity with tension near the top of the slab was equal to M_{us} = 2506 k-in. Equilibrium of external forces resulted in a column shear force of 2506/87 = 28.8 kips. The tensile force in the slab, T_s, was calculated assuming that 5 No. 7 and 2 No. 4 Grade 40 bars were effective:

$T_s = 1.1\ (\ (5)(0.6)(48.0) + (2)(0.2)(51.0)\ ) = 180.8$ kips.

The joint shear force and shear stress were then calculated as:

V_j = 180.8 -28.8 = 152.0 kips.

γ = (152.0)(1000) / (13.4)(13.4) $\sqrt{4000}$ =13.4

The joint shear stress of 13.4 $\sqrt{f_c'}$ was considered to be close enough to the target value of 14 $\sqrt{f_c'}$ and the design of the slab was considered acceptable.

As explained in Section 3.1.5 of this report, due to large flexural cracks observed during the tests which crossed the entire width of the slab, it was later decided that in calculating the flexural strength ratio for specimens with transverse beams and slabs, all slab longitudinal reinforcement should be considered effective in tension.

A.4 Flexural Design of Columns

For each specimen the width of the column was 1.6 in. larger than the width of the beam framing into it. After selection of number and size of reinforcing steel, the column sections were analyzed. The measured yield stress for the reinforcing steel and a compressive strength of 4000 psi for the concrete were used. Several points on the column axial load vs. column flexural capacity interaction diagram were calculated by assuming different locations for the neutral axis. For each column a point on the interaction diagram below the balanced condition was selected to give the required

flexural strength ratio for the subassemblage. If the corresponding axial load for this point on the interaction diagram was less than 40 percent of the balanced axial load and the required axial load was less than the capacity of the existing hydraulic jack, the flexural design of the column would be considered satisfactory. Otherwise, the number or size of the longitudinal reinforcement in the column would be modified until satisfactory results were obtained.

Figure A.1 shows the interaction diagram for the columns used in specimens 9 and 10. With an axial load of 80 kips, the flexural capacity of this column is 2456 k-in. This axial load was 30 percent of the balanced axial load of 265 kips, and within the range of the capacity of the hydraulic jack. The flexural strength ratios for specimens 9 and 10 were 2(2456) / 2511 = 1.96 and 2(2456) / 2506 = 1.96 respectively. These figures are very close to the target flexural strength ratio of 2.0. Hence, the flexural design of the column was considered satisfactory.

A.5 Design of Shear Reinforcement

The maximum shear force in the beam, $V_b(max)$, was calculated as:

$V_b(max) = M_{ub} / L_b = 2511 / 42 = 59.8$ kips

where, M_{ub} = ultimate flexural capacity of beam, k-in.,

and L_b = distance between beam loading point and front face of column, in.

The maximum beam shear stress, $v_b(max)$, was calculated as:

$$v_b(max) = V_b(max) / b_b d_b = (59.8)(1000)/(11.8)(16.0)$$
$$= 317 \text{ psi}$$

where, b_b = width of the beam, in.,

and d_b = effective depth of beam, in.

Allowing a maximum shear stress of $2\sqrt{f_c'} = 126$ psi to be carried by the concrete, the shear stress to be resisted by the the transverse reinforcement, v_s, was:

$$v_s = v_b(max) - v_c = 317 - 126 = 191 \text{ psi.}$$

The required spacing of No. 3 stirrups to resist this shear force was calculated from the following relationship:

$$s = \frac{A_v f_y}{b_b v_s} = \frac{(2)(0.11)(48800)}{(11.8)(191)} = 4.75 \text{ in.}$$

However, according to section A.5.11 of ACI 318-77 (12), the maximum allowable spacing for shear reinforcement over a distance equal to four times the depth of the member from the joint is limited to $d_b/4 = 4.0$ in. Therefore, No. 3 Grade 40 stirrups were provided at a spacing of 4.0 in.

The above criterion governed the design of shear

reinforcement for beams and columns of all specimens. Therefore, for beam and slab of specimen 10 a spacing of $d_b/4$ = 4.0 in. and for column of specimens 9 and 10 a spacing of $d_{lc}/4$ = 2.5 in. was used.

Because it was felt that the provisions of section A.5.11 of ACI 318-77 were very conservative, the shear reinforcement spacing of d/4 was provided over a distance equal to twice the depth of the member from the joint. These distances are shown as regions "a" and "d" in Fig. B.1 for beams and columns respectively. The spacing of shear reinforcement was usually increased by forty to fifty percent for the remaining portions of the beams and columns which were further away from the joint. In all cases additional shear reinforcement was provided near the beam and column loading points.

A.6 Joint Transverse Reinforcement

Two or three sets of transverse reinforcement were placed in the joint of the specimens. The amount of transverse reinforcement provided in the joint of the specimens was always lower than the recommendations of ACI-ASCE Committee 352 (12) except for specimen 4 where the provided transverse reinforcement was equal to the amount required. The transverse reinforcement ratio in the joint was calculated as:

$\rho = (n)(A_{sh}) / (b)(d-d')$

where, A_{sh} = area of transverse reinforcement in each set,

b = total width of column,

$d-d'$ = distance between the centroid of tensile and compressive reinforcement in beam or beam and slab,

and n = number of sets of transverse reinforcement in the joint.

For the specimens tested, the area of transverse reinforcement in each set, A_{sh}, was equal to two No. 4 bars for the outside square hoop, plus two No. 4 bars at a 45 degree angle for the diamond shaped tie. This resulted in:

$A_{sh} = 0.2(2 + 2\ Cos45°) = 0.68\ in^2$.

The transverse reinforcement ratio in the joint of specimen 9 was calculated as:

$\rho = (2)(0.68) / (13.4)(13.0) = 0.0078$

and that for specimen 10 was equal to:

$\rho = (2)(0.68) / (13.4)(15.0) = 0.0068$

A.7 Development of Reinforcement

All beam longitudinal reinforcement was anchored in the core of the beam to column joint with standard 90 degree hooks. The tensile stress developed by the hook,

f_h, was calculated according to the code recommendations (12) as:

$$f_h = 700\ (1 - 0.3d_b')\ \psi\sqrt{f_c'}$$

where, d_b' = nominal diameter of hooked bar, in.,

and ψ = anchorage effectiveness coefficient = 1.4

For No. 7 bars used in specimens 9 and 10, the hooks were allowed to carry the following stress:

$$f_h = 700\ (1 - 0.3\ (0.875)\ )\ (1.4)\ \sqrt{4000} = 45{,}700 \text{ psi.}$$

The required straight embedment length, l_s, measured from the outside of the core of the column to the beginning of the bar hook was then calculated as:

$$l_s = 0.4\ A_b\ (\alpha f_y - f_h)\ /\psi\ \sqrt{f_c'}$$

where, A_b = area of hooked bar, $in.^2$,

α = stress multiplier factor to account for strain hardening in steel = 1.25,

and f_y = specified yield stress of steel, psi.

However, the value of l_s should be larger than $4d_b$ and 4.0 in. The product αf_y was conservatively taken as 1.1 times the measured yield stress of the reinforcing steel. The required straight embedment length for No. 7 bars used in specimens 9 and 10 was equal to:

$$l_s = (0.04)(0.6)\ ((1.1)(48000)-(45700))/1.4\ \sqrt{4000} = 1.9 \text{ in.}$$

Hence, a minimum required straight embedment length of 4.0 in. was needed. This was less than the provided l_s of 5.9 in. for specimens 9 and 10.

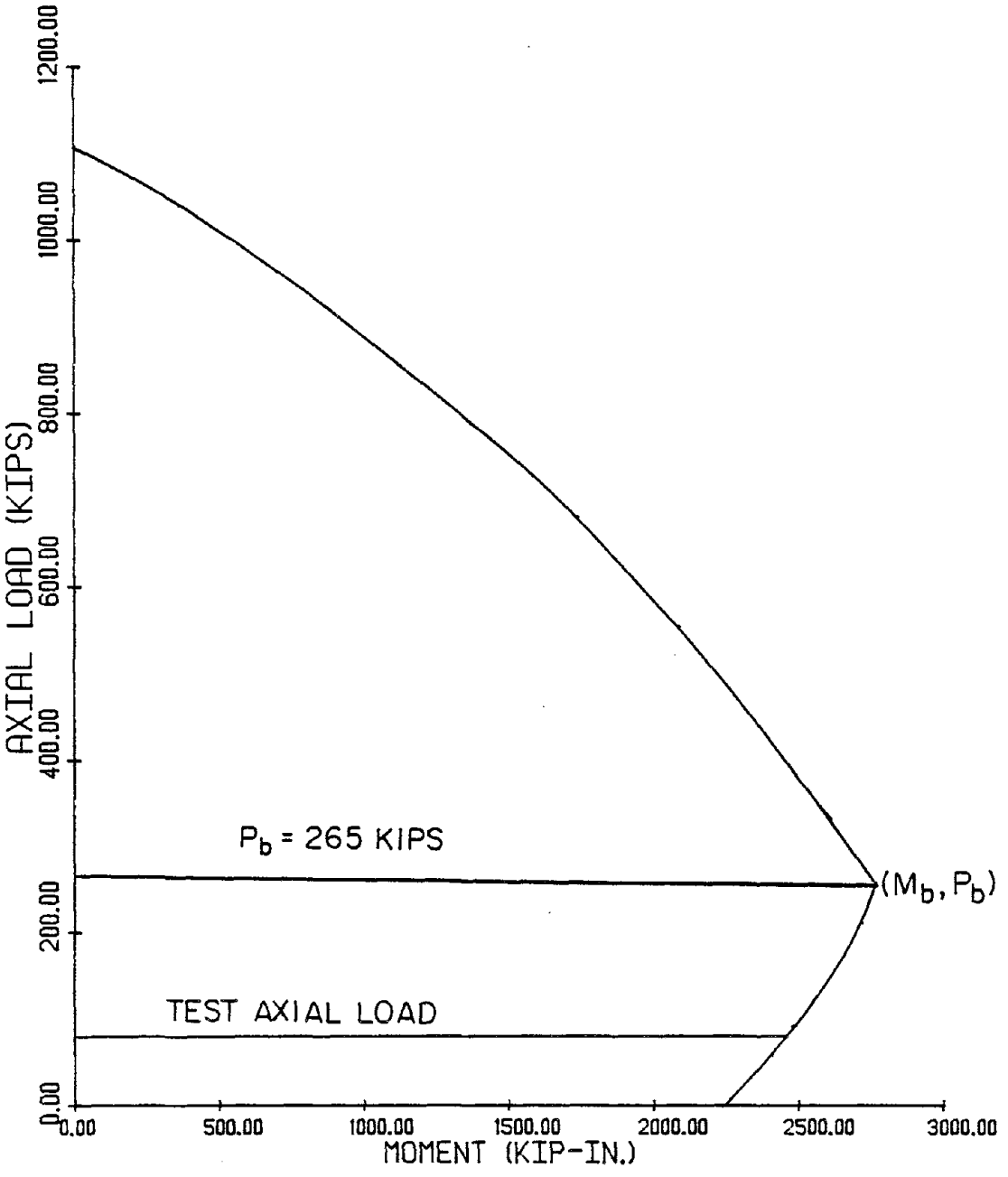

Fig. A.1. Interaction Diagram for Columns Used in Specimens 9 and 10.

APPENDIX B

SHEAR REINFORCEMENT DETAIL

Shear reinforcement was designed as explained in Appendix A. All web reinforcement in beams and columns consisted of closed, one-piece ties. Grade 40 bars were used for shear reinforcement in all beams and columns. Grade 60 No. 4 bars were used for joint transverse reinforcement.

In order to avoid congestion, the free ends of the ties were overlapped and welded together. Several samples of welded ties were tested under uniaxial tension to test the strength of the welds, and in all cases the failure occured outside the welded region. The size and spacing of web reinforcement was selected according to the recommendations of ACI 318-77 (1) for buildings located in seismic zones. Figure B.1 illustrates the location of shear reinforcement in specimens. The number of bars used in each specimen is listed in Table B.1.

For all transverse beams in specimens with transverse beams and slab, four No. 3 grade 40 shear stirrups were provided at a spacing of 2.5 in.

TABLE B.1

SHEAR REINFORCEMENT DETAIL

Specimen Number	Number, Size and Spacing of shear reinforcement at locations shown in Fig. B.1				
	Region (a)	(b)*	(c)**	(d)	(e)
1	8#3 @4 in.	7#3 @6 in.	2#4	8#3 @2.5 in.	6#3 @3 in.
2	8#3 @3.5 in.	8#3 @5 in.	2#4	8#3 @2.5 in.	6#3 @3 in.
3	8#3 @4 in.	7#3 @6 in.	3#4	8#3 @2.5 in.	6#3 @3 in.
4	8#3 @3.5 in.	8#3 @5 in.	3#4	8#3 @2.5 in.	6#3 @3 in.
5	8#3 @4 in.	3#3 @6 in.	2#4	8#3 @2.5 in.	6#3 @3 in.
6	8#3 @4 in.	3#3 @6 in.	3#4	8#3 @2.5 in.	6#3 @3 in.
7	8#3 @3.5 in.	4#3 @5 in.	2#4	8#3 @2.5 in.	6#3 @3 in.
8	8#3 @3.5 in.	4#3 @5 in.	3#4	8#3 @2.5 in.	6#3 @3 in.
9	8#3 @4 in.	4#3 @4 in.	2#4	8#3 @2.5 in.	4#3 @4 in.
10	8#3 @4 in.	4#3 @4 in.	2#4	8#3 @2.5 in.	4#3 @4 in.
11	8#3 @3 in.	8#3 @3 in.	2#4	8#3 @2.5 in.	4#3 @4 in.
12	8#3 @3 in.	8#3 @3 in.	2#4	8#3 @2.5 in.	4#3 @4 in.

*Additional web reinforcement was always provided on both sides of the main beam loading point.

**Grade 60 reinforcement; each set consisted of a square hoop plus a diamond shaped hoop.

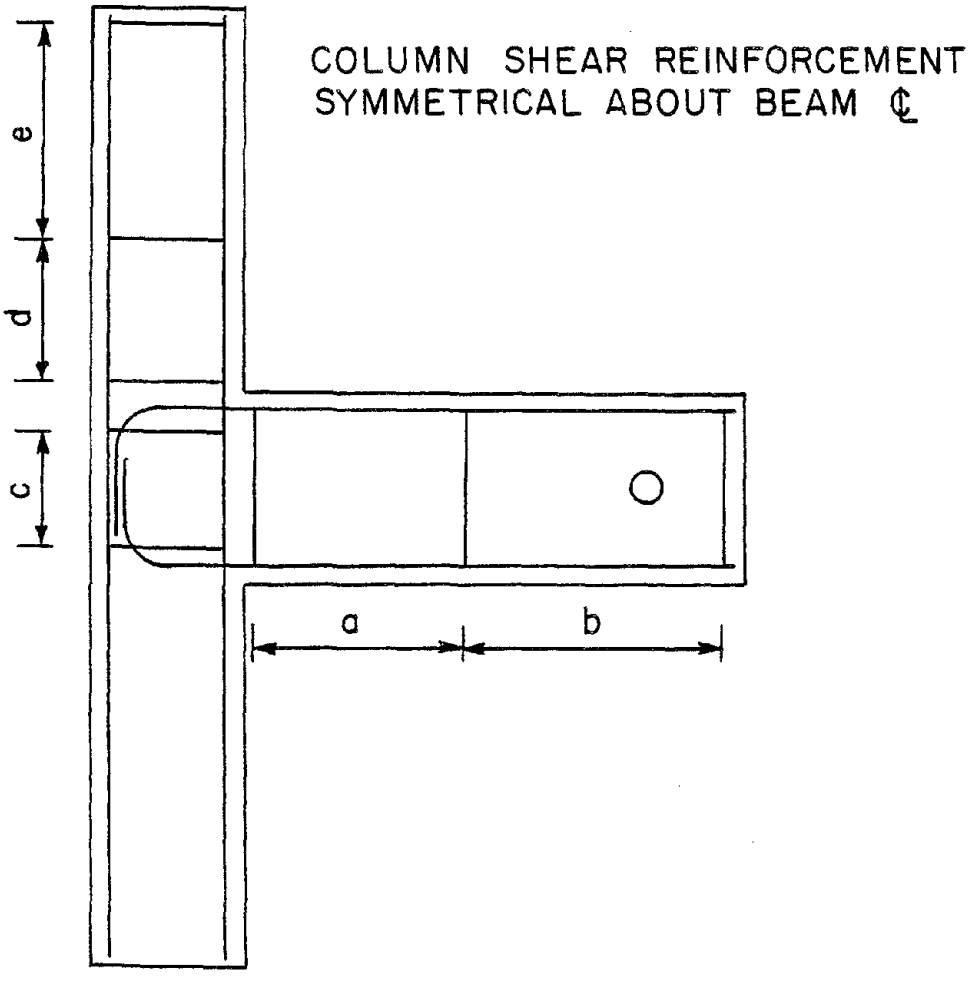

Fig. B.1. Shear Reinforcement Detail.

APPENDIX C

MATERIAL PROPERTIES

C.1 Concrete

Concrete for specimens 1 through 4 was ordered commercially from Ann Arbor Construction Company, specifying a coarse aggregate of 3/8 in. pea pebble and a compressive strength of 4000 psi at 28 days. The mix proportions for one cubic yard of concrete were:

Coarse aggregate (3/8 in. pea pebble)	1225 lb.
Sand	1785 lb.
Cement (Type 1 Portland)	493 lb.
Water	180 lb.

At the time of casting, additional water was added to the mix to obtain a slump of 5 inches. Seven 4 in. by 8 in. cylinders were cast and cured simultaneously with each specimen. The cylinders for the 28 day strength test of the first four specimens were not capped before testing. Results from these specimens were unreasonably low. All subsequent cylinders were capped with a sulphur compound following the recomendations of the American Society for Testing and Materials ASTM C39-71.

Because the strength of the above mix was found to be too high, based on several trial mixes the following mix was designed for specimens 5 through 12. The mix proportions for one cubic yard of concrete were:

Coarse aggregate (1 in. max. size)	1810 lb.
Sand	1155 lb.
Cement (Type 1 Portland)	667 lb.
Water	380 lb.

Additional water was added at the time of casting to produce a slump of approximately 5 inches. Six standard 6 in. by 12 in. cylinders were cast with each batch of concrete. The cylinders were always cured in the same condition as the specimens. Three cylinders were capped and tested after 28 days. The remaining cylinders were capped and tested on the test day. Results of concrete cylinder tests are shown in Table C.1.

An extensometer was attached to some of the 4 in. by 8 in. cylinders and the shortening of the cylinder height over a length of 6 inches was recorded through a dial gage. Strains were recorded at uniform stress intervals for all cases and were averaged to obtain the stress vs. strain curve for the concrete in that specimen. A typical concrete compressive stress vs. strain curve obtained for the concrete used in the lower column half of specimen 7 is shown in Fig. C.1.

C.2 Reinforcing Steel

Samples of reinforcing bars were randomly selected and subjected to uniaxial tension. Elongation of the bar over a gage length of 8 inches was measured following the ASTM-A615 recommendations. Elongation of the bars were recorded at uniform stress levels and converted to strains. The stress vs. strain curve for each sample was plotted and the yield stress, yield strain, strain at onset of strain hardening, and the ultimate stress and strain were recorded.

The average of the measured properties for all samples tested is listed in Table C.2. A typical plot of tensile stress vs. reinforcing bar strain for No. 6 grade 40 and grade 60 bars is shown in Fig. C.2.

TABLE C.1

RESULTS OF CONCRETE CYLINDER TESTS

Specime Number	Part of Specimen	Slump (in.)	f_c' (psi) 28 day	f_c' (psi) Test day
1	Entire	5.0	2020*	5090
			2190*	4730
			2310*	5250
			2270*	—
			Avg. 2200	Avg. 4870
2	Entire	5.0	2020*	5170
			2190*	5370
			2310*	5330
			2270*	5010
			Avg. 2200	Avg. 5070
3	Entire	4.0	2490*	6210
			2310*	5970
			2520*	6090
			—	6170
			Avg. 2440	Avg. 5930
4	Entire	4.0	2490*	6210
			2310*	6720
			2520*	6170
			—	6840
			Avg. 2440	Avg. 6470
5	Lower Column	4.5	3780	4400
			3630	4240
			3800	4070
			Avg. 3740	Avg. 4240
	Beams, Slab	4.5	5480	6210
			4810	6070
			5480	6280
			4620	—
			Avg. 5100	Avg. 6180
	Upper Column	5.5	3930	4530
			3910	4260
			4030	—
			Avg. 3960	Avg. 4390

TABLE C.1 (Cont'd)

RESULTS OF CONCRETE CYLINDER TESTS

Specime Number	Part of Specimen	Slump (in.)	f_c' (psi) 28 day	f_c' (psi) Test day
6	Lower Column	6.0	3480	3980
			3800	3820
			3700	4010
			Avg. 3660	Avg. 3940
	Beams, Slab	6.0	5640	5230
			5780	6050
			5480	5910
			Avg. 5630	Avg. 5730
	Upper Column	6.0	3840	4210
			3590	3450
			3840	4070
			Avg. 3760	Avg. 3910
7	Lower Column	5.5	**	4200
			**	3750
			**	3890
				Avg. 3950
	Beams, Slab	6.5	**	4100
			**	4170
			**	4330
				Avg. 4200
	Upper Column	6.0	**	4140
			**	3670
			**	3980
				Avg. 3930
8	Lower Column	6.0	**	4200
			**	3750
			**	3890
				Avg. 3760
	Joint, Transv. Beams	5.5	**	4280
			**	4240
			**	4240
				Avg. 4260

TABLE C.1 (Cont'd)

RESULTS OF CONCRETE CYLINDER TESTS

Specime Number	Part of Specimen	Slump (in.)	f_c' (psi) 28 day	Test day
8	Main Beam, Slab	5.5	**	4760
			**	4540
			**	4740
				Avg. 4680
	Upper Column	6.0	**	4100
			**	3960
			**	3640
				Avg. 3900
9	Entire	6.0	3430	3480
			3410	3620
			3450	3480
			Avg. 3430	Avg. 3530
10	Lower Column	6.0	3270	3480
			3310	3590
			3500	3390
			Avg. 3360	Avg. 3490
	Beams, Slab, Upper Column	6.0	3430	3480
			3410	3390
			3450	3520
			Avg. 3430	Avg. 3470
11	Entire	5.0	4970	5710
			4990	5940
			5090	5660
			Avg. 5020	Avg. 5770
12	Lower Column	6.0	3850	3610
			3910	3380
			3980	3910
			Avg. 3910	Avg. 3630
	Beams, Slab, Upper Column	5.0	4810	5160
			4510	5320
			4860	4770
			Avg. 4730	Avg. 5090

*Cylinders were not capped before testing.

**No cylinders were tested for the 28-day strength.

TABLE C.2

PROPERTIES OF REINFORCING STEEL

Bar Size	Grade	E_s	σ_y	ε_y	ε_{sh}	E_{sh}	ε_{max}^*	σ_{max}^*
#3	40	28.7	48.8	1.70	12.5	0.98	180	73.0
#4	40	28.5	51.0	1.79	13.1	1.05	172	78.1
#4	60	29.1	63.4	2.18	4.9	1.35	140	102.4
#6	40	27.9	50.0	1.79	12.8	1.04	195	82.0
#6	60	28.9	71.0	2.46	4.8	1.42	110	129.0
#7	40	28.4	48.0	1.69	11.2	0.97	185	80.3
#8	60	29.2	60.0	2.05	5.1	1.63	135	102.0

All stresses are expressed in units of (ksi)x10^3.

All strains are expressed in units of (in/in)x10^{-3}.

*Maximum stresses and strains measured at the last loading point prior to the failure.

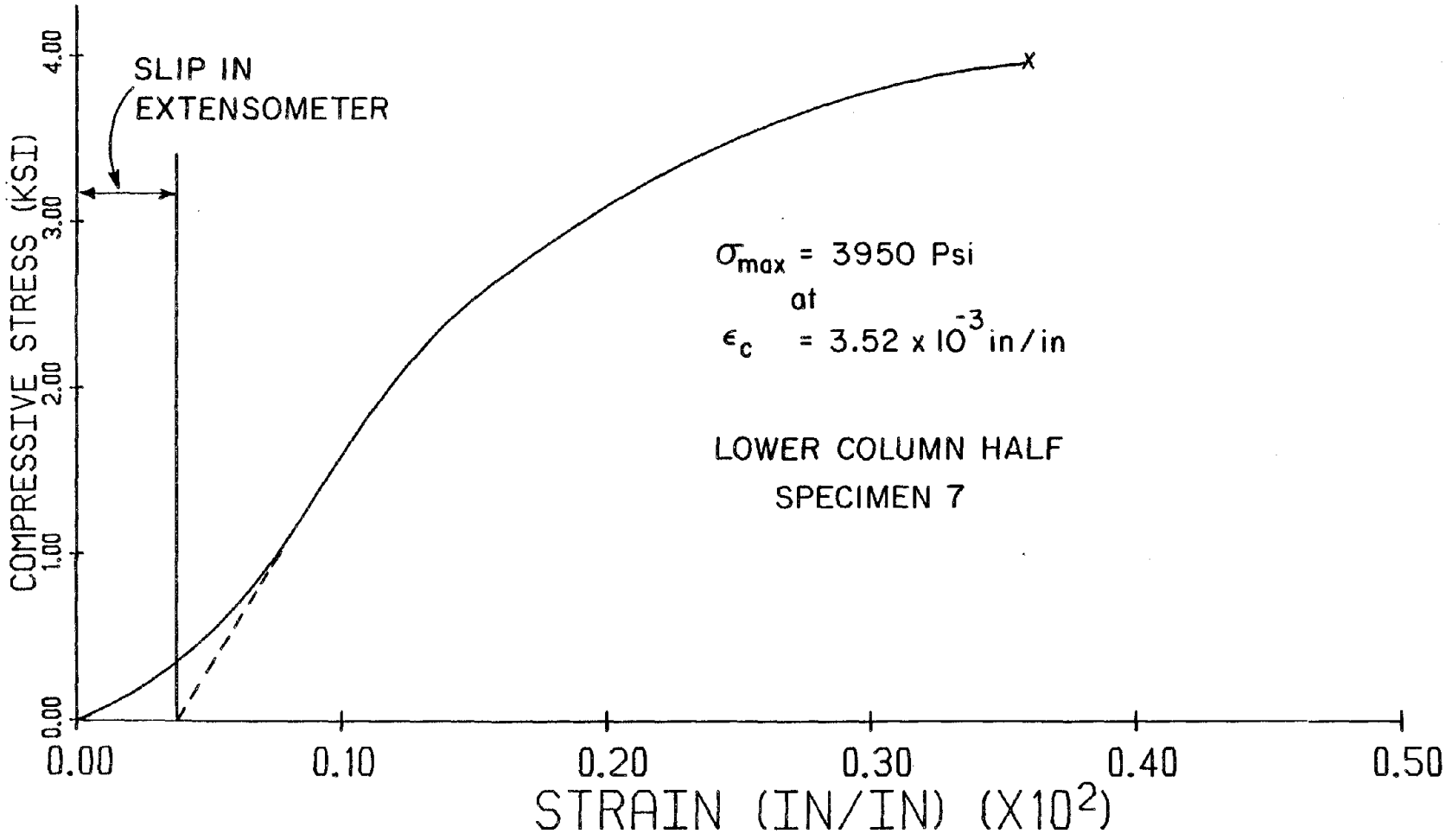

Fig. C.1. Plot of Measured Stress vs. Strain for Concrete Cylinders Tested in Conjunction with Subassemblages.

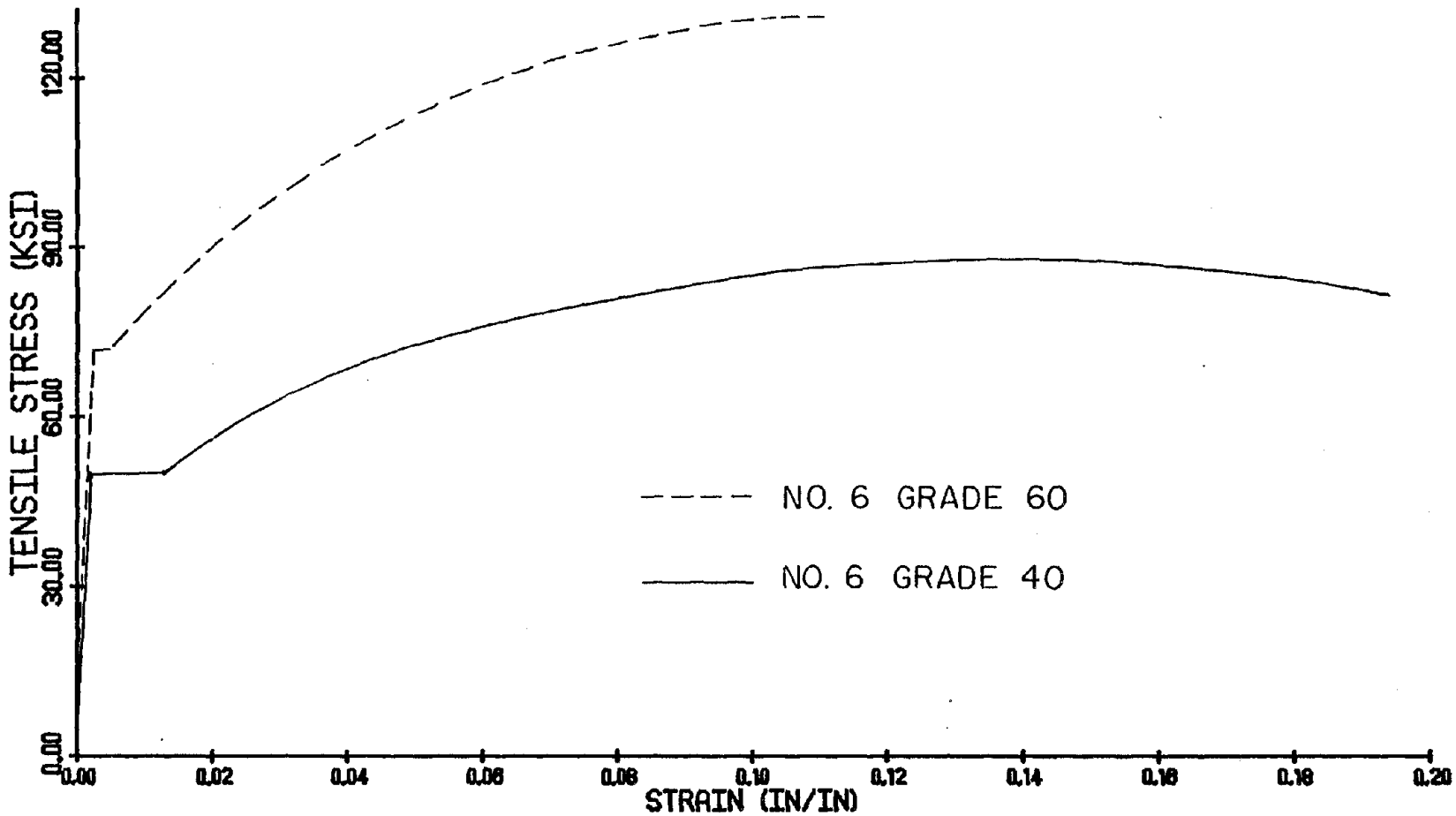

Fig. C.2. Typical Plot of Stress vs. Strain for Reinforcing Steel Used in the Specimens.

APPENDIX D

CONSTRUCTION OF SPECIMENS

Fabrication of specimens was entirely performed by student research assistants. Six sets of reusable forms were constructed in the wood shop of the Engineering 1-A Building. Forms were constructed using 3/4 in. exterior grade plywood with 1 1/2 in. square fir wales, screwed into the plywood using 2 in. wood screws, to stiffen the forms. Forms were then waterproofed by applying two coats of Orange Bulls Eye Shellac. Different sections of the formwork were bolted together with 5 in. long, 1/4 in. diameter machine bolts and caulked at all seams with modeling clay. Forms were coated with oil before casting to ease removal from finished specimens.

All reinforcing bars were bent manually in G. G. Brown Laboratory using a Hasstfeld #2 reinforcing bar bender. Dimensions of the finished bars conformed to the applicable specifications of ACI 318-77 Building Code. In order to avoid congestion in the joints, it was decided to bend the ties as full rectangles with two legs overlapping. The overlap was then welded with 1/8 in. diameter 7018 rods. Several welded #3 and #4 bars were

tested under uniaxial tension and the performance of the welding quality was proved satisfactory. Using templates made out of plywood, the free ends of the longitudinal bars were supported while ties were fastened to them with eighteen gage annealed wire. Two different fabrication techniques were used for specimens with or without transverse beams and slab.

Specimens without transverse beams and slab were cast flat on the floor. Beam reinforcement was mated to the completed column cage and installation of beam ties completed reinforcement fabrication. Steel cages were placed in the oiled forms and supported with small concrete cubes to provide proper concrete cover and hold the steel in position during casting. Steel pipes used for loading the specimens were placed near the end of the beam and tied to the reinforcing cage to make sure that they would remain vertical and in position during casting. Concrete was mixed and delivered in a ready mix truck by Ann Arbor Construction company according to the mix design specified in Appendix C. Additional water was added to the mix to give a slump of approximately 5 inches. Concrete was placed in the form and consolidated with a hand held internal spud electric vibrator.

Specimens with transverse beams and slab were cast vertically in three separate pours. The prepared column

cage was placed and supported vertically in the forms for the lower column half. The concrete for the lower column half was hand mixed in the laboratory and placed using a chute to avoid segragation of the constituent materials. The form was vibrated from the outside to give adequate consolidation of the concrete. Within a few working days the formwork for the slab and the beams were connected to the formwork for the lower column half and the reinforcing bars for the beams and slab were tied in place. The steel pipe for transfer of load to the beam portion of the specimen was secured horizontally in place near the end of the beam. Four wooden pegs, 1 in. in diameter and 5 in. in height, were placed vertically near the free end of the slab. The pegs were to be removed prior to the testing of the specimens to connect the stiffeners to the slab. Figure D.1 shows specimen 7 ready for casting of the slab.

Concrete for the beams and the slab was mixed and delivered by Ann Arbor Construction Company. For specimen nummber 8, however, the concrete for the beams and slab was hand mixed in the laboratory in two separate batches. Except for specimens 10 and 12, concrete for the upper column half was hand mixed in the laboratory and placed a few days after casting of the slab. For specimens 10 and 12 the upper column half was cast at the

same time with the slab, utilizing the same concrete which was used for slabs 10 and 12 respectively.

In all cases the excess concrete was removed with wooden screeds and the exposed surface of the specimen was smoothed with a trowel. A few hours later the specimen was covered with wet burlap and plastic sheets to reduce evaporation. The burlap was regularly sprayed with water. After a week the formwork was removed allowing the specimen to cure uncovered until it was tested. Prior to testing, the specimens were painted with a diluted cement paste mix to ease the detection of cracks during testing. The schedule of casting and testing dates for all specimens is shown in Table D.1.

Concrete cylinders, which were cast in reusable molds, were always cured in the same way as the specimens. For each specimen, half of the cylinders were tested after 28 days and the remaining cylinders were tested on the same day that the specimen was tested. Details of testing of the concrete cylinders were presented in Appendix C.

TABLE D.1

CASTING AND TESTING TIMETABLE

Specime Number	Part of Specimen	Date Cast	Date Tested	Age at Test-days
1	Entire*	17 Jul 79	21 Jan 80	187
2	Entire*	17 Jul 79	25 Jan 80	191
3	Entire*	7 Aug 79	1 Feb 80	178
4	Entire*	7 Aug 79	8 Feb 80	185
5	Lower Column	17 Oct 80	22 Dec 80	66
	Beams, Slab*	20 Oct 80		63
	Upper Column	24 Oct 80		59
6	Lower Column	11 Nov 80	12 Mar 81	121
	Beams, Slab*	18 Nov 80		114
	Upper Column	21 Nov 80		111
7	Lower Column	3 Feb 81	24 Mar 81	50
	Beams, Slab*	12 Feb 81		41
	Upper Column	17 Feb 81		36
8	Lower Column	3 Mar 81	21 Apr 81	48
	Joint, Transv. Beams	5 Mar 81		46
	Main Beam, Slab	5 Mar 81		46
	Upper Column	6 Mar 81		45
9	Entire*	16 Apr 81	26 Jun 81	71
10	Lower Column	14 Apr 81	20 Jun 81	63
	Beams, Slab, Upper Column*	16 Apr 81		65
11	Entire*	1 May 81	6 Jul 81	67
12	Lower Column	24 Apr 81	23 Jun 81	61
	Beams, Slab, Upper Column*	1 May 81		54

*Concrete was mixed and delivered by Ann Arbor Construction Company.

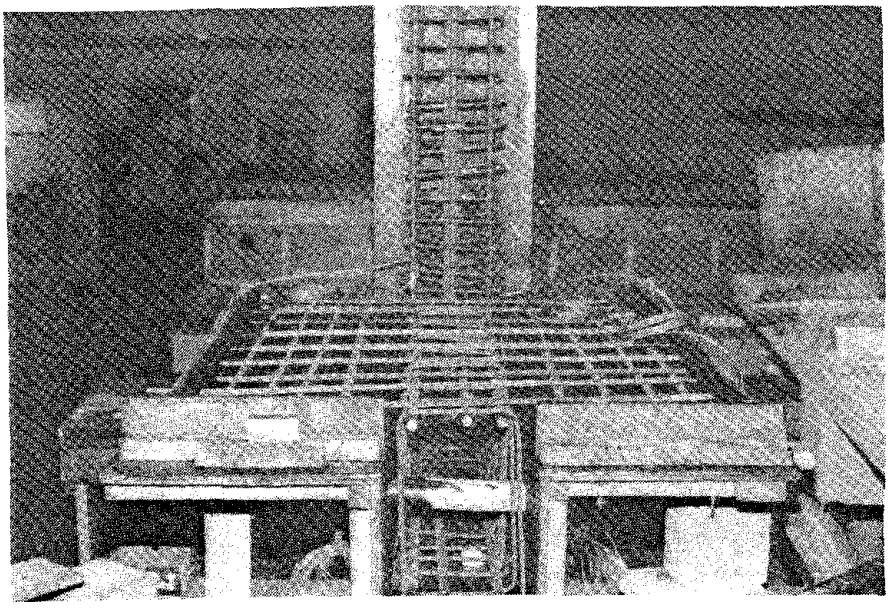

Fig. D.1. Specimen 7 Prior to Casting of the Beam and Slab Concrete.

APPENDIX E

APPLICATION OF STRAIN GAGES

Special annealed Constantan foil, high-elongation strain gages were applied to some of the reinforcing bars in the specimens tested. A 1½ in by ½ in. area of the reinforcing bar was filed to remove the deformation and surface scale. Care was taken to file as small an area as possible to prevent any local yielding of the bars. The filed surface was sanded with 220 grit sand paper. The surface was chemically cleaned with Conditioner A and Neutralizer 5.

The gages (EP-08-250BG-120) and the terminals (CEG-50D) were positioned on a cellophane tape and the assemblage was placed on the reinforcing bars at prescribed locations. One end of the tape was lifted at a shallow angle to surface and a two-component M-Bond AE-10 adhesive was applied to the back of the gage and the terminal. The tape was then replaced on the reinforcing bar. Using a curved pressure pad and heavy rubber bands, pressure was applied to the subassemblage for 24 hours.

Belden #22 AWG stranded three-conductor cable was soldered to each terminal. Two leads were connected to one of the gage tabs and the remaining lead was attached to the other tab. This procedure compensated for the lead wire length. Cables were tied to the reinforcing bars with steel tie wires to prevent any tension on the gage connection.

Gages were covered with air-drying acrylic coating (M-Coat D), and Nitrile Rubber coating (M-Coat B). A two-part polysulfide modified epoxy compound (M-Coat G) was applied to cover the gage and the lead wire area. Sufficient drying time was allowed between subsequent application of coatings. To protect the gage from any impact during construction of the specimens, the entire subassemblage was covered with M-Coat FB-2 Butyle Rubber Sealant and wrapped with friction cloth tape or Scotch Brand electrical tape.

Unless otherwise noted, the above products were manufactured by Micro-Measurement Corporation.

APPENDIX F

TESTING EQUIPMENT AND DATA ACQUISITION

F.1 Specimen Loading

Specimens 1 through 4 were tested such that the column portion of the specimen was placed horizontally and the beam portion of the specimen remained vertically in the testing frame. The column was tied down to the loading frame near the end points with roller bearings to simulate points of cotraflexure. A Templeton Model RC5065SB hydraulic jack with a maximum compressive capacity of 100 kips was used to apply the axial load to the secured specimen. A Templeton manual pump was used to drive the jack with a Templeton #7097 inline pressure gage to monitor jack loads.

A Gilmore Model 433-50 fatigue actuator with a capacity of 50 kips and a 12 in. stroke was used to apply the shear force to the beam loading point near the free end of the beam. The actuator was driven by a Vicker Model T40-VB20C-10 hydraulic pump with a capacity of 15 gpm at 3000 psi. Displacement of the actuator end was manually controlled through a Gilmore Model 660 servo

controller, 454 channel control, 435 pump controller, 431 servo amplifier, 416A position signal conditioner, and 416D control module. These control amplifiers also provided outlets to record and monitor the load cell and position transducer of the actuator.

Specimens 5 through 12 were placed in the testing frame such that the column portion of the specimen remained vertical. The column was tied to the testing frame with roller bearings near its ends. The beam portion of the specimen was also tied to the testing frame such that it could rotate freely. A Templeton Model HFJ-75 hydraulic jack with a maximum compressive capacity of 75 kips and a maximum stroke of 5/8 in. was used to apply the axial load to the column. A Templeton Model 785-4 manual pump was used to drive the jack with a Templeton #19182 inline pressure gage to monitor jack loads.

An MTS Model 207.16A hydraulic actuator with a capacity of 250 kips and a 16 in. stroke was used to apply the shear forces to the top of the upper column half. Displacement of the actuator was manually controlled through an MTS Model 406.11 controller. This unit provided outlets which allowed recording and monitoring of the actuator forces and displacements.

F.2 Data Acquisition

Three major sources were used to collect data during the tests: (1) a load cell and a displacement transducer attached to the hydraulic actuator, (2) electrical resistance strain gages bonded to the longitudinal and shear reinforcement, and (3) two Linear Variable Differential Transducers (LVDTs) positioned over the lateral face of the joint in the specimens without transverse beams and slab.

Load vs. Displacement

The applied actuator load vs. the load point displacement was plotted continuously throughout the test using a Honeywell Model 530 X-Y recorder. Signals to drive the X-Y recorder were provided by the Gilmore control module or the MTS controller described in section F.1.

Strain Gages

In each specimen thirty electrical resistance strain gages were bonded to the reinforcing steel at different locations to measure the elongation or shortening of the reinforcing bars. The position of these gages are shown in Figs. 2.12 and 2.13. A digital data acquisition system manufactured by Accurex Autodata Corporation was

used to measure strains. The system consisted of Visig 611 signal conditioning modules, a Vidar 606 master scanner, a Vidar 502B integrating digital voltmeter, a Vidar 111 power module, and a Vidar D-DAS system controller.

At each load point, the loading was temporarily stopped and the output voltages from the strain gages and the LVDTs were scanned and the results were printed on a 3320-5JE Teletype. The teletype was equipped with paper tape onto which the readings were punched. The paper tapes were compatible with the paper tape reader at the University of Michigan Computer Center. The paper tapes were directly copied into a computer disk file after the completion of each test. Figure F.1 shows the X-Y plotter, the Vidar console, the Gilmore control, and the teletype in preparation for a test.

LVDTs

Two Linear Variable Differential Transducers (LVDTs) were used in specimens without transverse beams and slab to measure the shear deformations of the joint. The location of the LVDTs are shown in Fig. 2.14. The brackets to support the LVDTs were constructed with 1¼ in. and 1½ in. square perforated tubing. The brackets were secured to the column portion of the specimen with

hex-head bolts.

Direct current Model 1000DC-D S/N758 LVDTs manufactured by Schaevitz were used. A Lambda LOD-Z-152 power supply was used to provide 15 VDC input power. The output voltage from these transducers was fed to the Vidar digital voltmeter. This output volatge was processed and recorded on the paper tape similar to the output voltage from the strain gages.

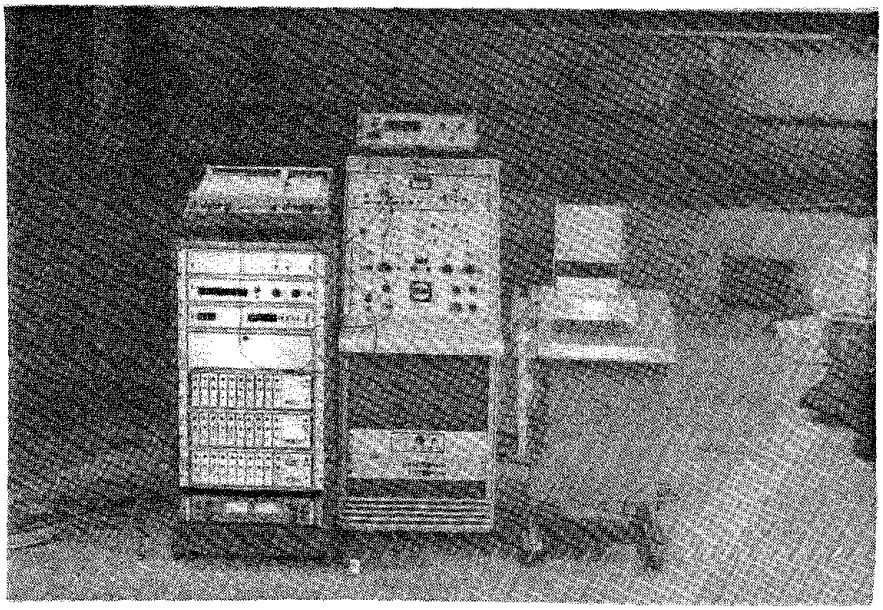

Fig. F.1. X-Y Plotter, Vidar Console, Gilmore Control and Teletype in Position for Operation.